# FRACTALS IN SOIL SCIENCE

Volume 88/3-4

Y. Pachepsky

*Developments in Soil Science 27*

# FRACTALS IN SOIL SCIENCE

*Further Titles in this Series*

*5A. G.H. BOLT and M.G.M. BRUGGENWERT (Editors)*
SOIL CHEMISTRY. A. BASIC ELEMENTS

*8. M. SCHNITZER AND S.U. KAHN (Editors)*
SOIL ORGANIC MATTER

*11A. L.P. WILDING, N.E. SMECK and G.F. HALL (Editors)*
PEDOGENESIS AND SOIL TAXONOMY. I. CONCEPTS AND INTERACTIONS

*11B. L.P. WILDING, N.E. SMECK and G.F. HALL. (Editors)*
PEDOGENESIS AND SOIL TAXONOMY. II. THE SOIL ORDERS

*13. P. KOOREVAAR, G. MENELIK and C. DIRKSEN*
ELEMENTS OF SOIL PHYSICS

*14. G.S. CAMPBELL*
SOIL PHYSICS WITH BASIC-TRANSPORT MODELS FOR SOIL-PLANT SYSTEMS

*15. M.A. SMULDERS*
REMOTE SENSING IN SOIL SCIENCE

*16. K. KUMADA*
CHEMISTRY OF SOIL ORGANIC MATTER

*19. L.A. DOUGLAS (Editor)*
SOIL MICROMORPHOLOGY: A BASIC AND APPLIED SCIENCE

*20. H.W. SCHARPENSEEL, M. SCHOMAKER AND A. AYOUB (Editors)*
SOIL ON A WARMER EARTH

*21. S. SHOJI, M. NANZYO and R. DAHGREN*
VOLCANIC ASH SOILS

*22. A.J. RINGROSE-VOASE and G.S. HUMPHREYS (Editors)*
SOIL MICROMORPHOLOGY: STUDIES IN MANAGEMENT AND GENESIS

*23. J. DVORÁK and L. NOVÁK*
SOIL CONSERVATION AND SILVICULTURE

*24. N. AHMAD and A. MERMUT*
VERTISOLS AND TECHNOLOGIES FOR THEIR MANAGEMENT

*25. E.G. GREGORICH and M.R. CARTER (Editors)*
SOIL QUALITY FOR CROP PRODUCTION AND ECOSYSTEM HEALTH

*26. S. KISS, D. PAŞCA and M. DRĂGAN-BULARDA (Editors)*
ENZYMOLOGY OF DISTURBED SOILS

*Developments in Soil Science 27*

# FRACTALS IN SOIL SCIENCE

Reprinted from Geoderma Volume 88/3-4

Edited by

**Y. PACHEPSKY, J.W. CRAWFORD and W.J. RAWLS**

*USDA-ARS, Hydrology Laboratory*
*10300 Baltimore Avenue,*
*Beltsville, MD 20705, USA*

*Scottish Crop Research Institute, Soil-Plant Dynamics Unit*
*Invergowrie, Dundee DD2 5DA, UK*

*USDA-ARS, Hydrology Laboratory*
*10300 Baltimore Avenue,*
*Beltsville, MD 20705, USA*

2000

**ELSEVIER**

Amsterdam - Lausanne - New York - Oxford - Shannon - Singapore - Tokyo

ELSEVIER SCIENCE B.V.
Sara Burgerhartstraat 25
P.O. Box 211, 1000 AE Amsterdam, The Netherlands

© 2000 Elsevier Science B.V. All rights reserved.

This work is protected under copyright by Elsevier Science, and the following terms and conditions apply to its use:

Photocopying
Single photocopies of single chapters may be made for personal use as allowed by national copyright laws. Permission of the Publisher and payment of a fee is required for all other photocopying, including multiple or systematic copying, copying for advertising or promotional purposes, resale, and all forms of document delivery. Special rates are available for educational institutions that wish to make photocopies for non-profit educational classroom use.

Permissions may be sought directly from Elsevier Science Global Rights Department, PO Box 800, Oxford OX5 1DX, UK; phone: (+44) 1865 843830, fax: (+44) 1865 853333, e-mail: permissions@elsevier.co.uk. You may also contact Global Rights directly through Elsevier's home page (http://www.elsevier.nl), by selecting 'Obtaining Permissions'.

In the USA, users may clear permissions and make payments through the Copyright Clearance Center, Inc., 222 Rosewood Drive, Danvers, MA 01923, USA; phone: (978) 7508400, fax: (978) 7504744, and in the UK through the Copyright Licensing Agency Rapid Clearance Service (CLARCS), 90 Tottenham Court Road, London W1P 0LP, UK; phone: (+44) 171 631 5555; fax: (+44) 171 631 5500. Other countries may have a local reprographic rights agency for payments.

Derivative Works
Tables of contents may be reproduced for internal circulation, but permission of Elsevier Science is required for external resale or distribution of such material.
Permission of the Publisher is required for all other derivative works, including compilations and translations.

Electronic Storage or Usage
Permission of the Publisher is required to store or use electronically any material contained in this work, including any chapter or part of a chapter.

Except as outlined above, no part of this work may be reproduced, stored in a retrieval system or transmitted in any form or by any means, electronic, mechanical, photocopying, recording or otherwise, without prior written permission of the Publisher.
Address permissions requests to: Elsevier Science Global Rights Department, at the mail, fax and e-mail addresses noted above.

Notice
No responsibility is assumed by the Publisher for any injury and/or damage to persons or property as a matter of products liability, negligence or otherwise, or from any use or operation of any methods, products, instructions or ideas contained in the material herein. Because of rapid advances in the medical sciences, in particular, independent verification of diagnoses and drug dosages should be made.

First edition 2000

Library of Congress Cataloging in Publication Data
A catalog record from the Library of Congress has been applied for.

ISBN: 0-444-50530-x

♾ The paper used in this publication meets the requirements of ANSI/NISO Z39.48-1992 (Permanence of Paper).
Printed in The Netherlands.

*Fractals in Soil Science*
Editors: Ya.A. Pachepsky, J.W. Crawford and W.J. Rawls
© 2000 Elsevier Science B.V. All rights reserved.


# Preface

This book is intended to provide a balanced account of the application of fractal models to soil science. Fractal models offer the soil scientist the possibility of relating soil properties at different scales and quantifying the intrinsic heterogeneity of soils. The application of fractal geometry to these problems is a recent development in soil science, the first papers only appearing in eighties. The set of papers in this issue represents the state of science.

Authors from a broad background explore topics from geochemistry to microbiology, and from scales of micrometres to the landscape. Limitations of the approach are discussed as well as the level of success in the hope that opportunities for future work will become clear. Challenges encountered in the measurement and interpretation of fractal properties are discussed. The first paper written by the editors presents a conceptual overview. The first bibliography on applications of fractals in soil science is included in the book.

It is hoped that the areas of application of fractal models in soil science will grow rapidly as a consequence of the focus provided by this book. The notion of fractals inevitably fascinates those who become familiar with it. A multitude of paths from fascination to application waits to be explored. May be these paths themselves are fractal.

YAKOV A. PACHEPSKY
JOHN W. CRAWFORD
WALTER J. RAWLS
(Editors)

# Contents

Preface v

Integrating processes in soils using fractal models
J.W. Crawford, Ya.A. Pachepsky and W.J. Rawls 1

Conventional and fractal geometry in soil science
Ya. A. Pachepsky, D. Giménez, J. W. Crawford, and W. J. Rawls 7

Surface fractal characteristics of preferential flow patterns in field soils: evaluation and effect of image processing
Susumu Ogawa, Philippe Baveye, Charles W. Boast, Jean-Yves Parlange, Tammo Steenhuis 19

Generalizing the fractal model of soil structure: the pore--solid fractal approach
Edith Perrier, Nigel Bird, Michel Rieu 47

Silty topsoil structure and its dynamics: the fractal approach
V. Gomendy, F. Bartoli, G. Burtin, M. Doirisse, R. Philippy, S. Niquet, H. Vivier 75

Simulation and testing of self-similar structures for soil particle-size distributions using iterated function systems
F.J. Taguas, M.A. Martín, E. Perfect 101

Scaling properties of saturated hydraulic conductivity in soil
D. Giménez, W.J. Rawls, J.G. Lauren 115

Estimating soil mass fractal dimensions from water retention curves
E. Perfect 131

Influence of humic acid on surface fractal dimension of kaolin: analysis of mercury porosimetry and water vapour adsorption data
Z. Sokolowska, S. Sokolowski 143

Applications of light and X-ray scattering to characterize the fractal properties of soil organic matter
James A. Rice, E. Tombácz, Kalumbu Malekani 161

Fractal and the statistical analysis of spatial distributions of Fe--Mn concretions in soddy-podsolic soils
Yu.N. Blagoveschensky, V.P. Samsonova 175

Fractal concepts in studies of soil fauna
Christian Kampichler 193

Fractal analysis in studies of mycelium in soil
Lynne Boddy, John M. Wells, Claire Culshaw, Damian P. Donnelly 211

The distribution of anoxic volume in a fractal model of soil
Cornelis Rappoldt, John W. Crawford 239

Fractal analysis of spatial and temporal variability
Bahman Eghball, Gary W. Hergert, Gary W. Lesoing, Richard B. Ferguson 259

Bibliography on applications of fractals in soil science
Ya. A. Pachepsky, D. Giménez, J. W. Crawford, and W. J. Rawls 273

This Page Intentionally Left Blank

*Fractals in Soil Science*
Editors: Ya.A. Pachepsky, J.W. Crawford and W.J. Rawls
© 2000 Elsevier Science B.V. All rights reserved.


Editorial

# Integrating processes in soils using fractal models

## Modeling heterogeneity using fractals

Soil structure affects and relates physical, chemical and biological processes in soil. Progress in quantifying the relationship is hampered by the complexity of soil structure and the intrinsic opacity of soil which makes it difficult to introduce directly measurable parameters of soil structure. To avoid this difficulty, simplifying assumptions are made that often involve the introduction of characteristic scales. For example, the representative elementary volume (REV) concept assumes that a single spatial scale exists below which the effects of heterogeneity on the process concerned can be averaged out. Another example is the macropore–micropore concept where it is assumed that transport processes occur over two distinct time scales: a time scale associated with fast macropore transport; and a time scale associated with slow micropore transport. Unfortunately working with characteristic scales in mind often leads to a quandary. First, there is no evidence for sharp boundaries between characteristic scales in soil. Second, and perhaps more importantly, characteristic scales are usually defined with reference to a particular process in soil. Therefore they are not useful in integrating processes of a different nature occurring at different scales or across different ranges in scale. This seems to be an obstacle impeding both the understanding of the interaction between processes, and the progress in multidisciplinary studies in soil science. Integrating knowledge on soil processes and gathering new knowledge in coherent manner become exigent as greater constraints are imposed on agricultural inputs to the soil, and global population growth and the potential effects of climatic change place increased pressure on agricultural and natural resources.

Fractals were found to provide an appropriate mathematical tool to address the issues of structure and scale in soil science. Fractal geometry was developed to describe the hierarchy of ever-finer detail in the real world. Natural objects often have similar features at different scales. Measures of these features, e.g., total number, total length, total mass, average roughness, total surface area, abundance, etc. are dependent on the scale on which the features are observed.

Reprinted from Geoderma 88 (1999)
© 1999 Elsevier Science B.V. All rights reserved

Fractal models assume that this dependence is the same across the range of scale, i.e., scale invariant within this range. Fractal models contain parameters which relate features at one scale to those at all others and as such they present an appealing methodology for linking processes across scales. They provide a framework within which multidisciplinary studies of soil can be conducted and the complex relation between different soil processes can be understood. However, use of fractal models is far from being straightforward. There exist many subtleties in the application and interpretation of the techniques.

This special issue of *Geoderma* has been conceived to demonstrate both the challenges and opportunities presented by fractals for modelling processes in soils. The objectives of assembling the publication were three-fold: (1) to introduce and critically discuss the methods for identifying fractal structure and for measuring fractal dimension; (2) to demonstrate the wide-ranging applicability of the fractal techniques in soil physics, biology and chemistry; and (3) to indicate the potential for a common framework within which the interaction of many complex soil processes can be addressed.

This publication provides an account of the state of the art in applying fractals to modelling processes in soil science after ten years since the start of intensive application.

## Methodologies

Much confusion in the soil science literature has arisen because of the literal translation of the properties of mathematical fractal to soil. While it is true that soil is not made up of spheres and straight lines, it is also true that soil is not precisely fractal. Rather, it is hoped that fractal models may lead to a more accurate description of soil in process models than methods of classic geometry. Given this stance, the choice of the most appropriate fractal model, and the measurement or estimation of the corresponding parameters is central to the successful application of the theory to soil processes.

There are two possible ways of measuring structure and the challenges presented by each of these is discussed in the chapters by Ogawa et al., Perrier et al., Perfect, Gomendy et al., Taguas et al. and Blagoveschensky and Samsonova. The first and most straightforward way is to image the structure and measure the structural units directly. This approach is discussed by Ogawa et al. and it is clear that both the measurement and interpretation of the resulting parameters can be as much dependent on image resolution and image processing as on the assumed model for the fractal distribution.

The second way of quantifying structure is based on an indirect evaluation of structural parameters from data on some soil process which is dependent on the underlying structure. Here two methodological approaches are possible. First, one can begin with a particular model for the structure and, using the process

model, obtain the values for the parameters that lead to the closest agreement between theory and observation. This approach is illustrated in the papers by Perfect and Gomendy et al. Alternatively, one can compare a range of different models for the structure and choose those which are most consistent with the observed properties. This approach is illustrated in the papers by Taguas et al. and Blagoveschensky and Samsonova. The results in the latter papers show that no single model need be clearly appropriate and the final decision can be a matter of choice among several models which each provide statistically acceptable fits to the data. Perrier et al. present a general model for a random porous structure which includes most of the existing fractal models as a subset, but also includes non-fractal models.

As with all indirect measurements, the parameter estimates are only as good as the model relating the underlying process to the structure. A comparison between direct (i.e., image analysis) and indirect (water retention and mercury porosimetry) measures of soil structure in the paper by Gomendy et al. shows that each method gives rise to different estimates for the fractal parameters. It is suggested by these authors that the discrepancy between the direct and indirect methods is due to an incomplete model of the processes (water retention and mercury porosimetry) from which the fractal parameters are derived.

## Applications

The significance of the theoretical developments will only emerge when they have been validated in application and demonstrated to yield new insight. Therefore, the emphasis in the major part of this publication is the construction and application of models of soil processes which are based on fractals. The utility of fractals in integrating processes in soil is demonstrated by the broad range of application to chemical, physical and biological processes. The papers by Eghball et al. and Boddy et al. show how models based on fractals can discriminate between effects on the state of a system due to variation in external factors and form the basis of hypotheses testing. The opportunity to relate parameters derived at different scales as a means of scaling soil processes is demonstrated in the papers by Giménez et al. and Rappoldt and Crawford. Links between soil physical, chemical and biological processes occurring at the same scale are derived using fractal models in the papers by Kampichler, Rappoldt and Crawford, and Blagoveschensky and Samsonova.

The matching of scales of the model to the particular application is crucial and this is covered in some detail by Gomendy et al. This is particularly important, since any observed fractal scaling cannot extend indefinitely. Extrapolation beyond the scale of observation is always fraught with uncertainty. Since many of the parameters derived in applications of fractal models appear as exponents in process models, any errors in their estimation can result in substantial quantitative, as well as qualitative, error in the predictions.

## Opportunities

One of the most important opportunities provided by the application of fractals to soil science, is the scope for integrating processes within or across scales. In the papers by Rice et al., Sokołowska and Sokołowski, and Blagoveschensky and Samsonova, however, it is clear that integrative approaches have their own special challenges. In the work of these papers, the underlying behaviour is controlled by both the distribution of reactive sites and the heterogeneity of the soil structure. Discriminating between the contribution of each to the integrated behaviour presents special challenges and it is clear that a combination of measurements together with modelling is required.

We recognise that not all important developments are reflected in this publication. There is no report on the application of fractals to the interaction between soil structure and roots. There have been noticeable attempts to describe root systems using fractals (van Noordwijk and Purnomosidhi, Agroforestry Systems 30 (1995) 161–173; Akasaka et al., Annals of Botany 81 (1998) 355–362; Isumi et al., Japanese Journal of Soil Science 66 (1997) 418–426). There is clear scope for using fractals to integrate soil and root processes to understand the interaction between soil structure, root architecture and competition for resources, as well as plant/soil pathogen interactions. Another example of an area not covered in the book is the application of fractals to soil surface topography, roughness and erosion (Huang and Bradford, Soil Sci. Soc. Am. J. 56 (1992) 14–21; Pardini, and Gallart, Eur. J. Soil. Sci. 49 (1998) 197–202).

Most applications of fractals to soil processes deal with steady state conditions or with a snapshot of the dynamic soil system. However, steady-state hypothesis is almost never applicable in the environmental problems, and it is under such non-steady conditions that fractal behaviour in natural structures is most pronounced. For example, for hydraulic conductivity and hydraulic diffusivity fields modelled as fractals between upper and lower bounds in spatial scale, non-Fickian dispersion terms reflecting the fractal behaviour appear during early times following infiltration (Grindrod and Impey, Water Resour. Res. 29 (1993) 4077–4089; Pachepsky and Timlin, J. Hydrol. 204 (1998) 98–107). Over longer times, and under constant infiltration, the dispersion follows classical Fickian behaviour. Therefore there is a need for more research into the role of fractal structure in non-steady dynamical processes in soils.

Structure formation is yet another topic that is not covered in this publication and is important at least for two reasons. The first is that almost all applications of fractals to soil rely on a parameterisation of the fractal properties that is a snapshot in time. An understanding of structural genesis is required to include the time dimension. Second, as was pointed out by Avnir et al. (Science 279 (1998) 39–40) there are many ways in which non-fractal distributions can appear fractal when measured. It is therefore often difficult to be confident that

the distributions are fractal and the strongest support comes from models of the processes which generate the observed structures. Some work on 2-D aggregation processes (Crawford et al., Eur. J. Soil Sci. 48 (1998) 643–650) indicate that rather general models for soil aggregation can yield fractal structures. However, there is substantial scope for combining theoretical and experimental studies of both aggregation and soil cracking to advance in understanding how soil structure evolves.

An outstanding feature of the works presented in this publication is the variety of techniques used to measure the parameters of the fractal distributions, and in particular the fractal dimension. It should be stressed that the definition of the fractal dimension, i.e., the property of the spatial structures, that is actually being measured by each technique, can, and indeed usually will, be different. There is thus ambiguity in the use of notation, and often the letter 'D' refers to quite different structural properties. This is of particular significance when the measured fractal parameters are used in some process model where a mismatch between different definitions will lead to error. A standardisation of notation may be appropriate although it is likely to be cumbersome in light of the variety of measurement techniques. Perhaps it is more important that the requirement be made that a clear account of the fractal model that the measurement is based on is provided. In particular, it is most important to be precise about how the measurements taken are interpreted in terms of such a model. This detail should remove all ambiguity, and make it clear that both the author and the reader understand the measurements and their application.

Finally, we stress that fractals should not be considered as an ultimate model of heterogeneity in the soil system. Rather they provide a balance between accuracy and clarity that may aid us in gaining insight into sources and results of the observed soil complexity. Fractals may become an especially useful tool for summarising increasingly large data sets obtained from remote sensing, image analysis, etc. However, once a greater insight into key processes is obtained, we would expect that the processes causing apparent fractal scaling will be revealed and quantified.

We thank all participants for their cooperation and contribution. Our thanks and appreciation are due to reviewers for their valuable help and comments.

J.W. CRAWFORD
Ya.A. PACHEPSKY
W.J. RAWLS

This Page Intentionally Left Blank

*Fractals in Soil Science*
Editors: Ya.A. Pachepsky, J.W. Crawford and W.J. Rawls
© 2000 Elsevier Science B.V. All rights reserved.


# Conventional and fractal geometry in soil science

Yakov A. Pachepsky[a], Daniel Giménez[b],
John W. Crawford[c], Walter J. Rawls[a]

[a] *USDA-ARS, Hydrology Laboratory, Beltsville, MD 20705, USA*
[b] *Department of Environmental Sciences, Rutgers, The State University of New Jersey, New Brunswick, NJ 08901, USA*
[c] *Scottish Crop Research Institute, Soil–Plant Dynamics Unit, Invergowrie, Dundee DD2 5DA, UK*

---

Geometric properties of soil elementary particles, aggregates, peds, pores, exposed soil surfaces, contours, etc., are of utmost importance for understanding and managing soils. Lengths, areas, volumes, mutual positions in space, counts per range of sizes, etc., are values to operate for anyone who studies or uses soils.

Both direct and indirect measurements of geometric quantities are in use in soil studies. Indirect, or proxy, geometrical measurements are very common. Non-geometrical values are converted into a geometrical value using a physical model thought to be approximately valid in soils. For example, to obtain particle size distribution, time of the transport of particles of a particular size is estimated from the Stokes model of viscous flow, and then the time is converted to diameters. To obtain pore size distribution, pore radii are computed using capillary models, and pressures are converted to radii. To estimate surface area, the model of ideal monolayer is used so that masses of adsorbed molecules are converted to area values. This list can be expanded easily.

Ideal geometrical objects, such as spheres, circles, and segments, are widely used as models in indirect and direct measurements in soil science. Soil particles are assumed to be spheres when the Stokes model is applied. Pores are presumed to be cylinders to compute radii of pores from capillary pressure values. Molecules are thought to be spheres in calculations of the surface area from the monomolecular coverage. Soil aggregates are viewed as spheres when their diameters are measured by the sieve analysis. Using ideal geometrical models is an approximation that introduces uncontrollable errors in the measurements.

Fractal geometry appeared not more than 30 years ago and gained enormous attention and popularity in science. Fractal geometry assumes that its objects have similar features at different resolutions. Because of the similarity, measures of these features such as total length, total number, average roughness, total surface area, etc., have dependencies on resolution that remain the same across the range of resolutions, i.e., are scale invariant within this range. For that reason, fractal geometry can relate features at one scale to those at all others within the resolution range. For a wide class of geometrical fractals, the dependencies of their geometric measures on resolution have the form of a power law $M \propto R^d$, where $M$ is the measure of features under study, and $R$ is the resolution. Such power dependencies are often called fractal scaling laws. The exponent $d$ reflects the irregularity of the features in terms of their ability to fill the space as the resolution decreases.

Power-law dependencies, such as those defining fractal scaling, have been known in soil science since James (1936) showed the applicability of the power law to the dependency of total particle mass on the minimum size of particles. Therefore, when fractal geometry came into existence, soil scientists in many countries saw in it a tool to explain and parameterize the accumulated body of knowledge about dependencies of soil parameters on scale. Pioneering works of Burrough (1983), Armstrong (1986), Culing (1986), Ahl and Niemeyer (1989), Tyler and Wheatcraft (1989), and Sokolowska (1989) showed opportunities for a broad spectrum of applications of fractal geometry in soil science. Rieu and Sposito (1991) developed the first mathematical fractal especially designed to simulate specific soil features.

The application of fractal models in soil science is a new developing field as demonstrated by the exponential growth in the number of publications (Figs. 1a, 1b). Table 1 shows a list of soil properties that have been shown to follow the fractal scaling. Several topical reviews and collections of papers were published recently (Perfect and Kay, 1995; Senesi, 1996; Giménez et al., 1997; Baveye et al., 1998; Anderson et al., 1998). Several books have appeared that describe applications of fractal geometry in disciplines closely interacting with soil science (Birdi, 1993; Christopher and La Pointe, 1995; Harrison, 1995; Hastings and Sugihara; 1993; Jullien and Botet, 1987; Korvin, 1992; Kruhl, 1995; Lam and de Cola, 1993; Liebovitch, 1998; Turcotte, 1997), in addition to several excellent monographs on fractal geometry (Mandelbrot, 1982; Feder, 1988, Kaye, 1994; Russ, 1994; Falconer, 1997; Meakin, 1998).

Two main reasons triggered interest in fractal geometry among soil scientists. First, fractal geometry was developed to describe irregular natural shapes having hierarchies of ever-finer detail. The founder of fractal geometry, Benoit Mandelbrot, asserted that "clouds are not spheres, mountains are not cones, coastlines are not circles, and bark is not smooth, nor does lightning travel in a straight line ..." (Mandelbrot, 1982). Shapes observed in soils are irregular, and us-

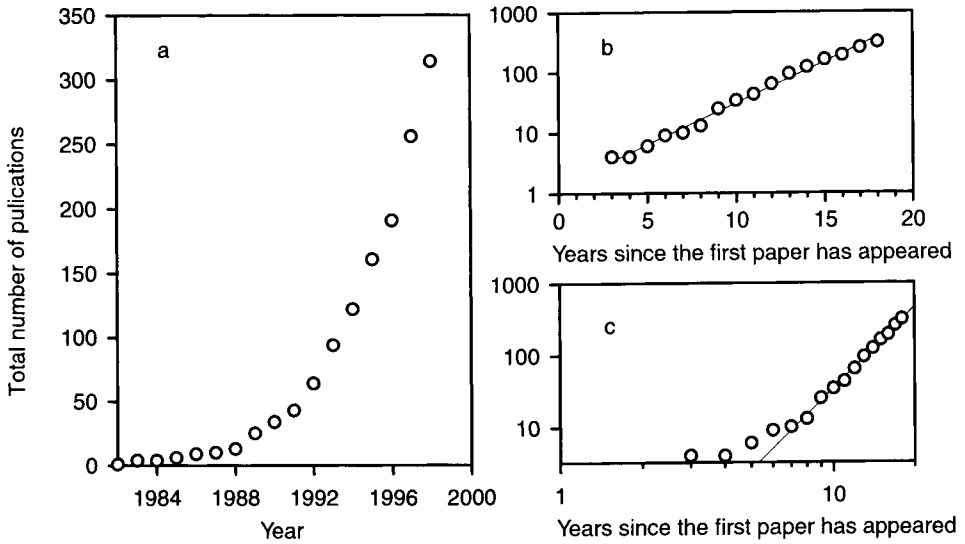


Fig. 1. Growth of the total number of publications on application of fractal models in soil studies: (a) dependence with linear scales on coordinates; (b) semi-logarithmic graph, linear time axis; (c) logarithmic scale, both axes logarithmic.

ing regular shapes like cylinders, circles, spheres, and segments to measure and simulate soil properties has always left a researcher dissatisfied to some extent. Therefore, geometrical techniques capable of dealing with irregularities at various scales are attractive. Second, fractal geometry was developed to relate features of natural objects observed at different scales. Soils are studied at spatial scales from nanometers to megameters, and relating soil properties observed at different scales remains a challenging problem in soil science from the moment it had been born as a science.

Applications of fractal geometry in soil science showed that fractal techniques provided a viable methodology to link processes and properties across scales. At the same time, it became clear that the use of fractal models was far from being straightforward. Subtleties in the application and interpretation of the techniques were caused, in particular, by the complexity of the scale concept in soil science, by the wide use of indirect measurements, by the uncertainty in processes underlying fractal scaling, and by the absence of ideal fractals in soils.

The concept of scale in soil science is more complex than the one usually used in fractal geometry. Fractal geometry defines scale by the resolution of measurements. Scale in soil studies can be defined by the resolution, or support, size, and by the extent, or size of the soil volume to be studied (Hoosbeek and Bryant, 1992). As the support size increases, direct measurement at this resolution becomes impossible. For example, measuring water content in a particular horizon for a soil pedon is impractical. Then the measurements are actually taken

Table 1
Applications of fractal geometry in soil studies

| Fractal scaling observed in soil properties and parameters | | Modeling soil properties and processes using fractal geometry | |
|---|---|---|---|
| Direct measurements | Indirect measurements[a] | Soil properties | Processes in soils |
| Aggregate bulk density. | Particle size distributions. | Hydraulic properties: | Fragmentation. |
| Number-size distributions for pores, aggregates, macropores, and cracks. | Surfaces of clay minerals. | water retention, saturated and unsaturated hydraulic conductivity. | Aggregation. |
| Pore surface area. | Surface and mass of humic substances. | Mechanical properties: | Preferential flow. |
| Water flow patterns. | Volume of solid particles from water retention data. | strain–stress relationships, strength, cohesion, aggregate strength. | Solute transport. |
| Architecture of plant roots. | Pore surface area. | Erodibility. | Water transport. |
| Mycelium patterns. | Pore connectivity. | Spatial variability of soil properties and crop yields. | Microbial transport. |
| Soil fauna pathways. | Pathways of solute particles. | Soil–landscape–vegetation relations. | Gas transport. |
| Distribution of the biomass of soil fauna. | | | Dissolution of soil minerals. |
| Soil surface roughness. | | | Adsorption. |
| | | | Movement of soil organisms. |
| | | | Root growth. |

[a] Indirect geometrical measurements employ a physical model to convert non-geometrical values, i.e. time, pressure, mass, light intensity, etc., into a geometrical values, i.e. length, area, volume.

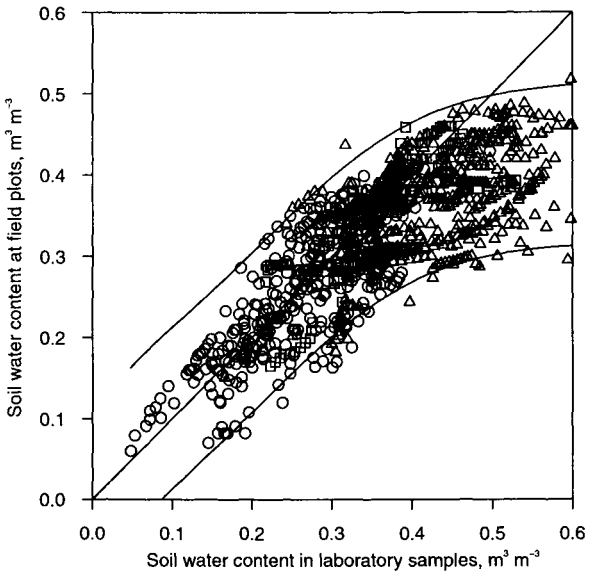


Fig. 2. Volumetric water contents at 5-cm laboratory and 2-5 m plot resolutions at the same soil matric potentials measured in drainage experiments. Data for 130 soil horizons from the UNSODA database (Leij et al., 1996). Symbols: circles, sand content greater than 80%; squares, sand content between 50% and 80%; triangles, sand content less than 50%. Lines show 95% prediction interval of the polynomial regression.

at some finer resolutions corresponding to volume averaged by a neutron probe, core sampler, TDR probe, etc. Results of these measurements are averaged to characterize a soil over the extent size. Whether this averaging is actually satisfactory for the extent-size-resolution characterization and how to average the measurement data often remain open questions. Figure 2 presents one example of scale effects induced by the change in the support size without change in the extent size resolution. The figure shows the comparison of averaged laboratory water retention data obtained at 5-cm resolution and the water retention data obtained in the field with several different resolutions and averaged over plots of 2 to 5 m sizes. As the soil texture becomes heavier and water contents become larger, average volumetric water contents over plots are smaller than average volumetric water contents over small core samples at the same soil water potential. For such type of measurements, Western and Blöschl (1999) noted recently that the spacing, i. e. distance between sampling locations, significantly affects results and conclusions of soil moisture studies. These authors suggested that a triplet 'support–spacing–extent' should be used to characterize the scale in soil studies.

It should be noted that introducing distinct characteristic scales has important methodological advantages since variables characterizing an ecological system vary with scale (Hoosbeek and Bryant, 1992; Bouma and Hoosbeek, 1996; Farina, 1998). Research at different scales brings different types of information about the ecological systems and its components (Bouma and Hoosbeek, 1996).

Also, studies at different scales differ in the potential for experimental manipulation, number of important factors or variables and types of variables, range of soil/landscape variables, and importance of temporal scale (Meentemeyer and Box, 1988). Nevertheless, working with characteristic scales in mind may lead to a quandary. Firstly, there is no evidence for sharp boundaries between characteristic scales in soil. Secondly, and perhaps more important, characteristic scales are usually defined with reference to a particular process in soil. Therefore, they may be not useful in integrating processes of a different nature occurring at different scales or across different ranges of scales. This seems to be an obstacle impeding both understanding the interaction between processes, and progress in multidisciplinary studies in soil science. A prospective of bridging between scales and resolutions became more attainable as the fractal models were researched and applied in soil science.

While it is true that soil is not made up of spheres and straight lines, it is also true that soil is far from being precisely fractal. Rather it is hoped that fractal models may lead to a more accurate description of soil in process models than methods of classic geometry. However, relationships of fractal geometry can be only approximately true in soils. This sometimes creates uncertainties in applications of fractal geometrical models. One example of such uncertainty comes from using cumulative values that are obtained from measurements giving amounts within ranges of size rather than continuous distributions of the measured value. For example, particle size distributions are reported as percentages within adjacent ranges of diameters. Scaling of particle sizes within these narrow diameter ranges may deviate from the scaling over all ranges simply because soil is never an ideal fractal. Different assumptions about the within-range distributions may give significantly different results in fractal model applications (Kozak et al., 1997). Indirect measurements as a source of data may be an impediment in the application of fractal models since all physical models used for conversions and assumptions about the pore and particle shapes inevitably are approximations for the heterogeneous soil materials and structures. Therefore, results of the proxy measurements can deviate from actual geometric values that they are deemed to represent.

Several mathematical fractal models can be applied to soil and result in the power law relating particular soil parameter to the resolution. This opens a Pandora's box of questions about criteria of applicability of fractal models and acceptable accuracy of these models. Answers to these questions cannot actually prove the validity of a fractal model. They can only show that the difference between predictions of a fractal model and experimental data are not significant in statistical sense. There are statistical techniques well suited for that (Dowdy and Wearden, 1985). However, this may not be easy if the span of resolutions is not large. The example in Fig. 1c shows that a power law fits the data on the number of publications on the time better than the exponential law in Fig. 1b in the range

of years 1988–1998. Yet, there is no model to explain this power law dependence whereas the exponential growth of publications in the new scientific field is a known and a researched phenomenon (Price, 1956). As was pointed out by Avnir et al. (1998), there are many ways in which nonfractal distributions can appear fractal when measured. It is obvious that, without a physical concept behind, an application of fractal models may be just an exercise in fitting.

This book has been conceived to demonstrate both the challenges and opportunities presented by fractals for modeling processes in soils, and to provide a state-of-the-art account on applying fractals to modeling processes in soil science ten years since the start of intensive application. The objectives of assembling the book were threefold: (a) to introduce and critically discuss the methods for identifying fractal structure and for measuring fractal dimensions; (b) to demonstrate the wide-ranging applicability of the fractal techniques in soil physics, biology and chemistry; and (c) to indicate the potential for a common framework within which the interaction of many complex soil processes can be addressed.

Two main directions in search for and construction of mathematical fractals that are suited to mimic soil structure are represented in this book in the chapters written by Perrier et al. and Taguas et al. The former chapter presents a general model for a random porous structure. The model includes most of the existing fractal models as a subset, but also includes nonfractal models. Analytical results in form of closed-form equations make this model directly suitable for testing with experimental data on soil structures. A different way to observe and study fractals is to construct them numerically using iterative algorithms. The chapter by Taguas et al. shows how to construct a fractal that has properties similar to properties of soil texture. Although direct fitting of this model to data is not possible, the iterative algorithm of the construction sheds light on the mechanism underlying the distributions of soil textural particles.

Fundamental challenges encountered in measurements to apply fractal models in soil are (a) using indirect, or proxy measurements, and (b) applying measurements based on conventional geometry to objects that are presumably fractal. The seemingly straightforward way to quantify soil structure is to image the structure and measure the structural units directly. This approach is discussed by Ogawa et al., and it is clear that both the measurement and interpretation of the resulting parameters can be as much dependent on image resolution and image processing as on the assumed model for the fractal distribution. A comparison between direct (i.e., image analysis) and indirect (water retention and mercury porosimetry) measures of soil structure in the chapter by Gomendy et al. shows that each method gives rise to different estimates for the parameters of the same fractal model. These authors suggest that the discrepancy between the direct and indirect methods is due to an imperfect model used to convert proxy measurements in soil structure characteristics.

If a particular mathematical fractal model is chosen to represent soil heterogeneity, then fitting it to data produces values of the parameters of heterogeneity that can be interpreted within the framework of this model. This approach is illustrated in the chapters written by Perfect and Gomendy et al. Alternatively, one can compare a range of different fractal models and choose the one which is most consistent with the observed properties. Such approach is presented in chapters by Taguas et al. and Blagoveschensky and Samsonova. The results in the latter chapter show that no single model need be clearly appropriate, and the final decision can be a matter of choice among several models all of which provide statistically acceptable fits to the data. Then criteria to choose the model come outside of geometrical construings.

Matching scales of the model and of the particular application is crucial, and this is covered in some detail by Gomendy et al. This is particularly important since any observed fractal scaling cannot extend indefinitely. Such scaling always exists only in a range of resolutions. Extrapolation beyond the scale of observation is always fraught with uncertainty. Since many of parameters derived in applications of fractal models appear as exponents in process models, any errors in their estimation can result in a substantial quantitative, as well as qualitative, error in the predictions. Sokołowska and Sokołowski present an example of using a statistical technique to define the resolution range where the fractal scaling holds.

The significance of the theoretical developments will only emerge when they have been validated in application and demonstrated to yield new insight. Therefore, the emphasis in the major part of this book is on the application of fractal models. The utility of fractals in integrating processes in soil is demonstrated by the broad range of application to chemical, physical, and biological processes. The chapters by Eghball et al. and Boddy et al. show how models based on fractals can discriminate between effects on the state of a system due to variation in external factors and form the basis of hypotheses testing. The opportunity to relate parameters derived at different scales as a means of scaling soil processes is demonstrated in the chapters by Giménez et al., Rice et al., Sokołowska and Sokołowski, and Rappoldt and Crawford. Links between soil physical, chemical, and biological processes occurring at the same scale are derived using fractal models in the chapters by Kampichler and Rappoldt and Crawford.

It needs to be conceded that only selected applications of fractal geometry in soil science are reflected in chapters of this book. For example, no report is given on the application of fractals to the interaction between soil structure and roots. There have been noticeable attempts to describe root systems using fractals. There is clear scope for using fractals to integrate soil and root processes to understand the interaction between soil structure, root architecture, and competition for resources, as well as plant/soil pathogen interactions. Another example of an area not covered in the book is the application of fractals to soil surface topography,

roughness, and erosion. Structure formation and aggregation is yet another topic that is not covered in this book. There is substantial scope for combining theoretical and experimental studies of both aggregation and soil cracking to advance in understanding how soil structure evolves. The reader is referred to the bibliography section of the book where examples of these and other applications can be found. The bibliography comprises publications in peer review journals. Recent conference papers reflect the vitality of fractal models in soil science as they demonstrate a variety of new fractal geometry applications in studies of soil penetrability, reflectance, electrical and thermodynamic properties, diffusion, etc.

An outstanding feature of the works presented in this book is the variety of techniques used to measure the parameters of the fractal distributions, and, in particular, the fractal dimension. It should be stressed that the definition of the fractal dimension, i.e., the property of the spatial structures that is actually being measured by each technique, can, and indeed usually will, be different. It remains model- and measurement-dependent. Thus there is an ambiguity in the use of notation, and often the letter '$D$' refers to quite different soil properties. This is of particular significance when the measured fractal parameters are used in some process model where a mismatch between different definitions will lead to error. A standardization of notation may be appropriate although it is likely to be cumbersome in light of the variety of measurement techniques. Perhaps it is more important that the requirement be made that a clear account of the fractal model that the measurement is based on is provided. It is also most important to be precise about how the measurements taken are interpreted in terms of such a model. This will remove all ambiguity about the measurements and their application.

What is next in applications of fractal geometry to soils? Presently, applications of fractals to soil processes mostly deal with steady-state conditions or with a snapshot of the dynamic soil system. However, the steady-state hypothesis is almost never applicable in environmental problems, and it is under such non-stationary conditions that fractal behavior in natural systems is most pronounced. Solute transport in soils seems to be a likely field for applications of fractal geometry to non-stationary phenomena. The first attempt to interpret solute transport using fractal model to describe pathways of solute particles yielded promising results (Flury and Flühler, 1995). In particular, dependencies of solute transport parameters on scale were successfully generated in a fractal framework.

Applications of more complex fractal models should be expected. Multifractal models and models based on continuous-time random walks and Lévy statistics seem to be most likely candidates. More efforts are anticipated in development of mathematical fractals that mimic scale dependencies of specific soil features. Data-intensive sensor technologies, such as remote sensing imagery, time domain reflectometry, laser altimetry, etc., gradually penetrate in soil studies. It becomes challenging to compress these observations into small number of parameters for comparison and classification purposes. Fractals have successfully been used for

data compression (Turner et al., 1998), and the techniques may be borrowed and developed to be applied to soil data.

Successful applications of fractal models in relating properties at different spatial scales hint at possible applications of such models to relate different temporal scales. Cycles of various durations are enclosed in each other in biological turnover occurring in soils and ecosystems. Similarities in these cycles can be explored at different time resolutions. Applications of such temporal scaling laws would become valuable in research of the global changes in atmospheric carbon content and carbon sequestration in soils. It was found in several research fields that fractal features arise as a result of the underlying chaos, and this has important implications in scales of predictability of systems (Addison, 1997). Growing interest in the predictability of soil behavior in changing environment may induce the search for chaos in soils to relate it to observed fractal scaling in soil properties.

Finally, we stress that fractals should never be considered as an ultimate model of heterogeneity in the soil system. Rather they provide a balance between accuracy and clarity that may aid us in gaining insight into sources and results of the observed soil complexity. Eventually, once a greater insight into key processes is obtained, we expect causes of the apparent fractal scaling to be revealed and quantified.

## References

Addison, P.S., 1997. Fractals and Chaos: an Illustrated Course. Inst. of Physics Pub., Bristol.

Ahl, C., Niemeyer, J., 1989. Fractal geometric objects in the soil. Mitt. Deutsch. Bodenk. Gesellschaft 59, 93–98.

Anderson, A.N., McBratney, A.B., Crawford, J.W., 1998. Applications of fractals to soil studies. Advances in Agronomy 63, 1–76.

Avnir, D., Biham, O., Lidar, D.A., Malcai, O., 1998. Is the Geometry of Nature Fractal? Science 279, 39–40.

Armstrong, A.C., 1986. On the fractal dimensions of some transient soil properties. Journal of Soil Science 37, 641–652.

Baveye, P., Parlange, J.-Y., Stewart, B.A., 1998. Fractals in Soil Science. CRC Press, Boca Raton.

Birdi, K.S., 1993. Fractals in Chemistry, Geochemistry, and Biophysics: An Introduction. Plenum Press, New York.

Blöschl, G., Sivapalan, M., 1995. Scale Issues in Hydrological Modelling: a Review. Hydrological processes 9, 251–292.

Bouma, J., Hoosbeek, M.R., 1996. The contribution and importance of soil scientists in interdisciplinary studies dealing with land. pp. 1–15. In: Wagenet, R.G., Bouma, J. (Eds.), The Role of Soil Science in Interdisciplinary Research. Soil Sci. Soc. Am. Publ. 45.

Burrough, P.A., 1983. Multiscale sources of spatial variation in soil. I. The application of fractal concepts to nested levels of soil variation. Journal of Soil Science 34, 577–597.

Christopher, C.B., La Pointe, P.R. (Eds.), 1995. Fractals in Petroleum Geology and Earth Processes. Plenum Press, New York.

Culling, W.E.H., 1986. Highly erratic spatial variability of soil-pH on Iping Common, West Sussex, CATENA 13, 81–98.

Dowdy, S., Wearden, S., 1985. Statistics for Research. John Wiley and sons, New York–Chichester.

Falconer, K.J., 1997. Techniques in Fractal Geometry. Wiley, Chichester–New York.

Farina, A., 1998. Principles and Methods in Landscape Ecology. Chapman & Hall. London–New York.

Feder, J., 1988. Fractals. Plenum Press, New York.

Flury, M., Flühler, H., 1995. Modeling solute leaching in soils by diffusion-limited aggregation: Basic concepts and application to conservative solutes. Water Resources Research 31, 2443–2452.

Giménez, D., Perfect, E., Rawls, W.J., Pachepsky, Y., 1997. Fractal models for predicting soil hydraulic properties: a review. Engineering Geology 48, 161–183.

Harrison, A., 1995. Fractals in Chemistry. Oxford University Press, New York.

Hastings, H.M., Sugihara, G., 1993. Fractals: a user's guide for the natural sciences. Oxford University Press, Oxford–New York.

Hoosbeek, M.R., Bryant, R.B., 1992. Towards the quantitative modeling of pedogenesis – a review. Geoderma 55, 183–210.

James, R.J., 1936. A simpler method of expressing the mechanical analysis of many common soils. Soil Science 32, 271–275.

Jullien, R., Botet, R., 1987. Aggregation and Fractal Aggregates. World Scientific, Singapore–Philadelphia.

Kaye, B.H., 1994. A random Walk Through Fractal Dimensions. VCH, Weinheim–New York.

Korvin, G., 1992. Fractal Models in the Earth Sciences. Elsevier, Amsterdam–New York.

Kozak, E., Pachepsky, Ya.A., Sokołowski, S., Sokołowska, Z., Stepniewski, W., 1996. A modified number-based method for estimating fragmentation fractal dimensions of soils. Soil Science Society of America Journal 60, 1291–1297.

Kruhl, J.H. (Ed.), 1995. Fractals and Dynamic Systems in Geoscience. Springer-Verlag, Berlin–New York.

Lam, N.S., de Cola, L. (Eds.), 1993. Fractals in Geography. Prentice Hall, Englewood Cliffs, N.J.

Leij, F., Alves, W.J., van Genuchten, M.Th., Williams, J.R., 1996. The UNSODA unsaturated soil hydraulic database. User's manual version 1.0. EPA/600/R-96/095. National Risk Management Laboratory, Office of Research and Development, Cincinnati, OH.

Levin, S.A., 1992. The problem of pattern and scale in ecology. Ecology 73, 1943–1967.

Liebovitch, L.S., 1998. Fractals and Chaos Simplified for the Life Sciences. Oxford University Press, New York.

Mandelbrot, B.B., 1982. The Fractal Geometry of Nature. W.H. Freeman, San Francisco.

Meakin, P., 1998. Fractals, Scaling and Growth far from Equilibrium. Cambridge University Press, Cambridge, U.K.–New York.

Meentemeyer, V., Box, E.O., 1987. Scale effects in landscape studies. In: Turner, M.G. (Ed.) Landscape heterogeneity and disturbance. Springer-Verlag, New York, pp. 15–34.

Perfect, E., Kay, B.D., 1995. Applications of fractals in soil and tillage research: a review. Soil and Tillage Research 36, 1–20.

Price, D.J., 1956. The exponential curve of science, Discovery 17, 240–243.

Rieu, M., Sposito, G., 1991. Fractal fragmentation, soil porosity, and soil water properties: I. Theory. Soil Science Society of America Journal 55, 1231–1238.

Russ, J.C., 1994. Fractal Surfaces. Plenum Press, New York.

Senesi, N., 1996. Fractals in general soil science and in soil biology and biochemistry. In: Stotzky, G., Bollag, J.-M. (Eds.), Soil Biochemistry Vol. 9, Marcel Dekker, New York. pp. 415–472.

Sokolowska, Z., 1989. On the role of energetic and geometric heterogeneity in sorption of water vapour by soils: Application of a fractal approach. Geoderma 45, 251–265.

Turcotte, D.L., 1997. Fractals and Chaos in Geology and Geophysics. Cambridge University Press, Cambridge, U.K.–New York.

Turner, M.J., Blackledge, J.M., Andrews, P.R., 1998. Fractal Geometry in Digital Imaging. Academic Press, San Diego, C.A.

Tyler, S.W., Wheatcraft, W., 1989. Application of fractal mathematics to soil water retention estimation. Soil Science Society of America Journal 53, 987–996.

Western, A.W., Blöschl, G., 1999. On the spatial scaling of soil moisture. J. Hydrol., 217, 203–224.

*Fractals in Soil Science*
Editors: Ya.A. Pachepsky, J.W. Crawford and W.J. Rawls
© 2000 Elsevier Science B.V. All rights reserved.


# Surface fractal characteristics of preferential flow patterns in field soils: evaluation and effect of image processing

Susumu Ogawa [a], Philippe Baveye [a,b,*], Charles W. Boast [b,1], Jean-Yves Parlange [a], Tammo Steenhuis [a]

[a] *Department of Agricultural and Biological Engineering, Riley-Robb Hall, Cornell University, Ithaca, NY 14853, USA*
[b] *Laboratory of Environmental Geophysics, Bradfield Hall, Cornell University, Ithaca, NY 14853, USA*

Received 5 December 1997; accepted 28 September 1998

**Abstract**

In the last few decades, preferential flow has become recognized as a process of great practical significance for the transport of water and contaminants in field soils. Dyes are frequently used to visualize preferential flow pathways, and fractal geometry is increasingly applied to the characterization of these pathways via image analysis, leading to the determination of 'mass' and 'surface' fractal dimensions. Recent work by the authors has shown the first of these dimensions to be strongly dependent on operator choices (related to image resolution, thresholding algorithm, and fractal dimension definition), and to tend asymptotically to 2.0 for decreasing pixel size. A similar analysis is carried out in the present article in the case of the surface fractal dimension of the same stained preferential flow pathway, observed in an orchard soil. The results indicate that when the box-counting, information, and correlation dimensions of the stain pattern are evaluated via non-linear regression, they vary anywhere between 1.31 and 1.64, depending on choices made at different stages in the evaluation. Among the parameters subject to choice, image resolution does not appear to exert a significant influence on dimension estimates. A similar lack of dependency on image resolution is found in the case of a textbook surface fractal, the quadratic von Koch island. These parallel observations suggest that the observed stain pattern exhibits characteristics similar to those of a surface fractal. The high statistical significance ($R > 0.99$) associated with

* Corresponding author. Department of Agricultural and Biological Engineering, Riley-Robb Hall, Cornell University, Ithaca, NY 14853, USA. E-mail: pcb2@cornell.edu

[1] Permanent address: Department of Natural Resources and Environmental Sciences, University of Illinois at Urbana-Champaign, 1102 South Goodwin Avenue, Urbana, IL 61801, USA.

Reprinted from Geoderma 88 (1999)
© 1999 Elsevier Science B.V. All rights reserved

each dimension estimate lends further credence to the fractality of the stain pattern. However, when proper attention is given to the fact that the theoretical definition of the surface 'fractal' dimension, in any one of its embodiments, involves the passage to a limit, the fractal character of the stain pattern appears more doubtful. Depending on the relative weight given to the available pieces of evidence, one may conclude that the stain pattern is or is not a surface fractal. However, this conundrum may or may not have practical significance. Indeed, whether or not the stain pattern is a surface fractal, the averaging method proposed in the present article to calculate surface dimensions yields relatively robust estimates, in the sense that they are independent of image resolution. These dimensions, even if they are not 'fractal', may eventually play an important role in future dynamical theories of preferential flow in field soils. © 1999 Elsevier Science B.V. All rights reserved.

*Keywords:* mass fractal dimensions; surface fractal dimensions; preferential flow patterns; field soils; quadratic von Koch island

## 1. Introduction

Preferential flow involves the transport of water and solutes via preferred pathways through a porous medium (Helling and Gish, 1991; Steenhuis et al., 1995). During preferential flow, local wetting fronts may propagate to considerable depths in a soil profile, essentially bypassing the matrix pore space (Beven, 1991). Although the term preferential flow does not imply any particular mechanism, it usually refers to one (or more) of three physically distinct processes: macropore flow, fingering (unstable flow), and funnelled flow.

Macropore flow involves transport through non-capillary cracks or channels within a profile, reflecting soil structure, root decay, or the presence of wormholes, and of ant or termite tunnels. A well-structured soil, for example, has at least two more or less interconnected flow regions for liquids applied at the surface: (1) through the cracks between blocks (interpedal transport), and (2) through the finer pore sequences inside the blocks (intrapedal, or matrix transport). Fingering occurs as a result of wetting front instability. Fingering may cause water and solutes to move in columnar structures through the vadose zone at velocities approaching the saturated hydraulic conductivity (Glass et al., 1988). Fingering may occur for a number of reasons, including changes in hydraulic conductivity with depth and compression of air ahead of the wetting front (Helling and Gish, 1991). Funnelled flow, finally, occurs when sloping geological layers cause pore water to move laterally, accumulating in a low region (Kung, 1990). If the underlying region is coarser-textured than the material above, finger flow may develop.

In a number of studies, the occurrence of preferential flow has been deduced indirectly from the inability of traditional transport equations (e.g., the Richards equation) to predict the outcome of breakthrough experiments in undisturbed soil columns, lysimeters or tile-drained field plots (e.g., Radulovich and Sollins, 1987; Radulovich et al., 1992; McCoy et al., 1994). Various experimental techniques have been used to gain insight into the processes that control

preferential flow and in particular to identify the soil characteristics (e.g., macropores, cracks, etc.) that cause it. Examples of such experimental techniques include X-ray computed tomography (Grevers et al., 1989; Peyton et al., 1994) or micromorphological analysis of soil thin sections (Grevers et al., 1989; Aguilar et al., 1990). Most of the studies on preferential flow, however, have relied on the use of dyes to visualize the preferential flow of water and solutes in soils, in laboratory experiments or under field conditions (e.g., Bouma and Dekker, 1978; Hatano et al., 1983; Ghodrati and Jury, 1990; Flury et al., 1994; Flury and Flühler, 1995; Natsch et al., 1996).

Color or black-and-white pictures of dye-stained soil profiles may be analyzed to provide the percentage of stained areas in vertical or horizontal cuts in the soil (e.g., Natsch et al., 1996). As useful as the information contained in these percentages may be to predict the extent and the kinetics of preferential flow in soils, one would undoubtedly want a more detailed description of the geometry of stained patterns and some way to relate this geometry to known morphological features of the soils. In this respect, the close similarity that is often apparent between these stained patterns and the very intricate details exhibited by fractals has encouraged a number of researchers to apply the concepts of fractal geometry to characterize preferential flow pathways. This approach was pioneered by Hatano et al. (1992) and Hatano and Booltink (1992). These authors found that the geometry of stained patterns in 2-D images of soil profiles may be characterized very accurately with two numbers; a 'surface' fractal dimension associated with the perimeter of the stained patterns and a 'mass' fractal dimension, relative to the area. The first fractal dimension varied little among, or with depth within, the five soils tested by Hatano et al. (1992). However, the mass fractal dimension varied appreciably both among soils and with depth for a given soil, with a total range extending from 0.59 to 2.0.

The wide range of values assumed by the 'mass fractal dimension' in the work of Hatano et al. (1992) suggests that this parameter may serve as a far better basis for comparison among soils than the virtually constant surface fractal dimension. Baveye et al. (1998) have shown, however, that estimates of the mass fractal dimensions of stained preferential flow patterns in field soils depend strongly on various subjective (operator-dependent) choices made in the estimation, in particular on the resolution (pixel size) of the pictures of the stained soil profiles. When picture resolution is taken into account, the dimensions of stain patterns converge to a value of 2.0 for pixel sizes tending to zero, indicating that the stain patterns are not mass fractals, and that apparent 'mass fractal' dimensions lower than 2.0 are artefactitious.

At present, no information is available concerning the effects that subjective, operator-dependent choices that must be made in the analysis of digitized images may have on the surface 'fractal' dimensions of preferential flow pathways in field soils. Furthermore, the theoretical framework necessary to

interpret the influence of some of these choices is lacking. In the following, (a) we attempt to provide such a conceptual framework, in part through a detailed analysis of the surface fractal characteristics of images of a textbook surface fractal, the quadratic von Koch island, (b) we assess in detail the practical consequences of several of the choices that are made in the evaluation of fractal dimensions of preferential flow pathways, using the same images of a dye-stained soil facies described by Baveye et al. (1998), and (c) we suggest a practical approach for making the estimation of surface fractal dimensions more robust.

## 2. Theory

### *2.1. The quadratic von Koch island*

The theoretical framework needed for the interpretation of the results reported in this article is probably best described on the basis of a 'textbook' surface fractal, the quadratic von Koch island. The iterative algorithm that generates this geometrical fractal is presented in detail in many publications (e.g., in the work of Baveye et al. (1998)), and is illustrated in Fig. 1. By definition, the quadratic

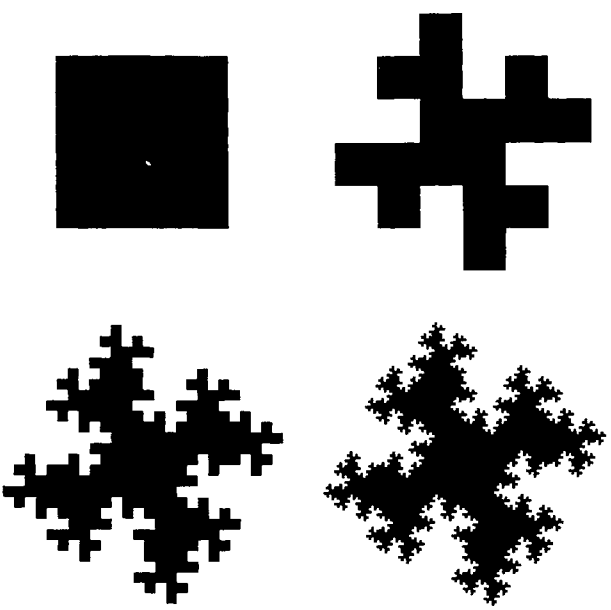

Fig. 1. Illustration of the first steps in the iterative construction of the quadratic von Koch island. The (square) initiator is in the upper left. A first application of the generator leads to the structure in the upper right. Steps two and three correspond to the structures at the bottom left and right, respectively.

von Koch island is obtained when the iterative algorithm in Fig. 1 is carried out ad infinitum. Geometrical structures obtained at finite steps in the iteration, like those illustrated in Fig. 1, are termed prefractals.

It is straightforward to show that the quadratic von Koch island has the same area as each one of its prefractals, including the starting square initiator. Also, the perimeter of the $i$ level prefractal is equal to $L_i = 4 \times 8^i \times (1/4)^i$, which diverges as $i \to \infty$. Therefore, it is clear that the perimeter, or coastline, of the quadratic von Koch island is infinitely long.

As a result of these features, the quadratic von Koch island is a surface fractal (we shall adhere to this terminology here, even though it is clear that 'perimeter fractal' would be more appropriate). The fractal character of the quadratic von Koch island may be quantified by calculating its similarity dimension, $D_s$. Since the generator of the island consists of eight line segments of length $r = 1/4$, $D_s$ is given by the ratio $-\ln 8/\ln(1/4) = 1.5$, which turns out to be identical to the Hausdorff dimension, $D_H$, of the island (e.g., Feder, 1988; Baveye and Boast, 1998). Both $D_s$ and $D_H$ are often used indiscriminately to denote the surface 'fractal dimension' of the island.

Another way to evaluate the surface 'fractal' dimension of the quadratic von Koch island involves so-called 'edge' squares. The $i$th prefractal of the island may be viewed as an assemblage of squares of side $\varepsilon_i = (1/4)^i$, with a fraction of squares touching or intersecting with the perimeter (Fig. 2). In selecting the squares that are at the edge, one may decide to include or not to include diagonal squares that touch the perimeter at only one point. This choice can sizably influence the slope of the line representing the number of squares vs. the square side length, in a log–log plot like that of Fig. 3a (where only the first 10 prefractals are considered). Indeed, under these conditions, the absolute value of the slope is higher when diagonal squares are counted (1.549) than when they are not (1.531). However, calculations show that the slope $\mathrm{d}\log_{10} N/\mathrm{d}\log_{10}(\varepsilon)$ in these two cases converges rapidly to a value of 1.5 as $\varepsilon$ is decreased, whether or not one includes diagonal squares (cf. Fig. 3b).

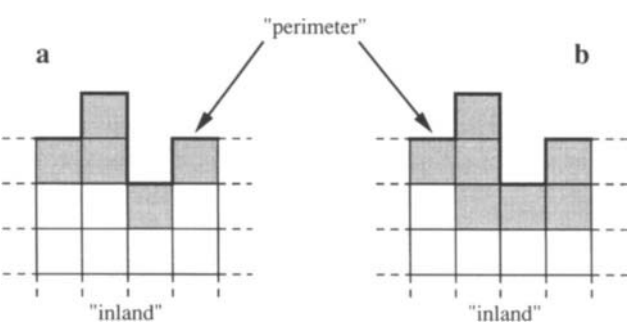


Fig. 2. Boundary of a prefractal of the quadratic von Koch island when one excludes (a) or

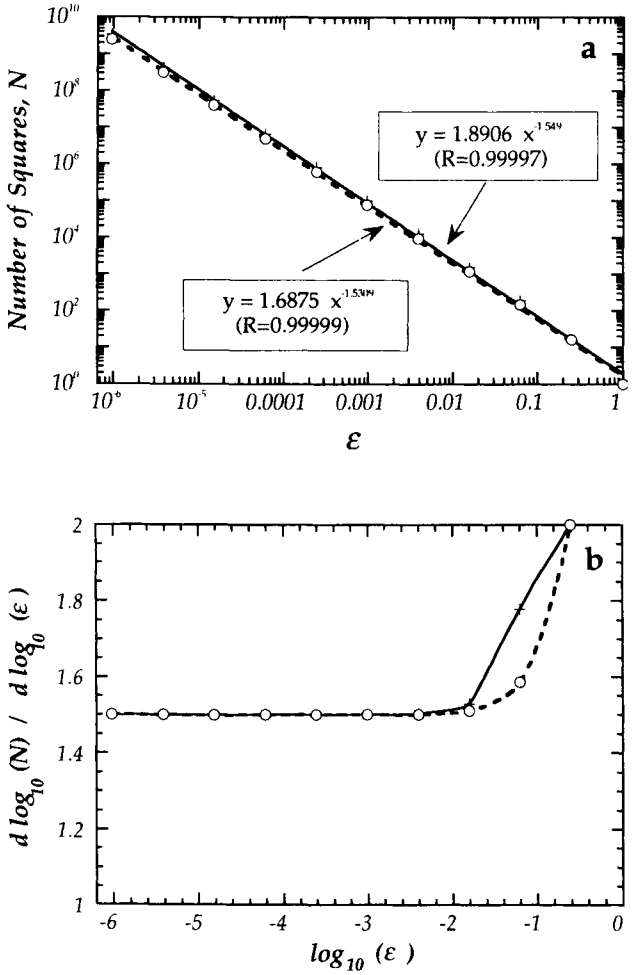


Fig. 3. (a) Logarithmic graph, vs. $\varepsilon$, of the number $N$ of 'inland' squares of side length $e$ associated with the perimeter of prefractals of the quadratic von Koch island when diagonal squares are included (crosses and solid line) or excluded (open circles and dashed line). The power–law equations in the boxes correspond to the straight lines obtained via non-linear regression. (b) Illustration of the asymptotic behavior of the slope $d\log_{10}(N)/d\log_{10}(\varepsilon)$ vs. $\varepsilon$. The meaning of the symbols is the same as in (a).

Another method to characterize the dimensionality of random or non-exactly-self-similar sets of points involves the so-called box-counting dimension (e.g., Falconer, 1992), commonly denoted by $D_{BC}$ and defined as

$$D_{BC} = \lim_{\varepsilon \to 0} \frac{\log_{10} N_\varepsilon(F)}{-\log_{10} \varepsilon} \tag{1}$$

for an arbitrary set $F \subseteq R^n$. In this definition, $N_\varepsilon(F)$ is the number of 'boxes' (i.e., squares, in the present situation) of size $\varepsilon$ needed to completely cover $F$.

The calculation of the number of squares of a given side length $\varepsilon$ needed to completely cover the quadratic von Koch island is greatly simplified if one takes as values of $\varepsilon$ the segment lengths of the island's prefractals, i.e., $\varepsilon = (1/4)^i$ for $i = 0, \ldots, \infty$, and if one uses a square grid, four of whose corners coincide with the four corners of the initiator. Such a coverage is illustrated in Fig. 4. When one includes 'diagonal' boxes (touching the edge at one and only one point) both inside and outside the island, one finds a value of $D_{BC}$ equal to 1.488 ($R = 1$). Removal of the diagonal boxes outside the island leads to $D_{BC} = 1.507$ ($R = 1$), whereas removal of all diagonal boxes yields $D_{BC} = 1.497$ ($R = 1$). These different values of $D_{BC}$ are obtained by starting with a box equal in size to the island's initiator and by halving the side length 10 times. Regardless of which diagonal boxes are included or excluded, the slope $\mathrm{d}\log_{10}(N)/\mathrm{d}\log_{10}(\varepsilon)$ of the $N(\varepsilon)$ relationship always converges rapidly to a value of 1.5 as $\varepsilon$ is decreased, a value that is identically equal to $D_S$ and $D_H$ (Fig. 5).

### 2.2. *Images, resolution and thresholding*

The discussion in Section 2.1 presumed that the evaluation of the 'fractal' dimension, using any particular definition, could be carried out on prefractals of a fractal or on the geometric fractal itself. This assumption is valid in the case of

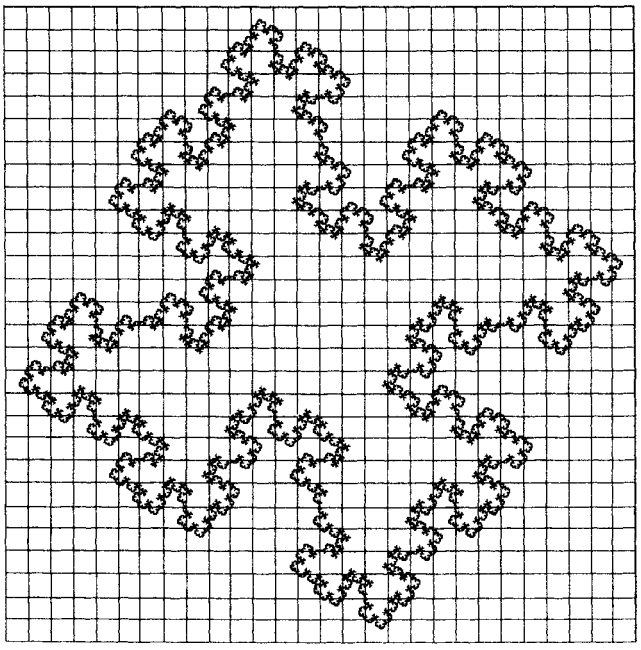

Fig. 4. Schematic illustration of the coverage of the edge of the quadratic von Koch island with boxes of size $\varepsilon$ equal to 1/16th the side length of the island's initiator. Boxes that are in contact with the island's perimeter at only one point, either inside or outside the island, are not included.

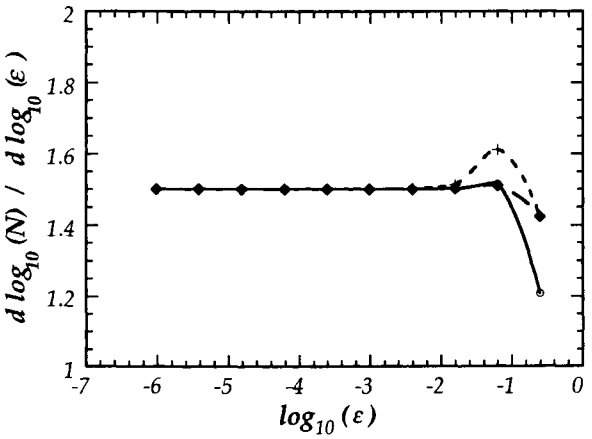


Fig. 5. Asymptotic behavior of the slope $d\log_{10}(N)/d\log_{10}(\varepsilon)$ vs. $\varepsilon$, where $N$ represents the number of boxes of relative side length $\varepsilon$ needed to cover the edge of the quadratic von Koch island. Open circles correspond to the case where diagonal boxes are counted both inside and outside. Crosses are for cases where diagonal boxes outside the island are not counted. Finally, full diamonds correspond to the situation of Fig. 4, where diagonal boxes are included neither inside nor outside the island.

mathematical fractals like the quadratic von Koch island, but is never met for real, or natural, fractals such as clouds, river networks or soil samples. These objects do not have 'prefractals' and, for physical reasons, it is impossible to obtain a representation of these systems with an infinite level of detail. Any attempt to depict them via, e.g., digitized photographs, radar traces, or tomographic 3-D reconstructions, unavoidably involves some coarse-graining of the features of the original systems.

Usually, at least one aspect of this coarse-graining process is analogous to the application of the box-counting method illustrated in Fig. 4 in that a regular square grid is superimposed on the system. In the application of the box-counting method to the perimeter of the quadratic von Koch island, for example, a given square is tallied if it intersects the perimeter of the island. In a digitized image of the island, contrastedly, a square grid defines the image pixels and the degree of overlap of each pixel with the island determines, via a proportionality rule, the grayscale level associated with the pixel. Grayscale levels customarily range from 0 to 255 (i.e., there are 256 grayscale values in total). In the following, it will be assumed that white and black correspond to grayscale values of 0 and 255, respectively.

A digitized image of the quadratic von Koch island with square pixels of size $\lambda = 1$, and, for convenience, positioned such that one pixel coincides with the initiator of the fractal, has three grayscale levels (Fig. 6a). The outer diagonal pixels touch the island at only one point, and therefore remain completely white (grayscale level = 0). In comparison, the four outer non-diagonal pixels overlap

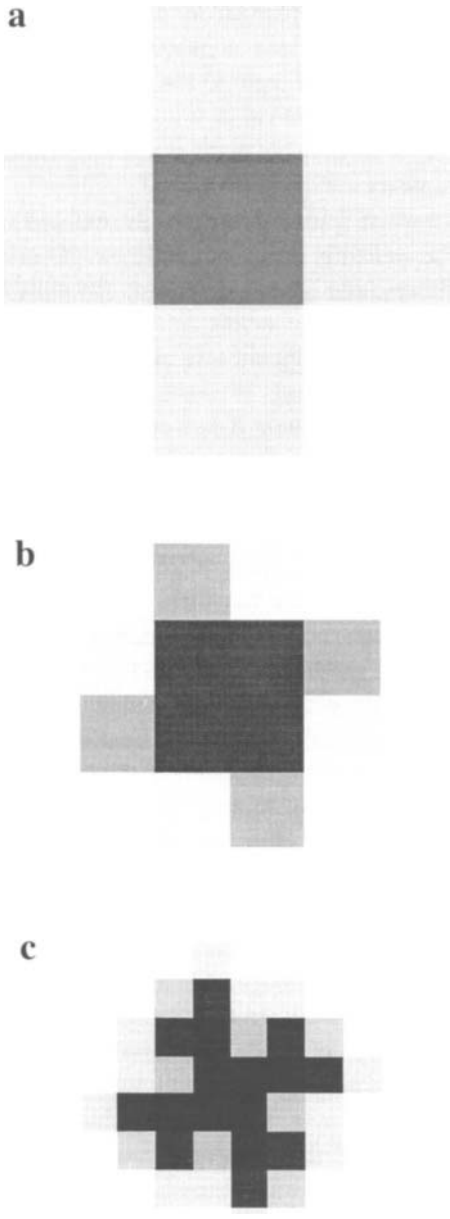


Fig. 6. Grayscale images of the quadratic von Koch island with pixels of size (a) $\lambda = 1$, (b) $1/2$ and (c) $1/4$. As with the box size $\varepsilon$ in Figs. 3–5, $\lambda$ is relative to the length of the sides of the square initiator in Fig. 1.

significantly with the von Koch island. The extent of this coverage may be

von Koch island. The overlap converges to $1/14$ as $i \rightarrow \infty$, i.e., for the island itself. This percentage translates into a grayscale level equal to 18 (255/14, truncated to an integer). Since the area of the island is one, the central pixel in Fig. 6a must have a grayscale level of $255(1-4/14) = 182$. In digitized images at higher resolution (i.e., with smaller pixel size), the number of grayscale levels increases (cf. Fig. 6b and c)

In practical applications of fractal geometry to real systems, images like those of Fig. 6 constitute the starting point of analyses. Available methods for the evaluation of fractal dimensions however require the number of grayscale levels to be reduced to just two; black and white. In other words, the images need to be thresholded. Various automatic algorithms, such as those described briefly in Section 3, could be used to this end. However, given the intrinsic symmetry of the histograms of images of the von Koch island obtained by coarse-graining and the lack of dispersion of grayscale levels outside of certain narrow ranges of values, it is sufficient for the purposes of the present analysis to consider three special cases of thresholding. The first, or high-threshold, consists of considering that any pixel with a grayscale value $< 255$ should become white (grayscale level = 0). Alternatively, adopting a low-threshold, one could consider that any pixel with a grayscale level $> 0$ should become black. Between those two extremes, one may take as a medium-threshold the value that splits the grayscale into two equal parts; pixels with grayscale value $\leq 127$ become white, and pixels with grayscale value $> 127$, black. Application of these three approaches to the quadratic von Koch island, coarse-grained with pixels of size $\lambda = 1/256$ (Fig. 7) shows that the resulting binary images have significantly different appearances. The high-threshold (Fig. 7a) yields an image composed of the pixels that are entirely contained within the island. Implicitly, this is the threshold adopted by De Cola and Lam (1993) in their analysis of photographs at different resolutions. The medium-threshold (Fig. 7b) yields a prefractal of the quadratic von Koch island. Finally, the low-threshold (Fig. 7c) produces a fattened version of the island, with a total number of pixels (of size $\varepsilon$) equal to the number of boxes of size $\varepsilon$ needed to cover the island. The edge in the high-threshold case appears very prickly, whereas that for the low-threshold is very rounded.

For each of the images of the quadratic von Koch island, with different resolutions and obtained with different thresholds, the relationship between the number of covering boxes and the box size $\varepsilon$ suggests very convincingly that the image's representation of the quadratic von Koch island is a surface fractal. For example, the log–log plots associated with the three highest-resolution images are presented in Fig. 8a. For practical reasons, the regression lines in this figure are restricted to the range of box sizes considered by the computer code fd3 (cf. Section 3). In all three cases in Fig. 8a, the $R$ values are remarkably high, which is typical of values found in the present research; none of the 'fractal' dimensions reported in this article had an associated $R$ value lower

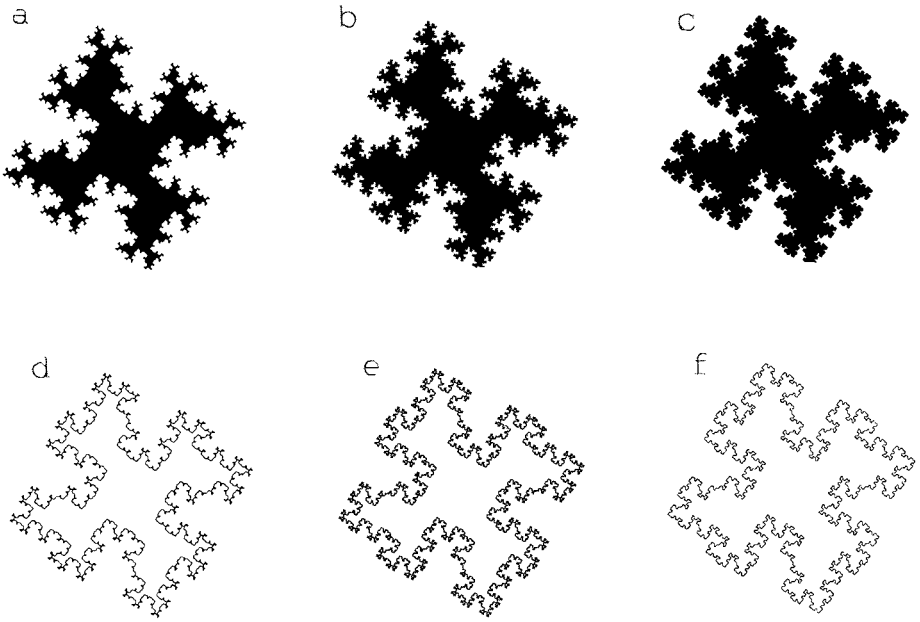


Fig. 7. Images of the quadratic von Koch island and of its edge obtained with (a and d) a high-threshold, (b and e) a medium-threshold at grayscale level 127 and (c and f) a low-threshold. See text for details.

than 0.99. The extremely high statistical significance associated with the regression lines in Fig. 8a suggests that, in the three images to which this figure relates, the representation of the quadratic von Koch island is a surface fractal. In other words, the coarse-graining associated with the images and the further approximation caused by thresholding apparently manage to preserve the fractal character of the initial object. This point of view rests implicitly on the premise that the slope of the regression line in log–log plots like that of Fig. 8a is a good estimate of the true box-counting dimension.

By looking at the data points in Fig. 8a from a different perspective, more in line with the definition of the box-counting dimension in Eq. (1), one finds a number of perplexing features, which clearly point in another direction. Instead of fitting a power–law relationship to the observed $N(\varepsilon)$ values, yielding a straight line in a $\log_{10}(N)$ vs. $\log_{10}(\varepsilon)$ plot, one can compute differences between the logarithms of neighboring values of $N$, and divide these differences by $\log_{10}(2)$ to obtain a piecewise approximation of the slope. This approach, for the three cases considered in Fig. 8a, leads to the points presented in Fig. 8b. All three sets of points show a pronounced decrease, from 2.0 at the largest box sizes to 0.0 when the box size equals the pixel size of the image. Between these two extremes, the points that are based on data included in the regressions in Fig. 8a are connected, pairwise, in Fig. 8b. In the left half of this intermediate

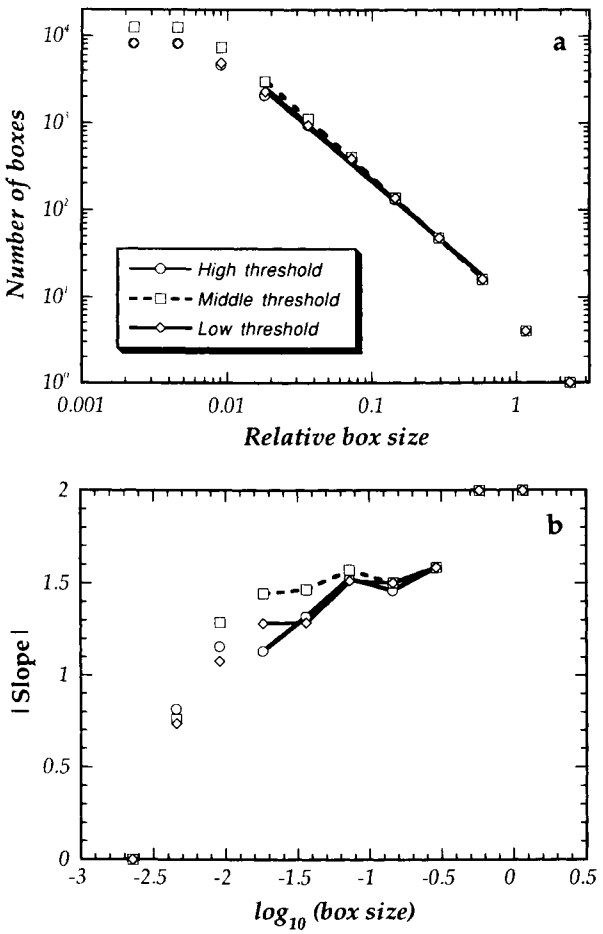


Fig. 8. (a) Relationship between the number of covering boxes, as counted using the fd3 sofware, and box size for images d, e and f in Fig. 7. The average box-counting dimension (i.e., the absolute value of the slope) associated with the regression lines are equal to 1.426 ('high-threshold', $R = 0.9964$), 1.515 ('middle-threshold', $R = 0.9999$) and 1.437 ('low-threshold', $R = 0.9989$). (b) Absolute value of the slope $d\log_{10}(N)/d\log_{10}(\varepsilon)$ vs. box size, obtained by calculating differences between adjacent points in (a). The straight lines in Fig. 8b connect the points corresponding with the data used to calculate the regression lines in Fig. 8a.

range, the high- and low-threshold curves decrease strongly. In the same range of box sizes, the middle-threshold curves exhibits a form of limit behavior, with an apparent plateau value near to 1.5.

The slopes shown in Fig. 8b do not correspond to the theoretical limit embodied in the definition of the box-counting dimension in Eq. (1), since they do not result from taking the limit of |slope| as $\varepsilon \to 0$. Since the limit of vanishing $\varepsilon$ does not make sense for finite-resolution images of the von Koch island, one might be tempted, for the low- and middle-threshold data in Fig. 8b,

to discern a tiny (two-point) plateau for the left hand of the data connected by lines. The values of 1.285 and 1.445, respectively, associated with these plateaux could then be viewed as the best available estimates of the box-counting dimension of the geometrical structures in Fig. 7f and e. A similar approach applied to the data points for the high-threshold curve in Fig. 8b leads however to no such conclusion. This approach is probably meaningless, that is, it probably does not make sense to examine the left end of the curves in Fig. 8b too closely.

Another way to look at Fig. 8b is to consider that the region of the graph in which 'fractal' behavior is exhibited is roughly in the range of $\log_{10}$(box size) between $-1.2$ and $-0.5$. Indeed, if one considers the five rightmost points in Fig. 8b, one is struck by the clear similarity that exists between the pattern of these points and that of the data points in Fig. 3b. After a sharp drop of |slope| as $\varepsilon$ is decreased, |slope| stabilizes around a stable plateau value. The three data points in the right half of the curves in Fig. 8b exhibit a slight wiggle, but one may consider this to be merely a random oscillation, due perhaps to the position of the boxes relative to the images. At smaller box sizes (below $\log_{10}$(box size) $= -1.2$), the finite resolution of the images reduces more and more the number of boxes needed for full coverage, compared with the number required to cover the true quadratic von Koch island. As a result, |slope| decreases sharply until it vanishes. From this viewpoint, only in a narrow range of $\log_{10}$(box size) do the images of the quadratic von Koch island exhibit a 'fractal' behavior, in spite of the fact that the initial structure, the quadratic von Koch island, is an acknowledged surface fractal. The box-counting dimensions associated with the plateaus in this range are equal to 1.523 ($\pm 0.063$), 1.553 ($\pm 0.044$) and 1.533 ($\pm 0.045$) for the high-, middle- and low-threshold cases, respectively. These mean values are higher than 1.5, but not significantly so (at $P = 0.05$ level).

The three approaches just described (i.e., regression analysis in Fig. 8a, search for a plateau in the left or in the right part of the curves in Fig. 8b) will be discussed again, later in this article, in connection with the evaluation of the surface fractal dimensions of stain patterns in a field soil. To simplify the rest of the analysis of images of the quadratic von Koch island, only the average 'fractal' dimensions, obtained via regression, will be addressed here. Patterns that this analysis reveals are qualitatively similar when dimensions based on the 'right' plateau approach are used instead.

In Fig. 9a, the variability due to thresholding appears commensurate with that due to image resolution. A similar observation pertains when one considers alternative dimensions (Fig. 9b); the discrepancies among values obtained for the box-counting, information, and correlation dimensions (for definitions of these dimensions see, e.g., Korvin, 1992; Baveye et al., 1998) are of the same order of magnitude as the variability due to image resolution. At small pixel sizes, the theoretical inequalities $D_{BC} \geqslant D_I \geqslant D_C$ (e.g., Korvin, 1992; Baveye and Boast, 1998) are verified. However, at the largest pixel size, the dimensions

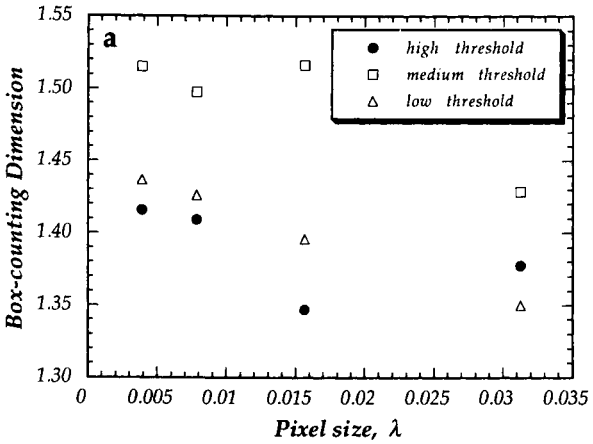
a
high threshold
medium threshold
low threshold
Box-counting Dimension
1.55
1.50
1.45
1.40
1.35
1.30
0
0.005
0.01
0.015
0.02
0.025
0.03
0.035
Pixel size, λ

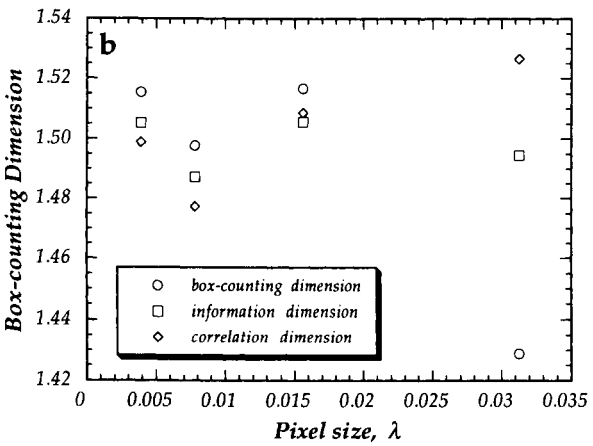
b
box-counting dimension
information dimension
correlation dimension
Box-counting Dimension
1.54
1.52
1.50
1.48
1.46
1.44
1.42
0
0.005
0.01
0.015
0.02
0.025
0.03
0.035
Pixel size, λ

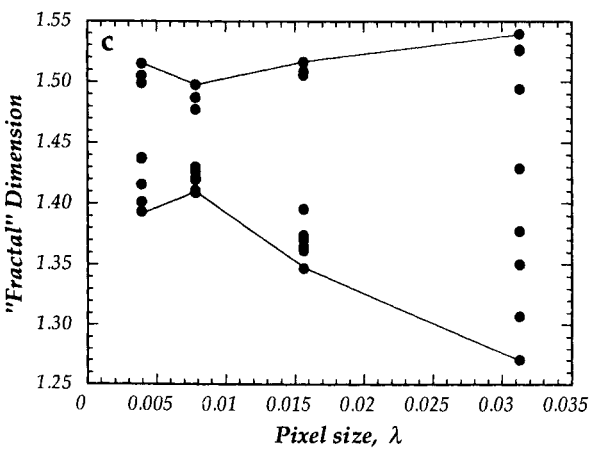
c
"Fractal" Dimension
1.55
1.50
1.45
1.40
1.35
1.30
1.25
0
0.005
0.01
0.015
0.02
0.025
0.03
0.035
Pixel size, λ

follow a reverse ordering, as do the corresponding mass fractal dimensions (see the work of Baveye et al. (1998)).

The overall effect of resolution, thresholding and choice of a 'fractal' dimension on the surface dimensions obtained for the quadratic von Koch island is depicted in Fig. 9c. In contrast with a similar graph obtained earlier by Baveye et al. (1998) for the apparent mass fractal dimensions of the quadratic von Koch island, this figure does not suggest either an upward or a downward trend of the surface dimensions at increasing image resolutions (decreasing pixel sizes).

## 3. Materials and methods

### *3.1. Field site*

The field site is located in the old Cornell University orchard, in Ithaca (NY). Soils in this orchard are moderately well-drained, were formed on a lacustrine deposit, and have been classified alternatively as a fine, illitic, mesic Glossaquic Hapludalf (Vecchio et al., 1984) or as a mixed, mesic Udic Hapludalf (Merwin and Stiles, 1994). The orchard was originally planted in 1927, but the trees were removed in 1977–1978. Between 1979 and 1983, a variety of test crops, including tobacco, sunflower and vegetables were grown on the plot. In 1985, the site was deep plowed with 12 t/ha of dolomite lime, and ryegrass and red fescue were planted (Merwin and Stiles, 1994). In April 1986, dwarf apple trees were planted 3 m apart in rows spaced 6 m. Sod grass ground cover has since been maintained between the tree rows and has been regularly mowed to a height of 6–10 cm.

### *3.2. Dye experiment*

On July 14, 1995, a 68.6-cm i.d. metal ring was pushed into the surface layer of the soil. A total of 20 l of a 1% solution (10 g/l) of blue food coloring (F&DC #1) were poured inside the cylinder and rapidly infiltrated into the soil. A total of 15 min later, a 1.8-m deep trench was dug, tangential to the outer surface of the metal ring. Initial digging was done with a backhoe, followed by carefully removing soil with shovels in order to obtain as vertical as possible a

Fig. 9. (a) Influence of thresholding on the relationship between box-counting dimension and pixel size in four different images of the edge of the quadratic von Koch island, (b) values of three 'fractal' dimensions of the edge in images of the quadratic von Koch island thresholded at grayscale level 127 (medium-threshold) and (c) summary of all the 'surface fractal' dimensions obtained with images thresholded in three different ways. The solid lines connect extreme points and provide a general idea of the envelope in which data points are located.

soil profile. Color pictures were taken of the exposed soil facies with a hand-held camera. Then a 5-cm thick slice of soil was further excavated toward the center of the ring. This same procedure was repeated three times, at 15-cm intervals, to obtain evidence of dye preferential transport at various points underneath the metal ring.

### *3.3. Image manipulation*

Two different color pictures of a single soil facies were used in the present study. These pictures, labeled '16' and '17', differ slightly with respect to viewing angle and exposure. Color prints and slides were obtained in both cases. The slides were scanned and the resulting (2048 × 3072 pixels) digitized images were stored in RGB (red–green–blue) color-coding format on a Kodak CD-ROM.

The software Adobe Photoshop™ (version 4.0, Adobe Systems) was used to manipulate and analyze soil images. Using features of this software, images 16 and 17 were retrieved at five different resolutions (2048 × 3072, 1024 × 1536, 512 × 768, 256 × 384, 128 × 192 pixels).

To ensure that all digitized images would receive identical treatments, precisely the same field of view was cropped (i.e., delineated and cut) in each case. In addition, to maximize the contrast between stained and background soil material, the storage format of the cropped images was changed from RGB to CYMK (cyan–yellow–magenta–black), and the cyan channel was retained for further analysis. This channel corresponds very closely with the color of the dye used in the field experiment, a feature that makes the stain patterns much more sharply contrasted than for any of the other channels available in Adobe Photoshop™. For the remainder of the work, the cyan channel of each image was converted to a grayscale image.

### *3.4. Thresholding algorithms*

To threshold or 'segment' a digitized image, one could in principle proceed by trial and error until one achieves a thresholding that appears reasonable, i.e., coincides with some a priori idea one may have about the two categories of pixels one attempts to separate. Unfortunately, this procedure is very subjective and may lead to biases when one is trying to compare images, or in the analysis of time sequences of images of a given object (e.g., under evolving lighting conditions). To palliate these difficulties, numerous automatic, non-subjective thresholding algorithms have been developed (e.g., Glasbey and Horgan, 1995). Two of the most commonly used were adopted in the research described in the present article. Both are iterative.

The *intermeans* algorithm is initiated with a starting 'guess' for the threshold. Then the mean pixel value of the set of pixels with grayscale level greater than

the initial threshold is calculated, and likewise for the set of pixels with grayscale level less than or equal to the initial threshold. The average of these two means is calculated, and truncated to an integer, to give the next 'guess' for the threshold. This process is continued, iteratively, until it converges, i.e., until there is no change in the threshold from one iteration to the next.

In the *minimum-error* algorithm, the histogram is visualized as consisting of two (usually overlapping) Gaussian distributions. As with the intermeans algorithm, a starting 'guess' for the threshold is made. The fraction of the pixels in each of the two sets of pixels defined by this threshold is calculated, as are the mean and variance of each of the sets. Then, in effect, a composite histogram is formulated, which is a weighted sum of two Gaussian distributions, each with mean and variance as just calculated, and weighted by the calculated fraction. The (not necessarily integer) grayscale level at which these two Gaussian distributions are equal is calculated (involving solution of a quadratic equation). This grayscale level, truncated to an integer, gives the next 'guess' for the threshold. Again, the process is continued, iteratively, until it converges.

Both thresholding algorithms suffer from the fact that the choice of the starting guess used to initiate the iterative calculations influences the convergence to a final threshold value. The resulting indeterminacy was avoided by using an objective approach developed by Boast and Baveye (submitted).

### *3.5. Removal of islands and lakes*

After thresholding the images of soil profiles with one of the algorithms described above, the resulting geometrical structure is generally very disconnected; besides two or three large 'continents' that extend downward from the soil surface, there is a myriad of 'islands' of various sizes and shapes. Some of these islands may in fact be peninsulas, artificially separated from the continents by the coarse-graining associated with the generation of images at a specified resolution. Some of the islands, however, may be truly disconnected from the continents, and may be manifestations of 3-D flow, not strictly in the plane of the images.

For the purpose of describing 1-D preferential flow in field soils, one may want to restrict application of fractal geometry to the part of a stain pattern that is connected to the inlet surface. This can be achieved with Adobe Photoshop™ by selecting the continents with the magic wand tool, inverting the selection (i.e., selecting everything but the continents), and making the latter selection uniformly white by adjusting its contrast and brightness. This procedure effectively eliminates islands.

In a similar manner, even though a physical justification is less obvious in this case, it is possible to remove the 'lakes', or patches of unstained soil within the continents.

### *3.6. Edge delineation*

After thresholding and removal of islands/lakes (in case they are removed), the filtering capability of Adobe Photoshop™ is used to isolate the edge pixels of the stain patterns, using the Adobe Photoshop™ 'Laplacian' filter, which isolates all inside edge pixels, including diagonal ones, and requires a subsequent inversion of grayscale values to produce a final image where the edge pixels, in black, contrast with the white background.

This procedure is applied to digitized images without any prior change in pixel size, which in Adobe Photoshop™ may be modified arbitrarily. To isolate the edge of stain patterns, however, it may be tempting to decrease substantially the pixel size. Every pixel would then be replaced by, for example, 4, 9, 16, 25, 36,... smaller pixels. In this manner, the 'edge' pixels would approximate more closely the perimeter of the stained patterns. Preliminary tests have shown that this approach significantly affects the final values found for the surface fractal dimensions of the stain patterns. However, in the range of pixel sizes analyzed, there was no obvious optimal pixel size reduction factor, common to all images. Therefore, until this question is better understood, it was decided not to modify the pixel size in the present research. Also, since in the relevant literature previous fractal analyses based on digitized images make no mention of the role of pixel size in the delineation of edges, it was decided not to involve it as one of the possible 'subjective' choices analyzed in the present work.

### *3.7. Calculation of fractal dimensions*

The box-counting, information and correlation dimensions were calculated using the C + + code 'fd3' written by John Saraille and Peter Di Falco (California State University at Stanislaus). This code, widely available on the Internet, e.g., via anonymous ftp at ftp.cs.csustan.edu, is based on an algorithm originally proposed by Liebovitch and Toth (1989). As do virtually all other algorithms that are meant to evaluate fractal dimensions of geometrical structures in a plane, fd3 only considers the centroids of the various pixels constituting the images of these structures. The side of the smallest square that fully covers the given set of points is successively halved 32 times, yielding box coverages with progressively smaller boxes. The two largest box sizes are considered too coarse and are therefore not taken into account in the calculation of the box-counting, information, and correlation dimensions. Similarly, at the low end of the range of box sizes, the data points for which the number of boxes is equal to the total number of points (= number of pixels in the image) are ignored.

The box-counting dimensions of several of the stain patterns were also calculated using a Pascal code written especially for the present work.

## 4. Results and discussion

In all the (grayscale) images resulting from selecting the cyan layer in the CMYK representation of pictures 16 and 17 at various resolutions, the preferential pathways appear darker than the background soil, both in the surface and in the deeper horizons (e.g., Fig. 10a).

Application of the thresholding algorithms to these images gives the threshold values reported in Table 1. The systematic differences between the threshold values for the images derived from pictures 16 and 17 correspond to differences in the exposure of the pictures, picture 16 being slightly underexposed compared with picture 17. Beside this influence of picture exposure, it appears that the minimum-error algorithm yields threshold values that are generally, but not always (cf. images 17-1 and 17-5), larger than those obtained with the intermeans algorithm. This discrepancy, when it is large, affects a sizeable portion of the pixels, e.g., in image 16-5, 17.2% of the pixels that are above the intermeans threshold are not above the minimum-error threshold.

After thresholding of a grayscale image with one of the two algorithms, and delineation of the edge using the Laplacian filter, one obtains an image like that of Fig. 10b. Further removal of islands and lakes produces the much 'cleaner' image of Fig. 10c. In each case, the solid lines correspond to the inside edge pixels, including diagonal pixels.

Not surprisingly, the differences between threshold values in Table 1 translate into different surface fractal dimensions, as shown in Fig. 11. Without exception, for a given image and a given definition of fractal dimension, the surface fractal dimension is larger in the binary image obtained with the lowest threshold value. In most cases (except in images 17-1 and 17-5), the intermeans threshold is smaller than its minimum-error counterpart, and the surface fractal dimensions determined using the intermeans threshold are higher than those based on the minimum-error threshold (open symbols generally higher than full symbols in Fig. 11). Quantitatively, the influence of the thresholding method on fractal dimensions remains relatively small. The largest difference, 0.029, is found in the case of the box-counting dimension in image 16-4 (circles in the fourth set of points from the right in Fig. 11).

More significant, quantitatively, is the influence of the choice of a 'fractal' dimension among the three candidates envisaged in the present research. These dimensions satisfy the inequalities $D_{BC} < D_I < D_C$, with $D_{BC}$ often appreciably lower than the other two. The largest difference, 0.08, is found in image 17-5 between the box-counting dimension and the other two dimensions.

Removal of the islands and/or lakes introduces another level of subjectivity in the evaluation of the surface fractal dimensions of stained preferential flow patterns. The decision to remove islands and, particularly, that to remove both islands and lakes appear to have a much more significant effect on the final dimension values than did either the choice of a thresholding algorithm or the

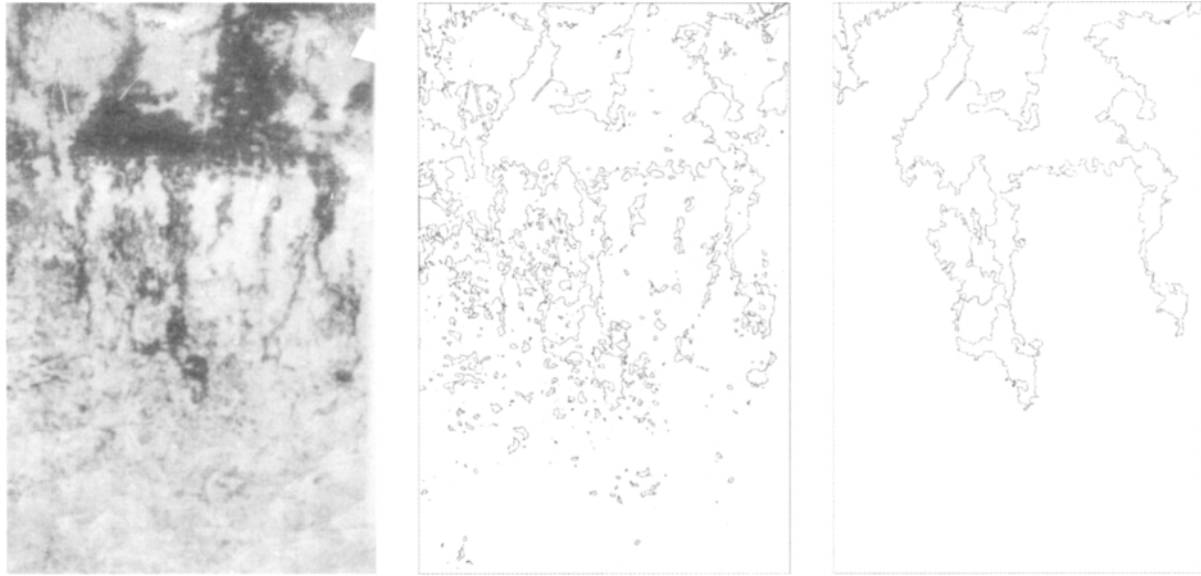

. 10. (a) Grayscale image, labeled 16-2-c, of the cyan layer of picture 16, retrieved from disk at the second highest possible resolution, (b) ck-and-white (binary) image obtained by thresholding the image with the intermeans algorithm and isolating the edge, and (c) same image as in (b) with removal of 'islands' and filling of 'lakes' prior to identifying the edge (see text for details).

Table 1
Values of the physical pixel size (cm), and of intermeans and minimum-error thresholds (grayscale levels) for the various digital versions of the available pictures of the soil profile, sorted in order of pixel size

| Picture number | Physical pixel size (cm) | Intermeans threshold (grayscale level) | Minimum -error threshold (grayscale level) |
|---|---|---|---|
| 16-1 | 0.042 | 117 | 120 |
| 17-1 | 0.053 | 112 | 111 |
| 16-2 | 0.083 | 118 | 122 |
| 17-2 | 0.105 | 113 | 115 |
| 16-3 | 0.167 | 118 | 122 |
| 17-3 | 0.211 | 113 | 114 |
| 16-4 | 0.333 | 118 | 123 |
| 17-4 | 0.420 | 113 | 115 |
| 16-5 | 0.667 | 118 | 125 |
| 17-5 | 0.846 | 109 | 109 |

selection of a specific definition of fractal dimension (cf. Fig. 12, similar graphs existing for the information and correlation dimensions). With dimensions for the untransformed state clustered around 1.55, removal of the islands alone makes the dimension values drop to approximately 1.42, whereas after removal of both islands and lakes, the dimension values range between 1.31 and 1.40.

In both Figs. 11 and 12, the resolution of the images used for the evaluation of the surface dimensions does not appear to have a significant influence on the

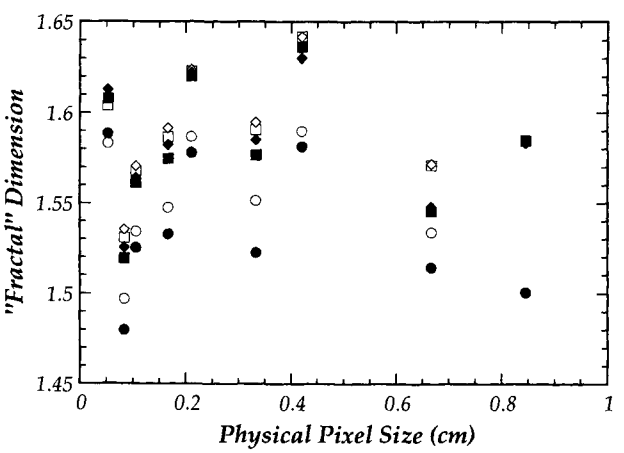


Fig. 11. Effect of thresholding and of the choice of a fractal dimension on the relationship between surface 'fractal dimensions' and physical pixel size. Open symbols correspond to the intermeans algorithm and full symbols to the minimum-error algorithm. Circles, squares and diamonds are associated with the box-counting, information and correlation dimensions, respectively. The analysis was carried out without prior removal of the islands or lakes.

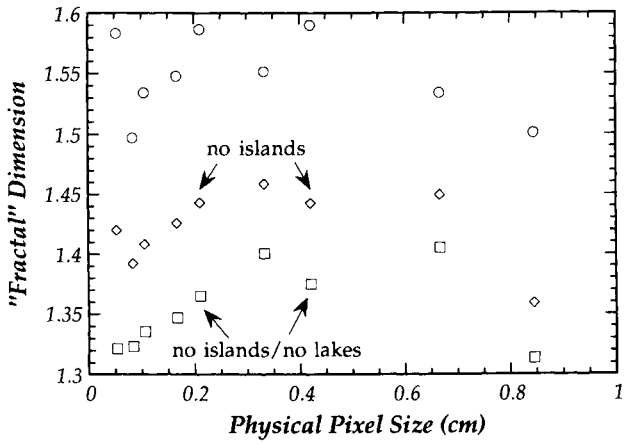


Fig. 12. Influence of the removal of islands, and of islands and lakes, on the values of the surface box-counting dimension in images thresholded with the intermeans algorithm. The circles correspond to the original images, whereas the diamonds and squares represent the dimensions obtained after removal of the islands, and islands and lakes, respectively.

observed dimensions. In all cases, there is significant scatter in the values found for the different dimensions over the range of image resolutions considered, and there is never any clear overall convergence pattern. In some rare instances, like the 'no islands/no lakes' values in Fig. 12, there seems to be a coherent trend at small pixel sizes. Whether or not this is more than a fortuitous occurrence, these trends all suggest a convergence to a non-integer value, in sharp contrast with the behavior identified by Baveye et al. (1998) for the (apparent) mass fractal characteristics of the same stain pattern.

If it is assumed that there are no coherent trends with pixel size and if the scatter in the dimension values is viewed as random, one can calculate a mean and standard deviation for each case. The resulting estimates, provided in Table 2, depend on the choice of a thresholding algorithm, on which fractal dimension is evaluated, and on whether or not islands and/or lakes are removed. However, they present the distinct advantage of being independent of the resolution of images. In this sense, the estimates in Table 2 are somewhat more robust than traditional estimates, oblivious of most of the vicissitudes of image resolution.

The lack of an overall trend towards an integer value over the range of image resolutions considered here is also clearly illustrated by the 'summary' graph in Fig. 13. In practical terms, this graph means that different observers, making different choices at various stages in the evaluation of the surface 'fractal' dimension of the stain pattern, are likely to end up with dimensions anywhere between 1.32 and 1.64. If these observers used several image resolutions and estimated the means as in Table 2, the range of observed dimension values would narrow somewhat, to between 1.35 and 1.59. Either way, the resulting

Table 2
Means and standard deviations of fractal dimensions obtained by averaging out the effect of image resolution

| | Intermeans threshold | Minimum-error threshold |
|---|---|---|
| *Untransformed image* | | |
| Box-counting dimension | $1.55 \pm 0.03$ | $1.54 \pm 0.04$ |
| Information dimension | $1.59 \pm 0.03$ | $1.58 \pm 0.04$ |
| Correlation dimension | $1.59 \pm 0.03$ | $1.58 \pm 0.03$ |
| *No islands* | | |
| Box-counting dimension | $1.42 \pm 0.03$ | $1.43 \pm 0.03$ |
| Information dimension | $1.48 \pm 0.03$ | $1.48 \pm 0.02$ |
| Correlation dimension | $1.49 \pm 0.03$ | $1.49 \pm 0.03$ |
| *No islands / no lakes* | | |
| Box-counting dimension | $1.35 \pm 0.03$ | $1.37 \pm 0.04$ |
| Information dimension | $1.39 \pm 0.03$ | $1.40 \pm 0.03$ |
| Correlation dimension | $1.40 \pm 0.03$ | $1.41 \pm 0.04$ |

range of fractal dimensions is a sizable fraction (25% or 33%) of the total permissible range for this fractal dimension (1 to 2).

The graph of Fig. 13 lends strong credence to the contention that the stain pattern is a surface fractal, i.e., that its surface fractal dimension is non-integer. Further support for this viewpoint is provided by the fact that each of the data points in the graph has been obtained (via non-linear regression) with a very high $R$ value, always larger than 0.99. A representative illustration of the estimation procedure is provided in Fig. 14a for image 17-1. The evidence of

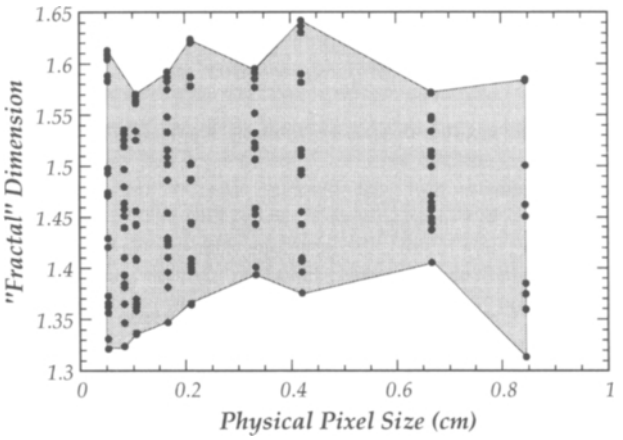


Fig. 13. Compilation of all the surface fractal dimensions obtained in the present study, vs. the physical pixel size. The gray region represents the global envelope of the plotted data, determined

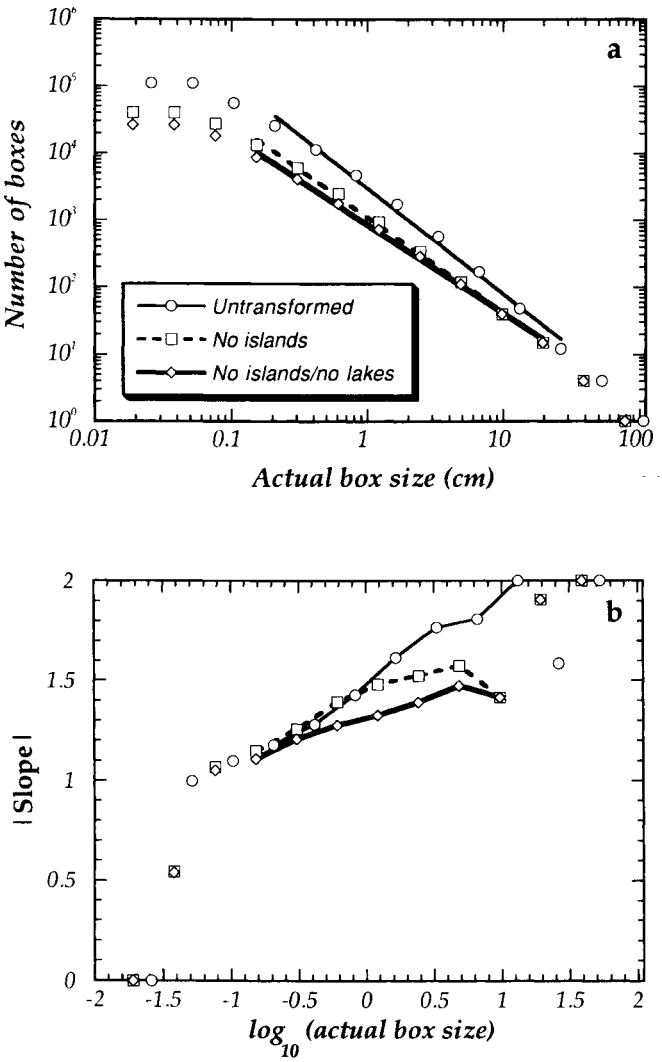


Fig. 14. (a) Relationship between the number of covering boxes and their size for image 17-1, the highest-resolution image derived from picture 17, thresholded with the intermeans algorithm. The average box-counting dimension (i.e., the absolute value of the slope) associated with the regression lines is equal to 1.58 ('untransformed', $R = 0.993$), 1.42 ('no islands', $R = 0.997$) and 1.32 ('no islands/no lakes', $R = 0.998$). (b) Absolute value of the slope $d\log_{10}(N)/d\log_{10}(\varepsilon)$ vs. box size, obtained by calculating differences between adjacent points in (a). The straight lines in Fig. 14b connect the points corresponding with the data used to calculate the regression lines in Fig. 14a.

extremely high $R$ values, combined with the more than two decades of pixel sizes over which power–law behavior is observed, would be considered convincing enough by most authors to conclude that the stain pattern is a surface fractal.

However, as was done earlier with the quadratic von Koch island, the results of Fig. 14a may be analyzed from another perspective, leading in a very different direction (Fig. 14b). Indeed, for all images, the graphs of |slope| vs. $\log_{10}$(actual box size) like that in Fig. 14b reveal a largely monotonic decrease of |slope| as the box size decreases. There is no tendency in the left part of the fd3 range (connected points) for the points to form plateaux, i.e., for |slope| to be more or less constant for a range of box sizes. To the left of the fd3 range, the predominant behavior seems to be a convergence to unity. In the right part of the fd3 range, one would be hard pressed to identify a plateau for the 'untransformed' case (open circles). For the 'no islands' and 'no islands/no lakes' cases, one might perhaps view the wiggles in the range of $\log_{10}$(actual box size) between 0 and 1.1 (first four connected points from the right) as a random fluctuation around stable values of $1.50 \pm 0.07$ ('no islands') and $1.40 \pm 0.06$ ('no islands/no lakes'). These box-counting dimensions are somewhat higher than those obtained via regression (Fig. 14a) and leftmost set of points in Fig. 12. This is not surprising, given the fact that the slope of the regression lines in Fig. 14a is in some sense an average over the whole fd3 range, whereas the estimates just calculated are based solely on the subrange of box sizes where |slope| is largest. Unfortunately, the estimates of the box-counting dimensions obtained by considering plateaus in Fig. 14b suffer from a great deal of subjectivity, associated with the range of box numbers considered in the analysis. Indeed, if for some reason, one were to remove the rightmost connected data point in either of the 'no islands' cases, evidence of a plateau would be significantly weakened and one would be tempted to conclude that the corresponding pattern is non-fractal. The decision to include the rightmost point in the graph is linked to the (subjective) choice made in the computer code fd3 to ignore the two largest box sizes when calculating the box-counting dimension (see Section 3). This choice seems very sound, yet one could very well have opted to ignore only the largest, or to be more restrictive and to ignore the three largest box sizes. These alternate choices would affect significantly the decision to consider or not to consider that images of the stain pattern are surface fractals. Of course, as is certainly the case with the quadratic von Koch island, this decision may only pertain to images of the stain pattern and *not* to the stain pattern itself.

## 5. Conclusions

The key results of the research reported in the present article are contained in Figs. 13 and 14. The first of these figures shows that operator choices, made during the analysis of images of the stain pattern, cause the final surface 'fractal' dimension estimates to vary over a sizable range, approximately from 1.32 to 1.64. This range may be reduced somewhat by averaging out the influence of image resolution (cf. Table 2).

In spite of the subjectivity associated with the evaluation of the surface fractal dimensions, Fig. 13 shows no tendency for the dimensions to tend to an integer value at small pixel sizes. This observation suggests that the stain pattern is a genuine surface fractal. This conclusion is also supported by the very good fit of regression lines to data in Fig. 14a, giving remarkably high $R$ values. Contrastedly, Fig. 14b casts doubt on the fractality of representations of the stain pattern in digitized images. In the range of box sizes considered appropriate for the evaluation of fractal dimensions, there is no appearance of a plateau at the lower end of the range, and although one could conceivably identify plateaux for two of the three curves at the high end of the fd3 range, evidence in this sense is not particularly strong and the choice of where to see a plateau is quite subjective.

The resulting conundrum about the fractality of images of the stain pattern illustrates vividly some of the difficulties associated with the application of fractal geometry to physical systems. To some extent, however, it may be largely academic. The method described above, giving estimates of surface dimensions by averaging out the effect of image resolution, yields numbers that are more robust than traditional estimates, ceteris paribus. Whether or not the observed stain pattern is a surface fractal, these numbers may prove useful in mathematical descriptions of the preferential transport of water and solutes in field soils. Beyond the interest that there may be in characterizing the geometry of a complicated pattern or object with a number, perhaps of even greater interest is the question of what can be done with the number once it is obtained. Further research in the direction explored by Crawford et al. (in press) will be needed to provide answers to this important question.

## Acknowledgements

The research reported in the present article was supported in part by grant No. DHR-5600-G-1070-00 PSTC Project Number 11.243 awarded to one of us (P.B.) by the United States Agency for International Development and by a BARD grant awarded to Tammo Steenhuis. Gratitude is expressed to Stokely Boast, who wrote a computer program to generate the prefractals of the quadratic von Koch island, and to an anonymous reviewer for very thoughtful comments.

## References

Aguilar, J., Fernández, J., Ortega, E., de Haro, S., Rodríguez, T., 1990. Micromorphological characteristics of soils producing olives under non-ploughing compared with traditional tillage methods. In: Douglas, L.A. (Ed.), Soil Micromorphology: A Basic and Applied Science. Elsevier, Amsterdam, pp. 25–32.

Baveye, P., Boast, C.W., 1998. Fractal geometry, fragmentation processes and the physics of scale-invariance: an introduction. In: Baveye, P., Parlange, J.Y., Stewart, B.A. (Eds.), Fractals in Soil Science. Lewis Publishers, Boca Raton, FL, pp. 1–54.

Baveye, P., Boast, C.W., Ogawa, S., Parlange, J.Y., Steenhuis, T., 1998. Influence of image resolution and thresholding on the apparent mass fractal characteristics of preferential flow patterns in field soils. Water Resources Research 34, 2783–2796.

Beven, K., 1991. Modelling preferential flow: An uncertain future? In: Gish, T.J., Shirmohammadi, A. (Eds.), Preferential Flow: Proceedings of National Symposium. American Society of Agricultural Engineers, St. Joseph, MI, pp. 1–11.

Boast, C.W., Baveye, P., submitted. Avoiding indeterminacy in iterative image thresholding algorithms. Pattern Recognition.

Bouma, J., Dekker, L.W., 1978. A case study on infiltration into dry clay soil: I. Morphological observations. Geoderma 20, 27–40.

Crawford, J.W., Baveye, P., Grindrod, P., Rappoldt, C., in press. Application of fractals to soil properties, landscape patterns and solute transport in porous media. In: Corwin, D.L., Loague, K., Ellsworth, T.R. (Eds.), Advanced Information Technologies for Assessing Non-point Source Pollutants in the Vadose Zone. American Geophysical Union, Washington, DC.

De Cola, L., Siu-Ngan Lam, N., 1993. Introduction to fractals in geography. In: Siu-Ngan Lam, N., De Cola, L. (Eds.), Fractals in Geography. Prentice-Hall, Englewood Cliffs, NJ, pp. 3–22.

Falconer, K.J., 1992. Fractal Geometry: Mathematical Foundations and Applications. Wiley, Chichester, UK.

Feder, J., 1988. Fractals. Plenum, New York.

Flury, M., Flühler, H., 1995. Tracer characteristics of brilliant blue FCF. Soil Sci. Soc. Am. J. 59, 22–27.

Flury, M., Flühler, H., Jury, W.A., Leuenberger, J., 1994. Susceptibility of soils to preferential flow of water: a field study. Water Resources Research 30, 1945–1954.

Ghodrati, M., Jury, W.A., 1990. A field study using dyes to characterize preferential flow of water. Soil Sci. Soc. Am. J. 54, 1558–1563.

Glasbey, C.A., Horgan, G.W., 1995. Image Analysis for the Biological Sciences. Wiley, Chichester, UK.

Glass, R.J., Steenhuis, T.S., Parlange, J.Y., 1988. Wetting front instability as a rapid and far-reaching hydrologic process in the vadose zone. J. Contam. Hydrol. 3, 207.

Grevers, M.C.J., De Jong, E., St. Arnaud, R.J., 1989. The characterization of soil macroporosity with CT scanning. Can. J. Soil Sci. 69, 629–637.

Hatano, R., Booltink, H.W.G., 1992. Using fractal dimensions of stained flow patterns in a clay soil to predict bypass flow. J. Hydrol. 135, 121–131.

Hatano, R., Sakuma, T., Okajima, H., 1983. Observations on macropores stained by methylene blue in a variety of field soils. Jpn. J. Soil Sci. Plant Nutr. 54, 490–498, in Japanese.

Hatano, R., Kawamura, N., Ikeda, J., Sakuma, T., 1992. Evaluation of the effect of morphological features of flow paths on solute transport by using fractal dimensions of methylene blue staining pattern. Geoderma 53, 31–44.

Helling, C.S., Gish, T.J., 1991. Physical and chemical processes affecting preferential flow. In: Gish, T.J., Shirmohammadi, A. (Eds.), Preferential Flow: Proceedings of a National Symposium. American Society of Agricultural Engineers, St. Joseph, MN, p. 77.

Korvin, G., 1992. Fractal Models in the Earth Sciences. Elsevier, Amsterdam.

Kung, K.J.S., 1990. Preferential flow in a sandy vadose soil: 1. Field observations. Geoderma 46, 51.

Liebovitch, L.S., Toth, T., 1989. A fast algorithm to determine fractal dimensions by box counting. Phys. Lett. A 141, 386–390.

Merwin, I.A., Stiles, W.C., 1994. Orchard groundcover management impacts on apple tree growth and yield, and nutrient availability and uptake. J. Am. Soc. Hort. Sci. 119 (2), 209–215.

McCoy, E.L., Boast, C.W., Stehouwer, R.C., Kladivko, E.J., 1994. Macropore hydraulics: taking a sledgehammer to classical theory. In: Lal, R., Stewart, B.A. (Eds.), Soil Processes and Water Quality. Lewis Publishers, Boca Raton, FL, pp. 303–348.

Natsch, A., Keel, C., Troxler, J., Zala, M., Von Albertini, N., Défago, G., 1996. Importance of preferential flow and soil management in vertical transport of a biocontrol strain of *Pseudomonas fluorescens* in structured field soil. Appl. Environ. Microbiol. 62 (1), 33–40.

Peyton, R.L., Gantzer, C.J., Anderson, S.H., Haeffner, B.A., Pfeifer, P., 1994. Fractal dimension to describe soil macropore structure using X-ray computed tomography. Water Resources Research 30, 691–700.

Radulovich, R., Sollins, P., 1987. Improved performance of zero-tension lysimeters. Soil Sci. Soc. Am. J. 51, 1386–1388.

Radulovich, R., Sollins, P., Baveye, P., Solorzano, E., 1992. Bypass water flow through unsaturated microaggregated tropical soils. Soil Sci. Soc. Am. J. 56, 721–726.

Steenhuis, T.S., Parlange, J.Y., Aburime, S.A., 1995. Preferential flow in structured and sandy soils: Consequences for modelling and monitoring. In: Wilson, L.G., Everett, L.G., Cullen, S.J. (Eds.), Handbook of Vadose Zone Characterization and Monitoring. Lewis Publishers, Boca Raton, FL, pp. 61–77.

Vecchio, F.A., Armbruster, G., Lisk, D.J., 1984. Quality characteristics of New Yorker and Heinz 1350 tomatoes grown in soil amended with a municipal sewage sludge. J. Agric. Food Chem. 32, 364–368.

*Fractals in Soil Science*
Editors: Ya.A. Pachepsky, J.W. Crawford and W.J. Rawls
© 2000 Elsevier Science B.V. All rights reserved.


# Generalizing the fractal model of soil structure: the pore–solid fractal approach

Edith Perrier [a,1], Nigel Bird [b,2], Michel Rieu [a,*]

[a] *ORSTOM, Laboratoire d'Informatique Appliquée, 32 av. Henri Varagnat, 93143 Bondy Cedex, France*

[b] *Silsoe Research Institute, Soil Science Group, Wrest Park Silsoe, Bedford MK45 4HS, UK*

Received 28 October 1997; accepted 28 September 1998

**Abstract**

We review a generalized approach to modeling soil structures, which exhibit scale invariant, or self-similar local structure over a range of scales. Within this approach almost all existing fractal models of soil structure feature as special albeit degenerate cases. A general model is considered which is shown to exhibit either a fractal or nonfractal pore surface depending on the model parameters. With the exception of two special cases corresponding to a solid mass fractal and a pore mass fractal the model displays symmetric power law or fractal pore size and solid size distributions. In this context the model provides an example of a porous structure in which pore sizes can be inferred from associated solid particle sizes through this symmetry. Again with two exceptions the model is shown to exhibit scaling of solid and pore volumes as a function of the resolution of measurement contrary to that of a mass fractal structure and to possess porosity other than zero or unity when local structure is included at arbitrarily small scales contrary to the situation arising in the case of a solid mass fractal and a pore mass fractal model respectively. Consequently the model not only generalizes the fractal approach to modeling soil structure but introduces properties central to the characterization of a soil which are quite distinct from those exhibited by existing fractal models. The model thus offers a wider scope for modeling self-similar multiscale soil structures than that currently operating. © 1999 Elsevier Science B.V. All rights reserved.

*Keywords:* fractal; soil structure; pore surface; pore mass

* Corresponding author. E-mail: rieu@paris.orstom.fr
[1] E-mail: perrier@bondy.orstom.fr
[2] E-mail: bird@bbsrc.ac.uk

Reprinted from Geoderma 88 (1999)
© 1999 Elsevier Science B.V. All rights reserved

## 1. Introduction

Fractals are becoming increasingly popular in soil physics research as a means for characterizing various properties of porous media. They have been used both in theoretical and practical studies to model: (i) fractal number–size distributions (pore size distributions: Friesen and Mikula, 1987; Ahl and Niemeyer, 1989; Tyler and Wheatcraft, 1990; Rieu and Sposito, 1991c; Perrier et al., 1996; particle size distributions: Tyler and Wheatcraft, 1989, 1992; Wu et al., 1993); (ii) fractal surfaces (pore–solid interface: Pfeifer and Avnir, 1983, de Gennes, 1985, Friesen and Mikula, 1987; Davis, 1989, van Damme and Ben Ohoud, 1990; Toledo et al., 1990; Bartoli et al., 1991; Crawford et al., 1995) and (iii) mass fractal properties (solid mass fractal: Friesen and Mikula, 1987; Bartoli et al., 1991; Rieu and Sposito, 1991c; Young and Crawford, 1991; Crawford, 1994; Bird et al., 1996; Crawford et al., 1995; Perrier et al., 1995; or associated aggregate distributions: Perfect and Kay, 1991; Crawford et al., 1993; or pore mass fractal: Katz and Thompson, 1985; Ghilardi et al., 1993). The main purpose of these studies is to analyze or characterize complex multiscale porous structures. As far as soil structure is concerned, attention to date has focused mainly on modeling soil structures and, in particular, soil aggregate structures in terms of solid mass fractals and on modeling the pore–solid interface within the soil in terms of fractal surfaces. The essential feature common to each fractal model is scale invariance, that is the structure in question is composed of parts which appear similar to the whole. Examples include the now familiar Menger sponge (or Sierpinski carpet) in the context of a mass fractal model and the Von Koch curve, or the internal surface of a Menger sponge in the context of a fractal surface model. Our purpose is to review a new approach to modeling multiscale porous media and soil structures in particular. This involves an alternative class of models which can be viewed as a generalization of the previously quoted fractal models. Like any fractal model, the new class exhibits self-similar properties. In other important respects, central to the characterization of a porous medium, it is quite distinct. We will call it a 'pore–solid fractal' model (PSF).

The PSF model originates from two studies. Neimark (1989) developed the 'self-similar multiscale percolation system', a representation of a disordered, disperse medium that exhibits a fractal interface between solid and pore phases. Perrier (1994) independently proposed a multiscale model of soil structure which combines a fractal pore number–size distribution and a fractal solid number–size distribution. Although these two models have been developed in different contexts, using slightly different definitions, and presenting different local geometrical shapes, they are nevertheless equivalent in terms of the features considered in this paper. After a quick review of the principles of modelling a fractal porous medium we will define the PSF model within this conceptual framework using Neimark's definition. Equivalence with Perrier's

definition is given in Appendix A. First we will show how the PSF model actually gathers in a single structure the previous properties of fractal pore and solid number–size distributions and a pore–solid fractal interface. Then we will examine further properties of the PSF model: we will show that it combines in a geometrical pattern pores and solids at any stage of its development, and we will derive its scaling properties as regards the solid or pore mass, showing that a PSF in its general form is not a mass fractal. Finally, in Section 4, we will see that the PSF model reduces to a classic solid or pore mass fractal in two symmetric limiting cases, and, more generally, that the PSF model constitutes a general framework for analysing and comparing most of the previous fractal models of porous structures in soil science.

## 2. Fractal objects

### *2.1. Basic construction*

Construction of a deterministic self-similar fractal object of fractal dimension $D$, embedded in an Euclidean space of dimension $d$, is based on the following: First, an initiator (Fig. 1a) which defines a region of linear size $L$ in a space of Euclidean dimension $d$. This region can be divided into $N$ equal parts or subregions of linear size $L/n$ paving the whole object. Second, a generator (Fig. 1b) which (i) divides the $N$ parts into two sets of $Nz$ (shown in light gray in

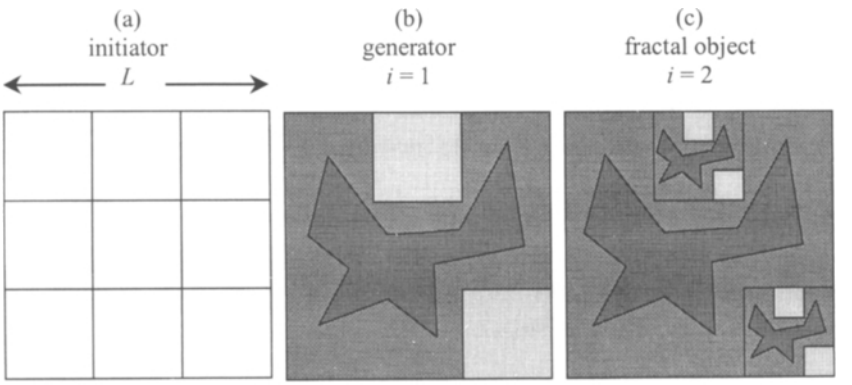


$d = 2, n = 3, z = 2/9, D = \log 2/\log 3 = 0.631, Nz = 2$

Fig. 1. Basic construction of a fractal object. In a space of Euclidean dimension $d$, the initiator (a) defines a region of linear size $L$ divided into $N$ equal parts. At the first iteration step, the generator (b) divides the $N$ parts into two sets of $Nz$ (light gray) and $N(1-z)$ (dark gray) subregions, determines the location of the $Nz$ subregions and defines a pattern inside the $N(1-z)$ subregions. At the next step, each of the $Nz$ subregions is replaced by a reduced replicate of the

Fig. 1b) and $N(1-z)$ (shown in dark gray in Fig. 1b) subregions ($z < 1$); (ii) defines a pattern inside the $N(1-z)$ subregions; (iii) defines the location of the $Nz$ subregions where the whole shape will be replicated.

Then a recursive process replaces each of the $Nz$ subregions by the generator reduced by the same ratio $1/n$ (Fig. 1c for step 2) and so forth at subsequent steps $i$.

### 2.2. *General properties*

The smaller subregions pave the whole initiator so that $N(L/n)^d = L^d$, that is

$$N = n^d \tag{1}$$

The fractal dimension $D$ follows from the number of replicates and the similarity ratio by

$$D = \frac{\log(Nz)}{\log(n)}. \tag{2}$$

Eq. (2) may be rearranged as:

$$Nz = n^D. \tag{3}$$

Combining Eqs. (1) and (3) we obtain

$$z = n^{D-d}, \tag{4}$$

and

$$nz = n^{D-(d-1)}. \tag{5}$$

Let $\mathcal{N}_z(r_i)$ be the number of replicates of size $r_i$ created at each step $i$ of the development of the structure. $r_i$ is defined by

$$r_i = L(n)^{-i} \quad \text{or} \quad n^i = L/r_i. \tag{6}$$

The number of replicates created at step 1 is: $\mathcal{N}_z(r_1) = Nz$.

At the next iteration step, $Nz$ replicates of size $r_2$ are created in each replicate of size $r_1$. Then at step $i$,

$$\mathcal{N}_z(r_i) = (Nz)\mathcal{N}_z(r_{i-1}) = Nz(Nz)^{i-1}.$$

or

$$\mathcal{N}_z(r_i) = (Nz)^i. \tag{7}$$

Using Eqs. (3) and (6) we obtain

$$(Nz)^i = (n^D)^i = (n^{-i})^{-D} = \left(L^{-1}r_i\right)^{-D} = L^D r_i^{-D}, \tag{8}$$

and

$$\mathcal{N}_z(r_i) = L^D r_i^{-D}. \tag{9}$$

Eq. (9) expresses the relationship between the number of replicates and their size as a power law function with an exponent equal to $-D$, where $D$ is the fractal dimension.

In a similar way, several parameters of the fractal object can also be expressed as power law functions of the resolution scale $r_i$. Formulas (10) to (12) will be useful in further derivations:From Eqs. (1) and (6)

$$N^i = L^d r_i^{-d}. \tag{10}$$

From Eqs. (4) and (6)

$$z^i = L^{D-d} r_i^{d-D}. \tag{11}$$

From Eqs. (5) and (6)

$$(nz)^i = L^{D-(d-1)} r_i^{(d-1)-D}. \tag{12}$$

### *2.3. Classical ways to model a porous medium*

Depending on the modeling context, the $N(1-z)$ subregions may represent different patterns. When fractal objects are used to model porous media made of a solid phase and a pore phase, the set of these $N(1-z)$ subregions represents generally an homogeneous material (shown in dark gray in Fig. 2) rather than a heterogeneous one (Fig. 1).

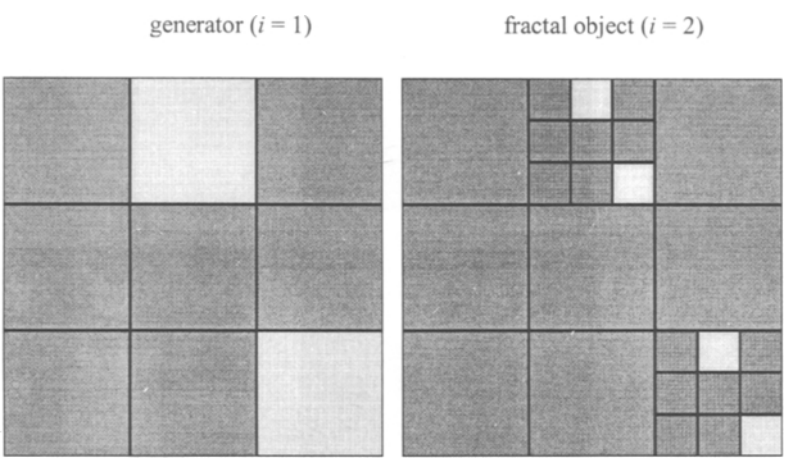


$d = 2, n = 3, z = 2/9, D = 0.631$

Fig. 2. The first two steps of the development of a fractal porous medium. The $N(1-z)$ (dark

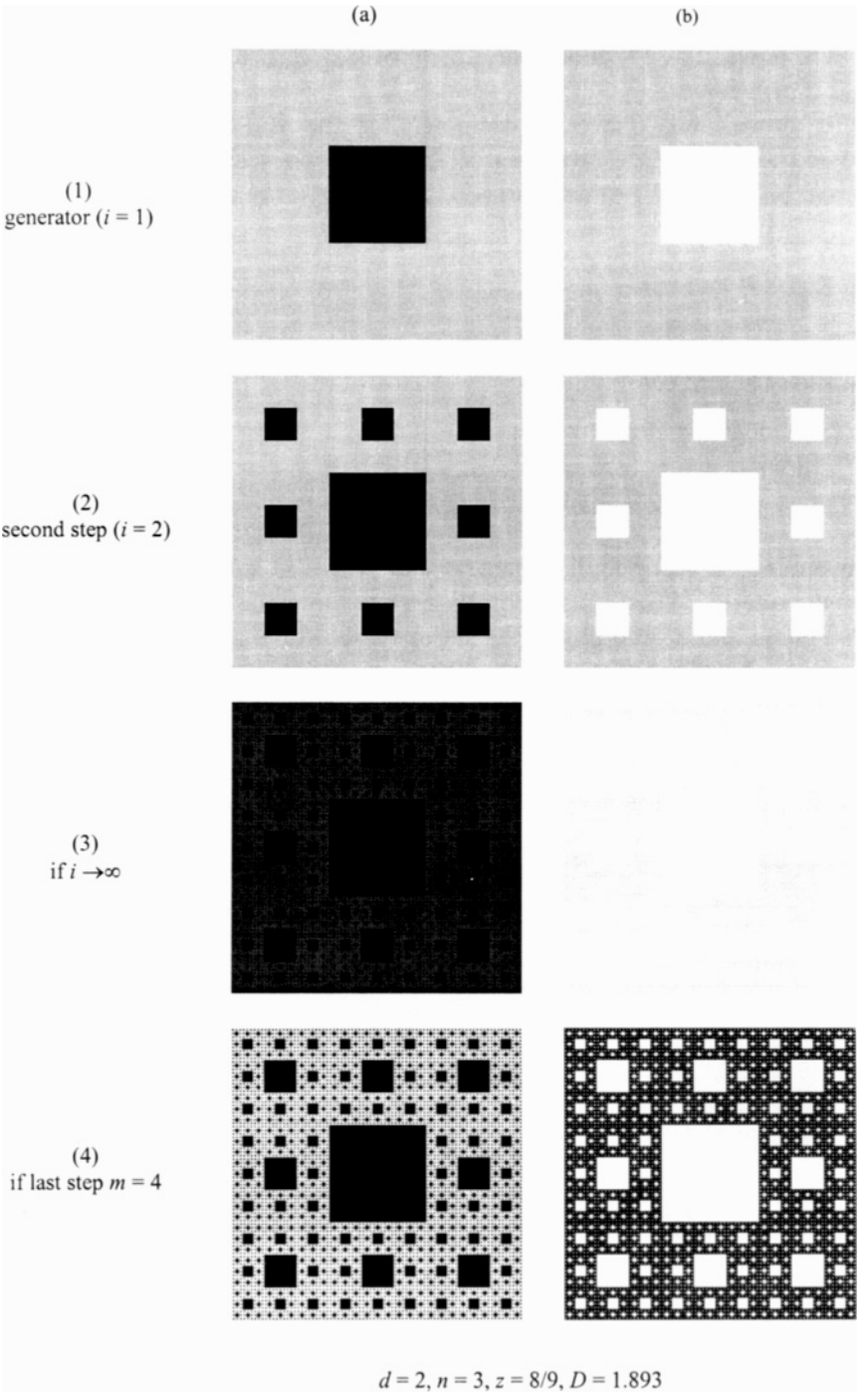
(a)
(b)
(1)
generator ($i = 1$)
(2)
second step ($i = 2$)
(3)
if $i \to \infty$
(4)
if last step $m = 4$
$d = 2, n = 3, z = 8/9, D = 1.893$

This homogeneous material can be identified either with the solid phase of the porous medium (shown in black in Fig. 3a.1) ('pore mass fractal') or the pore phase (shown in white in Fig. 3b.1) ('solid mass fractal').

At each step $i$, reduced copies of the generator in the $Nz$ subregions (shown in light gray in Fig. 3a.1) reveal new details at finer resolution scales (Fig. 3a.2 and b.2). These subregions constitute the 'fractal set'.

Two main options have been considered in previous studies: (i) Iterations are carried out ad infinitum, and the fractal set of $(Nz)^i$ subregions vanishes. The model represents only solid in the so-called pore mass fractal (Fig. 3a.3) or only pores in the solid mass fractal (Fig. 3b.3). (ii) A lower cutoff of scale is assumed, considering a finite number of recursive iterations $m$. The $(Nz)^m$ subregions created at the last iteration step $i = m$ will undergo no further division and the fractal set is assumed to model the complementary phase: in a pore mass fractal it is associated with the pore phase (shown in very light gray in Fig. 3a.4), and in a solid mass fractal it is associated with the solid phase (shown in black in Fig. 3b.4).

## 3. The PSF model

### *3.1. Definition*

Following the approach of Neimark, which combines pores and solids in the model in an interesting symmetrical setting, we define the $(1 - z)$ proportion of the generator as a mixture of pore and solid defined as follows:

$$(1 - z) = (x + y) \tag{13}$$

where $x$ denotes the proportion of pore phase, $y$ the proportion of solid phase and $z$ represents the proportion of the generator where the whole shape is replicated at each step. Solids and pores generated at each step are kept whereas the fractal set is transformed (Fig. 4).

Combining Eqs. (13), (1) and (2) we can express the fractal dimension as:

$$D = d + \frac{\log(1 - x - y)}{\log n}. \tag{14}$$

Eq. (14) shows that for a given Euclidean dimension $d$, the value of the fractal dimension $D$ of a PSF model depends only on the value of parameters $n$, $x$ and $y$.

Fig. 3. Classical example of a pore mass fractal (a) and a solid mass fractal (b) modeling a porous medium. The pore phase is shown in white or very light gray and the solid phase is shown in black. If infinite iterations are carried out, the pore mass fractal represents only solid (a.3) and the solid mass fractal only void (b.3). If a lower cutoff of scale is assumed, the fractal set (shown in light gray) is associated with the pore phase (a.4) or the solid phase (b.4).

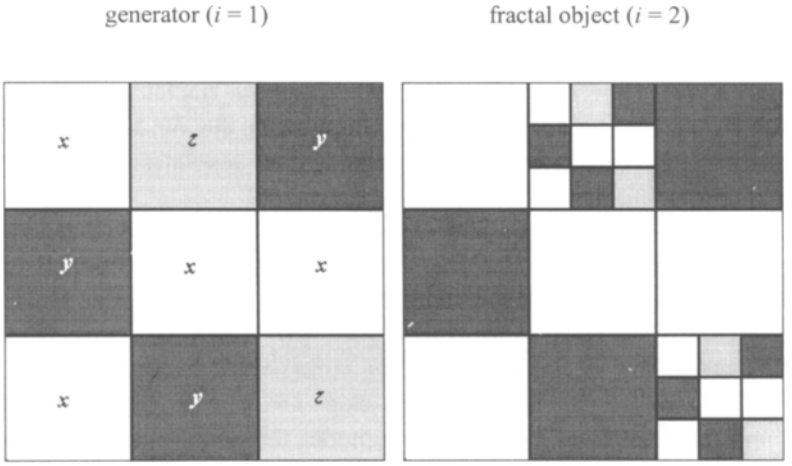


$d = 2, n = 3, z = 2/9, x = 4/9, y = 3/9, D = 2 + \log(1\text{-}7/9)/\log 3 = 0.631$

Fig. 4. Definition of a PSF model. The $N(1-z)$ subregions are divided into $Nx = 4$ pore subregions (white) and $Ny = 3$ solid subregions (black). The fractal set (iight gray) corresponds to $Nz = 2$ subregions where the whole shape is replicated at next iteration step.

Parameters $x$, $y$ and $z$ can be considered as probabilities ($x + y + z = 1$) and mathematical calculations can be done in a probabilistic way (Neimark, 1989). However, for sake of simplicity, we will consider here that $x$, $y$ and $z$ are proportions and $Nx$, $Ny$, $Nz$ refer to the number of subregions of each type, to get simple proofs based only on counting.

### *3.2. Counting elements*

At step 1, there are only elements of size $L/n$: $Nx$ pores, $Ny$ solids and $Nz$ subregions where the whole shape will be replicated at the next step.

At step 2, some elements of size $L/n$ are kept: $Nx$ pores, $Ny$ solids, whereas new elements of size $L(n)^{-2}$ are added: $Nx(Nz)$ pores, $Ny(Nz)$ solids, and $Nz(Nz)$ subregions where the whole shape will be replicated at the next step.

At step $i$, let $\mathcal{N}_x(r_i)$ and $\mathcal{N}_y(r_i)$ be the respective numbers of pores and solids of size $r_i$. Then

$$\mathcal{N}_x(r_i) = (Nx)\mathcal{N}_z(r_{i-1}) \quad \text{and} \quad \mathcal{N}_y(r_i) = (Ny)\mathcal{N}_z(r_{i-1}).$$

Using Eq. (7) we obtain

$$\mathcal{N}_x(r_i) = Nx(Nz)^{i-1}, \tag{15a}$$

and using Eq. (8),

$$\mathcal{N}_x(r_i) = \frac{Nx}{Nz}(Nz)^i = \frac{x}{z}L^D r_i^{-D}. \tag{15b}$$

In a symmetric way, we can write

$$\mathcal{N}_y(r_i) = Ny(Nz)^{i-1} \tag{16a}$$

or

$$\mathcal{N}_y(r_i) = \frac{Ny}{Nz}(Nz)^i = \frac{y}{z}L^D r_i^{-D}. \tag{16b}$$

More generally, the number of elements of size $r_i$ added at each step scales as a power $-D$ of the size:

$$\mathcal{N}_x(r_i) \propto r_i^{-D}, \quad \mathcal{N}_y(r_i) \propto r_i^{-D}, \quad \mathcal{N}_z(r_i) \propto r_i^{-D}. \tag{17}$$

### *3.3. Porosity*

Since $x$ represents the proportion of pores kept at step 1 by the generator, $zx$ is the proportion of pores added in the replicates generated at step 2, and so on. Thus the porosity $\phi_i$ at step $i$ is the following sum:

$$\phi = x + zx + z^2x + \ldots + z^{i-1}x = x\sum_{j=0}^{i-1} z^j = x\left(\frac{z^i - 1}{z - 1}\right). \tag{18}$$

From Eq. (13) we obtain

$$\phi_i = \frac{x}{x + y}(1 - z^i). \tag{19}$$

As the number of iterations $i$ increases to infinity, $z^i \to 0$ and Eq. (19) becomes (cf. Neimark, 1989 and Perrier, 1994):

$$\phi = \frac{x}{x + y} \tag{20}$$

Eq. (20) shows that a PSF model exhibits a finite value of the total porosity which depends only on the value of parameters $x$ and $y$.

### *3.4. Cumulative number–size distributions of pores and solids*

It is commonly assumed that, when a collection of self-similar objects exhibits a cumulative number–size distribution of objects in the form:

$$N(r) \propto r^{-D}. \tag{21}$$

the collection may be called fractal of dimension $D$ (Mandelbrot, 1983).

Let $N_x(r_i)$ and $N_y(r_i)$ be the respective numbers of pores and solids of size greater than or equal to $r_i$.

At iteration step $i = 1$, the number of pores is $N_x(r_1) = \mathcal{N}_x(r_1) = Nx$.

For $i = 2$, $N_x(r_2) = N_x(r_1) + \mathcal{N}_x(r_2) = Nx + Nx(Nz) = Nx(1 + Nz)$, and at any step $i$:

$$N_x(r_i) = N_x(r_{i-1}) + \mathcal{N}_x(r_i) = Nx\left(1 + Nz + (Nz)^2 + \ldots + (Nz)^{i-1}\right).$$

Summation of this geometric series of ratio $Nz$ yields:

$$N_x(r_i) = Nx\sum_{j=0}^{i-1}(Nz)^j = Nx\left(\frac{(Nz)^i - 1}{Nz - 1}\right). \tag{22}$$

If $Nz > 1$, as $i \to \infty$, $(Nz)^i \gg 1$ and $((Nz)^i - 1) \cong (Nz)^i$. Using Eq. (8) one gets

$$N_x(r_i) \cong \frac{Nx}{Nz - 1}(Nz)^i = \frac{Nx}{Nz - 1}L^D r_i^{-D}. \tag{23a}$$

In a symmetric way, the cumulative number of solids greater than or equal to $r_i$ is obtained by substituting $x$ by $y$ in Eq. (23a)

$$N_y(r_i) \cong \frac{Ny}{Nz - 1}(Nz)^i = \frac{Ny}{Nz - 1}L^D r_i^{-D}. \tag{23b}$$

Eqs. (23a) and (23b) are discrete analogs of Eq. (21). They can be rewritten as:

$$N_x(r_i) \propto r_i^{-D}, \tag{24a}$$

and

$$N_y(r_i) \propto r_i^{-D}. \tag{24b}$$

Eqs. (24a) and (24b) show the symmetry exhibited by the PSF model: both the pore number–size distribution and the solids number–size distribution assume a power law form with identical exponent $-D$, where $D$ is the fractal dimension.

### *3.5. Pore–solid interface*

Another fractal property commonly observed in some porous media is related to the measurement of the pore–solid interface.

A surface is called fractal of dimension $D$ when its area $S(l)$ measured with units $l^{d-1}$ scales as $l^{d-1-D}$ where $d - 1 < D < d$, that is:

$$\frac{S(l)}{l^{d-1}} \propto l^{-D}. \tag{25}$$

Neimark (1989) has studied the properties of "the surface of a self similar multiscale percolation system". For completeness, we include here our own derivation of the interface behavior in a PSF model. The area $S(i)$ of the pore–solid interface (perimeter when $d = 2$, surface when $d = 3$) can be first approximated by summing the surfaces of all the boundaries of the solid elements which have been created after $i$ iteration steps. These solid elements are squares ($d = 2$) or cubes ($d = 3$) of size greater than or equal to $r_i$. Each solid subregion of linear size $r_i$ has a surface $2dr_i^{d-1}$ and the cumulative boundary of the solid elements, denoted $S_y(i)$ is equal to:

$$S_y(i) = \sum_{j=1}^{i} \left(\mathcal{N}_y(r_j)\right)\left(2dr_j^{d-1}\right). \tag{26}$$

Introducing Eqs. (16a) and (6), we obtain

$$S_y(i) = 2d\sum_{j=1}^{i} Ny(Nz)^{j-1}\left(Ln^{-j}\right)^{d-1}, \tag{27}$$

$$S_y(i) = 2dNyL^{d-1}\sum_{j=1}^{i}(Nz)^{j-1}\left(n^{-(d-1)}\right)^{j} = 2dNy\left(\frac{L}{n}\right)^{d-1}\sum_{j=1}^{i}\left(\frac{Nz}{n^{d-1}}\right)^{j-1}. \tag{28}$$

Using Eq. (1), we get

$$S_y(i) = 2dn^d y\left(\frac{L}{n}\right)^{d-1}\sum_{j=1}^{i}\left(\frac{n^d z}{n^{d-1}}\right)^{j-1} = 2dy\left(\frac{L}{n}\right)^{-1}L^d\sum_{j=1}^{i}(nz)^{j-1}. \tag{29}$$

The value of the geometric series in Eq. (29) depends on the value of $nz$. If $nz = 1$,

$$S_y(i) = 2dy\left(\frac{L}{n}\right)^{-1}L^d i. \tag{30}$$

From Eq. (6) we obtain $i = (\log\ L/r_i)/(\log\ n)$ and Eq. (30) becomes

$$S_y(i) = \frac{2dnyL^{d-1}}{\log n}\log\frac{L}{r_i}. \tag{31}$$

If $nz \neq 1$,

$$S_y(i) = 2dy\left(\frac{L}{n}\right)^{-1}L^d\frac{(nz)^i - 1}{nz - 1}. \tag{32}$$

From Eq. (12) we have $(nz)^i = L^{D-d+1} r_i^{d-1-D}$ and Eq. (32) becomes

$$S_y(i) = y\frac{2dnL^{d-1}}{1-nz} + y\frac{2dnL^D}{nz-1} r_i^{d-1-D}. \tag{33a}$$

In a symmetric way, the cumulative area of the boundaries of pores created at $i$ iteration steps is given by

$$S_x(i) = x\frac{2dnL^{d-1}}{1-nz} + x\frac{2dnL^D}{nz-1} r_i^{d-1-D}. \tag{33b}$$

The actual interface $S(i)$ between solids and pores cannot be calculated so simply, because the location of the solid and pores subregions in the model must be taken into account. At each step $i$, we consider a constant number $Ny$ (or $Nx$) of solid (or pore) subregions but randomly distributed in space. If two solid subregions have a common side, this side belongs to the total boundary measured by $S_y(i)$, but not to the solid–pore interface. Thus $S(i) < S_x(i)$ and $S(i) < S_y(i)$.

In a random realization, assuming $x \neq 0$, $y \neq 0$, the calculation of $S(i)$ can be done in a probabilistic manner. As the number of iterations increases to infinity, the fractal set of $(Nz)^i$ subregions vanishes and the probability $p_x(i)$ that an arbitrary chosen point on the solid boundary belongs to the interface is equal to the probability that the neighboring point outside the solid is located in a pore subregion. Thus as infinite iterations are carried out, $p_x(i) \to_{i\to\infty} \phi$, where $\phi$ is the porosity.

Then, using Eq. (19)

$$S(i) = p_x(i)S_y(i) = \phi S_y(i) = \frac{x}{x+y} S_y(i) \tag{34a}$$

or in a symmetrical way we could get

$$S(i) = p_y(i)S_x(i) = (1-\phi)S_x(i) = \frac{y}{x+y} S_x(i). \tag{34b}$$

and from Eqs. (33a) and (33b), Eqs. (34a) and (34b) are strictly identical.

Three cases must be distinguished.

(i) If $D = d-1$ (that is $nz = 1$). From Eqs. (31) and (34a) we obtain

$$S(i) = \frac{xy}{x+y}\frac{2dnL^{d-1}}{\log n}\log\frac{L}{r_i}. \tag{35}$$

The surface of the solid–pore interface approaches infinity approximately as the logarithm of the inverse of $r_i$.

If $nz \neq 1$

(ii) if $D < d-1$ (that is $nz < 1$).

Using Eqs. (33a) and (34a) we get

$$S(i) = \frac{x}{x+y}\left(\frac{2dynL^{d-1}}{1-nz} + \frac{2dynL^{D}}{nz-1} r_i^{d-1-D}\right) \tag{36a}$$

or from Eqs. (33b) and (34b)

$$S(i) = \frac{y}{x+y}\left(\frac{2dxnL^{d-1}}{1-nz} + \frac{2dxnL^{D}}{nz-1} r_i^{d-1-D}\right). \tag{36b}$$

As $i \to \infty$, $r_i \to 0$, $r_i^{d-1-D} \to 0$ thus

$$S(i) \xrightarrow[i\to\infty]{} \frac{xy}{x+y} \frac{2dnL^{d-1}}{1-nz}. \tag{37}$$

The surface of the solid–pore interface approaches a finite value.

(iii) If D > d − 1 (that is $nz > 1$).

Eqs. (36a) and (36b) may be rewritten as

$$S(i) = \frac{xy}{x+y} \frac{2dnL^{d-1}}{1-nz} + \frac{xy}{x+y} \frac{2dnL^{D}}{nz-1} r_i^{d-1-D} \tag{38}$$

As $i \to \infty$, $r_i \to 0$, and $r_i^{d-1-D} \to \infty$. As the second term of the right side of Eq. (38) grows without limit, the first constant term becomes negligible. Thus

$$S(i) \xrightarrow[i\to\infty]{} \frac{xy}{x+y} \frac{2dnL^{D}}{nz-1} r_i^{d-1-D}, \tag{39}$$

or (cf. Eq. (25)):

$$\frac{S(i)}{r_i^{d-1}} \xrightarrow[i\to\infty]{} C_1 r_i^{-D} \tag{40}$$

where $C_1$ is a constant. The area of the pore–solid interface approaches infinity as a power law function of the resolution scale. It is fractal of dimension $D$.

### *3.6. Mass of pores and solids*

Fractal models often refer to so-called mass fractal properties, where the term mass actually means the solid or pore volume (the mass is proportional to the volume if a uniform density is assumed).

An object is called a mass fractal if the number $B(r)$ of boxes of size $r$ needed to cover it scales as $r^{-D}$

$$B(r) \propto r^{-D} \tag{41a}$$

or if its mass $M(r)$ measured with units $r^d$ scales as $r^{-D}$

$$\frac{M(r)}{r^d} \propto r^{-D}. \tag{41b}$$

In the PSF model, measuring mass with a box-counting method, let $B_y(i)$ be the number of boxes of size $r_i$ needed to cover the volume of solids.

At the start, $B_y(0) = 1$ box of size $r_0 = L$ covers the whole structure.

At first step, $B_y(1) = Ny + Nz$ boxes of size $r_i$ are needed to cover the solids.

At step 2, there are $B_y(2) = N(Ny) + NzB_y(1)$ boxes of size $r_2$, and at step $i$, there will be: $B_y(i) = N^i y + NzB_y(i-1)$ boxes of size $r_i$ covering the volume of solids. We can show by recurrence that

$$B_y(i) = N^i y\left(\frac{z^i - 1}{z - 1}\right) + (Nz)^i \tag{42}$$

$$\begin{aligned} B_y(i) &= N^i y + NzB_y(i-1) = N^i y + Nz\left(N^{i-1} y\left(\frac{z^{i-1} - 1}{z - 1}\right) + (Nz)^{i-1}\right) \\ &= N^i y + Nz\left(N^{i-1} y\left(\frac{z^{i-1} - 1}{z - 1}\right)\right) + (Nz)^i = N^i y\left(1 + z\left(\frac{z^{i-1} - 1}{z - 1}\right)\right) + (Nz)^i \\ &= N^i y\left(\frac{z - 1 + z^i - z}{z - 1}\right) + (Nz)^i = N^i y\left(\frac{z^i - 1}{z - 1}\right) + (Nz)^i. \end{aligned}$$

Thus

$$B_y(i) = N^i y\left(\frac{z^i - 1}{z - 1}\right) + (Nz)^i = \frac{N^i yz^i - N^i y + z(Nz)^i - (Nz)^i}{z - 1}$$

$$= \frac{(Nz)^i(y + z - 1) - N^i y}{z - 1}$$

or

$$B_y(i) = \frac{x(Nz)^i + N^i y}{1 - z},$$

and introducing Eq. (13)

$$B_y(i) = \frac{x}{x + y}(Nz)^i + \frac{y}{x + y}N^i. \tag{43}$$

Using Eqs. (8) and (10), Eq. (43) can be rewritten as

$$B_y(i) = \frac{y}{x + y}L^d r_i^{-d} + \frac{x}{x + y}L^D r_i^{-D}. \tag{44a}$$

In the same way, covering the pores needs a number $B_x(i)$ of boxes varying as

$$B_x(i) = \frac{x}{x + y}L^d r_i^{-d} + \frac{y}{x + y}L^D r_i^{-D}. \tag{44b}$$

The symmetric expressions for $B_x(i)$ and $B_y(i)$ assume the form of the sum of two power law functions of the box size $r_i$ with exponents $-d$ and $-D$, where $d$ is the Euclidean dimension and $D$ the fractal dimension. We conclude that, in a PSF model, neither the solid phase nor the pore phase exhibit fractal scaling. The PSF in its general form is not a true mass fractal.

The volumes of pores and solids measured with resolution $r_i$, which we denote by $M_x(i)$ and $M_y(i)$ respectively follow immediately from Eqs. (44a) and (44b) as

$$M_x(i) = B_x(i) r_i^d = \frac{x}{x+y} L^d + \frac{y}{x+y} L^D r_i^{d-D}, \tag{45a}$$

$$M_y(i) = B_y(i) r_i^d = \frac{y}{x+y} L^d + \frac{x}{x+y} L^D r_i^{d-D}. \tag{45b}$$

If infinite iterations are carried out, $M_x(i)$ and $M_y(i)$ approach finite values

$$M_x(i) \to \frac{x}{x+y} L^d = \phi L^d, \tag{46a}$$

$$M_y(i) \to \frac{y}{x+y} L^d = (1-\phi) L^d, \tag{46b}$$

as required.

## 4. Discussion

### *4.1. A new, consistent geometric representation of a two-phase porous structure*

Many attempts to model fractal properties of complex real porous media involve rather simple geometric figures: the Sierpinki carpet, the Menger sponge, the fractal cube considered by Rieu and Sposito and many types of fractal, lacunar models (see Rieu and Perrier, 1997, for a review). Several models of fractal surface have been first proposed based on the Von Koch curve (Pfeifer and Avnir, 1983) or similar shapes. These theoretical models generally represent only the pore–solid interface and their use to model soil structure is limited. Mass fractals constitute a great improvement in the sense that they closely associate both solid and pore phases in a geometrical frame. Two main types of mass fractal model are commonly used (Rieu and Perrier, 1997). Pore mass fractals exhibit a fractal pore 'mass' by introducing a fractal cumulative number–size distribution of elements identified with solids in a fractal set identified with the pore phase (Fig. 3a). Solid mass fractals exhibit a fractal solid mass by introducing a fractal cumulative number–size distribution of elements identified with pores in a fractal set identified with a solid phase (Fig. 3b). However it should be noted that if, as in a true mathematical fractal, infinite

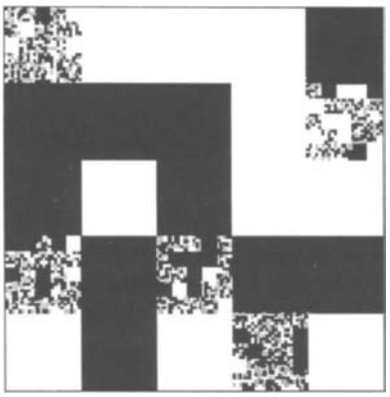

$d = 2, n = 5, z = 0.2, x = y = 0.4, D = 1, i = 3$

Fig. 5. Randomized PSF based on a square pattern. In this example, $D = 1$.

iterations are carried out in the recursive construction of the mass fractal, the pore space vanishes in pore mass fractals while the solid space vanishes in solid mass fractals. Paradoxically in this limit a pore mass fractal can represent a particle size distribution but no pores (Tyler and Wheatcraft, 1992, cf. Fig. 3a.3) and a solid mass fractal can represent a pore size distribution but no solids (Tyler and Wheatcraft, 1990, cf. Fig. 3b.3). Both may represent a purely theoretical fractal pore–solid interface, but neither in the limit is able to represent a two-phase porous medium.

Since it always associates in a single geometric shape two fractal cumulative number–size distributions of elements with a fractal set, the PSF model presented in this paper, is a more advanced fractal model of porous medium. Irrespective of the range of scale over which the structure is developed, both a solid phase and a pore phase are modelled by two power law distributions whereas the fractal set can be identified with either the solid or the pore phase if a lower cut-off of scale is considered or vanishes if infinite iterations are carried out (Figs. 5 and 6). This matter is not addressed by Neimark (1989) who was not interested in the properties of the solid whereas it is a central point of view in the approach of Perrier (1994).

A PSF and a mass fractal exhibit structure over a range of scales specified by the modeller. A well-known property of a solid mass fractal is that when this structure extends to arbitrarily small scales the porosity of the model approaches unity, assuming that the fractal set is identified with the solid phase and its complement is identified with the pore phase. When these identifications are reversed (pore mass fractal), the porosity approaches zero. These limiting values of porosity clearly have no physical relevance. This is in marked contrast to the porosity of the new model which is designed to attain limiting value of total

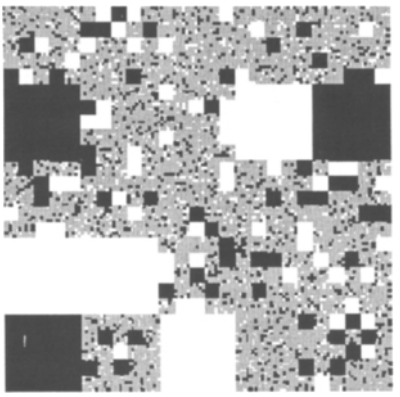

$d = 2, n = 5, z = 0.72, x = y = 0.14, D = 1.796, i = 3$

Fig. 6. Randomized PSF based on a square pattern. General case of $d - 1 \leq D < d$.

porosity $\phi$ lying between these two extremes and depending only on the values of the parameters $x$ and $y$, that is the proportion of pore space and solid kept at each step. This peculiarity of PSF model is thus an important extension to the range of models available for modelling multiscale porous media and specifically soil structures.

*4.2. The PSF model compared to classic mass fractal models*

The scaling of the mass of solid or pores is a crucial point in modelling soil structures. This matter is not developed by Neimark (1989) neither by Perrier (1994), but the interesting scaling properties of a PSF deserve attention. A mass fractal possesses characteristic scaling properties which identify it as a fractal structure (see Rieu and Perrier, 1997 for a review). A PSF in its general form is not a mass fractal and its scaling properties are different. For a mass fractal a power law scaling relation is obtained from which the mass fractal dimension may be inferred. For a PSF, as shown by Eqs. (44a) and (44b), the corresponding relation assumes the form of the sum of an Euclidean power law function and a fractal power law function. Thus neither the solid mass nor the pore mass properly exhibit a fractal scaling. Whilst the scaling relations identify the PSF as a structure other than a mass fractal, it is important to note that it can nevertheless easily be confused with that of a mass fractal if it is examined over a narrow range of scales. Some degree of caution is thus required in the use of any algorithm to analyse soil data, and the theory suggests that some soils might have been called mass fractals on approximate grounds and might be better modelled by a PSF.

In the case $x = 0$, the PSF model reduces to a fractal number–size distribution of solids and a fractal set. If the latter is associated with the pore phase, the result is a pore mass fractal. From Eqs. (44a) and (44b) we then have that $B_v(i)$

exhibits Euclidean scaling while $B_x(i)$ exhibits fractal scaling as required. Similarly, if $y = 0$ and the fractal set is associated with the solid phase we obtain a solid mass fractal. Then Eqs. (44a) and (44b) show that $B_y(i)$ exhibits fractal scaling whilst $B_x(i)$ exhibits Euclidean scaling. Thus mass fractal models appear as degenerate cases of a PSF.

Both a PSF in its general form and a mass fractal exhibit self-similar properties in the sense that where local structure occurs, it is similar to the whole. The essential difference between the two which leads to the different scaling properties as shown above is that a PSF model is in places devoid of such local structure, whereas a mass fractal is not.

### *4.3. Pore and solid number–size distributions*

In this paper, we use the expression 'solid' or 'solid element' instead of 'particle' or 'grain' used in other works (e.g., Haverkamp and Parlange, 1986). But we do not mean 'solid, porous aggregate' in the sense of Rieu and Sposito (1991a,b) or Crawford et al. (1995). We clarify this statement by noting that we identify 'particles' with the primary elements of a soil structure. The number–size distribution of solids and pores differ significantly between a mass fractal and a PSF. If a lower cut-off of scale is considered, in a solid mass fractal, i.e., a fractal set identified with the solid phase, the solids are of equal size (cf. Bird et al., 1996), whilst the complementary pore space exhibits a power law number–size distribution of pores, with a power law exponent equal to $-D$. Similarly for a pore mass fractal, i.e., a fractal set identified with the pore phase, the pores are of equal size while the solids size distribution is power law. In contrast, in a PSF symmetry exists between the pore-size and solid-size distributions. Specifically both distributions assume a power law form with identical power law exponent $-D$ (cf. Perrier, 1994), where $D$ is the fractal dimension of the pore–solid interface. The existence of such a symmetry is interesting in relation to the established view that solid-size distributions convey information relating to porosity and pore–size distributions and consequently soil hydraulic properties, through relations which map known solid sizes onto inferred pore sizes (e.g., Arya and Paris, 1981; Haverkamp and Parlange, 1986). A PSF provides an example of a porous material where this view appears to some extent valid. Also of interest are previous suggestions that power law fractal pore-size and particle-size distributions can coexist within a soil (e.g., Tyler and Wheatcraft, 1992, who acknowledged that "a theoretical development is not yet available"). Again a PSF, in contrast to a mass fractal, provides an explicit example of one such model where this situation occurs.

### *4.4. Pore–solid interface*

In a mass fractal the pore–solid interface is the boundary between the solid (or the pores) distributed in the fractal pore (or solid) mass. This surface grows

as a power law of the resolution scale. It is fractal of dimension $D$. When the fractal structure is developed ad infinitum, the fractal pore (or solid) mass vanishes and the interface has no physical relevance. However, if a lower cut-off of scale is used, the area of the interface has a finite value and the fractal surface can model a real solid–pore interface. Neimark (1989) has shown that in his 'self-similar multiscale percolation system' both fractal and nonfractal surfaces can arise depending on the value of $nz$ and consequently $D$. When a fractal surface occurs, this $D$ is also the dimension of the surface. In our own derivation of the scaling behavior of the interface, based on the number–size distribution, we obtain the same result. Because it always associates both solid and pore phases, the PSF model exhibits a pore–solid interface even if the structure is developed towards infinity. Depending on the value of the fractal dimension, the area of the interface assume the form of a logarithmic function of the length scale $r_i$ (in the case of $D = d - 1$, cf. Eq. (35)), or of a fractal power law ($D > d - 1$; cf. Eq. (39)), or it tends towards a constant finite value (for $D < d - 1$; cf. Eq. (37)).

It follows from the above that whilst a porous material can exhibit self-similar properties and fractal number–size distributions of its elements (pores, solids or both) this does not imply a fractal surface. This only occurs when $D > d - 1$ (see e.g., Pfeifer and Avnir, 1983; Friesen and Mikula, 1987; Toledo et al., 1990). Here mathematical calculation of the area of the interface brings evidence of this critical value $d - 1$. Fig. 5 presents the particular case of a PSF model with a fractal dimension $D = d - 1$. It is interesting to note that although not visually obvious, the solid–pore interface is not fractal in this instance as it

Table 1
Scaling properties of the PSF model and of pore and solid mass fractal models

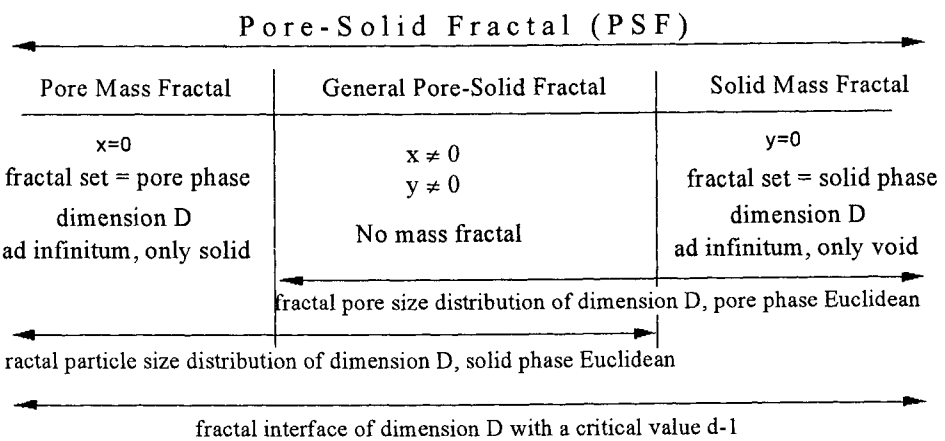
Pore-Solid Fractal (PSF)
Pore Mass Fractal
General Pore-Solid Fractal
Solid Mass Fractal
x=0
fractal set = pore phase
dimension D
ad infinitum, only solid
x ≠ 0
y ≠ 0
No mass fractal
y=0
fractal set = solid phase
dimension D
ad infinitum, only void
fractal pore size distribution of dimension D, pore phase Euclidean
ractal particle size distribution of dimension D, solid phase Euclidean
fractal interface of dimension D with a critical value d-1

Table 2
Summary of the features of the PSF model

| PSF model parameters:<br>[$x$→pore sub-regions]<br>[$y$→solid sub-regions]<br>[z→fractal set]<br>[1/n = similarity ratio] | Pore Mass Fractal<br>$x = 0$ | General PSF<br>$x \neq 0,\ y \neq 0$ | Solid Mass Fractal<br>$y = 0$ |
|---|---|---|---|
| Basic relations<br>(Equations 1 & 13) | $N = n^d$<br>$1 - z = y$ | $N = n^d$<br>$1 - z = x + y$ | $N = n^d$<br>$1 - z = x$ |
| Fractal dimension<br>(Equation 14) | $D = d + \dfrac{\log(1-y)}{\log n}$ | $D = d + \dfrac{\log(1-x-y)}{\log n}$ | $D = d + \dfrac{\log(1-x)}{\log n}$ |
| Total porosity<br>(Equation 20) | $\phi = 0$ | $\phi = \dfrac{x}{x+y}$ | $\phi = 1$ |
| Number-size distribution<br>of pores (Equation 23a) | none | $N_x(r_i) \cong \dfrac{Nx}{Nz-1} L^D r_i^{-D}$ | $N_x(r_i) \cong \dfrac{Nx}{Nz-1} L^D r_i^{-D}$ |
| Number-size distribution<br>of solids (Equation 23b) | $N_y(r_i) \cong \dfrac{Ny}{Nz-1} L^D r_i^{-D}$ | $N_y(r_i) \cong \dfrac{Ny}{Nz-1} L^D r_i^{-D}$ | none |

| | | | |
|---|---|---|---|
| Mass of pores<br>(Equations 8 & 45a) | If fractal set $(Nz)^i \equiv$ pores<br>$\frac{M_z(i)}{r_i^d} = (Nz)^i = L^D r_i^{-D}$ | $\frac{M_x(i)}{r_i^d} = \frac{x}{x+y} L^d r_i^{-d} + \frac{y}{x+y} L^D r_i^{-D}$ | $\frac{M_x(i)}{r_i^d} = L^d r_i^{-d}$ |
| Mass of solids<br>(Equations 45b & 8) | $\frac{M_y(i)}{r_i^d} = L^d r_i^{-d}$ | $\frac{M_y(i)}{r_i^d} = \frac{y}{x+y} L^d r_i^{-d} + \frac{x}{x+y} L^D r_i^{-D}$ | If fractal set $(Nz)^i \equiv$ solids<br>$\frac{M_z(i)}{r_i^d} = (Nz)^i = L^D r_i^{-D}$ |
| Pore-solid interface<br>$D = d - 1$<br>(Equation 35) | If fractal set $(Nz)^i \equiv$ pores<br>$r_i > 0$<br>$S_y(i) = y \frac{2dnL^{d-1}}{\log n} \log \frac{L}{r_i}$ | No condition on fractal set $(Nz)^i$<br>No limitation on $r_i$<br>$S(i) = \frac{xy}{x+y} \frac{2dnL^{d-1}}{\log n} \log \frac{L}{r_i}$ | If fractal set $(Nz)^i \equiv$ solids<br>$r_i > 0$<br>$S_x(i) = x \frac{2dnL^{d-1}}{\log n} \log \frac{L}{r_i}$ |
| $D < d - 1$<br>(Equations 33 & 37) | $S_y(i) = y \frac{2dnL^{d-1}}{1-nz} + y \frac{2dnL^D}{nz-1} r_i^{d-1-D}$ | $S(i) \xrightarrow[i \to \infty]{} \frac{xy}{x+y} \frac{2dnL^{d-1}}{1-nz}$ | $S_x(i) = x \frac{2dnL^{d-1}}{1-nz} + x \frac{2dnL^D}{nz-1} r_i^{d-1-D}$ |
| $D > d - 1$<br>(Equations 33 & 39) | $S_y(i) = y \frac{2dnL^{d-1}}{1-nz} + y \frac{2dnL^D}{nz-1} r_i^{d-1-D}$ | $S(i) \xrightarrow[i \to \infty]{} \frac{xy}{x+y} \frac{2dnL^D}{nz-1} r_i^{d-1-D}$ | $S_x(i) = x \frac{2dnL^{d-1}}{1-nz} + x \frac{2dnL^D}{nz-1} r_i^{d-1-D}$ |

grows in a logarithmic fashion when the structure is developed. Apart from the relatively small extension of the fractal set, nothing points out why the area of the solid–pore interface is on the critical point between a nonfractal surface whose area tends towards a finite constant value and a fractal surface whose area tends towards infinity when the structure is developed ad infinitum (Fig. 6).

Calculations of the area of the interface have been derived for $x \neq 0$, $y \neq 0$. Fig. 3 gives an illustration of the limiting cases $x = 0$, $y = 0$. When $x = 0$, the PSF becomes a pore mass fractal combining a fractal distribution of solids and a fractal set. Now if the supplementary assumption is made that the fractal set of $(Nz)^i$ subregions represent pores we can still define and measure a pore–solid interface. Symmetrically a pore–solid interface can be defined when $y = 0$. The general results concerning the fractal character of the pore–solid interface hold in these limiting cases.

### *4.5. Summary*

The scaling properties of the PSF model are summarized in Table 1. It can be observed how the PSF is a generalization of mass fractal which may be viewed as special albeit degenerate case. Thus the PSF model can be used in many cases for the following purposes.

1. Either to represent soils which have been shown to be surface fractals, in the same way as simple surface models have already been used (e.g., Pfeifer and Avnir, 1983; de Gennes, 1985).

2. Or to represent soils which exhibit a fractal pore size distribution, in the same way as simple lacunar fractal models have already been used (e.g., Tyler and Wheatcraft, 1990; Rieu and Sposito, 1991a).

3. Or to represent soils which exhibit a fractal solid size distribution, in the same way as simple models of fractal number–size distributions have already been used (e.g., Tyler and Wheatcraft, 1992; Wu et al., 1993)

4. Or to represent soils which exhibit a fractal solid mass, in the same way as simple models of a fractal solid phase have already been used (e.g., Rieu and Sposito, 1991a; Young and Crawford, 1991).

5. Or to represent soils which exhibit a fractal pore mass, in the same way as simple models of a fractal pore phase have already been used (e.g., Katz and Thompson, 1985; Ghilardi et al., 1993).

In addition, because the PSF model is a self-consistent geometric model of the whole porous structure, whatever the particular fractal property it has be designed to model, it gives also information about the possible scaling behaviour of the other properties of the porous structure (cf. Table 2). For example, if we consider a soil exhibiting a fractal pore size distribution (Perrier et al., 1996), the PSF model suggests which properties of the solid phase and which hydraulic properties could be associated to this particular pore size distribution.

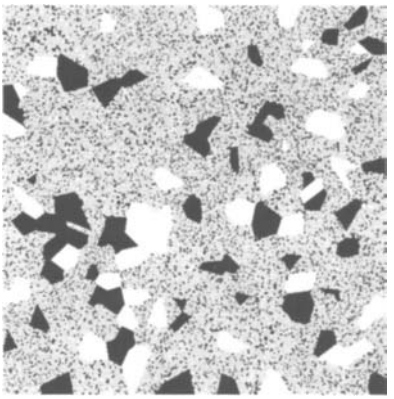

$d = 2, n = 20, z = 0.75, x = y = 0.125, D = 1.904, i = 2$

Fig. 7. Randomized PSF based on a polyedral pattern, with a division process obtained by a Voronoï tessellation. General case of $d - 1 \leq D < d$.

### *4.6. Extension: effect of different local geometric patterns*

The ability of a fractal model of porous medium to represent a soil structure depends on its structural features: number–size distribution of its components, porosity, fractal scaling of the pore and solid phases, fractal scaling of the pore–solid interface, and on the behaviour ad infinitum of these properties. But this ability also depends strongly on the geometric patterns of the model. As an example, two realizations of the PSF model are presented Figs. 6 and 7. The first one is based on a square pattern. In the second, the division of the initiator is obtained by a Voronoï tessellation process (Perrier, 1994) and the basic pattern is polyhedral. In both cases, the proportions $x$, $y$ and $z$ have a constant value and the location of the pore and solid subregions is randomly determined at each iteration step. At any stage of its development, both structures exhibit the same properties: total porosity value lying between 0 and 1, fractal number–size distribution of pores and solids, nonfractal scaling of the pore and solid phases and fractal scaling of the pore–solid interface.

Improved geometric patterns may help in the construction of more realistic models of soil structure. As an example Figs. 8 and 9 present structures equivalent respectively to those presented in Figs. 6 and 7 in terms of their basic properties, but here the pores are located around the solids. Instead of keeping $Ny$ solids and $Nx$ pores among the $N(1 - z)$ subregions, an homothetic reduction of ratio $k$ replaces each subregion of size $r_i^d$ among the $N(1 - z)$ ones by one solid of size $k^d r_i^d$ surrounded by one pore of size $(1 - k^d) r_i^d$. This pattern proposed by Perrier (1994) is defined by a set of three parameters ($N$, $z$ and $k$) whereas Neimark's percolation system and PSF model use ($N$, $x$ and $y$). Equivalence between these two approaches is given in Appendix A.

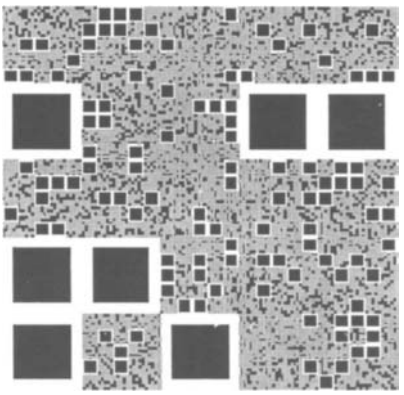

$d = 2, n = 5, z = 0.72, x = y = 0.14, D = 1.796, k = 0.707, i = 3$

Fig. 8. PSF numerically equivalent to the example presented in Fig. 6. Here, the void phase is located around the solid, resulting in a very different shape.

Obviously, some of these examples resemble soil structures more than others. In particular, each of them exhibits a specific kind of pore connectivity. As an illustration of this latter, Fig. 10 presents a mass fractal variation of the Sierpinski Carpet carried out by Perrier (1994). This degenerate form of PSF model is a 2D representation of a random realization of the fractal cube considered by Rieu and Sposito (1991a), fragmented by a Voronoï tessellation (Perrier et al., 1995). This fractal object is a solid mass fractal where a fractal cumulative number–size distribution of fractures is associated with a solid phase that exhibits a fractal scaling. As in the model presented in Fig. 3b, when this structure extends to arbitrarily small scales its porosity approaches unity.

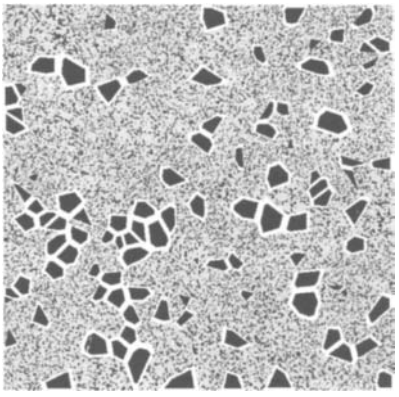

$d = 2, n = 20, z = 0.75, x = y = 0.125, D = 1.904, k = 0.707, i = 2$

Fig. 9. PSF numerically equivalent to the example presented in Fig. 7, with a void phase

$d = 2, n = 2.65, z = 0.92, x = 0.08, y = 0, D = 1.919, i = 5$

Fig. 10. 2D representation of a random realization of the fractal cube considered by Rieu and Sposito (1991a,b,c), fragmented by a Voronoï tessellation. In this solid mass fractal, the fractal set is associated to the solid phase.

Unfortunately the network of fractures appears excessively connected for modelling a soil pore space.

## 5. Conclusion

In conclusion, the PSF model originating with Neimark (1989) and Perrier (1994) can be viewed as a fully self-consistent fractal model of general application in the sense that it is not tied to a specific local geometry. Whilst this is equally true of a mass fractal, the generality of a PSF obviously exceeds that of a mass fractal. Mass fractals have already featured prominently in modelling complex porous materials and it remains to be seen to what extent the wider class of PSF models follows this trend.

Neither the pore phase nor the solid phase of a general PSF exhibit mass fractal scaling. On the other hand the pore–solid interface is fractal for $D > d - 1$. At any stage of its development, the PSF can model a two-phase porous structure. When the structure extends ad infinitum, its porosity approaches a finite value that can be chosen by the modeller between the extreme value 0 or 1 independently of the fractal dimension. Finally the main peculiarity of the PSF is the association in the same geometric shape of a distribution of pores and a distribution of solids which both assume a power law form with the same fractal exponent. As a result of this symmetry, the PSF model appears promising in terms of modelling hydraulic properties based on structural properties of the solid phase. If in addition an appropriate geometric shape is used, the connectivity of the pore network can be taken into account in pore network

simulations. Intrinsic to a mass fractal and a PSF model as presented in this paper are the notions of multiscale structure and self-similarity of structure. Further generalization is possible when the latter notion is relaxed. Construction of a model in which similarity of structure at different scales is not required further widens its scope of application. These points will be developed in forthcoming papers.

## 6. List of symbols

| | |
|---|---|
| $D$ | fractal dimension |
| $d$ | Euclidean space dimension |
| $L$ | linear size of the initiator |
| $N$ | number of subregions paving the initiator |
| $n$ | inverse of the similarity ratio |
| $z$ | proportion of subregions where the whole shape is replicated |
| $x$ | proportion of subregions kept as pores |
| $y$ | proportion of subregions kept as solids |
| $\mathcal{N}_z(r_i)$ | total number of replicates of size $r_i$ created at iteration step $i$ |
| $\mathcal{N}_x(r_i)$ | total number of pores of size $r_i$ created at iteration step $i$ |
| $\mathcal{N}_y(r_i)$ | total number of solids of size $r_i$ created at iteration step $i$ |
| $N_z(r_i)$ | total number of replicates of size greater than or equal to $r_i$ |
| $N_x(r_i)$ | total number of pores of size greater than or equal to $r_i$ |
| $N_y(r_i)$ | total number of solids of size greater than or equal to $r_i$ |
| $m_*$ | last step of division if any |
| $\alpha$ | means 'proportional to' |
| $\phi$ | porosity |
| $\phi_i$ | partial porosity at step $i$ |
| $B_x(i)$ | number of boxes of size $r_i$ needed to cover the pores |
| $B_y(i)$ | number of boxes of size $r_i$ needed to cover the solids |
| $B_z(i)$ | number of boxes of size $r_i$ needed to cover the fractal set |
| $M_x(i)$ | volume (or mass) of pores at iteration step $i$ |
| $M_y(i)$ | volume (or mass) of solids at iteration step $i$ |
| $S(i)$ | area of the pore–solid interface |
| $S_x(i)$ | cumulative boundary of pores at iteration step $i$ |
| $S_y(i)$ | cumulative boundary of solids at iteration step $i$ |
| $p_x(i)$ | probability that an arbitrary chosen point on the solids boundary belongs to the solid–pore interface |
| $p_y(i)$ | probability that an arbitrary chosen point on the pores boundary belongs to the solid–pore interface |
| $k$ | ratio of the similarity transformation used by Perrier (1994) to define the size of the solids and pores associated to any subregion |

## Appendix A

### *A.1. Equivalence between the model of Perrier (1994) and the PSF model*

Perrier's model is defined on the basis of three parameters ($N$, $z$, $k$) which are equivalent to the set ($N$, $x$, $y$) defining the PSF model.

Perrier's model involves $Nz$ and $N(1-z)$ subregions as does the PSF. The parameter $k$ defines the ratio of the contracting similarity used to replace each of the $N(1-z)$ subregions of linear size $r$ by one solid of volume $k^d r^d$ surrounded by one pore of volume $(1-k^d)r^d$ (see Figs. 8 and 9). An equivalent PSF model can be created by choosing the same $N$ and the following $x$ and $y$ proportions: $x=(1-z)(1-k^d)$, $y=(1-z)k^d$

Conversely, if a PSF model is defined by the parameters ($N$, $x$, $y$), an equivalent model is obtained using Perrier's definitions by choosing the same $N$ and the following $z$ and $k$ values:

$$z=1-x-y, \quad k=\left(\frac{y}{x+y}\right)^{1/d}$$

All the results obtained in this paper could have been also derived using Perrier's definition. For instance, the equivalent of the total porosity given in Eq. (20), $\phi=x/(x+y)$, is: $1-k^d$. Limiting cases $x=0$ and $y=0$ correspond respectively to $k=1$ and $k=0$.

## References


Ahl, C., Niemeyer, J., 1989. The fractal dimension of the pore volume inside soils. Z. Pflanzenernährungu. Bodenkunde 152, 457–458.

Arya, L.M., Paris, J.F., 1981. A physico-empirical model to predict the soil moisture characteristic from particle-size distribution and bulk density data. Soil Sci. Soc. Am. J. 45, 1023–1030.

Bartoli, F., Philippy, R., Doirisse, M., Niquet, S., Dubuit, M., 1991. Silty and sandy soil structure and self-similarity: the fractal approach. J. Soil Sci. 42, 167–185.

Bird, N., Bartoli, F., Dexter, A.R., 1996. Water retention models for fractal soil structures. Eur. J. Soil Sci. 47, 1–6.

Crawford, J.W., 1994. The relationship between structure and the hydraulic conductivity of soils. Eur. J. Soil Sci. 45, 493–502.

Crawford, J.W., Sleeman, B.D., Young, I.M., 1993. On the relation between number–size distributions and the fractal dimensions of aggregates. J. Soil Sci. 44, 555–565.

Crawford, J.W., Matsui, N., Young, I.M., 1995. The relation between the moisture release curve and the structure of soil. Eur. J. Soil Sci. 46, 369–375.

Davis, H.T., 1989. On the fractal character of the porosity of natural sandstone. Europhys. Lett. 8, 629–632.

de Gennes, P.G., 1985. Partial filling of a fractal structure by a wetting fluid. In: Adler, D., et al. (Eds.), Physics of Disordered Materials, Plenum, New York, NY, pp. 227–241.

Friesen, W.I., Mikula, R.J., 1987. Fractal dimensions of coal particles. J. Colloid Interf. 120, 263–271.

Ghilardi, P., Kaikai, A., Menduni, G., 1993. Self-similar heterogeneity in granular porous media at the representative elementary volume scale. Water Resour. Res. 29, 1205–1215.

Haverkamp, R., Parlange, J.Y., 1986. Predicting the water retention curve from particle-size distribution: sandy soils without organic matter. Soil Sci. 142, 325–339.

Katz, A.J., Thompson, A.H., 1985. Fractal sandstones pores: implication for conductivity and pore formation. Phys. Rev. Lett. 54 (12), 1325–1328.

Neimark, A.V., 1989. Multiscale percolation systems. Sov. Phys.-JETP 69, 786–791.

Mandelbrot, B.B., 1983. The Fractal Geometry of Nature. Freeman, San Francisco.

Perfect, E., Kay, B.D., 1991. Fractal theory applied to soil aggregation. Soil Sci. Soc. Am. J. 55, 1552–1558.

Perrier, E., 1994. Structure géométrique et fonctionnement hydrique des sols. Simulations exploratoires. Thèse Université Paris VI (Ed. Orstom, Paris, 1995).

Perrier, E., Mullon, C., Rieu, M., de Marsily, G., 1995. A computer construction of fractal soil structures. Simulation of their hydraulic and shrinkage properties. Water Resour. Res. 31, 2927–2943.

Perrier, E., Rieu, M., Sposito, G., de Marsily, G., 1996. A computer model of the water retention curve for soils with a fractal pore size distribution. Water Resour. Res. 32, 3025–3031.

Pfeifer, P., Avnir, D., 1983. Chemistry in non integer dimensions between two and three: I. Fractal theory of heterogeneous surfaces. J. Chem. Phys. 79, 3558–3564.

Rieu, M., Perrier, E., 1997. Fractal models of fragmented and aggregated soils, In: Baveye, P., et al. (Eds.), Fractals in Soil Science. CRC Press, Boca Raton, FL, pp. 169–202.

Rieu, M., Sposito, G., 1991a. Fractal fragmentation, soil porosity, and soil water properties: I. Theory. Soil Sci. Soc. Am. J. 55, 1231–1238.

Rieu, M., Sposito, G., 1991b. Fractal fragmentation, soil porosity, and soil water properties: II. Applications. Soil Sci. Soc. Am. J. 55, 1239–1244.

Rieu, M., Sposito, G., 1991c. Relation pression capillaire-teneur en eau dans les milieux poreux fragmentés et identification du caractère fractal de la structure des sols. C.R. Acad. Sci., Ser. II 312, 1483–1489.

Toledo, P.G., Novy, R.A., Davis, H.T., Scriven, L.E., 1990. Hydraulic conductivity of porous media at low water content. Soil Sci. Soc. Am. J. 54, 673–679.

Tyler, S.W., Wheatcraft, S.W., 1989. Application of fractal mathematics to soil water retention estimation. Soil Sci. Soc. Am. J. 53, 987–996.

Tyler, S.W., Wheatcraft, S.W., 1990. Fractal processes in soil water retention. Water Resour. Res. 26, 1047–1054.

Tyler, S.W., Wheatcraft, S.W., 1992. Fractal scaling of soil particle-size distributions: analysis and limitations. Soil Sci. Soc. Am. J. 56, 362–369.

van Damme, H., Ben Ohoud, M., 1990. From flow to fracture and fragmentation in colloidal media. In: Disorder and Fracture, NATO ASI Series. Plenum, New York, pp. 105–116.

Wu, Q., Borkovec, M., Sticher, H., 1993. On particle-size distributions in soils. Soil Sci. Soc. Am. J. 57, 883–890.

Young, I.M., Crawford, J.W., 1991. The fractal structure of soil aggregates: its measurement and interpretation. J. Soil Sci. 42, 187–192.

*Fractals in Soil Science*
Editors: Ya.A. Pachepsky, J.W. Crawford and W.J. Rawls
© 2000 Elsevier Science B.V. All rights reserved.


# Silty topsoil structure and its dynamics: the fractal approach

V. Gomendy [a], F. Bartoli [a,*], G. Burtin [a], M. Doirisse [a], R. Philippy [a], S. Niquet [b], H. Vivier [c]

[a] *Centre de Pédologie Biologique U.P.R. 6831 du C.N.R.S. associée à l'Université Henri Poincaré, Nancy 1, B.P. 5, F-54501 Vandœuvre-les-Nancy Cedex, France*
[b] *Centre Interrégional de Ressources Informatiques de Lorraine, château du Montet, F-54500 Vandœuvre-les-Nancy, France*
[c] *Laboratoire des Sciences du Génie Chimique UPR 6811 du CNRS, BP 451, F-54001 Nancy Cedex, France*

Received 10 October 1997; accepted 28 September 1998

**Abstract**

This paper describes the application of fractal geometry to the study of the structure and dynamics of tilled silty topsoil. The soil structure of each topsoil sample has been experimentally quantified directly by image analysis and indirectly by both water retention and mercury porosimetry. Any fractal scaling laws were mostly determined within a relevant common pore radius yardstick scale. Their scale invariants were fractal dimensions of either the matrix ($D_m$) or the solid:pore interfaces ($D_s$). We showed that the $D_m$ or $D_s$ values computed from water retention data were higher than their $D_m$ or $D_s$ value counterparts computed from mercury porosimetry data, which were themselves much higher than their microscopic fractal dimension value counterparts (only $D_m$). This was attributed to (i) partial pore-volume filling by either water or mercury and (ii) hysteresis between water drainage and mercury intrusion. A positive relationship between the fractal dimensions of the solid:pore interfaces and their solid mass fractal dimension counterparts have also been found, with the value of $D_m$ being higher than the corresponding value of $D_s$, characterizing complex fractal structures with interconnected pores. We also showed that clay content has a positive effect on both $D_m$ and $D_s$ values from either water retention or mercury porosimetry data as well on the positive relationship occurring between the $D_s$ values and their $D_m$ value counterparts. The physical process underlying this behaviour is proposed to be partial volume-pore filling by clays and, concomitantly, an increase in the rugosity of the microscopic solid:pore interfaces. In contrast, the temporal variability of either $D_m$ or $D_s$

* Corresponding author. Tel.: +33-83-51-08-60; E-mail: bartoli@cpb.cnrs-nancy.fr

Reprinted from Geoderma 88 (1999)
© 1999 Elsevier Science B.V. All rights reserved

values was moderate and can be attributed to both increase of pore connectivity and water hysteresis which occurred during the drying and wetting cycles of the studied cultivation period.
© 1999 Elsevier Science B.V. All rights reserved.

*Keywords:* fractal; image analysis; mercury porosimetry; silty topsoils; soil structure; water retention

## 1. Introduction

Transport processes in variably-saturated porous media can be described at the macroscopic scale using mathematical models such as the Darcy–Buckingham or the Richards equation. They have been extensively used to predict and model the transport of water, ions and colloids in soils. In a number of situations, particularly in very heterogeneous soils, the use of these macroscopic models has faced serious difficulties in recent years (e.g., Vauclin and Vachaud, 1984; Kutilek and Nielsen, 1994). Soils are complex multiscale and hierarchical porous media with a continuous set of organization levels going from nano- (clay domains) to micro- (aggregates) and macro-scale (clods, horizons). It is therefore believed that quantitative characterization of spatial geometric variability is required to improve the modelling of transport processes in such heterogeneous porous media.

This has motivated the recent introduction in soil science of a unified conceptual framework, fractal geometry (Mandelbrot, 1982; Feder, 1988; Avnir, 1989; Gouyet, 1992), which at least in principles allows one to get a handle on the geometric complexity of soils and to characterize it fully with just a few numbers, the fractal dimensions. These fractal dimensions could be used to extrapolate measurements of soil hydraulic properties to a larger scale than the experimental observation scale. Fractal scaling of soil structures were measured both directly from image analysis and indirectly from mercury porosimetry or water retention data. Such fractal scale invariances of soil structure have been recently reviewed by van Damme (1995) and Bartoli et al. (1998) and further analyzed in the increasing recent papers devoted to fractals and soil structure (e.g., Peyton et al., 1994; Crawford et al., 1995, 1997; Pachepsky et al., 1995a,b, 1996; Perrier et al., 1995, 1996; Anderson et al., 1996; Bird et al., 1996; Crawford and Matsui, 1996; Zeng et al., 1996; Bird, 1997; Bird and Dexter, 1997; Gimenez et al., 1997; Bartoli et al., 1999).

The fractal approach has been so extensively explored and discussed in soil water retention modeling (Toledo et al., 1990; Rieu and Sposito, 1991a,b; Perrier et al., 1995, 1996; Crawford et al., 1995; Pachepsky et al., 1995a; Bird et al., 1996) but, as recently suggested by Perrier et al. (1996), "A fractal analysis of the water retention curve cannot be done without also analyzing the underlying fractal object in respect to its geometrical interpretation. Thus only experi-

ments carried out to measure, on the same soil, both water retention data and structural properties will enable progress to occur in understanding the fractal nature of soils.''

Few works have attempted to relate the fractal scaling analysis of soil structure images to the corresponding mercury porosimetry (Bartoli et al., 1991, 1999) or water retention curve data (Crawford et al., 1995, with an unfortunate overlap between the range of pore radii scales covered by image analysis and the range covered by water retention by drainage; Bird, 1997; Crawford et al., 1997). The aim of the present paper is therefore to compare image analysis, mercury porosimetry and water retention data within a relevant common pore radius scale and a unified framework assessing the applicability of fractal geometry to the study of soil structure.

Reliable estimates of soil hydraulic properties are also especially difficult to obtain because the soil structure is both spatially and temporally variable and heterogeneous. Little information is available on temporal changes of structural and hydraulic properties of soils (e.g., Cassel and Nelson, 1985; Mapa et al., 1986; Mackie-Dawson et al., 1989a,b; Messing and Jarvis, 1993; Scott et al., 1994). The second aim of the present paper is therefore to study the temporal variability of silty tilled topsoil structures, and their fractal dimension values, during a 3- to 4-month cultivation period, from Spring to Autumn, characterized by drying and wetting cycles (Fig. 1).

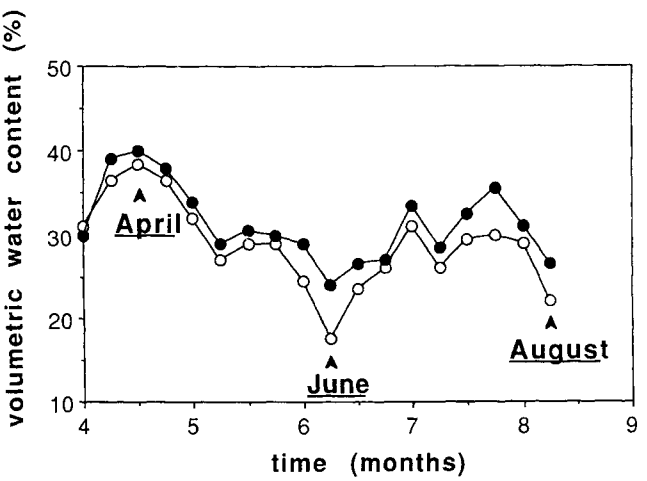


Fig. 1. Temporal variability of mean in situ volumetric topsoil content during the studied 1993 cultivation period occurring from the beginning of wheat plant growing to harvesting. TDR measurements in soil volumes of 0–30 cm soil depth have been carried out within metric stations of permanent topographic positions. Open and full circle symbols correspond to the studied plateau and midslope topsoils, respectively (after Gomendy, 1996).

## 2. Material and methods

### *2.1. Soils and soil sampling*

The study was conducted on a silty glossic leached brown soil (Typic Haplustalf) developed in quaternary silty materials, at the experimental Mélarchez catchment (7 $km^2$) which is located 80 km east of Paris (Bartoli et al., 1995). $B_{tg}$ illuvial horizons (up to 0.3–0.5 m depth) were homogeneous, with $31 \pm 1\%$ of total clays. In contrast, three topsoil units, organized within toposequences, have been distinguished by Bartoli et al. (1995).

Samples of the three topsoil units were collected at 5–15 cm depth within 100 $m^2$ squared stations and one unique cultivation plot, with winter wheat and pea for the 1993 and 1994 sampling periods, respectively. Our research effort has been focused on the plateau and midslope topsoil samples of the 1993 cultivation period, with the following sampling dates: 15–16 April (wetting period and beginning of plant growing), 14–15 June (end of the most important drying event) and 16–17 August 1993 (Autumnal harvest occurring at the end of the drying and wetting cycles period) (Fig. 1). The studied topsoils have also been sampled in 9–10 May and 23–24 June 1994 in order to have complementary bulk density, water retention and mercury porosimetry data.

Undisturbed soil in the field was sampled vertically using (i) metal Kubiena boxes to give blocks of soil measuring $60 \times 100 \times 40$ mm for micromorphology, (ii) PVC cylinders (50 mm high and 80 mm diameter) to give blocks of soils for soil bulk density and (iii) PVC cylinders (50 mm high and 26.5 mm diameter) to give blocks of soils for soil bulk density, soil retraction by drying, water retention by drainage, and mercury porosimetry.

Selected mean characteristics of the three topsoil samples are listed in Table 1. Mean clay content values and associated standard deviations were $16.3 \pm 0.5\%$, $25.6 \pm 0.7\%$ and $14.9 \pm 0.1\%$ for the plateau, midslope and downslope topsoil units, respectively, with similar clay mineralogy characterized by smectites (40–55% of the clay fraction), illite and kaolinite (Bartoli et al., 1995). Conversely, the mean proportions of volumetric topsoil retraction, measured following the method described by Braudeau (1987), were moderate for the 1993 samples, and related to their clay content: $4.3 \pm 1.5\%$, $8.9 \pm 2.1\%$ and $2.5 \pm 1.2\%$ for the plateau, midslope and downslope 1993 undisturbed wet topsoil samples, respectively. No significant temporal variations have been established for organic carbon (OC) contents of the 1993 soil samples. Mean OC was also related to clay content (Table 1).

### *2.2. Bulk density and micromorphology*

Bulk density was calculated on 105°C oven-dried 28 and 251 $cm^3$ cylindrical cores (three replicates of each type of cylinders for each soil sample). Soil total

Table 1
Main soil characteristics

| Topsoil sample | Distance from the brook (m) | Mean slope (%) | Mean particle-size distribution (%) | | | | | Mean volumetric retraction (%) | Mean organic carbon (%) |
|---|---|---|---|---|---|---|---|---|---|
| | | | Coarse sand > 200 μm | Fine sand 50–200 μm | Coarse silt 20–50 μm | Fine silt 2–20 μm | Clay < 2 μm | | |
| Plateau | 700 | 0.5 | 1.9 | 4.0 | 46.4 | 29.5 | 16.3 | 4.3 | 0.8 |
| Midslope | 440 | 4.5 | 1.3 | 3.9 | 37.5 | 29.2 | 26.6 | 8.9 | 1.1 |
| Downslope | 370 | 1.5 | 2.9 | 4.4 | 46.5 | 28 | 14.9 | 2.5 | 0.8 |

porosity, expressed in percentage of 'pore volume:soil core volume' ratio, was determined from bulk density data assuming that soil particle density was equal to 2.65 g $cm^{-3}$.

Soil structure has been characterized for the plateau and downslope topsoils sampled during the 1993 cultivation period, using two scales of observation: (i) photographs of vertically oriented soil blocks under UV lights, 43 $mm^2$, and with a resolution length of 0.1 mm, and (ii) backscattered SEM micrographs of vertically-oriented soil thin sections, 250 $\mu m^2$, and a resolution length of 0.5 $\mu$m. The samples were air-dried, impregnated with a polyester resin containing a fluorescent dye (Uvitex OB; Ciba-Geigy) and hardened. A fluorescent dye added to the impregnation mixture enabled pores (pore size $> 0.2$ mm) to be seen clearly and photographed within vertically oriented soil blocks, 10 mm thick, under two UV lights, as described by Murphy (1986). Binary images of these photographs have been analyzed.

Neighboring soil blocks were sawn, mounted on glass slides and ground to sections, 25 $\mu$m thick, which were covered with thin carbon layers under high vacuum for analysis with a Cambridge scanning electron microscope operated at 20 kV. Images were obtained using the backscattered electron technique (Bisdom and Thiel, 1981). The Backscattered-Electron Scanning Images (BESI) of soil thin sections correspond to a range of pore sizes relevant to the study of soil structure by mercury intrusion or water retention. Five 1-$mm^2$-squared zones without cracks were selected randomly on each soil thin section within a square centimeter network.

Analysis of the binary BESI have been described and discussed elsewhere (Bartoli et al., 1999). They included (i) the square box method for computing both the porosity $\Phi$ as a function of the observation scale $R$ and the solid mass fractal dimension $D_m$ using an observation scale $R$ fractal law, (ii) the chord length method for calculating the pore size distribution and the $D_m$ values using a yardstick scale $r$ fractal law. The porosity value for each pore chord length $L$ (linear horizontal intersections of the pore space: e.g., Dehoff and Rhines, 1972; Ringrose-Voase, 1990) was computed by multiplying the number of these chords with the one pixel cross-sectional area associated with each chord. The sum of the pore surface area $S_{IA}$ for all pore chord lengths was normalized to one. Pore surface area was plotted as a function of half the chord length ($L/2$), which was comparable to the pore radius $r$, assuming that the normalized pore surface area for a two dimensional-space equals the normalized pore volume (Dehoff and Rhines, 1972).

In this study, we also explored 1,000 pore networks and used a customized image analysis package to compute one main pore connectivity parameter: the normalized percolation probability, $Pr$, defined as the ratio between the surface area of the percolation networks extending from the top to the bottom of the image without interruption and the surface area of the whole pore network. The normalized percolation probability is similar to the 'effective porosity:porosity'

ratio recently determined by Eggleston and Peirce (1995) on simulated binary images.

### 2.3. *Porosimetry by mercury intrusion*

A Carlo Erba (Series 2000) mercury depression and intrusion porosimeter associated with the Macropore Unit Series 120 linked to a IBM PC computer, was used to determine the pore size distribution (p.s.d.) as a function of either pressure ($P$) from 1.25 $10^{-3}$ to 200 MPa or pore radii ($r$) from 3.75 $10^{-3}$ to 600 μm, using 1-$cm^3$ individual soil cubic fragments which were sawed from air-dried 251 $cm^3$ cylindrical cores soil samples. These 1-$cm^3$ soil samples were previously oven-dried at 105°C for 48 h and outgassed at room temperature for 2 h thereafter. A value for the surface tension of mercury of 0.485 N $m^{-1}$ and a contact angle on soil of 141.3° was used with the Washburn equation, assuming cylindrical pores in the calculation. The pressure was increased automatically when less than $3 \times 10^{-4}$ $cm^3$ of mercury was intruded in 1 min, over a period of 3–5 h. Porosity was computed from mercury pore volume data assuming soil particle density of 2.65 g $cm^{-3}$.

### 2.4. *Soil water retention by drainage*

The 28-$cm^3$ cylindrical soil samples, with their PVC envelopes, were water-saturated by capillarity within a closed volume at room temperature for 48 h and desaturated at a constant matric potential thereafter, using the classical Richards membrane method (Klute, 1986). Four replicates by matric potential value (−10, −20, −30 and −160 kPa) were carried out and the time for drainage equilibrium varied from 2 weeks at −160 kPa to 4 weeks at −10 kPa. Porosity was also computed from water-filled pore volume data assuming soil particle density of 2.65 g $cm^{-3}$.

### 2.5. *Fractal dimensions and statistics*

In this study, the methods under consideration imply self-similarity of the hierarchical structure of the soil samples studied. However, in many situations, especially for rough surfaces (e.g., Neimark, 1996), scaling invariance corresponds to self-affine rather than self-similar properties (Mandelbrot, 1982; Feder, 1988; Avnir, 1989; Gouyet, 1992). All the calculations of the fractal dimensions used have been previously reviewed, described and discussed elsewhere (van Damme, 1995; Bartoli et al., 1998, 1999).

In this paper, the computation of the solid mass fractal dimensions $D_m$ was first carried out within a 0.245- to 250-μm scale range, on digitized binary BESI

of thin soil sections using the fitted square boxes method, with a solid surface area, approximately at the center of each micrograph, as the center of the fitted squares. The solid mass fractal dimension $D_m$ equals the slope of the surface area $S_m$ ($R$) vs. the observation scale R plot on a doubly logarithmic scale (Bartoli et al., 1991, 1998, 1999). The three-dimensional $D_m$ value was obtained by adding 1 to the corresponding $D_m$ value measured in the porous medium intersection plane, with the assumption that the studied porous medium is isotropic. Each mean $D_m$ value and its standard error were calculated from five $D_m$ values each corresponding to randomly selected thin section areas (1 $cm^2$ square network).

The computation of the solid mass fractal dimensions $D_m$ was also carried out using (i) both water retention data and simplified mercury porosimetry data corresponding to the same calculated 1 to 15 μm pore radii range than the one used in the water retention experimental sets and (ii) the fractal fragmentation theory of Rieu and Sposito (1991a,b) who showed that water retention curves may be approximated reasonably well with the following analytical expression:

$$\theta(P) + 1 - \theta_{max} = (P_{min}/P)^{3-D_m} \quad (1)$$

In this expression, $\theta(P)$ and $\theta_{max}$ are the volumetric water content at matric potential $P$ and at saturation, respectively, $P_{min}$ is the air-entry pressure in the initially water-saturated porous medium, and $D_m$ is the solid mass fractal dimension of the wetted soil structure. For mercury porosimetry simplified data, content of volumetric air under vacuum replaces volumetric water content in Eq. (1) in which $P_{min}$ is then the mercury-entry pressure in the initially air under vacuum porous medium.

We also used the Rieu and Sposito conceptual approach for computing $D_m$ values by image analysis. Here the solid mass fractal dimension $D_m$ is the scale invariant parameter of a scale law which relates the solid surface area to a yardstick scale $r$ (cylindrical tube pore radius) and not to an observation scale $R$ as it is when using the fitted square boxes method. Combining Eq. (1) with the Washburn equation ($r \propto P^{-1}$), where $r$ is the cylindrical tube pore radius (yardstick scale) and $P$ the capillary pressure, it follows that:

$$\theta(r) + 1 - \theta_{max} = (r/r_{max})^{3-D_m} \quad (2)$$

or, similarly, normalized in terms of porosity $\Phi$:

$$\Phi(r) + 1 - \Phi_{max} = (r/r_{max})^{3-D_m} \quad (3)$$

where $r$ is the cylindrical tube pore radius corresponding to the capillary pressure $P$ and $r_{max}$ is the largest cylindrical tube pore radius corresponding to the capillary pressure $P_{min}$ of the fractal set.

The fractal dimensions of the solid:pore interfaces $D_s$ were computed using cumulative pore volume distributions of either the mercury porosimetry or the water retention data with the following proportionality:

$$V_{pdf}(P) \propto P^{D_s-3} - P_{max}^{D_s-3} + C \quad (4)$$

where $V_{pdf}$ is the cumulative volume of the defending fluid (either air under vacuum for mercury porosimetry or water for water retention by drainage), $P$ is the applied pressure, for either mercury or air intrusion, corresponding to the cylindrical tube pore radius $r$, $P_{max}$ is the capillary pressure corresponding to the smallest cylindrical tube pore radius $r_{min}$ of the fractal set and C is a constant which can be included to account for possible pore space existing at scales below the fractal regime (Perrier et al., 1996; Bird et al., 1996).

The linear parts of the cumulative log $V_{pdf}$ vs. log $P$ plots from the mercury porosimetry or water retention data are therefore interpreted as corresponding to fractal solid:pore interfaces. Fractal dimension values of the solid:pore interfaces, and their standard errors, were computed from the slopes of the straight lines of mercury porosimetry or water retention data plotted on double logarithmic scales (Eq. (4)), and standard errors of the slopes, respectively. Although only four sets of mean volumetric water content—matric potential value have been recorded for each water retention curve within a narrow $-10$ to $-160$ kPa matric potential value range (15- to 1-μm pore radii range), water retention curves have been fitted by power laws and $D_s$ values have been computed from Eq. (4). In contrast, the mercury porosimetry data of silty soils are difficult to interpret in terms of fractal geometry because of pore connectivity effects and this fractal dimension was only estimated on a rather small portion of the mercury intrusion curve, at lower capillary pressures than the ones corresponding to the main breakthrough phenomena of percolation as it was previously showed and discussed by Bartoli et al. (1999). The fractal mercury pressure or pore radii value range was mostly 2–30 MPa or 0.4–0.02 μm, respectively.

Simple regression analysis and one-way analysis of variance (ANOVA with 1 to 3 factors) were also carried out on our data. In order to quantify the effect of one parameter (e.g., clay or time) on the fractal dimension values, the least significant differences (LSD) were also used on our sets of data.

A key point on the fractal dimensions measured from either water retention or mercury porosimetry data is as follows. In these cases, we refer to the fractal dimensions as 'similitude' fractal dimensions because these two surface and pore volume probes only describe the solid:pore surface and the pore-volume accessible by the probes and not necessarily the real surface or pore-volume which can be directly captured by image analysis. Surface and pore-volume accessibility may vary with the scale and the probe-type used. However, a positive relationship may exist between, e.g., the Hausdorff–Besicovich dimension (Mandelbrot, 1982; Feder, 1988; Avnir, 1989; Gouyet, 1992) and the

similitude surface fractal dimension $D_s$ measured from either water retention or mercury porosimetry data.

## 3. Results and discussion

### *3.1. Porosity and pore size distributions from bulk density and image analysis*

Statistical treatments of total porosity data (bulk density analysis) of the 1993 topsoil samples lead to the conclusions that porosity is most sensitive to the topsoil unit ($F = 20{,}2$; $p < 0.0001$). Significantly higher total porosity values occur for the midslope topsoil, rich in clay, than for the two other plateau and downslope topsoils, with the exception of the plateau topsoil sampled in August (Fig. 2). Macro-porosity values (image analysis of photographs of soil blocks) are also higher, with larger pore diameters (Gomendy, 1996), for the midslope topsoil, rich in clay, than for the other two topsoils (Fig. 2).

Sampling date has also a significant effect on total porosity values ($F = 8{,}2$; $p = 0.011$) whereas cylinder size (251 or 28 $cm^3$) has no influence ($F = 4$; $p > 0.05$). This result confirms our fractal analysis of soil sample images from two embedded observation scales. Images of soil structure in a two-dimensional space were solid mass fractal from 0.005 to 0.5 mm square size (analysis of SEM micrographs of soil thin sections: this paper) whereas they were either non-fractal or poorly approximated by solid mass fractal from 0.5 to 50 mm square size, with high fractal dimension values of 1.98 to 2 (analysis of photographs of soil blocks: Gomendy, 1996), leading to the conclusion that, during this cultivation period, porosity was rather constant for volume sizes more than $1.25 \times 10^{-4}$ $cm^3$, with a slight increase of macro-porosity as a function of observation scale.

The mean total porosity values were also calculated from the balance of image analysis data considering that (i) the value of the soil porosity measured in a two-dimensional space by image analysis equals the value of the soil porosity measured in a three-dimensional space (stereological assumption) and (ii) the solid phase of the photographs of soil blocks is a single phase at this poor resolution scale (0.1 mm) but corresponds in reality to a binary solid:pore phase which is characterized by the mean porosity value determined on BESI of thin sections (resolution scale 0.5 $\mu$m). The mean total porosity values calculated from the balance of image analysis data were very close than those determined from the bulk density data, with less than 10% of variations between them (Fig. 2). This positive result validates both our stereological assumption and our BESI soil thin section sampling. It also allows us to properly use image analysis data of the studied BESI corresponding to a range of pore sizes relevant to the study of interrelationships between soil structure, mercury intrusion and water retention.

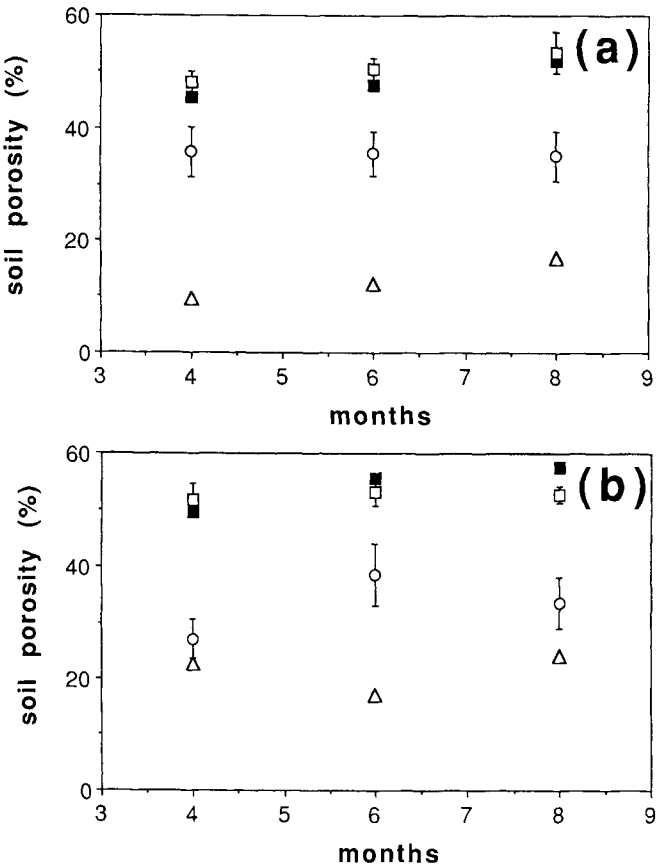


Fig. 2. Means and standard errors of topsoil porosities, expressed in soil porosity units (%), as a function of sampling month (1993 cultivation period) for the studied plateau (a) and midslope (b) topsoils sampled within metric stations of permanent topographic positions. Total topsoil porosity values were determined either in a three-dimensional space by the bulk density method (full square symbols) or in a two-dimensional space by the image analysis balance of photographs of soil blocks and of Backscattered Electron Scanning Images (BESI) of soil thin sections (open square symbols). Open triangle and circle symbols correspond to macro-porosity values of photographs of soil blocks and to micro- and meso-porosity values of BESI of thin sections, respectively.

The drying and wetting cycles which occurred during the cultivation period (Fig. 1) lead to pore volumes redistribution for the midslope topsoil, with an inverse temporal relationship between the soil block macro-porosity and the BESI porosity values (Fig. 2b), which should be attributed to shrinking and swelling processes. Both total and soil block macro-porosity values of the plateau topsoil also increased as a function of the drying and wetting cycles (Fig. 2a).

These drying and wetting cycles had also positive effects on both proportions of BESI percolative porosity values (Fig. 3a) and of their 30- to 200-μm pore diameter BESI counterparts (not shown). The temporal increase of the mean BESI percolative porosity (Fig. 3a) was higher, and conversely, the temporal decrease of its variation coefficient (Fig. 3b) was lower for the midslope topsoil, rich in clay, than for the plateau topsoil. This temporal increase of micro- and mesopore connectivity and, conversely, temporal decrease of its variability, may be attributed to (i) water menisci producing forces between these micro-aggregates leading to micro-aggregation of silty quartz:clay micro-aggregates during drying events and (ii) shrinking and swelling processes leading to micro-crack growth, particularly for the more compact midslope topsoil microstructure, rich in clays, as was observed on the BESI (Gomendy, 1996).

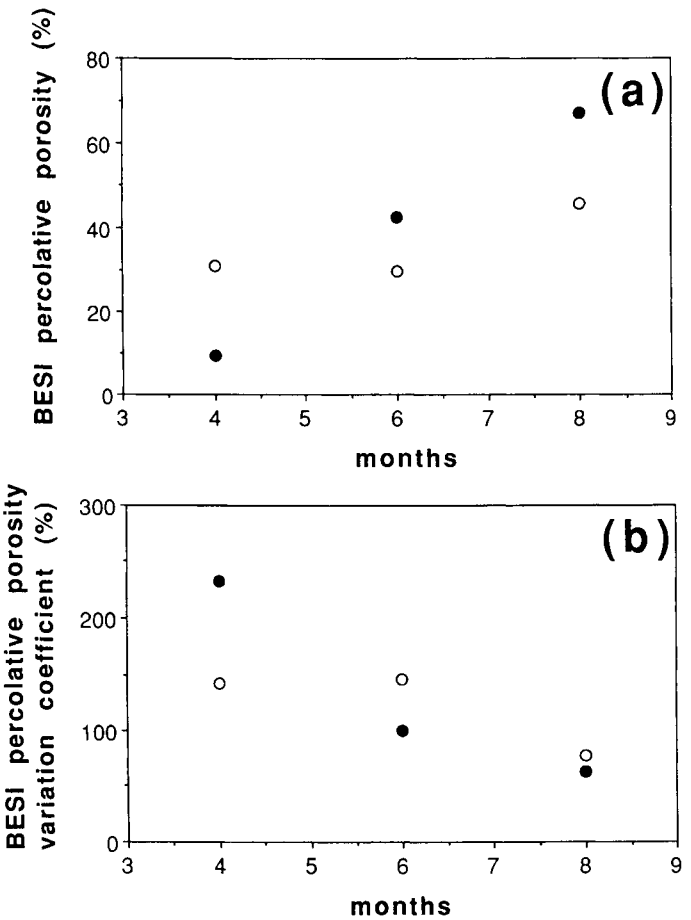


Fig. 3. Mean BESI percolative topsoil porosity values, expressed in soil porosity units (%) (a) and their variation coefficient counterparts (% of the means) (b) as a function of sampling month (1993 cultivation period) for the studied plateau (open circle symbols) and midslope (full circle symbols) topsoils sampled within metric stations of permanent topographic positions.

*3.2. Porosity and pore size distributions from water retention and mercury porosimetry*

The temporal variability of in situ volumetric water content (TDR data) showed that the midslope topsoil, rich in clays, had always a better in situ water retention than its plateau topsoil counterpart (Fig. 1).

Similarly, mercury porosimetry or water retention micro-porosity values corresponding to pore (throat) radii less than 1 μm were higher for midslope topsoil samples, rich in clays, than for their plateau and downslope topsoil counterparts (Fig. 4a). Conversely, mesoporosity values corresponding to pore (throat) radii of 1–15 μm were lower (Fig. 4b). This differential clay effect on

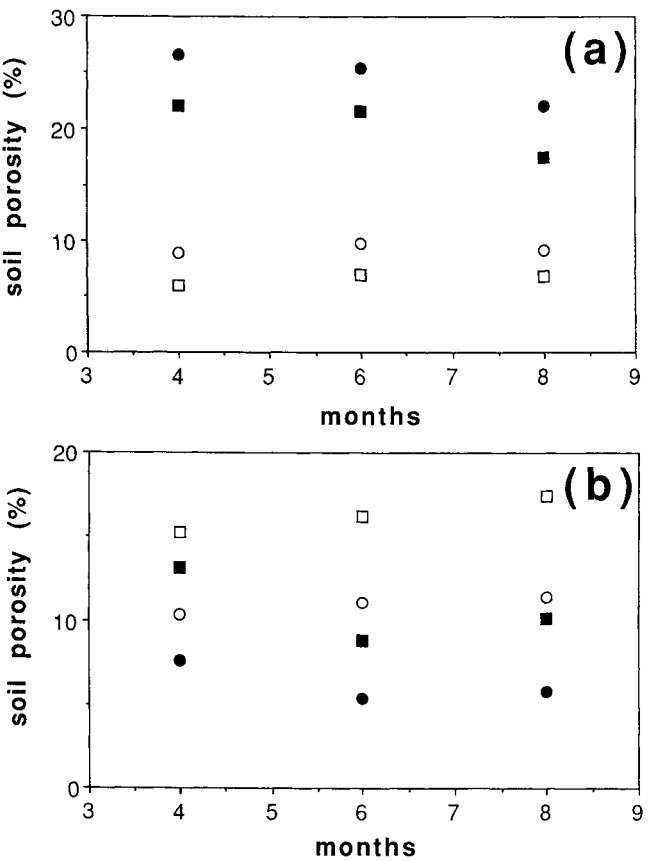


Fig. 4. Mean topsoil water retention (full symbols) and mercury intrusion (open symbols) porosities, expressed in soil porosity units (%), as a function of sampling month (1993 cultivation period) for the studied plateau (square symbols) and midslope (circle symbols) topsoils sampled within metric stations of permanent topographic positions. (a) and (b) correspond to porosity values of micro-porosity ( < 1-μm pore (throat) radii) (a) and of meso-porosity (1- to 15-μm pore (throat) radii) (b), respectively.

the pore-size distribution of mercury porosimetry and water retention data was previously reported, e.g., by Nagpal et al. (1972) who observed that the mercury intrusion data shifted as a function of clay content to larger pore diameters than the water retention data. These discrepancies might be caused (i) by a hysteresis effect because water retention by drainage is a 'receding' process while mercury intrusion is an 'advancing' process, as previously suggested by Wu et al. (1990) and (ii) partly by shrinking and swelling processes which were moderate in the studied topsoils (Table 1).

On the other hand, the drying and wetting cycles which occurred during the cultivation period (Fig. 1) had clear effects on both mercury porosimetry and water retention porosities, with a tendency to decrease both the water micro- and mesoporosity values and to increase both their corresponding mercury micro- and especially mesoporosity value (Fig. 4). The negative but scattered temporal relationship occurring between micro- and meso water retention porosity values and their BESI percolative porosity values counterparts (Fig. 5) indicates that the temporal decrease of water retention porosities (Fig. 4) was controlled by the increase of micro- and mesopore connectivity with time (BESI percolative porosity data: Fig. 3). This leads to a better pore accessibility by air and, conversely, to a better water drainage process by percolation when the topsoil is dried at an applied equilibrium pressure. Similarly, the temporal increase of mercury mesoporosity values (Fig. 4) can be attributed to the corresponding increase of BESI pore connectivity (Fig. 3). This will result in a better pore-volume accessibility by mercury (percolation: e.g., Bartoli et al., 1999). A greater difference between the two mesoporosity values has also been observed

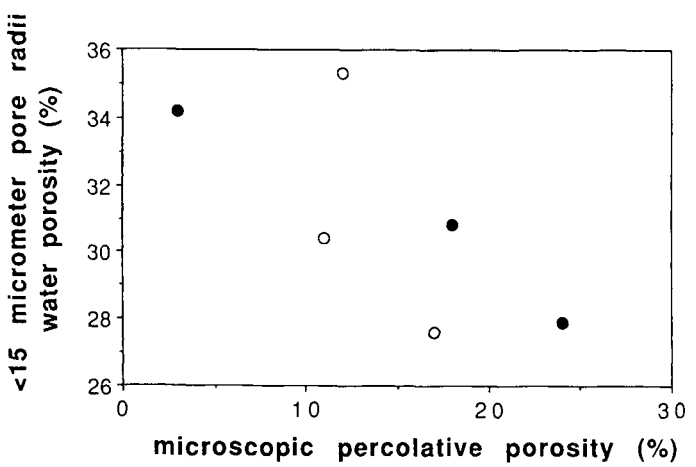


Fig. 5. Relationship between mean porosity values of micro- and meso-porosity ( < 15-μm pore (throat) radii) filled by water (water retention by drainage) and their BESI mean percolative porosity value counterparts, both porosities being expressed in soil porosity units (%). Open and full circle symbols correspond to the studied plateau and midslope topsoils, respectively.

for the plateau topsoil compared with the midslope one. This may be attributed to a more pronounced hysteresis effect between water retention and mercury intrusion due to a higher percolation pore network volume occurring for the plateau topsoil than for the midslope one (Gomendy, 1996; Fig. 4b).

Another more important discrepancy also exists between the water retention and mercury porosimetry micro- and meso pore volumes, and the corresponding pore volumes derived from image analysis. Those, which are both within the 1- to 15-μm pore (throat) radii range and filled by either water or mercury are characterized by lower porosity values than those which are determined by image analysis (Figs. 2, 4 and 8). This may be due to (i) larger pore size range for BESI analysis than for water retention and mercury porosimetry and (ii) non-analyses of proportions of micro- and mesopores which have been either water-drained (water retention) or not yet accessible to mercury intrusion (percolation: e.g., Bartoli et al., 1999).

### *3.3. Fractal dimensions of the solid phases*

Soil block macro-structures were mostly non-solid mass fractals (Gomendy, 1996) whereas soil thin section microstructures were solid mass fractal (Figs. 6–8) as it was usually demonstrated (e.g., Bartoli et al., 1998).

The variation of the $D_m$ values determined on the same BESI was narrower using the chord length method than the square box method and mean $D_m$ values tend to be slightly higher using the first method than using the second one (Fig. 6).

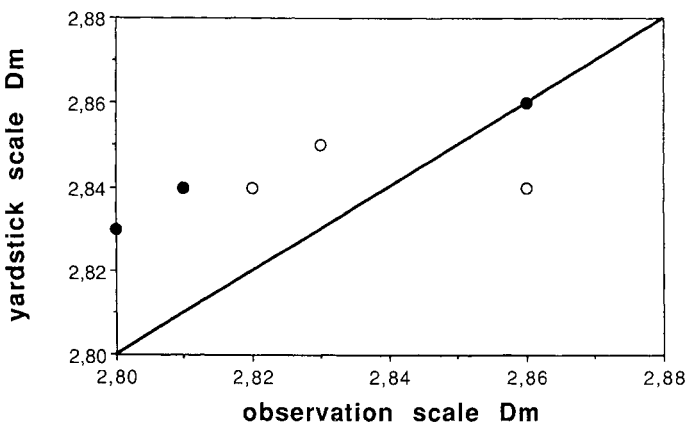


Fig. 6. Relationship between the solid mass fractal dimension values (three-dimensional space) computed from data obtained using the chord yardstick method and those computed from data obtained using the square box observation scale method. Open and full circle symbols correspond to the studied plateau and midslope topsoils, respectively, and the straight line corresponds to the bisector.

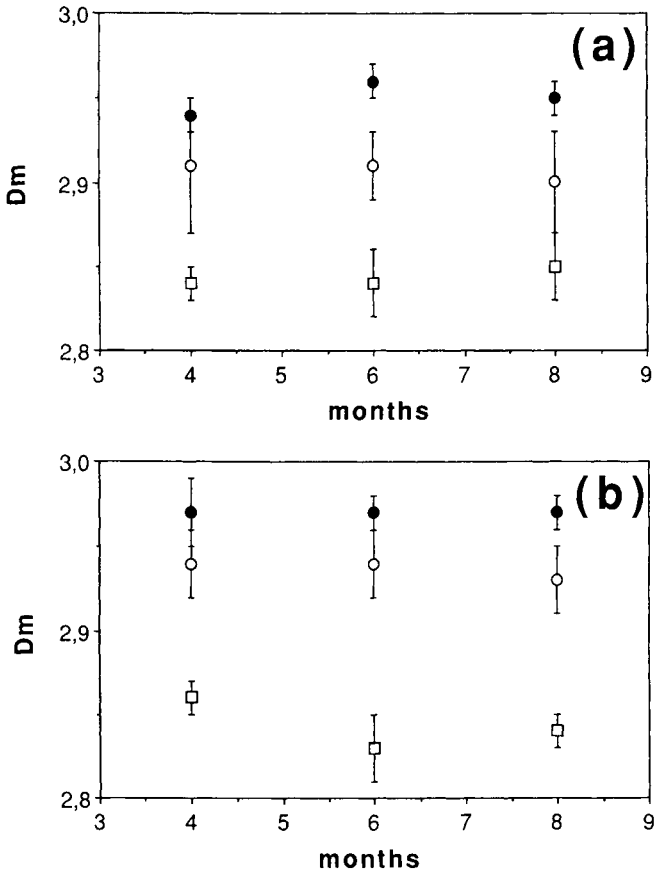


Fig. 7. Means and standard errors of the similitude solid mass fractal dimension (three-dimensional space) as a function of sampling month (1993 cultivation period) for the studied plateau (a) and midslope (b) topsoils sampled within metric stations of permanent topographic positions. Full and open circle symbols correspond to water retention and mercury porosimetry data, respectively, whereas open square symbols correspond to BESI analysis data.

Although more methodological and theoretical work is required in this area, we will focus, in this paper, on the $D_m$ values determined by the chord length method in order to use the same yardstick (pore radius) for micromorphology, water retention and mercury porosimetry data within a relevant common pore radius scale. However, if we want to use this yardstick concept more precisely, we have to consider the fact that the pore radii positions of the main peaks of the pore-volume distributions (p.v.d.) of silty topsoils were a factor of 10 less on the mercury porosimetry p.v.d. curve than on its BESI analysis counterpart (Bruand et al., 1993; Gomendy, 1996; Bartoli et al., 1999). In mercury porosimetry and water retention, the pore size is attributed to the size of the necks of the pore chamber network (percolation processes) whereas in image analysis (using the chord length method) the pore size is attributed to the larger pore chamber size.

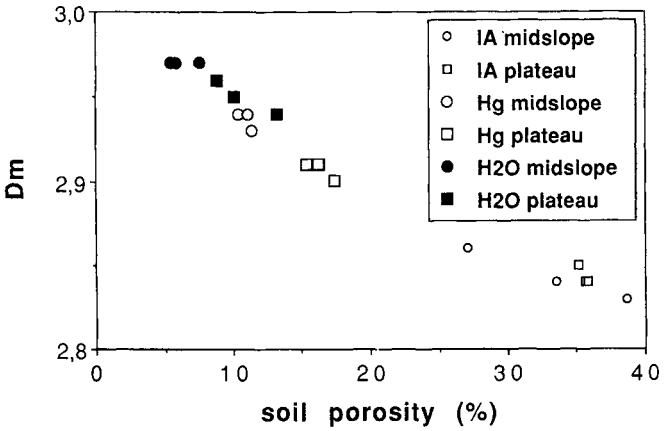


Fig. 8. Relationship between mean solid mass fractal dimension values (three-dimensional space) and their porosity value counterparts, expressed in soil porosity units (%). Fractal dimensions computed from either water retention or mercury porosimetry data are similitude fractal dimensions.

Another discrepancy occurred with the micro- and mesoporosity values which characterized either total micro- and mesopore volumes (image analysis) or partial 'functional' micro- and mesopore volumes (water retention and mercury porosimetry) whose values are controlled by both pore connectivity (e.g., Fig. 5) and hysteresis. As previously discussed, water retention by drainage is a 'receding' process whereas mercury intrusion is an 'advancing' process.

Bearing in mind the experimental difficulties in properly comparing direct and indirect analyses of soil structure, we will now consider the results of the solid mass fractal approach.

No significant clay effect has been observed on the $D_m$ values determined by image analysis as it was previously reported by Bartoli et al. (1999). The temporal variation of the solid mass fractal dimension values determined by image analysis was also narrow (Fig. 7), with the exception of the midslope topsoil, rich in clays, where intense drying from April to June (Fig. 1) leads to both an increase of BESI porosity value (Fig. 2) and a decrease of the corresponding value of $D_m$ (Fig. 7b). The latter observation is predicted by fractal theory and has been previously validated for sandy and silty soil BESI structures (Bartoli et al., 1998).

Although some caution should be exercised when using the $D_m$ values determined by water retention and by simplified mercury porosimetry (resulting from too few data and the occurrence of a main percolation event during mercury intrusion: Bartoli et al., 1999) we have compared these two solid mass fractal dimensions (i) with each other and (ii) with their microscopic fractal dimension counterparts (Fig. 7). The results are as follows.

The similitude fractal dimension values of the solid phases calculated either by water retention or by mercury porosimetry were also always higher for the

midslope topsoils than for their plateau topsoil counterparts (Fig. 7). This clay content effect is attributed to the partial filling of micro- and mesopores by clays (Fig. 8).

The water retention similitude $D_m$ values were higher than the corresponding mercury porosimetry values, which were in turn higher than the corresponding BESI values (Fig. 7). Similarly high values for the water retention-derived similitude dimension ($D_m$ values of 2.9 to 2.97) were previously obtained by Perrier et al. (1996) over the range of length scales probed by the values of matric potential for a set of sandy and silty soils. The discrepancy between the data from indirect soil structure analysis and those from direct soil structure analysis has been already discussed in Section 3.2. The negative relationship occurring between the $D_m$ values and the corresponding value for the porosity obtained by direct image analysis (Fig. 8) was confirmed from indirect soil structure analysis (Fig. 8). This indicates that similitude $D_m$ values are intrinsic measurements of the degree of pore-volume filling by either water (water retention by drainage) or mercury (mercury porosimetry) in the studied topsoil mesopore systems, confirming fractal theory (e.g., Mandelbrot, 1982; Bartoli et al., 1998).

### *3.4. Fractal dimensions of the solid:pore interfaces*

Although the similitude fractal dimensions of the solid:pore interfaces have been calculated over different ranges in pore radius (1-to 15-μm and mostly 0.02- to 0.4-μm pore (throat) radii for water retention and mercury porosimetry, respectively) we have compared these two types of fractal dimension values. Showing similarly trends as $D_m$, the values of $D_s$ were higher (i) for water retention than for mercury porosimetry and (ii) for the midslope topsoil than for the plateau topsoil, either for water retention or for mercury porosimetry (Fig. 9). The underlying reasons for theses effects are likely to be (i) hysteresis between water drainage ('receding' process) and mercury intrusion ('advancing' process) and (ii) pore-volume filling both by clays and by either water or mercury, as discussed in Section 3.3.

The fact that the similitude fractal dimension values of the solid:pore interfaces were higher for water retention than for mercury porosimetry have been previously reported Bartoli et al. (1992) for a set of silty topsoils aggregated with Fe(III) polycations and model humic macromolecules ($D_s$ values of 2.7–3.0 and of 2.45–2.65, respectively). Bartoli et al. (1992) also demonstrated that the similitude $D_s$ values from either water retention or mercury porosimetry data increased as a function of adsorbed iron and, conversely decreased as a function of their pore volume value counterparts, confirming that $D_s$ is an intrinsic measurement of the degree of pore filling by adsorbed poorly-ordered iron oxyhydroxides.

The similitude fractal dimension $D_s$ of the solid:pore interfaces, computed from the water retention curves has also been previously found to be inversely

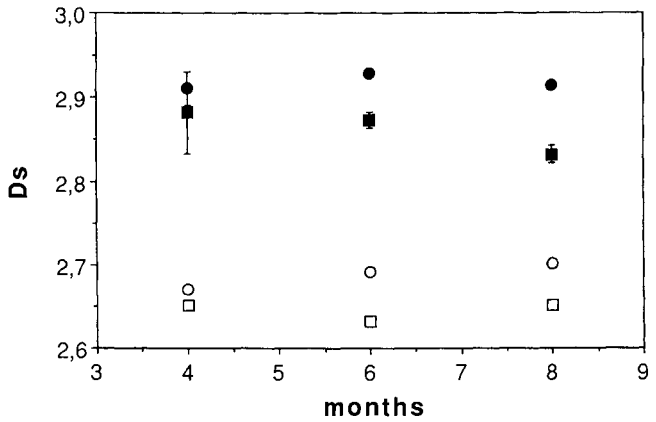


Fig. 9. Means and standard errors of the similitude fractal dimension of the solid:pore interface (three-dimensional space) as a function of sampling month (1993 cultivation period) for the studied plateau (square symbols) and midslope (circle symbols) topsoils sampled within metric stations of permanent topographic positions. Full and open symbols correspond to water retention and mercury porosimetry data, respectively.

related to soil clay content, larger values of $D_s$ corresponding to finer textured soils. The mean water retention similitude $D_s$ value so non-linearly increased from 2.41 to 2.87, when the texture went from coarse (sandy) to fine (clayey) (Brakensiek and Rawls, 1992). Another similar clay content effect has also been recently reported by Bartoli et al. (1999) on the mercury porosimetry similitude $D_s$ values of a range of silty soil horizons which have been sampled within the soil toposequence studied here.

Clay coatings occurred on and between silty quartz grains and micro-aggregates and were characterized by high micro-rugosity, as previously observed by TEM on ultra-thin topsoil sections by Bartoli et al. (1998, 1999). It may partly explain why solid:pore interfaces probed by either water or mercury are apparently disordered, with similitude fractal dimension $D_s$ values of 2.63–2.93. The fractal dimension values of the solid:pore interfaces of the Ca-saturated studied topsoils should be attributed, as previously suggested by Bartoli et al. (1999), to the complex association between the fractal surfaces of disordered Ca-clay microaggregates (BET surface area $D_s$ value of 2.86 for Ca-smectite, as determined by van Damme and Ben Ohoud, 1990) and the more regular surfaces of quartz grains (BET surface area $D_s$ values of 2.14–2.21 for quartz grains, as reviewed and determined by Avnir et al., 1985).

The water retention similitude $D_s$ values also tend to decrease from June (end of the drying global period) to August (almost end of the re-wetting global period) whereas, conversely, their mercury porosimetry $D_s$ value counterparts tend to increase (Fig. 9). Although it is still unclear, it should be both attributed to the hysteresis in situ behavior of topsoil water retention (Fig. 1) and to the

observed increase of percolative porosity (Fig. 3). Perrier et al. (1995) and Bird and Dexter (1997) have recently shown that the connectivity of either simulated deterministic or stochastic fractal porous media has a strong influence on the hysteric behavior of their water retention curves, and therefore on their solid:pore interfacial fractal dimension values.

More generally, the water retention and mercury porosimetry data of the three plateau, midslope and downslope topsoils sampled in 1993 and in 1994 show that a positive relationship between the water retention similitude $D_s$ values and their mercury porosimetry similitude $D_s$ value counterparts occurred for each sampling period (Fig. 10) leading to the conclusion that (i) the underlying soil geometry such as the fractal properties of the solid:pore interfaces and pore connectivity controls water retention similitude $D_s$ values and (ii) temporal variability (e.g., water retention hysteresis, pore connectivity) must be considered when modeling soil hydraulic properties.

Finally, a positive relationship between the similitude fractal dimensions of the solid:pore interfaces and their solid mass fractal dimension value counterparts have been founded from both water retention and mercury porosimetry data, with much more higher $D_m$ values than their $D_s$ value counterparts (Fig. 11), as it was previously reported by Bartoli et al. (1991, 1999) for other silty and sandy topsoil samples. Following the suggestions of Bartoli et al. (1991, 1999) this last result should characterized complex interconnected aggregates (statistical fractals), with a percolation pore network, as it was previously demonstrated by simulation and theoretical works (e.g., Kolb et al., 1983; Kolb and Herrmann, 1987; Saleur and Duplantier, 1987).

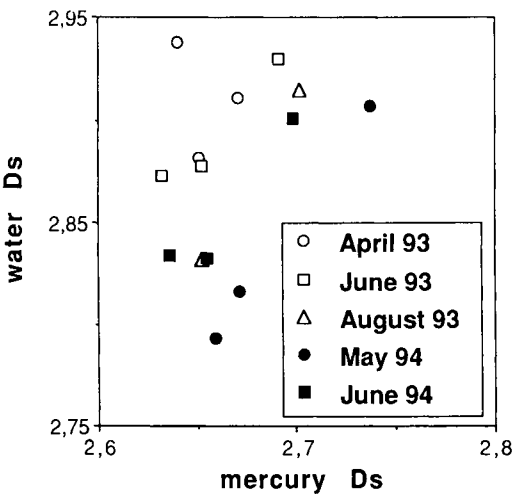


Fig. 10. Relationship between mean similitude fractal dimension values of the solid:pore interfaces (three-dimensional space) probed by either water or mercury for the studied plateau, mid- and downslope topsoils sampled within metric stations of permanent topographic positions during the 1993 and 1994 Spring to Autumn cultivation periods.

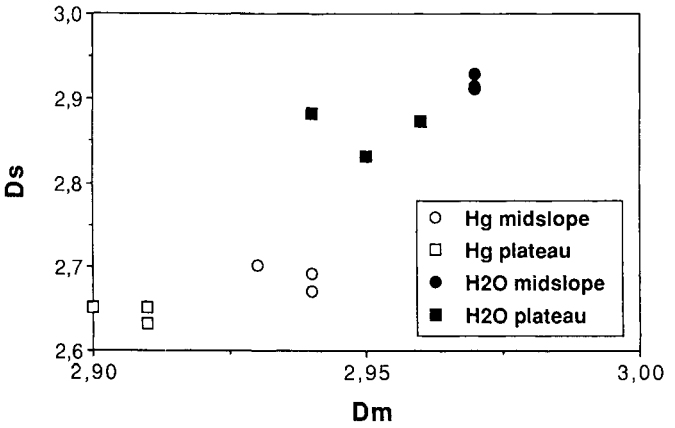


Fig. 11. Relationship between mean similitude fractal dimension values of the solid:pore interfaces and of the solid phases (three-dimensional space) probed by either water or mercury for the studied plateau and downslope topsoils sampled within metric stations of permanent topographic positions during the 1993 Spring to Autumn cultivation period.

The relationship between $D_s$ values and their $D_m$ value counterparts was also more pronounced for the midslope topsoil than for the plateau one, with a larger $D_m$ value range and, conversely, a lower $D_s$ value range (Fig. 11). It should be attributed to clays, rendering soil micro- and mesoporosity more compact and less variable (effects on $D_m$ values) and solid:pore interfaces more rugged and disordered (effects on $D_s$ values).

## 4. Conclusion

Three independent methods were compared for computing fractal dimensions of the matrix ($D_m$) or of the solid:pore interface ($D_s$) from image analysis, water retention and mercury porosimetry data of silty topsoils which have been sampled during a cultivation period, from Spring to Autumn.

The water retention similitude $D_m$ or $D_s$ values of the studied topsoils were higher than their mercury porosimetry similitude $D_m$ or $D_s$ value counterparts, themselves being considerably higher than their microscopic fractal dimension value counterparts (only $D_m$). These different $D_m$ values are intrinsic measurements of the degree of pore filling as demonstrated by the fact that they were negatively correlated with the corresponding values of porosity. The porosity values quantified either total micro- and mesoporosity (image analysis) or its functional porosity counterpart (pore-volume filled by either water within a 'receding' process, leading to the lowest porosity values, or, in contrast, by mercury within an 'advancing' process).

Both the water retention and mercury porosimetry similitude $D_m$ or $D_s$ values were also higher for the midslope topsoil, rich in clays, than for the other studied topsoil. The reason for this is likely to be partial volume-pore filling by clays and a corresponding increase of ruggedness of the microscopic solid:pore interfaces due to increase of clay coatings on and between silty quartz and micro-aggregates.

The temporal variability of the similitude fractal dimensions of either the solid phases or the solid:pore interfaces was moderate, and should be attributed both to an increase of pore connectivity and to water retention hysteresis occurring as a function of drying and wetting cycles.

Finally, a positive relationship between the similitude fractal dimensions of the solid:pore interfaces and their solid mass fractal dimension counterparts has also been found. The relation holds for each topsoil, with $D_m$ being higher than the corresponding values of $D_s$, characterizing complex fractal structures with interconnected pores (cf. a percolation pore network). The relationship between the $D_s$ values and their $D_m$ value counterparts was more pronounced for the midslope topsoil than for the plateau topsoil which may be attributed to clays, rendering soil micro- and mesoporosity more compact and less variable, and solid:pore interfaces more rough and more disordered.

In conclusion, the fractal approach to the study of soil structure, its dynamics, and slow fluid transport processes appears to be a useful tool in reaching a better physical understanding of fluid transport within complex multi-scaled soil structure. As a modeling tool, the most important gain is in extending our intuitive grasp of the significance of structural complexity for the physical interpretation of our data and thereby to produce better models of soil processes. However the relationship between matric potential, whose gradient controls water transport, and water content is complex (e.g., hysteresis, percolation) leading necessarily to further investigation on the effect of both pore connectivity and water hysteresis on fractal analyses.

## Acknowledgements

The authors would like to warmly thank M. Gury, CPB–CNRS Nancy, for his field expertise, P. Ansart, CEMAGREF Hydrology division Antony, J.M. De La Rivière and G. Bellier, ORSTOM Bondy for valuable technical assistance in TDR in situ soil volumetric water and soil shrinking measurements, respectively, and Béatrice Pechard-Presson, LSGC–CNRS Nancy, for her help in image analysis. They also thank Dr. Gimenez and the anonymous reviewer for their constructive comments and suggestions on an early draft of the paper. Trust and financial support from the PIREN Seine project, since 1992, the 'Méthodes, modèles et théories' Committee of the CNRS Environment programme (1993–1994) as well as the PhD French public research grant given to

the first author were greatly appreciated. The first author also thanks R. Grayson, Centre for Environmental Applied Hydrology, Melbourne University, Australia, for his kind hospitality during her 1997 post-doctorate stay in this Institute, with a Melbourne University postdoctorate fellowship.

## References

Anderson, A.N., McBratney, A.B., Fitspatrick, E.A., 1996. Soil mass, surface, and spectral fractal dimensions estimated from thin section photographs. Soil Science Society of America Journal 60, 962–969.

Avnir, D., 1989. The Fractal Approach to Heterogeneous Chemistry: Surfaces, Colloids, Polymers. Wiley, New York.

Avnir, D., Farin, D., Pfeifer, P., 1985. Surface geometric irregularity of particulate materials: the fractal approach. Journal of Colloid and Interface Science 103, 112–123.

Bartoli, F., Philippy, R., Doirisse, M., Niquet, S., Dubuit, M., 1991. Structure and self-similarity in silty and sandy soils: the fractal approach. Journal of Soil Science 42, 167–185.

Bartoli, F., Philippy, R., Burtin, G., 1992. Poorly-ordered hydrous Fe oxides, colloidal dispersion and soil aggregation: II. Modification of silty soil aggregation by addition of Fe(III) polycations and humic macromolecule models. Journal of Soil Science 43, 59–75.

Bartoli, F., Burtin, G., Royer, J.J., Gury, M., Gomendy, V., Philippy, Leviandier, T., Gaffrej, R., 1995. Spatial variability of topsoil characteristics within one silty soil type. Effects on clay migration. Geoderma 68, 279–300.

Bartoli, F., Dutartre, Ph., Gomendy, V., Niquet, S., Dubuit, M., Vivier, H., 1998. Fractals and soil structure. In: Baveye, P., Parlange, J.Y., Stewart, B.A. (Eds.), Fractals in Soil Science: Advances in Soil Science. CRC Press, pp. 203–232.

Bartoli, F., Bird, N., Gomendy, V., Vivier, H., 1999. The relationship between silty soil structures and their mercury porosimetry curve counterparts: fractals and percolation. European Journal of Soil Science 40, 1–4.

Bird, N.R.A., 1997. Comments 'The relation between the moisture-release curve and the structure of soil' by J.W. Crawford, N. Matsui and I.M. Young. European Journal of Soil Science 46, 188–189.

Bird, N.R.A., Dexter, A.R., 1997. Simulation of soil water retention using random fractal networks. European Journal of Soil Science 48, 633–641.

Bird, N.R.A., Bartoli, F., Dexter, A.R., 1996. Water retention models for fractal structures. European Journal of Soil Science 47, 1–6.

Bisdom, E.B.A., Thiel, F., 1981. Backscattered electron scanning images of porosities in thin sections of soils, weathered rocks and soil–gas reservoir rocks using SEM-EDXRA. In: Bisdom, E.B.A. (Ed.), Submicroscopy of Soils and Wheathered Rocks. 1st IWGSUSM Workshop, 1980, Wageningen. Pudoc, Wageningen, pp. 191–206.

Brakensiek, D.L., Rawls, W.J., 1992. Comments on 'fractal processes in soil water retention' by S.W Tyler and S.W. Wheatcraft. Water Resources Research 28, 601–602.

Braudeau, E., 1987. Mesure automatique de la rétraction d'échantillons de sols non remaniés. Science du Sol 25, 85–93.

Bruand, A., d'Acqui, L.P., Nyamugafata, P., Darthout, R., Ristori, G.G., 1993. Analysis of porosity in a tilled 'crusting soil' in Zimbabwe. Geoderma 59, 235–248.

Cassel, D.K., Nelson, L.A., 1985. Spatial and temporal variability of soil physical properties of Norfolk loamy sand as affected by tillage. Soil Tillage Research 5, 5–17.

Crawford, J.W., Matsui, N., 1996. Heterogeneity of the pore and solid volume of soil: distinguishing a fractal space from its non-fractal complement. Geoderma 73, 183–195.

Crawford, J.W., Matsui, N., Young, I.M., 1995. The relation between the moisture-release curve and the structure of soil. European Journal of Soil Science 46, 369–375.

Crawford, J.W., Matsui, N., Young, I.M., 1997. Reply to: Comments on 'The relation between the moisture-release curve and the structure of soil' by N.R.A. Bird. European Journal of Soil Science 46, 189–191.

Dehoff, J., Rhines, M., 1972. Microscopie Quantitative. Masson, Paris.

Eggleston, J.R., Peirce, J.J., 1995. Dynamic programming analysis of pore space. European Journal of Soil Science 46, 581–590.

Feder, J., 1988. Fractals. Plenum, New York.

Gimenez, D., Allmaras, R.R., Nater, E.A., Huggins, D.R., 1997. Fractal dimensions for volume and surface of interaggregate pores—scale effects. Geoderma 77, 19–38.

Gomendy, V., 1996. Spatial and temporal variabilities of structural and hydric silty topsoil properties (Orgeval catchment, Brie). PhD Thesis, Nancy University.

Gouyet, J.F., 1992. Physique et Structures Fractales. Masson, Paris.

Klute, A., 1986. Water retention: laboratory methods. Methods of soil analysis: Part 1. Physical and mineralogical methods. Soil Science Society of America, Agronomy Monograph 9, 635–662.

Kolb, M., Herrmann, H.J., 1987. Surface fractals in irreversible aggregation. Physical Review Letters 59, 454–457.

Kolb, M., Botet, R., Jullien, R., 1983. Scaling of kinetically growing clusters. Physical Review Letters 51, 1123–1126.

Kutilek, Nielsen, 1994. Soil Hydrology: GeoEcology Textbook. Catena Verlag, Cremlingen-Destedt, Germany.

Mackie-Dawson, L.A., Mullins, C.E., Fitzpatrick, E.A., Court, M.N., 1989a. Seasonal changes in the structure of clay soil in relation to soil management and crop type: I. Effects of crop rotation at Cruden Bay, NE Scotland. Journal of Soil Science 40, 269–281.

Mackie-Dawson, L.A., Mullins, C.E., Goss, M.J., Court, M.N., Fitzpatrick, E.A., 1989b. Seasonal changes in the structure of clay soil in relation to soil management and crop type: II. Effects of cultivation and cropping at Compton Beauchamp. Journal of Soil Science 40, 283–292.

Mandelbrot, B., 1982. The Fractal Geometry of Nature. Freeman, San Francisco.

Mapa, R.B., Green, R.E., Santo, L., 1986. Temporal variability of soil hydraulic properties with wetting and drying subsequent to tillage. Soil Science Society of America Journal 50, 1133–1138.

Messing, I., Jarvis, N.J., 1993. Temporal variation in the hydraulic conductivity of a tilled clay soil as measured by tension infiltrometers. Journal of Soil Science 44, 11–24.

Murphy, C.P., 1986. Thin Section Preparation of Soils and Sediments. AB Academics, Berkhamsted, UK.

Nagpal, N.K., Boersma, L., DeBacker, L.W., 1972. Pore size distributions of soils from mercury intrusion data. Soil Science Society of America Proceedings 36, 264–267.

Neimark, A.V., 1996. Characterization of rough surfaces. In: Le Van, M.DD. (Ed.), Fundamentals of Adsorption. Kluwer Academic Publishers, Boston, MA, pp. 659–666.

Pachepsky, Y.A., Polubesova, T.A., Hajnos, M., Sokolowska, Z., Jozefaciuk, G., 1995a. Fractal parameters of pore surface area as influences by simulated soil degradation. Soil Science Society of America Journal 59, 68–75.

Pachepsky, Y.A., Shcherbakov, R.A., Kornunskaya, L.P., 1995b. Scaling of soil water retention using a fractal model. Soil Science 159, 99–104.

Pachepsky, Y.A., Yakovchenko, V., Rabenhorst, M.C., Pooley, C., Sikora, L.J., 1996. Fractal parameters of pore surface as derived from micromorphological data: effect of long-term management practices. Geoderma 74, 305–319.

Perrier, E., Mullon, C., Rieu, M., de Marsily, G., 1995. Computer construction of fractal soil structures: simulation of their hydraulic and shrinkage properties. Water Resources Research 31, 2927–2943.

Perrier, E., Rieu, M., Sposito, G., de Marsily, G., 1996. Models of the water retention curve for soils with fractal pore-size distributions. Water Resources Research 31, 2927–2943.

Peyton, R.L., Gantzer, C.J., Anderson, S.H., Haeffner, B.A., Pfeifer, P., 1994. Fractal dimension to describe soil macropore structure using X-ray computed tomography. Water Resources Research 30, 691–700.

Rieu, M., Sposito, G., 1991a. Fractal fragmentation, soil porosity, and soil water properties: I. Theory. Soil Science Society of America Journal 55, 1231–1238.

Rieu, M., Sposito, G., 1991b. Fractal fragmentation, soil porosity, and soil water properties: II. Applications. Soil Science Society of America Journal 55, 1239–1244.

Ringrose-Voase, A.J., 1990. One-dimensional image analysis of soil structure I. Principles. Journal of Soil Science 41, 499–512.

Saleur, H., Duplantier, 1987. Exact determination of the percolation hull exponent in two dimensions. Physical Review Letters 58, 2325–2328.

Scott, H.D., Mauromoustakos, Handayani, P., Miller, D.M., 1994. Temporal variability of selected properties of loessial soil as affected by cropping. Soil Science Society of America Journal 58, 1531–1538.

Toledo, P.G., Novy, R.A., Davis, H.D., Scriven, L.E., 1990. Hydraulic conductivity of porous media at low water content. Soil Science Society of America Journal 54, 673–679.

van Damme, H., 1995. Scale invariance and hydric behaviour of soils and clays. Comptes Rendus à l'Académie des Sciences, Paris 320 (II a), 665–681.

van Damme, H., Ben Ohoud, M., 1990. From flow to fracture and fragmentation in colloidal media: II. Local order and fragmentation geometry. In: Charmet, J.C., Roux, S., Guillin, E. (Eds.), Disorder and Fracture. Plenum, New York, pp. 105–116.

Vauclin, M., Vachaud, G., 1984. Transferts hydriques dans les sols non saturés, non homogènes. Annales des Mines 1984, 63–74.

Wu, L., Vomocil, J.A., Childs, S.W., 1990. Pore size, particle-size, and water retention. Soil Science Society of America Journal 54, 952–956.

Zeng, Y., Gantzer, C.J., Payton, R.L., Anderson, S.H., 1996. Fractal dimension and lacunarity of bulk density determined with X-ray computed tomography. Soil Science Society of America Journal 60, 1718–1724.

This Page Intentionally Left Blank

*Fractals in Soil Science*
Editors: Ya.A. Pachepsky, J.W. Crawford and W.J. Rawls
© 2000 Elsevier Science B.V. All rights reserved.


# Simulation and testing of self-similar structures for soil particle-size distributions using iterated function systems

F.J. Taguas [a,*], M.A. Martín [a], E. Perfect [b]

[a] *Dpto. Matemática Aplicada, E.T.S.I. Agrónomos, Universidad Politécnica de Madrid, 28040 Madrid, Spain*
[b] *Department of Agronomy, University of Kentucky, Lexington, KY 40546-0091, USA*

Received 19 September 1997; accepted 28 September 1998

**Abstract**

Particle-size distribution (PSD) is a fundamental soil physical property. The PSD is commonly reported in terms of the mass percentages of sand, silt and clay present. A method of generating the entire PSD from this limited description would be extremely useful for modeling purposes. We simulated soil PSDs using an iterated function system (IFS) following Martín and Taguas [Martín, M.A., Taguas, F.J., 1998. Fractal modeling, characterization and simulation of particle-size distribution in soil. Proc. R. Soc. Lond. A 454, 1457–1468]. By means of similarities and probabilities, an IFS determines how a fractal (self-similar) distribution reproduces its structure at different length scales. The IFS allows one to simulate intermediate distributional values for soil textural data. A total of 171 soils from SCS [Soil Conservation Service, 1975. Soil taxonomy: a basic system of soil classification for making and interpreting soil surveys. Agricultural Handbook no. 436. USDA-SCS, USA, pp. 486–742] were used to test the ability of different IFSs to reconstruct complete PSDs. For each soil, textural data consisting of the masses in eight different size fractions were used, and different PSDs were predicted using different combinations of three similarities. The five remaining data points were then compared with the simulated ones in terms of mean error. Those similarities that gave the lowest mean error were identified as the best ones for each soil. Fifty-three soils had an error less than 10%, and 120 had an error less than 20%. The similarities corresponding to the sand, silt and clay fractions, i.e., IFS {0.002, 0.05}, did not, in general, produce good results. However, for soils classified as sand, silt loam, silt, clay loam, silty clay loam and silty clay, the same similarities always produced the lowest mean error, indicating the existence of a self-similar structure. This structure was not the same for all classes, although loams and clays were both best simulated by the IFS {0.002, 0.02}. It is concluded that IFSs are a

* Corresponding author. Fax: +34-1-3365817; E-mail: mamartin@mat.etsia.upm.es

Reprinted from Geoderma 88 (1999)
© 1999 Elsevier Science B.V. All rights reserved

powerful tool for identifying self-similarity in soil PSDs, and for reconstructing PSDs using data from a limited number of textural classes. © 1999 Elsevier Science B.V. All rights reserved.

*Keywords:* fractal; iterated function systems; soil particle-size distribution

## 1. Introduction

The statistical description of soil texture and particle-size distribution (PSD) is of great importance in the study of soil physical properties. One of the earliest attempts in this direction was due to Hatch and Choate (1929). Their work was later extended by Krumbein and Pettijohn (1938), Otto (1939) and Inman (1952). The usual classification of textures for particle sizes $\leq 2$ mm is made by giving the percentages of total masses of clay, silt and sand. Different classifications of soil texture have been proposed (Folk, 1954; Shepard, 1954; Baver et al., 1972; Soil Conservation Service, 1975; Vanoni, 1980). These systems differ in the particle-size limits chosen to separate the size groups and in the percentages of mass in each group chosen to define each textural class.

An enormous amount of soil PSD data has been reported in terms of the mass percentages of sand, silt and clay present. A method of reconstructing the entire PSD from this limited description would be extremely useful for modeling purposes.

Shirazi and Boersma (1984) used the proportions of clay, silt and sand to obtain the geometric mean of particle diameter $d_g$ and its geometric standard deviation $\sigma_g$. Using these parameters they converted the USDA textural triangle into an equivalent diagram based on $d_g$ and $\sigma_g$. This diagram provided greater resolution in detecting classified soil samples within a textural region. Later, Shirazi et al. (1988) extended and improved the above paper by using the log-normal distribution to interpolate between particle size limits within each fraction. Fractal geometry provides new ideas and concepts for the mathematical description of highly irregular and heterogeneous media as is the case of soil. A new intrinsic symmetry law is considered to characterize the apparent disorder, which consists of the repetition of the disorder itself over a certain range of scales. This property is called self-similarity and natural and real objects with this property are called fractals.

A fractal medium has a complex geometry which is statistically repeated across a wide range of scales, giving rise to scale-invariance. When a property of a fractal medium is measured at different scales, and irregularities of size less than a characteristic size are ignored, a power law appears reflecting this scale-invariance. The power scaling exponent is said to be the fractal dimension, and measures the degree of irregularity of the medium.

During last decade fractal ideas and concepts have been used to describe soil physical properties, to model physical processes and to quantify soil spatial

variability (for a complete review see Perfect and Kay, 1995). In particular, soil particle size distributions have been shown to obey power scaling of the type (Turcotte, 1986; Tyler and Wheatcraft, 1989, 1992; Wu et al., 1993):

$$N(l \geq L) \propto l^{-d} \tag{1}$$

where $N(l \geq L)$ is the number of particles of length $l$ greater than a characteristic length $L$, and the power exponent $d$ is a non-integer number ($0 < d < 3$). From this law, and under the usual hypothesis (particles of constant shape and density) power scalings of type:

$$M(l \leq L) \propto l^{3-d} \tag{2}$$

can be derived for the distribution of the mass of particles of size less than $L$, $M(l \leq L)$ (Tyler and Wheatcraft, 1992; Turcotte, 1992). The exponent $d$ is usually referred as the fragmentation fractal dimension and has become an important soil physical parameter (Perfect and Kay, 1995). However, the hope that the above fractal dimension could play an important role in the quantitative analysis of soil textures, has not been realized due to the fact that soils with quite different mass percentages of clay, silt and sand can have very similar fractal dimensions (Tyler and Wheatcraft, 1992). Furthermore the mass and number power laws by themselves do not provide a complete quantitative description of the PSD (Kozak et al., 1996).

Power law scaling indicates an underlying self-similar or scale-invariant structure, but does not provide information on the way the PSD reproduces this structure at different scales. This new aspect of self-similarity is considered in Martín and Taguas (1998), who developed a method to simulate the entire PSD based on a natural interpretation of self-similarity, coupled with a theoretical result from fractal geometry. This method provides a powerful way to generate an arbitrary number of intermediate distributional values from a few textural data. The present paper applies the method of Martín and Taguas to a wide range of PSDs in order to test the extent of self-similarity in soils, and investigate the influence of textural class on the different types of self-similarity observed.

## 2. Theory

The starting point in Martín and Taguas (1998) is to think about the fractal structure which causes, or is the genesis, of the power laws of Eqs. (1) and (2), and which effectively denotes the scale-invariance of the PSD. The PSD is defined by assigning to each interval $[l_1, l_2]$ the mass of soil particles whose length is in such an interval. Thus, the power scalings described by Eqs. (1) and (2) become a consequence of the highly irregular mass distribution. A crucial feature of this distribution is the absence of any proportionality between the

length of an interval and the mass of soil particles with characteristic length in such interval. Moreover, this distribution will exhibit scale invariant features. For example, from a photograph of soil grains one cannot determine the scale at which the photograph was taken. We give a new interpretation of the scale-invariance of PSD by assuming that the distribution statistically repeats its structure and irregularity at different scales.

If we observe a soil sample and we consider the particles grouped in different classes according to their sizes, the structure of the distribution at this scale is given by the mass of soil in each of these classes. If we now change the scale in one of these classes, new different classes would appear and it can be thought that they repeat the initial structure, that is, the mass soil proportion in each class agrees (statistically) with the above scale. If self-similarity is assumed this process would be repeated at different scales. This interpretation of self-similarity is quite natural since in the absence of more detailed information, it is appropriate to suppose that what you see at one scale also occurs at other scales. Another reason for our interpretation is, as fractal geometry shows, that fractal scalings of the PSD are a consequence of fractal structures of the type proposed above which are called multifractal distributions. This approach has the advantage that mathematical theorems concerning self-similar fractal distributions are applied in order to obtain interesting practical results.

Let us suppose that from textural data for a soil we have selected a set of $N$ relative proportions of mass corresponding to $N$ consecutive size classes. In order to simplify, let us further suppose that $N = 3$. First, we shall present how to apply mathematically the above idea to real PSD data. Later, we shall discuss how the results depend on the data selected and how to manage these ideas in order to get better practical results. Let us denote by $I_1 = [0, a]$, $I_2 = [a, b]$ and $I_3 = [b, c]$ the subintervals of sizes corresponding to the three size classes and $p_1$, $p_2$ and $p_3$ the relative proportions or probabilities ($p_1 + p_2 + p_3 = 1$) of mass for the intervals $I_1$, $I_2$ and $I_3$, respectively. Associated with these definitions, one may consider the following functions

$$\varphi_1(x) = r_1 x \tag{3}$$

$$\varphi_2(x) = r_2 x + a \tag{4}$$

$$\varphi_3(x) = r_3 x + b \tag{5}$$

where $r_1 = a/c$, $r_2 = (b - a)/c$, $r_3 = (c - b)/c$ and $x$ is any point (or value) of the interval $[0, c]$. That is, $\varphi_1$, $\varphi_2$ and $\varphi_3$ are the linear functions (similarities) which transform the points of the interval $[0, c]$ in the points of the subintervals $I_1$, $I_2$ and $I_3$, respectively. The set

$$\{\varphi_1, \varphi_2, \varphi_3; p_1, p_2, p_3\} \tag{6}$$

is called an iterated function system (IFS) (Barnsley and Demko, 1985).

By means of the similarities $\varphi_i$ and the probabilities $p_i$, an IFS determines how a fractal distribution reproduces its structure at different scales. As it is shown in Martín and Taguas (1998), the set of textural data together with the self-similarity assumption determines unequivocally a self-similar fractal distribution, which may be considered a model for the corresponding PSD.

In practice, the above ideas are used as follows: let us define, the same as before, the intervals $I_1$, $I_2$ and $I_3$, their relative proportions $p_1$, $p_2$ and $p_3$ respectively, and the IFS $\{\varphi_1, \varphi_2, \varphi_3; p_1, p_2, p_3\}$. If we construct $\varphi_j(I_i)$, then we obtain nine intervals $I_{ij}$ $(i = 1,2,3;\ j = 1,2,3)$ with relative mass proportions $p_i p_j$. In the next step, 27 intervals appear with their respective mass proportions, and so on successively. However, this procedure does not permit us to define, exactly, the mass proportion of any interval $J = [e, f]$ different from the intervals of any step obtained from the preceding process. A result from fractal geometry (Elton, 1987; see also Martín and Taguas, 1998) leads to an algorithm which allows us to simulate the distribution in an exact way. The mass proportion of soil formed by particles whose length is in the interval $J$ of sizes, may be computed using the associated IFS as follows: (a) take any starting value $x_0$ of $[0, c]$. (b) Choose, at random, an integer number $i$ of the set 1, 2, 3, with probability $p_i$, that is, the outcome may be 1 with probability $p_1$, may be 2 with probability $p_2$ and 3 with probability $p_3$. We denote by $x_1$ the value $\varphi_i(x_0)$. (c) Repeat the random experiment of (b), and suppose the new outcome is $j$ and compute $\varphi_j(x_1)$, which we denote by $x_2$.

We obtain in this way a sequence $x_0, x_1, \ldots, x_n$. Then, if $m_n$ is the number of $x_i$'s which belong to any interval $J$, the ratio

$$m_n/n \tag{7}$$

approaches the mass of the interval $J$ as the number of iterations $n$ goes to infinity.

In practice, the estimation of mass of the interval $J$ is achieved quickly. In fact, a computation of mass is practically invariable after $n = 3000$, and it gives the same value if we repeat this apparently random computation starting with a different point $x_0$.

## 3. Materials and methods

A great amount of textural data were used to test the self-similarity theory described above for soil PSDs. These data correspond to the two first horizons of soils described in Soil Conservation Service (1975).

The data refer to the proportions $m_i$ of mass of soil corresponding to particles whose lengths are in the following size classes (mm): clay ($< 0.002$), silt (0.002–0.02) and (0.02–0.05), very fine sand (0.05–0.1), fine sand (0.1–0.25), medium sand (0.25–0.5), coarse sand (0.5–1) and very coarse sand (1–2). In order to use these data to construct an associated IFS we shall denote by $[a, b]$

the lengths greater than or equal to $a$ and less than or equal to $b$. These size classes determine a set of seven intermediate cut points {0.002, 0.02, 0.05, 0.1, 0.25, 0.5, 1} and eight consecutive intervals corresponding to the eight size classes $I_1 = [0, 0.002]$, $I_2 = [0.002, 0.02]$, ..., $I_8 = [1, 2]$.

The data offer the possibility of using some of them to construct an IFS and thus, a fractal PSD associated with it. The above method allows us to simulate the distribution and to contrast the real data, not considered in the construction of the IFS, with the predicted ones resulting from the simulation. This is an inverse problem, in which the goal is to find those IFSs that most closely reproduce the target measure (Barnsley and Demko, 1985; Barnsley et al., 1985).

With these data it is possible to construct IFSs with a number of similarities which may vary from 2 to 8. Thus, the method provides a great number of potential simulated fractal PSDs. Each PSD preserves the textural data used to define the corresponding IFS, which determines the way the distribution repeats its own structure, that is, the type of self-similarity present in it.

In order to test the self-similarity, we used only three similarities. One reason for this is that three similarities include the IFS constructed when the mass percentages of clay, silt and sand are used, and these are the most commonly available textural data. However, we must emphasize that different testing can be done selecting a different number of similarities, and specially that using all available data, the model leads to a self-similar PSD whose simulation maintains the original data.

We constructed the different possible IFSs $\{\varphi_1, \varphi_2, \varphi_3; p_1, p_2, p_3\}$ using the following rules.

(a) Select two cut points $\alpha$ and $\beta$ among the seven possible choices. (b) Suppose $\alpha < \beta$ and let $\varphi_1$ be the linear function (similarity) which transforms the interval [0, 2] into the interval $J_1 = [0, \alpha]$, that is

$$\varphi_1(x) = \frac{\alpha}{2}x \tag{8}$$

and let $p_1$ be the mass proportion of soil particles in $J_1$.

(c) Let $\varphi_2$ be the linear function which transforms the interval [0, 2] into the interval $J_2 = [\alpha, \beta]$, that is

$$\varphi_2(x) = \frac{\beta - \alpha}{2}x + \alpha \tag{9}$$

and $p_2$ the mass proportion of particles in $J_2$.

(d) Let $\varphi_3$ be the linear function which transforms the interval [0, 2] into the interval $J_3 = [\beta, 2]$, that is

$$\varphi_3(x) = \frac{2 - \beta}{2}x + \beta \tag{10}$$

and $p_3$ the mass proportion of particles in $J_3$.

In order to simplify, we denote this IFS as $\{\alpha, \beta\}$. For example, if $\alpha = 0.05$ and $\beta = 0.25$, then $J_1 = [0, 0.05]$ (that is, the union of $I_1$, $I_2$ and $I_3$), $J_2 = [0.05, 0.25]$ ($I_4$ and $I_5$) and then, $J_3 = [0.25, 2]$ ($I_6$, $I_7$ and $I_8$). So, $p_1 = (m_1 + m_2 + m_3)/100$, $p_2 = (m_4 + m_5)/100$ and $p_3 = (m_6 + m_7 + m_8)/100$.

The rules (a), (b), (c) and (d) permit the construction of 21 different IFSs. The IFSs were used in conjunction with Elton's algorithm to simulate the PSD in length intervals of 0.05 mm. The result remained the same after approximately 3000 iterations. We used 5000 iterations for all of the simulations.

In order to evaluate how close the real and simulated PSDs were, we considered the mean error $\epsilon$. That is, if $m_i$ is the mass proportion in the size class $I_i$ and $m'_i$ is the mass proportion assigned by one of the IFSs constructed, then the mean error, $\epsilon$, is

$$\epsilon = \frac{\sum_{1}^{8} |mi - m'_i|}{2} \tag{11}$$

Notice that this error takes into account the mass proportions that are not in the correct size interval, adding them for the eight successive intervals. It follows that $\epsilon$ is an index which quantifies the accuracy of the different self-similar distributions to reproduce the original textural data. Vrscay (1991) used a similar distance function to evaluate the goodness of fit of an IFS to a target histogram.

## 4. Results and discussion

Textural data corresponding to 171 soils have been studied. The respective PSDs have been simulated in the way described above, using all the possible

Table 1
Average errors organized by textural class for the IFS {0.002, 0.05} and the best IFS for each soil

| Soil textural classes | Average error | |
|---|---|---|
| | [0.002, 0.05] | Other IFSs |
| Sand | 39.1 | 11.8 |
| Loamy sand | 31.1 | 17.0 |
| Sandy loam | 34.1 | 19.1 |
| Loam | 34.6 | 19.1 |
| Silt loam | 34.3 | 9.4 |
| Silt | 44.4 | 8.5 |
| Sandy clay loam | 29.0 | 19.2 |
| Clay loam | 28.0 | 19.7 |
| Silty clay loam | 30.9 | 7.6 |
| Silty clay | 19.1 | 9.3 |
| Clay | 14.3 | 10.1 |

IFSs constructed with three similarities. For soils in each textural class the simulation was made with every IFS, and the IFS with the smallest error $\epsilon$ was selected. Fifty-three soils had an error less than 10% and 67 had an error greater than 10% and less than 20%, with the best IFS, respectively.

Table 1 shows the average error for soils belonging to each textural class when the simulation was made with the IFS {0.002, 0.05}, i.e., using the mass percentages of clay, silt and sand. It is clear that relative to the other IFSs, the IFS {0.002, 0.05} does not produce, in general, good results. The average of the minimum error for soils in each textural class was the smallest for silty clay loam (an average minimum error of 7.6%). Silt (8.5%) and silty clay (9.3%) also

Table 2
Summary of the best IFSs for each soil in a textural class, including their maximum and minimum errors

| Soil textural classes | Number of soils | IFS | Error | |
|---|---|---|---|---|
| | | | Minimum | Maximum |
| Sand | 6 | {0.1, 0.25} | 7.6 | 14.0 |
| Loamy sand | 2 | {0.02, 0.05} | 18.8 | 22.4 |
| | 1 | {0.1, 0.25} | 21.5 | 21.5 |
| | 2 | {0.25, 0.5} | 9.8 | 12.5 |
| Sandy loam | 17 | {0.002, 0.02} | 10.4 | 27.4 |
| | 6 | {0.02, 0.05} | 12.1 | 21.9 |
| | 2 | {0.02, 0.1} | 16.2 | 18.5 |
| | 10 | {0.05, 0.1} | 9.1 | 27.8 |
| | 1 | {0.05, 1} | 25.2 | 25.2 |
| | 5 | {0.1, 0.25} | 8.5 | 24.3 |
| | 3 | {0.25, 0.5} | 22.9 | 24.6 |
| | 7 | {0.5, 1} | 6.1 | 24.5 |
| Loam | 15 | {0.002, 0.02} | 5.4 | 26.6 |
| | 1 | {0.002, 0.05} | 22.1 | 22.1 |
| | 1 | {0.05, 0.1} | 24.1 | 24.1 |
| | 1 | {0.5, 1} | 22.1 | 22.1 |
| Silt loam | 29 | {0.002, 0.02} | 1.5 | 26.4 |
| Silt | 2 | {0.002, 0.02} | 8.3 | 8.7 |
| Sandy clay loam | 2 | {0.02, 0.05} | 13.3 | 19.7 |
| | 2 | {0.05, 0.1} | 17.6 | 22.4 |
| | 1 | {0.1, 0.5} | 19.1 | 19.1 |
| | 1 | {0.5, 1} | 23.5 | 23.5 |
| Clay loam | 12 | {0.002, 0.02} | 15.5 | 25.1 |
| Silty clay loam | 15 | {0.002, 0.02} | 2.0 | 16.4 |
| Silty clay | 7 | {0.002, 0.02} | 1.6 | 16.3 |
| Clay | 15 | {0.002, 0.02} | 4.8 | 19.5 |
| | 1 | {0.1, 0.25} | 4.0 | 4.0 |
| | 1 | {0.1, 0.5} | 9.3 | 9.3 |
| | 1 | {0.25, 0.5} | 9.9 | 9.9 |
| | 2 | {0.5, 1} | 11.3 | 16.7 |

had low average minimum errors. On the other hand, the classes with the highest average minimum error were clay loam (19.7%) and sandy clay loam (19.2%).

Table 2 shows, for each textural class, the number of soils whose best simulation was made by means of a certain IFS and the minimum and maximum error of the simulation of these soils using that IFS. For example, twenty soils belonging to the clay textural class have been studied, all of them having been simulated with the 21 possible IFSs. The smallest error was obtained for fifteen soils with the IFS {0.002, 0.02}, for two soils with the IFS {0.5, 1}, for one soil with the IFS {0.1, 0.25}, for another soil with the IFS {0.1, 0.5} and for the last soil with the IFS {0.25, 0.5}. For all of the soils classified as sand, silt loam, silt, clay loam, silty clay loam and silty clay, the smallest error was reached by the same IFS (Table 2). This shows that, for these classes, there is a kind of self-similar PSD structure characteristic of the textural class, determined for the corresponding IFS. So, each of these classes should show a different type of self-similarity. This cannot be extrapolated to all textural classes, although in

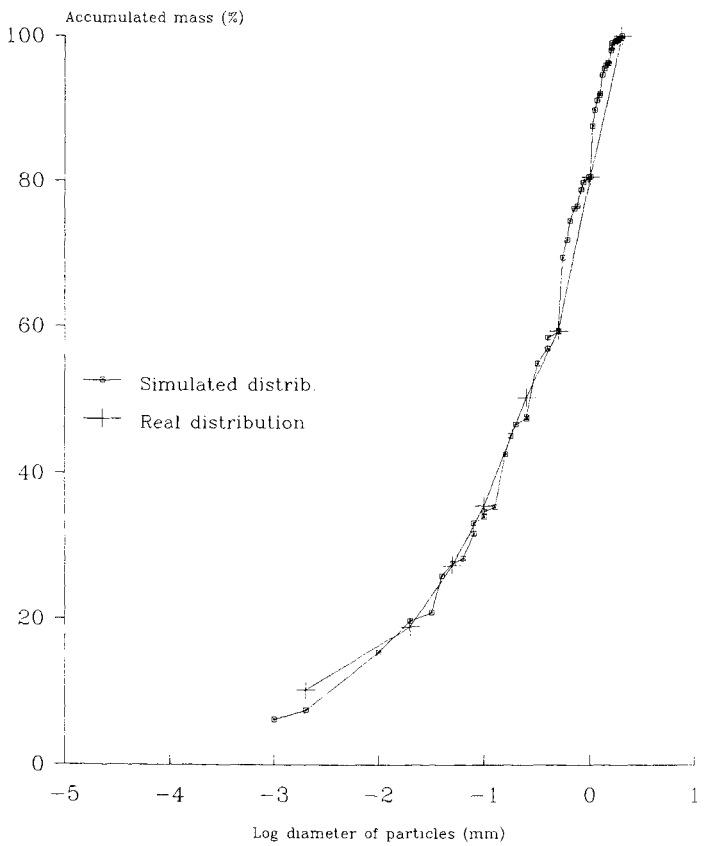


Fig. 1. PSD simulated using the IFS {0.5, 1} and PSD using the real textural data.

some of them, a distinctive IFS can be selected (for example, the IFS {0.002, 0.02} for textural classes loam and clay). It is possible that considering self-similar PSDs produced for IFSs with cut-off points different from than those that were present in the data we used might yield similar results. Further research is needed in this direction since use of different or additional distributional values could influence the evaluation of the degree of self-similarity. In order to investigate this possibility, more detailed soil textural data will be required for matching the IFSs, particularly in the finer fractions. This is in a different spirit from the present work, which sought to explore the fractal scaling properties of soil PSDs based on the limited number of separates that are normally available.

It must be pointed out that the above discussion concerns self-similar PSDs produced using three similarities. The method may also be applied using all available data, that is, in this case, using an IFS constructed with eight similarities. The simulation of PSD with this IFS preserves the eight textural values used and assigns a simulated mass to any subinterval $[a, b]$ for any intermediate values. It also updates the distribution using the natural assumption

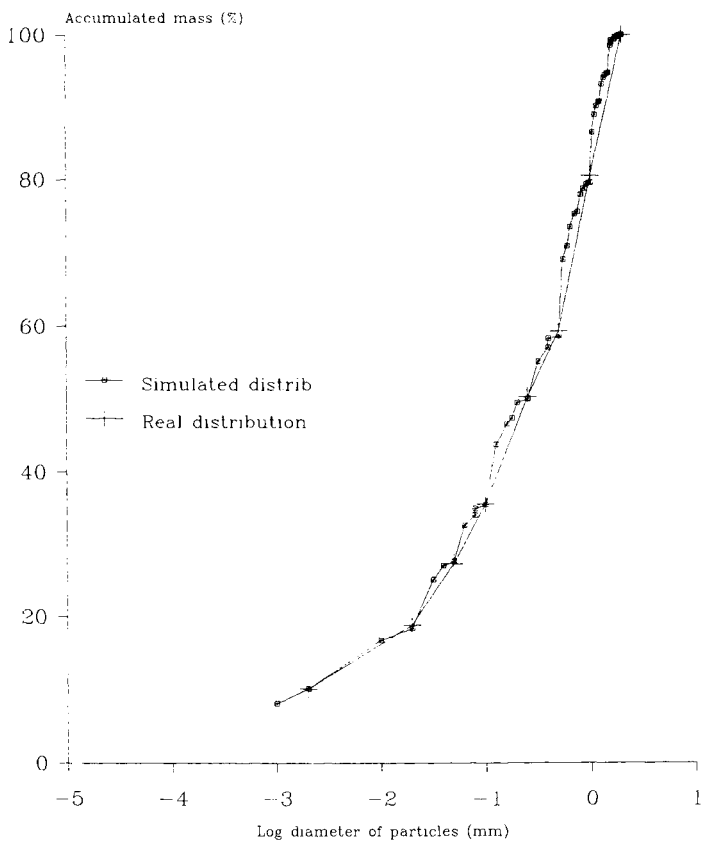


Fig. 2. PSD simulated with eight similarities and PSD using the real textural data.

of self-similarity for smaller scales, about which nothing is known. In Figs. 1–3, respectively, simulations have been made using three similarities for the IFS with the minimum error, {0.5, 1} in first case, eight in the second (the eight similarities corresponding to the eight textural data known) and in the third using the IFS {0.002, 0.05}. The data correspond to the soil horizon A11 described on p. 640 of Soil Conservation Service (1975). The accumulated mass was computed by dividing the intervals [0, 0.002], [0.002, 0.1], [0.1, 0.25] and [0.25, 2] in 2, 10, 6 and 35 subintervals, respectively. The mass corresponding to any subinterval was then simulated using 5000 iterations of Elton's algorithm.

Finally, as it is shown in Martín and Taguas (1998), different measurable properties or functions related to the PSD, and technically expressed by integrals with respect to the distribution, may be computed by an algorithm of the same type, with minimal computational cost. In particular, moments and other statistical parameters (such as mean particle length) of self-similar distributions may be determined using ad hoc formulas (Martín and Taguas, 1991) which involve the similarities $\varphi_i$ and the proportions $p_i$.

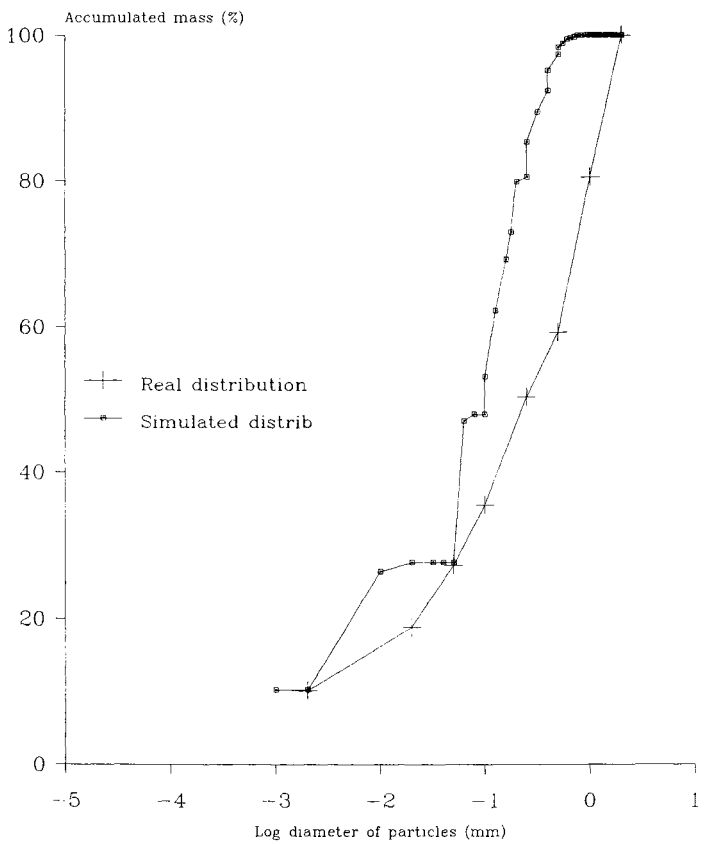


Fig. 3. PSD simulated using the IFS {0.002, 0.05} and PSD using the real textural data.

## 5. Conclusions

The irregularity and complexity of soil PSDs, together with their scale-invariant features suggest a fractal self-similar distribution as a suitable and natural model. The problem is to determine the type of self-similarity, or way of reproducing the structure at different scales, especially when the number of textural data is small. We have proposed an IFS model to simulate the particle-size distribution of soils based on the natural and usual assumption of self-similarity interpreted in a precise and new way which may be mathematically handled. Textural data allow us to construct IFSs which lead to self-similar PSD models, which can be simulated by means of a simple algorithm.

A total of 171 soils have been used to apply the model. For each soil, a set of eight textural data were used to construct different IFSs with three similarities determined by the same number of data. The five remaining data points were used to compare with the simulated ones coming from the corresponding IFS.

The IFS {0.002, 0.05} corresponding to the mass proportions of clay, silt and sand gave rather poor simulations. In contrast, other IFSs based on the three similarities resulted in excellent predictions. For some textural classes, all soils belonging to a particular class were best simulated by the same IFS. The most consistent results were obtained for the silty clay loam, silty clay, silt, silt loam, clay and sand textural classes. Although further research has to be done, this suggests the possibility of the existence of a characteristic type of self-similarity or way of reproducing the structure of the PSD at different scales for soils in these textural classes. For such self-similar soils, our model represents a powerful tool for simulating the PSD based on few data, and for computing soil parameters related to the PSD.

## References

Barnsley, M.F., Demko, S., 1985. Iterated function systems and the global construction of fractals. Proc. R. Soc. Lond. A 399, 243–275.

Barnsley, M.F., Erwin, V., Hardin, D., Lancaster, J., 1985. Solution of an inverse problem for fractals and other sets. Proc. Natl. Acad. Sci. U.S.A. 83, 1975–1977.

Baver, L.D., Gardner, W.H., Gardner, W.R., 1972. Soil Physics, 4th edn. Wiley, New York.

Elton, J., 1987. An ergodic theorem for iterated maps. J. of Ergodic Theory and Dynamical Systems 7, 481–488.

Folk, R.L., 1954. The distinction between grain size and mineral composition in sedimentary rock nomenclature. J. Geol. 62, 344–359.

Hatch, T., Choate, S., 1929. Statistical description of the size properties of nonuniform particulate substances. J. Franklin Inst. 207, 369–387.

Inman, D.L., 1952. Measures for describing the size distribution of sediments. J. Sediment. Petrol. 22 (3), 125–145.

Kozak, E., Pachepsky, Ya.A., Sokołowski, S., Sokołowska, Z., Stepniewski, W., 1996. A modified number-based method for estimating fragmentation fractal dimensions of soils. Soil Sci. Soc. Am. J. 60, 1291–1297.

Krumbein, W.C., Pettijohn, F.J., 1938. Manual of Sedimentary Petrography. Appleton-Century, New York.

Martín, M.A., Taguas, F.J., 1991. Some parameters of distribution of mass in self-similar fractals. Real Anal. Exchange 7 (2), 765–770.

Martín, M.A., Taguas, F.J., 1998. Fractal modeling, characterization and simulation of particle-size distributions in soil. Proc. R. Soc. Lond. A 454, 1457–1468.

Otto, G., 1939. A modified logarithmic probability graph for interpretation of mechanical analysis of sediments. J. Sediment. Petrol. 9 (2), 62–76.

Perfect, E., Kay, B.D., 1995. Applications of fractals in soil and tillage research: a review. Soil and Tillage Research 36, 1–20.

Shepard, F.P., 1954. Nomenclature based on sand–silt–clay ratios. J. Sediment. Petrol. 24 (3), 151–158.

Shirazi, M.A., Boersma, L., 1984. A unifying quantitative analysis of soil texture. Soil Sci. Soc. Am. J. 48, 142–147.

Shirazi, M.A., Boersma, L., Hart, J.W., 1988. A unifying quantitative analysis of soil texture: improvement of precision and extension of scale. Soil Sci. Soc. Am. J. 52, 181–190.

Soil Conservation Service, 1975. Soil taxonomy: a basic system of soil classification for making and interpreting soil surveys. Agricultural Handbook no. 436. USDA-SCS, USA, pp. 486–742.

Turcotte, D.L., 1986. Fractals and fragmentation. J. Geophys. Res. 91 (B2), 1921–1926.

Turcotte, D.L., 1992. Fractals and Chaos in Geology and Geophysics. Cambridge Univ. Press, Cambridge.

Tyler, S.W., Wheatcraft, S.W., 1989. Application of fractal mathematics to soil water retention estimation. Soil Sci. Soc. Am. J. 53, 987–996.

Tyler, S.W., Wheatcraft, S.W., 1992. Fractal scaling of soil particle-size distributions: analysis and limitations. Soil Sci. Soc. Am. J. 56, 362–369.

Vanoni, V.A., 1980. Sedimentation Engineering. Sedimentation Committee, Hydraulic Division, American Society of Civil Engineers, New York.

Vrscay, E.R., 1991. Moment and collage methods for the inverse problem of fractal construction with iterated function systems. In: Peitgen, H.-O., Henriques, J.M., Penedo, L.F. (Eds.), Fractals in the Fundamental and Applied Sciences. North Holland, pp. 443–461.

Wu, Q., Borkovec, M., Sticher, H., 1993. On particle-size distributions in soils. Soil Sci. Soc. Am. J. 57, 883–890.

This Page Intentionally Left Blank

*Fractals in Soil Science*
Editors: Ya.A. Pachepsky, J.W. Crawford and W.J. Rawls
© 2000 Elsevier Science B.V. All rights reserved.


# Scaling properties of saturated hydraulic conductivity in soil

D. Giménez [a,*], W.J. Rawls [a], J.G. Lauren [b]

[a] *USDA-ARS, Hydrology Laboratory, Bldg. 007, Rm. 104, BARC-West, Beltsville, MD, 20705, USA*

[b] *Department of Soil, Crop, and Atmospheric Sciences, Cornell University, Ithaca, NY 14853, USA*

Received 3 November 1997; accepted 28 September 1998

**Abstract**

Variability of saturated hydraulic conductivity, $k_{sat}$, increases when sample size decreases implying that saturated water flow might be a scaling process. The moments of scaling distributions observed at different resolutions can be related by a power-law function, with the exponent being a single value (simple scaling) or a function (mutiscaling). Our objective was to investigate scaling characteristics of $k_{sat}$ using the method of the moments applied to measurements obtained with different sample sizes. We analyzed three data sets of $k_{sat}$ measured in: (1) cores with small diameter and increasing length spanning a single soil horizon, (2) columns with increasing cross sectional area and constant length, and (3) columns with increasing cross sectional area and length, the longest column spanning three soil horizons. Visible porosity (macroporosity) was traced on acetate transparency sheets prior to measurement of $k_{sat}$ in situation (2). Six moments were calculated assuming that observations followed normal ($k_{sat}$, macroporosity) and/or log-normal ($k_{sat}$) distributions. Scaling of $k_{sat}$ was observed in all three data sets. Simple scaling was only found when flux occurred in small cross sectional areas of a simple soil horizon (data set (1)). Multiscaling of $k_{sat}$ distributions was found when larger soil volumes were involved in the flux process (data sets (2) and (3)). Moments of macroporosity distributions showed multiscaling characteristics, with exponents similar to those from $\ln k_{sat}$ distributions. The scaling characteristics of $k_{sat}$ reported in this paper agree with similar results found at larger scales using semivariograms. Scaling exponents from the semivariogram and the moment techniques could be

* Corresponding author. Present address: Department of Environmental Sciences, Rutgers University, 14 College Farm Rd., New Brunswick, NJ 08902-8551. Tel.: +1-732-932-9477; Fax: +1-732-932-8644; E-mail: dgimenez@envsci.rutgers.edu

Reprinted from Geoderma 88 (1999)
© 1999 Elsevier Science B.V. All rights reserved

complemented, as demonstrated by the agreement between macroporosity scaling exponents found with both techniques. © 1999 Elsevier Science B.V. All rights reserved.

*Keywords:* multiscaling; fractal; macroporosity

## 1. Introduction

Soils are heterogeneous systems with regions more or less favorable to flow distributed spatially in intricate patterns. The high spatial variability exhibited by measurements of saturated hydraulic conductivity, $k_{sat}$, is associated with heterogeneity in soil properties. Particularly important for the rapid movement of water is the presence and continuity of macropores (Bouma, 1982; Lauren et al., 1988). The variability in $k_{sat}$ measurements is a function of sample size (Anderson and Bouma, 1973; Zobeck et al., 1985; Lauren et al., 1988; Mallants et al., 1997). Highly variable $k_{sat}$ values are usually obtained with small cores that can enclose almost exclusively structural features responsible for extreme flow conditions, e.g., compacted clods or continuous macropores (Anderson and Bouma, 1973). Measurements with large cores are generally less variable because an increase in sample size is equivalent to measuring $k_{sat}$ with a decreased resolution (observations are averaged over larger areas).

Functional relationships between resolution and statistical properties of measurements has been used to define scaling properties of geophysical phenomena (Gupta and Waymire, 1990; Lovejoy and Schertzer, 1995; Rodriguez-Iturbe et al., 1995). A process is said to be scaling when statistical properties of a distribution vary as a power-law of the resolution (Feder, 1988). Soil properties measured at different scales show that behavior. Rodriguez-Iturbe et al. (1995) found that variance and spatial correlation of soil moisture determined from images covering 848 $km^2$ showed a power-law decay with distance. Sisson and Wierenga (1981) also observed a power-law decay of correlation with distance for infiltration rates. The same type of behavior is present in measurements of porosity from thin sections (Murphy and Banfield, 1978).

Processes that show simple scaling result from the additive contribution of various factors, and are characterized by a simple parameter, e.g., the fractal dimension $D$ (homogeneous fractal). In contrast, a multiplicative contribution of random variables results in a multiscaling process (non-uniform fractal) requiring more than one fractal dimension for a complete characterization (Gupta and Waymire, 1990).

Geophysical phenomena such as rain and river flow are better described by multiscaling models (Gupta and Waymire, 1990; Lovejoy and Schertzer, 1995). Multiscaling processes are characterized by extreme and more or less isolated events. For instance, high-resolution measurements are needed to detect rainfall of high intensity because such intensities occur only during very short periods of time (Lovejoy and Schertzer, 1995).

The spatial structure of soil properties have been investigated using models appropriate to characterize simple scaling. The most common model used is the fractional Brownian motion which is obtained from a semivariogram. Analyses of semivariograms have showed simple scaling over limited range of scales for various soil properties (Burrough, 1983, 1993). Li and Loehle (1995) used wavelet analysis to show that quasi-periodic behavior in semivariograms of air permeability was caused by a hierarchical distribution of heterogeneities at different scales. Also Folorunso et al. (1994) found multiscaling behavior of soil surface strength of dry soils. Morphological differences in the vertical and horizontal directions may result in anisotropic scaling of soil properties. For instance, vertical and horizontal transects of log-transformed $k_{sat}$ had different scaling parameters when fitted to a model of fractional Brownian motion (Kemblowski and Chang, 1993).

Scaling characteristics of $k_{sat}$ are important to infer statistical properties of a distribution at scales other than the measured one and to guide modeling efforts. Numerical simulations of three-dimensional flow in heterogeneous soil have shown scaling of hydraulic conductivity consistent with a fractal model (Zhang, 1997). These numerical experiments showed that the scale dependance of hydraulic conductivity increased with increasing degree of soil heterogeneity. Neuman (1994) has shown a scaling behavior of the log of soil hydraulic conductivities for separation intervals ranging between 0.1 to 500 m, with most of the data between 2 and 30 m. Scaling of $k_{sat}$ for scales smaller than 1 m has not being investigated. Analysis of the moments of distributions of $k_{sat}$ measurements obtained on soil volumes with dimensions mostly smaller than 1 m can provide evidence on the scaling nature of $k_{sat}$ at small intervals. The objective of this paper was to investigate scaling characteristics of $k_{sat}$ using the method of the moments.

## 2. Background

Scaling refers to a statistical invariance in the probability distributions of a process with respect to a scale function $C_\lambda$. Simple scaling implies that for values corresponding to each scale factor $\lambda$ larger than 0, a probability distribution $Y_\lambda$ can be related to the probability distribution obtained at the unit resolution, $Y_1$, by a scale function of the form $C_\lambda = \lambda^k$, where $k$ is a scaling exponent, that can be positive or negative (Gupta and Waymire, 1990; Kumar et al., 1994). The scale factor $\lambda$ can be applied to both contraction ($\lambda > 1$) and magnification ($\lambda < 1$). A consequence of simple scaling is that the moments of order $q$ of a distribution obtained with a scale factor $\lambda$ is related to the moments of the unit resolution distribution as:

$$E[Y_\lambda^q] = \lambda^{k(q)} E[Y_1^q] \tag{1}$$

where $E[]$ denote expected values. For a process that is simple scaling, $k$ is a single value parameter linearly related to the order of the moment $q$. For a multiscaling process, on the other hand, $k$ is not a linear function in $q$. Eq. (1) has been used to determine scaling properties of rainfall and soil moisture from images by studying distributions of pixel properties at several grouping levels (scale factors) or spatially distributed rain gauges (Gupta and Waymire, 1990; Rodriguez-Iturbe et al., 1995; Svensson et al., 1996; Dubayah et al., 1997).

The fractional Brownian motion is an example of a simple scaling process that has been used to describe the spatial structure of $k_{sat}$ (Kemblowski and Chang, 1993):

$$\gamma(\lambda) = 0.5E\left[(y_z - y_{z+\lambda})^2\right] = \lambda^{2H}\gamma_1 \tag{2}$$

where $\gamma(\lambda)$ is a semivariance, and $H = k$ is a scaling exponent known as the Hurst exponent. Eq. (2), known as a semivariogram, estimates an average semivariance of point measurements separated by a distance $\lambda$. Investigations of the spatial structure of $k_{sat}$ with Eq. (2) were made in the context of water management studies, usually involving separation intervals larger than 1 m. Gupta and Waymire (1990) presented other models of simple scaling.

## 3. Material and methods

We used published data to test the scaling characteristics of $k_{sat}$ according to Eq. (1). The three data sets selected have in common that $k_{sat}$ was measured in samples of different dimensions. A scale factor $\lambda$ is defined as $\lambda = E_1/E_i$, where $E_i$ is sample dimension (length, area, or volume) increasing from $i = 1$ to $i = n$.

Anderson and Bouma (1973) studied the effect of sample length on $k_{sat}$. They measured $k_{sat}$ on ten soil cores of constant diameter (0.075 m) and increasing length (0.05, 0.075, 0.10, and 0.17 m) sampled from a B2 horizon (silty clay loam) of a Batavia silt loam (Typic Argiudoll). Another set of $k_{sat}$ from the same soil horizon was measured in 0.10 m high and 0.075 m diameter cores, and a mix of Rhodamine B dye and water (ratio 1:10) was run through the cores. Length of colored planar voids at several cross sections along soil cores was determined from resin-impregnated sections.

Lauren et al. (1988) measured $k_{sat}$ on 37 sites along a 370-m transect on an argillic horizon. At each site, $k_{sat}$ was measured on soil rectangular columns of decreasing cross-sectional area: $1.60 \times 0.75$, $1.20 \times 0.75$, $0.50 \times 0.50$ m, and circular columns with diameters of 0.20 and 0.07 m. With the exception of the length of smallest circular column (0.06 m), sample length was 0.20 m. Measurements on rectangular columns were made in situ. Starting with the largest size, column walls were covered with plaster, and a thin layer of soil was

removed from the surface prior to ponding. Ponding was maintained for 3 to 4 h to establish steady-state flow that was assumed equal to $k_{sat}$. Measurements on circular columns were made on detached samples using a constant head method (Bouma, 1982). Prior to measurements of $k_{sat}$, visible pores were traced on an acetate transparency sheet (0.07 $m^2$) placed on the surface. Original acetate sheets were photocopied and reduced to 0.036 $m^2$, and scanned. Binary images ($901 \times 1201$ pixels) of the full acetate sheets and of the centered $601 \times 900$, $289 \times 601$, and $271 \times 301$ pixels were generated. Area of pores larger than 10 square pixels were obtained with NIH-Image.

Mallants et al. (1997) presented $k_{sat}$ data for the surface horizon of a sandy loam soil (Udifluvent) measured on columns of 0.05, 0.20, and 0.30 m in diameter; and respective lengths of 0.051, 0.20 and 1 m. A constant head method was used in the smallest two columns. Tensiometers were installed in the 1-m length column at several depths and the columns were saturated from the bottom. Water was ponded on the top to a maximum depth of about 0.01 m, and water flux and pressure potentials were measured once a day for 20 days. Values of $k_{sat}$ for the 0–0.15 m were estimated from flux measurements and tensiometer reading using Darcy's law. These values, however, are controlled by the length of the full column, i.e., 1 m.

### *3.1. Data analysis*

A distribution of measurements of $k_{sat}$ or macroporosity made on a particular soil volume was tested for normality according to Shapiro and Wilk (1965), and its moments were calculated assuming normal ($k_{sat}$, macroporosity) and log-normal ($k_{sat}$) distributions. Statistical moments of order $q$ of a normal distribution, $M$, were estimated from the derivative of order $q$ with respect to $t$ of the moment generating function

$$M(t) = \exp\left[\mu t + \frac{t^2\sigma^2}{2}\right] \tag{3}$$

by setting $t = 0$. Moments for the log-normal distribution were estimated according to

$$M_{ln}^q = \exp\left[q\left(\mu_{ln} + q/2\sigma_{ln}^2\right)\right] \tag{4}$$

where $\mu$, $\mu_{ln}$; and $\sigma$, $\sigma_{ln}$ are the mean and standard deviation of $k_{sat}$ and $\ln k_{sat}$, respectively.

Moments $M(t)$ and $M_{ln}^q$, estimated with Eqs. (3) and (4) were obtained for distributions representing different scale factors. The scaling parameter for a given moment order was estimated with linear regression (Statistix, 1996) from a log–log plot of moment order vs. scale factor.

## 4. Results and discussion

In this paper we used the method of the moments to infer a spatial structure of $k_{sat}$. Moments were estimated from distributions of $k_{sat}$ measurements obtained with samples of different volume. Changes in sample volume were achieved by changes in sample length, sample cross sectional area, or a combination of both. Thus, data was not aggregated to infer their scaling properties as is usually done when this technique is used in remote sensing studies (Rodriguez-Iturbe et al., 1995; Dubayah et al., 1997). The spatial location of a sample was not considered in the analysis as is commonly done in studies of spatial structure with semivariograms.

Saturated hydraulic conductivity is related to a mean equivalent pore diameter through Poiseuille's Law. For non-uniform pores composed by segments of varying length and diameter, total pore length, along with length and diameter of segments determine the mean equivalent diameter of a pore system (Dunn and Phillips, 1991). Systematic changes in pore diameter are likely to occur where soil properties change, e.g., at interfaces between horizons, or near the soil surface. In regions of a soil profile less subjected to changes, pore properties are probably more homogeneous and $k_{sat}$ measurements less variable. Typically, values measured on short cores sampled through areas of a soil profile with variable soil properties are more variable than those measured on longer samples. In the latter case a sample is more likely to enclose an area of relatively homogeneous soil that act regulating the flow. A small cross-sectional area usually increases the variability of measurements because a core may sample areas that are either favorable or restrictive to flow.

It is usually assumed that $k_{sat}$ follows a log-normal distribution (Kutílek and Nielsen, 1994). Horowitz and Hillel (1987), on the other hand, have shown that log-normality could be a consequence of analyzing a low number of samples. Tests of normality showed that a ln transformation increased normality in the distributions of the Lauren et al. (1988) and Mallants et al. (1997) data sets, whereas the Anderson and Bouma (1973) data was normally distributed regardless of the transformation (Table 1). Except for the latter data set, normality of a distribution was changed with sample dimension, but such differences decreased when data was ln-transformed (Table 1). Given the uncertainty on the overall distribution of $k_{sat}$, the analysis of the moments was performed assuming a normal and a log-normal distribution.

Anderson and Bouma (1973) showed that the mean and standard deviations of $k_{sat}$ measurements decreased with increasing sample length. They attributed this effect to a decrease in connectivity of the larger pores, i.e., the probability that pores will remain connected throughout the length of a core increases with decreasing core length. Large and connected pores result in high values of $k_{sat}$. Anderson and Bouma (1973) demonstrated a decrease in pore connectivity by a decrease in the total length of colored planar voids with depth. Measurement

Table 1
Summary of statistics of $k_{sat}$ values from three data sets assuming normal (subscript n) and log normal (subscript ln) distributions

| Sample dimension | $M_n$ | $\sigma_n$ | $W$ | $M_{ln}$ | $\sigma_{ln}$ | $W$ |
|---|---|---|---|---|---|---|
| Anderson and Bouma (1973) | | | | | | |
| $5.0\times10^{-2}$[a] | 74.10 | 20.12 | 0.958 | 4.25 | 0.29 | 0.959 |
| $7.5\times10^{-2}$ | 39.55 | 15.05 | 0.853 | 3.62 | 0.36 | 0.940 |
| $1.0\times10^{-1}$ | 14.97 | 4.90 | 0.974 | 2.65 | 0.36 | 0.957 |
| $1.7\times10^{-1}$ | 9.83 | 1.72 | 0.962 | 2.27 | 0.18 | 0.952 |
| Lauren et al. (1988) | | | | | | |
| $2.4\times10^{-1}$[b] | 2.48 | 1.96 | 0.792 | 0.66 | 0.70 | 0.967 |
| $1.8\times10^{-1}$ | 1.58 | 1.17 | 0.840 | 0.21 | 0.71 | 0.943 |
| $0.5\times10^{-2}$ | 1.76 | 1.80 | 0.661 | 0.23 | 0.75 | 0.850 |
| $6.3\times10^{-3}$ | 4.01 | 4.51 | 0.734 | 0.85 | 1.09 | 0.987 |
| $2.7\times10^{-4}$ | 3.88 | 5.36 | 0.661 | 0.69 | 1.22 | 0.978 |
| Mallants et al. (1997) | | | | | | |
| $0.5\times10^{-3}$[c] | 32.32 | 96.00 | 0.346 | 1.41 | 1.93 | 0.968 |
| $2.0\times10^{-1}$ | 14.34 | 25.93 | 0.460 | 1.84 | 1.28 | 0.959 |
| 1.0 | 4.78 | 1.71 | 0.879 | 1.51 | 0.33 | 0.941 |

$M$ and $\sigma$ are mean and standard deviation, respectively, and $W$ is a test statistics for deviation from normality.
[a]sample length (m), [b]sample volume ($m^3$), [c]sample length (m).

variability, imposed by a relatively small sample cross sectional area, increased with decreasing core length. Water flux in longer cores was controlled by a more homogeneous soil matrix with lower $k_{sat}$ values. The moments of the normal and log-normal distributions obtained with different core lengths showed a linear relationship in a log–log scale with almost identical scaling coefficients for both distributions (Table 2). When the scaling coefficients of the moments of

Table 2
Estimates of scaling exponent $k$, standard error of the estimates, (SE), residual sum of squares, RSS, and coefficient of determination, $R^2$, for moments of order $q$ estimated assuming normal and log-normal distributions of the $k_{sat}$ values of Anderson and Bouma (1973)

| Moment of order $q$ | Normal distribution | | | Log-normal distribution | | |
|---|---|---|---|---|---|---|
| | $k$(SE) | RSS | $R^2$ | $k$(SE) | RSS | $R^2$ |
| 1 | −1.72(0.319) | 0.031 | 0.936 | −1.73(0.315) | 0.030 | 0.937 |
| 2 | −3.49(0.625) | 0.117 | 0.940 | −3.50(0.599) | 0.107 | 0.945 |
| 3 | −5.29(0.922) | 0.255 | 0.943 | −5.32(0.855) | 0.219 | 0.951 |
| 4 | −7.11(1.216) | 0.443 | 0.945 | −7.19(1.089) | 0.355 | 0.956 |
| 5 | −8.94(1.508) | 0.681 | 0.946 | −9.10(1.308) | 0.513 | 0.960 |
| 6 | −10.70(1.804) | 0.975 | 0.946 | −11.06(1.520) | 0.692 | 0.964 |

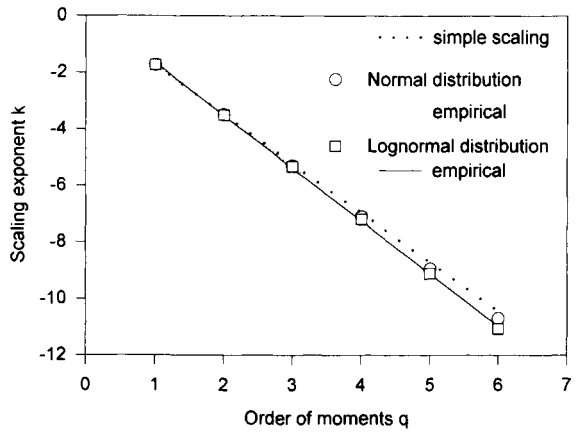


Fig. 1. Scaling exponent $k$ as a function of the order of the moments estimated from the distribution of $k_{sat}$ values of Anderson and Bouma (1973).

the normal and log-normal distributions where plotted as a function of the order of the moments they both showed simple scaling (Fig. 1), also evident in the similarity of the distributions across sample lengths (Table 1). Simple scaling could be the result of a dominant factor, i.e., pore connectivity, determining $k_{sat}$. At shallower depths there was an additive effect of more connected pores contributing to a $k_{sat}$ value.

The data set of Lauren et al. (1988) deals mainly with an increase in cross sectional area available to flow, but it also combines in situ measurements of $k_{sat}$ with determinations in detached columns. Plots of the value of the moments of the normal and log-normal distributions as a function of sample cross sectional area show significant scatter (Fig. 2). Experimental problems to

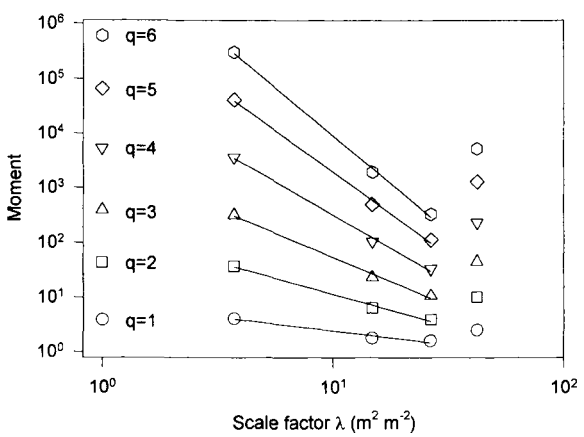


Fig. 2. Moments of a normal distribution as a function of scaling factor $\lambda$ for the data set of Lauren et al. (1988). Slopes of solid lines are the scaling exponents $k$ of a normal distribution shown in Fig. 3.

measure $k_{sat}$ on the largest and smallest soil columns may have introduced errors to those distributions. The increase in variability for the largest column may have resulted from experimental difficulties to saturate and measure $k_{sat}$ in such a large sample volume. The statistical distribution for the smallest core might have being influenced by a decrease of both cross-sectional area and sample length. Because of these limitations, slopes of the moments were obtained by considering the three samples with intermediate volume (Fig. 2 and Table 3). Even though measurements in cylindrical columns were made on detached samples, we assumed that the length of the detached cores (0.20 m) was enough to minimize the effect of high number of macropores open to the bottom of a sample (Anderson and Bouma, 1973).

The scaling properties of saturated flow in the soil of Lauren et al. (1988) depended on the type of distribution assumed. The growth of the scaling exponents with the order of the moments was larger for the moments of the log-normal distribution than the ones of the normal distribution (Table 3). The former case corresponds to a clear case of multiscaling, whereas moments for the normal distribution deviated only slightly from simple scaling (Fig. 3). The difference is caused by changes in the properties of the distributions of $k_{sat}$ and $\ln k_{sat}$ with sample size. Distributions of $k_{sat}$ deviated more from normality and were less homogeneous across sample sizes than those of $\ln k_{sat}$ (compare $W$-values for transformed and non-transformed distributions in Table 1). Deviations from normality may have resulted in more accurate determinations of the moments for the log-transformed $k_{sat}$ distributions.

An analysis of the scaling characteristics of macroporosity may shed light on the scaling of $k_{sat}$ since both properties are spatially related (Lauren et al., 1988; Mallants et al., 1997). Furthermore, Ahuja et al. (1984) found that the scaling properties of macroporosity and $k_{sat}$ (measured in the same sample volume) were similar. We applied the method of the moments to investigate scaling of the areal distribution of total visible porosity (macroporosity) obtained from

Table 3
Estimates of scaling exponent $k$, standard error of the estimates, (SE), residual sum of squares, RSS, and coefficient of determination, $R^2$, for moments of order $q$ estimated assuming normal and log-normal distributions of the $k_{sat}$ values of Lauren et al. (1988)

| Moment $q$ | Normal distribution | | | Log-normal distribution | | |
|---|---|---|---|---|---|---|
| | $k$(SE) | RSS | $R^2$ | $k$(SE) | RSS | $R^2$ |
| 1 | −0.50(0.094) | 0.003 | 0.965 | −0.53(0.132) | 0.007 | 0.941 |
| 2 | −1.16(0.097) | 0.004 | 0.993 | −1.40(0.333) | 0.042 | 0.946 |
| 3 | −1.76(0.132) | 0.007 | 0.994 | −2.61(0.602) | 0.139 | 0.949 |
| 4 | −2.41(0.138) | 0.007 | 0.997 | −4.15(0.939) | 0.338 | 0.951 |
| 5 | −3.03(0.155) | 0.009 | 0.997 | −6.04(1.343) | 0.693 | 0.953 |
| 6 | −3.50(0.145) | 0.008 | 0.998 | −8.26(1.816) | 1.267 | 0.954 |

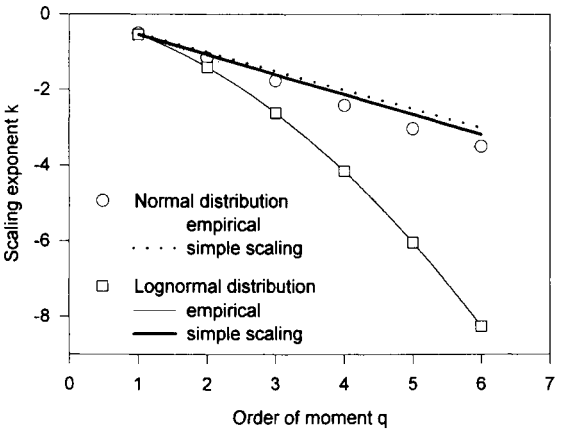


Fig. 3. Scaling exponent $k$ as a function of the order of the moment estimated from the distribution of $k_{sat}$ values of Lauren et al. (1988) by assuming normal and log-normal distribution of observations.

binary images of the original drawings of Lauren et al. (1988). The moments of macroporosity distributions were estimated assuming a normal distribution (a ln transformation is unlikely to change the properties of these distributions) in agreement with Lauren et al. (1988). The moments of macroporosity distributions showed scaling properties (Table 4), with the growth of the scaling exponents being multiscaling (Fig. 4). Macroporosity and $\ln k_{sat}$ exhibited similar scaling behavior as demonstrated by comparable relative deviations from simple scaling. The percentage of deviation from simple scaling for the scaling exponents of the 6th moments of macroporosity and $\ln k_{sat}$ were 55% and 61%. The better fit achieved with the log-normal model and the similarity between the scaling of macroporosity and $\ln k_{sat}$ suggest that the data of Lauren et al. (1988) was multiscaling.

The data of Mallants et al. (1997) combine changes in sample cross sectional area (diameters of 0.051, 0.20, and 0.30 m) and length (0.051, 0.20, and 1 m).

Table 4
Estimates of scaling exponent $k$, standard error of the estimates, (SE), residual sum of squares, RSS, and coefficient of determination, $R^2$, for moments of order $q$ estimated assuming normal distribution of the macroporosity values of Lauren et al. (1988)

| Moment $q$ | $k$(SE) | RSS | $R^2$ |
|---|---|---|---|
| 1 | −0.213(0.042) | 0.003 | 0.928 |
| 2 | −0.729(0.140) | 0.015 | 0.931 |
| 3 | −1.165(0.200) | 0.061 | 0.944 |
| 4 | −1.696(0.295) | 0.131 | 0.943 |
| 5 | −2.197(0.370) | 0.206 | 0.946 |
| 6 | −2.880(0.445) | 0.299 | 0.954 |

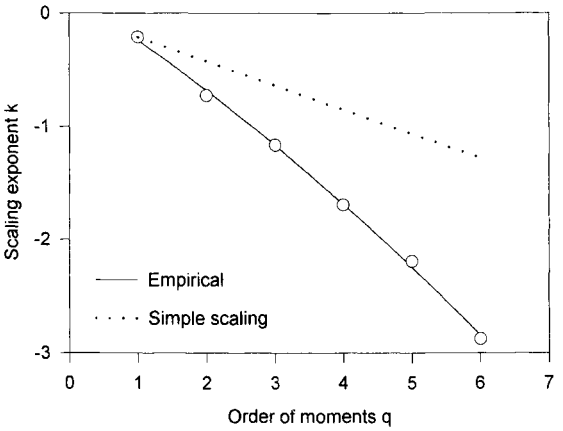


Fig. 4. Scaling exponent $k$ as a function of the order of the moments estimated from the distribution of the macroporosity values of Lauren et al. (1988).

Distributions of $k_{sat}$ deviated more from normality, and were less homogeneous across sample size than distributions of $\ln k_{sat}$ (Table 1). Sample length dominated scaling properties of this data set. Moments of the $k_{sat}$ distribution for the three sample sizes were linear in a log–log scale only when plotted as a function of sample length (Table 5). Simultaneous variations in length and cross-sectional area may have caused the non-linearity observed in the plot of the moments of the distribution vs. sample volume. Kemblowski and Chang (1993) found different scaling exponents for samples taken along transects parallel and perpendicular to soil surface.

Moments of both log-normal and normal distributions were multiscaling (Fig. 5). As with the data of Lauren et al. (1988), multiscaling behavior was more evident for the moments of the log-normal distribution. The data of Mallants et al. (1997) showed larger deviations from normality than the Lauren et al. (1988)

Table 5
Estimates of scaling exponent $k$, standard error of the estimates, (SE), residual sum of squares, RSS, and coefficient of determination, $R^2$, for moments of order $q$ estimated assuming normal and log-normal distributions of the $k_{sat}$ values of Mallants et al. (1997)

| Moment $q$ | Normal distribution | | | Log-normal distribution | | |
|---|---|---|---|---|---|---|
| | $k$(SE) | RSS | $R^2$ | $k$(SE) | RSS | $R^2$ |
| 1 | −0.64(0.025) | 0.001 | 0.998 | −0.57(0.070) | 0.004 | 0.985 |
| 2 | −2.02(0.113) | 0.011 | 0.997 | −2.34(0.148) | 0.000 | 1.000 |
| 3 | −2.94(0.246) | 0.051 | 0.993 | −5.31(0.256) | 0.056 | 0.998 |
| 4 | −4.29(0.345) | 0.100 | 0.994 | −9.47(0.653) | 0.361 | 0.995 |
| 5 | −5.32(0.507) | 0.215 | 0.991 | −14.83(1.206) | 1.233 | 0.993 |
| 6 | −6.59(0.510) | 0.217 | 0.994 | −21.38(1.914) | 3.107 | 0.992 |

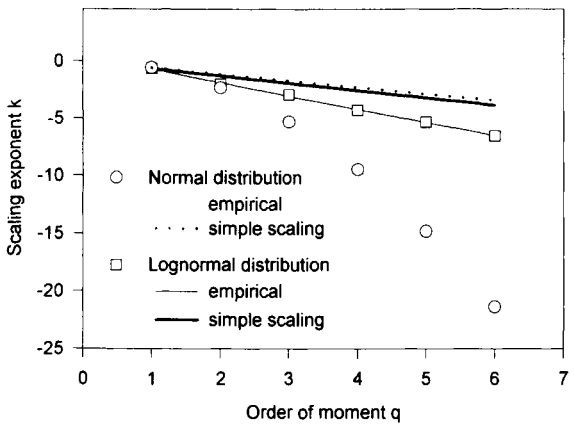


Fig. 5. Scaling exponent $k$ as a function of the order of the moment estimated from the distribution of $k_{sat}$ values of Mallants et al. (1997) by assuming normal and log-normal distribution of observations.

data, as demonstrated by the lower values of the test statistic $W$ attained by the former distributions (Table 1). An important difference between the data of Mallants et al. (1997) and Lauren et al. (1988) is that in the latter soil samples were from a single soil horizon whereas in the former the largest sample included three soil horizons with distinctive morphological characteristics and statistical properties of $k_{sat}$ distributions. Clay content increased with depth, whereas soil structure was moderate in the 0.25 to 0.55 m and weak in the rest of the profile (Mallants et al., 1997). Mallants et al. (1996) showed that coefficients of variation of $k_{sat}$ varied among soil horizons, being largest in the deepest soil horizon (0.55–1 m)—highest clay content and weak structure—and lowest in the intermediate one (0.25–0.55 m)—intermediate clay content and moderate soil structure. These differences in flow conditions may have determined the larger relative deviations from simple scaling in the Mallants et al. (1997) data as compared to the data of Lauren et al. (1988).

### *4.1. Scaling exponent from semivariograms*

Spatial structure at larger separation intervals are typically studied with semivariograms. Scaling exponents obtained with the method of the moments ($q = 2$) and the semivariogram model showed in Eq. (2) can be used together to obtain scaling parameters over a wide range of scales. Semivariograms of the Lauren et al. (1988) cylindrical and planar void distributions fitted Eq. (2) within a range of 70 m (Fig. 6). Furthermore, the scaling exponent of the second moment of macroporosity, $k = 0.36$, compared well with the scaling exponent $H = 0.39$ and $H = 0.31$ obtained from semivariograms of cylindrical and planar voids, respectively (Fig. 6). It should be noted, however, that semivariances at a

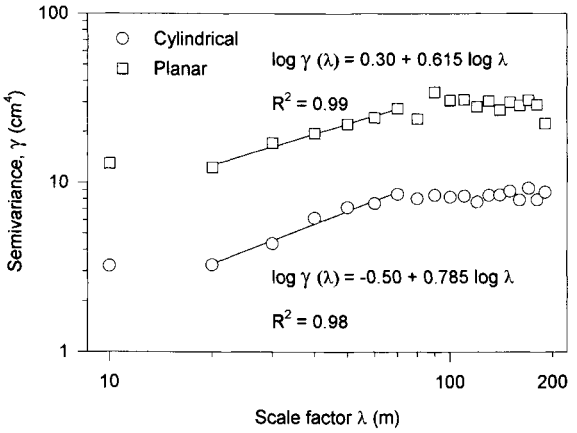


Fig. 6. Semivariograms of cylindrical and planar voids calculated by Lauren et al. (1988).

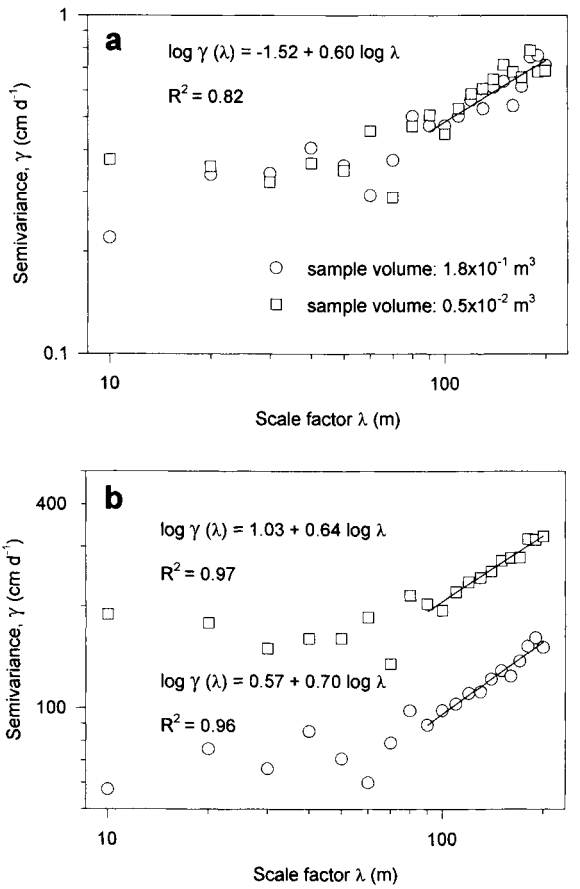


Fig. 7. Semivariograms of $k_{sat}$ measured on two sample volumes assuming log-normal (a) and normal (b) distribution of observations.

spacing of $\lambda = 10$ m deviated from the linear relation shown in Fig. 6 which suggest a discontinuity in the scaling properties of macroporosity between the scales covered by the method of the moments and the one shown in the semivariograms.

Eq. (2) was not a good model of the spatial structure of either $k_{sat}$ or $\ln k_{sat}$ measured by Lauren et al. (1988) in samples of $1.8 \times 10^{-1}$ and $0.5 \times 10^{-2}$ $m^3$ (particularly at spacings smaller than 90 m). Possibly, spatial structure of this property was confined to an area smaller than the minimum spacing used in the semivariograms. A linear section was noticeable in semivariograms from both sample sizes within separation intervals between 60 to 80 m and 200 m (Fig. 7). Average values of scaling exponents from semivariograms were $H = 0.30$ for $k_{sat}$, and $H = 0.34$ for $\ln k_{sat}$, and slightly smaller than the ones found with the method of the moments (Table 3). The cause(s) of the scaling at that range and the lack of scaling at shorter space intervals remain unclear, but it can be interpreted as being the result of the multiscale nature of soil which may result in semivariograms with a step-wise increase (Neuman, 1994).

Semivariograms calculated from data in Mallants et al. (1997) did not show any clear spatial structure for either $k_{sat}$ or $\ln k_{sat}$ when analyzed with Eq. (2). This can be the result of different scaling properties in the vertical and horizontal directions (Kemblowski and Chang, 1993; Li and Loehle, 1995).

## 5. Conclusions

Scaling parameters of $k_{sat}$ measured on samples with linear dimensions ranging from a few centimeters to over a meter were determined with the method of the moments. These scales were not considered in previous studies. The upper and lower sample dimensions were mainly determined by experimental limitations on measuring $k_{sat}$ beyond those dimensions.

Simple scaling was observed when $k_{sat}$ was measured on small soil volumes (constant cross sectional area and increasing length) sampled from a single soil horizon. Variation of pore connectivity with sample length was probably the dominant factor determining simple scaling. When water flow occurred through larger soil volumes, multiscaling was found by scaling either the cross sectional area or the length of soil available to flow. Multiscaling behavior was more clearly manifested by the log-transformed distributions of $k_{sat}$ than by the non-transformed data. A normal distribution may have not been representative of sample distributions involving large soil volumes. Consequently, the determination of the moments for the normal distribution may been less accurate than the ones from the log-transformed distributions.

Saturated flow through large soil volumes is most likely multiscaling as the result of several sources of flux control acting at different scales (Neuman, 1994). The simple scaling observed in the Anderson and Bouma (1973) data set

occurred when variability sources were limited (small samples of a single horizon).

Macroporosity and $k_{sat}$ were spatially related in the data set of Lauren et al. (1988). The scaling characteristics of both properties were similar, which suggests that prediction of $k_{sat}$ scaling could be attained by considering morphological indicators. A better understanding of the influence of soil structure on water flow in soil can be gained by studying scaling properties of different soil properties in relation to scaling characteristics of water flow.

The method of the moments is promising to studying scaling of $k_{sat}$ and other soil hydraulic properties at scales smaller than 1 m. More research is needed to evaluate the relation between scaling exponents obtained with this technique and with other methods involving point measurements such as the semivariogram method.

## References


Ahuja, L.R., Naney, J.W., Green, R.E., Nielsen, D.R., 1984. Macroporosity to characterize spatial variability of hydraulic conductivity and effects of land management. Soil Sci. Soc. Am. J. 48, 699–702.

Anderson, J.L., Bouma, J., 1973. Relationship between saturated hydraulic conductivity and morphometric data of an argillic horizon. Soil Sci. Soc. Am. Proc. 37, 408–421.

Bouma, J., 1982. Measuring the hydraulic conductivity of soil horizons with continuous macropores. Soil Sci. Soc. Am. J. 46, 438–441.

Burrough, P.A., 1983. Multiscale sources of spatial variation in soil: I. The application of fractal concepts to nested levels of soil variation. J. Soil Sci. 34, 577–597.

Burrough, P.A., 1993. Soil variability: a late 20th century view. Soils and Fertilizers 56, 529–562.

Dubayah, R., Wood, E.F., Lavallee, D., 1997. Multiscaling analysis in distributed modeling and remote sensing: An application using soil moisture. In: Quattrochi, D.A., Goodchild, M.F., (Eds.), Scale in Remote Sensing and GIS. CRC/Lewis Publishers, Boca Raton, FL, USA.

Dunn, G.H., Phillips, R.E., 1991. Equivalent diameter of simulated macropore systems during saturated flow. Soil Sci. Soc. Am. J. 55, 1244–1248.

Feder, J., 1988. Fractals. Plenum, New York.

Folorunso, O.A., Puente, C.E., Rolston, D.E., Pinzon, J.E., 1994. Statistical and fractal evaluation of the spatial characteristics of soil surface strength. Soil Sci. Soc. Am. J. 58, 284–294.

Gupta, V.K., Waymire, E., 1990. Multiscaling properties of spatial rainfall and river flow distributions. J. Geophys. Res. 95 (D3), 1999–2009.

Horowitz, J., Hillel, D., 1987. A theoretical approach to the areal distribution of soil surface conductivity. Soil Sci. 43 (4), 231–240.

Kemblowski, M.W., Chang, C.M., 1993. Infiltration in soils with fractal permeability distribution. Ground Water 31, 187–192.

Kumar, P., Guttarp, P., Foufoula-Georgiou, E., 1994. A probability-weighted moment test to assess simple scaling. Stochastic Hydrology and Hydraulics 8, 173–183.

Kutílek, M., Nielsen, D.R., 1994. Soil Hydrology. Catena Verlag, Cremlingen-Destedt, Germany.

Lauren, J.G., Wagenet, R.J., Bouma, J., Wösten, J.H., 1988. Variability of saturated hydraulic conductivity in a Glossaquic Hapludalf with macropores. Soil Sci. 145, 20–27.

Li, B.L., Loehle, C., 1995. Wavelet analysis of multiscale permeabilities in the subsurface. Geophys. Res. Lett. 22 (23), 3123–3126.

Lovejoy, S., Schertzer, D., 1995. Multifractals and rain. In: Kundzewicz, A.W. (Ed.), New Uncertainty Concepts in Hydrology and Hydrological Modelling. Cambridge Press, Cambridge, UK, pp. 61–103.

Mallants, D., Mohanty, B.P., Jacques, D., Feyen, J., 1996. Spatial variabilitity of hydraulic properties in a multi-layered soil profile. Soil Sci. 161, 167–181.

Mallants, D., Mohanty, B.P., Vervoort, A., Feyen, J., 1997. Spatial analysis of saturated hydraulic conductivity in a soil with macropores. Soil Technol. 10, 115–131.

Murphy, C.P., Banfield, C.F., 1978. Pore space variability in a sub-surface horizon of two soils. J. Soil Sci. 29, 156–166.

Neuman, S.P., 1994. Generalized scaling of permeabilities: Validation and effect of support scale. Geophys. Res. Lett. 21, 349–352.

Rodriguez-Iturbe, I., Vogel, G.K., Rigon, R., Entekhabi, D., Castelli, F., Rinaldo, A., 1995. On the spatial organization of soil moisture fields. Geophys. Res. Lett. 22, 2757–2760.

Shapiro, S.S., Wilk, M.B., 1965. An anlysis of variance test for normality (complete samples). Biometrika 3, 591–611.

Sisson, J.B., Wierenga, P.J., 1981. Spatial variability of steady-state infiltration rates as a stochastic process. Soil Sci. Soc. Am. J. 45, 699–704.

Statistix, 1996. User's Manual. Version 1.0. Analytical Software, Tallahassee, FL, USA.

Svensson, C., Olsson, J., Berndtsson, R., 1996. Multifractal properties of daily rainfall in two different climates. Water Resour. Res. 32, 2463–2472.

Zhang, R., 1997. Scale-dependent soil hydraulic conductivity. In: Novak, M.M., Dewey, T.G. (Eds.), Fractal Frontiers. World Scientific, New York, NY, pp. 383–391.

Zobeck, T.M., Fausey, N.R., Al-Hamdan, N.S., 1985. Effect of sample cross-sectional area on saturated hydraulic conductivity in two structured clay soils. Trans. ASAE 28, 791–794.

*Fractals in Soil Science*
Editors: Ya.A. Pachepsky, J.W. Crawford and W.J. Rawls
© 2000 Elsevier Science B.V. All rights reserved.


# Estimating soil mass fractal dimensions from water retention curves [1]

E. Perfect *

*Department of Agronomy, University of Kentucky, Lexington, KY 40546-0091, USA*

Received 13 November 1997; accepted 28 September 1998

**Abstract**

The drying branch of the water retention curve is widely used for modeling hydrologic processes and contaminant transport in porous media. A prefractal model is presented for this function based on the capillary equation and a randomized Menger sponge algorithm with upper and lower scaling limits. The upper limit is the air entry value ($\Psi_0$) and the lower limit is the tension at dryness ($\Psi_j$). Between these two limits the theoretical curve is concave when plotted as relative saturation ($S$) vs. the log of tension ($\Psi$). The mass fractal dimension ($D$) controls the degree of curvature, with decreasing concavity as $D \rightarrow 3$. The theoretical equation was fitted to water retention data for six soils from Campbell and Shiozawa [Campbell, G.S., Shiozawa, S., 1992. Prediction of hydraulic properties of soils using particle size distribution and bulk density data. International Workshop on Indirect Methods for Estimating the Hydraulic properties of Unsaturated Soils. University of California Press, Berkeley, CA, pp. 317–328]. These data consisted of between 31 and 39 paired measurements of $S$ and $\Psi$ for each soil, with $\Psi$ ranging from $3.1 \times 10^0$ to $3.3 \times 10^5$ kPa. All of the fits were excellent with adjusted $R^2$ values $\geq 0.96$. The resulting estimates of $D$ were all significantly less than three at $P < 0.05$. The lowest value of $D$ was 2.60 for a sandy loam soil, and the highest was 2.90 for a silty clay soil. Refitting the same data, but over a restricted subset of $\Psi$'s $\leq 1.5 \times 10^3$ kPa, produced errors in the estimation of $D$. Two of the estimates of $D$ were significantly greater than three at $P < 0.05$. To estimate $D$ accurately, water retention data covering the entire tension range from saturation to zero water content are required. In the absence of such data, it is possible to obtain physically reasonable estimates of $D$ by setting $\Psi_j = 10^6$ kPa, the approximate tension at oven dryness, and fitting the proposed equation as a two parameter model. © 1999 Elsevier Science B.V. All rights reserved.

*Keywords:* moisture characteristic; prefractals; pore-size distribution; oven drying

* Tel.: +1-606-257-1885; Fax: +1-606-257-2185; E-mail: eperfect@ca.uky.edu
[1] Kentucky Agric. Exp. Stn. Contribution No. 97-06-141.

Reprinted from Geoderma 88 (1999)
© 1999 Elsevier Science B.V. All rights reserved

## 1. Introduction

The drying branch of the water retention curve, $S(\Psi)$, is widely used for modeling hydrologic processes and contaminant transport in natural porous media such as soils and rocks. The $S(\Psi)$ is usually determined experimentally from paired measurements of relative saturation, $S$ (defined as the volumetric water content, $\theta$, divided by the volumetric water content at saturation, $\theta_{sat}$), and soil water tension, $\Psi$, made under quasi-equilibrium conditions, with both variables slowly changing over time (Topp et al., 1993).

Several theoretical models have been proposed for the $S(\Psi)$ of ideal fractal porous media. These can be classified as either surface- or mass-based models. The first type assumes the porous medium is a surface fractal, and that water is present only as thin adsorbed films on pore surfaces, all of the capillary water having drained as predicted by the well-known capillary equation (de Gennes, 1985; Toledo et al., 1990). The second type assumes the porous medium is a mass fractal, and that only capillary water is present, with complete drainage of each pore as predicted by the capillary equation (Ahl and Niemeyer, 1989; Tyler and Wheatcraft, 1990; Pachepsky et al., 1995).

Equations for the $S(\Psi)$ resulting from these two different modeling strategies have been compared by Crawford et al. (1995), Bird et al. (1996) and Giménez et al. (1997). A limitation of both approaches is that fractal scaling of the $S(\Psi)$ is assumed to hold over an infinite range of tensions. In reality, natural porous media have both upper and lower scaling limits, corresponding to the water tensions draining their largest and smallest pores, respectively. Systems that are fractal over a finite range of scales are called prefractals (Mandelbrot, 1982). Perfect et al. (1996, 1998) have proposed a mass-based prefractal model for the $S(\Psi)$ in which the capillary equation applies over a finite range of tensions. However, when this equation was fitted to experimental data from a wide range of porous media, many nonphysical estimates of $D > 3$ were obtained.

In fitting any fractal model to experimental data it is vital that the data cover as wide a range of scales as is possible. This often necessitates the use of different methods at different scales (e.g., Davis, 1989). Rossi and Nimmo (1994) reported differences in goodness of fit for an empirical equation fitted to $S(\Psi)$ data over a restricted range of tensions ($\Psi \leq 1.5 \times 10^3$ kPa), as compared to its performance over the range $\Psi \leq 1.8 \times 10^6$ kPa. While the four-decade tension range used by Perfect et al. (1996, 1998) exceeded the minimum of at least one decade required to compute an experimental $D$ value (Pfeifer and Orbert, 1989), it is likely that a wider range of tensions would have yielded better estimates of $D$. In order to cover the complete range of $S$, water retention data are needed over a six-decade tension range. This is because air entry commonly occurs at approximately $10^0$ kPa, while zero water content, as defined by oven drying, corresponds to a tension of approximately $10^6$ kPa (Ross et al., 1991; Rossi and Nimmo, 1994).

The objectives of this paper are to present a new derivation of the Perfect et al. (1996, 1998) equation, to fit the resulting equation to $S(\Psi)$ data covering a wide range of tensions, and to analyze the influence on $D$ of fitting over a reduced range of tensions. Since it is extremely difficult and time-consuming to determine the complete $S(\Psi)$ (different methods must be employed at different scales), previously published data were used for the fitting. These data were selected because they covered the entire range of $S$, and because they included soils from widely different textural classes.

## 2. Theoretical considerations

Water extraction from a saturated prefractal Menger sponge (Mandelbrot, 1982; Turcotte, 1992) can be modeled as a stepwise process. First pore space is created by applying a randomized Menger sponge generator, in which $\mu$ is the number of elements removed and $b$ is the scaling factor, to a solid initiator of unit length $j$ times. It follows that the mass fractal dimension, $D$, of the sponge is given by (Mandelbrot, 1982; Turcotte, 1992):

$$D = \log(b^3 - \mu)/\log(b) \tag{1}$$

The sponge is now assumed to be saturated with water in equilibrium with a hanging water column. It is further assumed that all of the pores are hydraulically connected to the atmosphere via larger pores. Thus, progressively smaller pores will desaturate as the length of the hanging water column, and the tension in the pore water, is increased.

From Rieu and Sposito (1991) and Perfect et al. (1998), the $i$th level volumetric water content, $\theta_{i,j}$, of the prefractal Menger sponge is given by:

$$\theta_{i,j} = (b^i)^{D-3} - (b^j)^{D-3} \tag{2}$$

where $0 \leq i \leq j$. The saturated water content, or total porosity, of the sponge, $\theta_{0,j}$ is obtained by setting $i = 0$ in Eq. (2), i.e.,

$$\theta_{0,j} = 1 - (b^j)^{D-3} \tag{3}$$

The relative saturation of the sponge, $S$, can now be defined as:

$$S = \theta_{i,j}/\theta_{0,j} = \left[(b^i)^{D-3} - (b^j)^{D-3}\right]/\left[1 - (b^j)^{D-3}\right] \tag{4}$$

From the capillary equation, the tension of water at the $i$th level, $\Psi_i$, can be related to the scaling factor $b$ by (Tyler and Wheatcraft, 1990):

$$\Psi_i/\Psi_0 = b^i \tag{5}$$

where $\Psi_0$ is the tension that desaturates the largest pores present, commonly known as the air entry value. It follows from Eq. (5) that:

$$\Psi_j/\Psi_0 = b^j \tag{6}$$

where $\Psi_j$ is the tension that desaturates the smallest pores present, sometimes referred to as the tension at dryness.

Substituting Eqs. (5) and (6) into Eq. (4) and rearranging yields the following water retention equation for the prefractal Menger sponge:

$$S = \left(\Psi_i^{D-3} - \Psi_j^{D-3}\right)/\left(\Psi_0^{D-3} - \Psi_j^{D-3}\right); \qquad \Psi_0 \le \Psi_i \le \Psi_j \tag{7}$$

where $S = 1$ for $\Psi_i < \Psi_0$ and $S = 0$ for $\Psi_i > \Psi_j$. Eq. (7) predicts a stepwise water retention curve. However, water retention curves for natural porous media are continuous functions (Topp et al., 1993). To eliminate this discrepancy, $\Psi_i$ in Eq. (7) will henceforth be replaced by the continuous variable $\Psi$.

The above analysis includes a number of important assumptions. For instance, every time an element is removed, the length of the resulting pore is assumed to be $1/b^j$. However, if the removal pattern is truly random, pores will sometimes coalesce to produce mean pore lengths $> 1/b^j$ at the $j$th level. The presence of such pores will effect the mean tension required to desaturate pores at each level in the hierarchy. An additional complication is hysteresis due to the presence of hydraulically connected and disconnected pores. Disconnected pores on exterior surfaces will be open to the atmosphere, while those in the interior will be atmospherically isolated. In the case of connected pores, small pores may be connected to the atmosphere via larger ones, and large pores may be connected to the atmosphere via smaller ones. At the $i$th level, disconnected exterior pores and small pores connected to the atmosphere via larger ones will drain at a tension of $\Psi_i$, while atmospherically isolated pores and large pores connected to the atmosphere via smaller ones will not. These phenomena can lead to discrepancies between mass fractal dimensions computed from the pore-size distribution and values estimated from water retention data (Crawford et al., 1995; Bird and Dexter, 1997).

An approximate version of Eq. (7) was derived previously by Perfect et al. (1996, 1998) for a prefractal Menger sponge with a tightly bound residual water phase. The present analysis is more direct and does not require the assumption of a negligibly small residual water content.

In soil physics practice zero water content is defined by oven drying at a temperature of between 100° and 110°C for 24 h (Gardner, 1986; Nimmo, 1991). This somewhat arbitrary definition means that estimates of $\Psi_j$ based on experimental data can only vary as related to pore size over the range $\Psi_0 < \Psi_j \le \Psi_{\text{oven}}$, where $\Psi_{\text{oven}}$ is the soil water tension produced by oven drying. For $\Psi_j > \Psi_{\text{oven}}$, $S = 0$ and Eq. (7) can be rewritten as:

$$S = \left(\Psi^{D-3} - \Psi_{\text{oven}}^{D-3}\right)/\left(\Psi_0^{D-3} - \Psi_{\text{oven}}^{D-3}\right); \qquad \Psi_0 \le \Psi \le \Psi_{\text{oven}} \tag{8}$$

where $S = 1$ for $\Psi < \Psi_0$ and $S = 0$ for $\Psi > \Psi_{\text{oven}}$.

Eq. (8) is identical in form to the empirical equation used by Ross et al. (1991) to extend the Campbell (1974) water retention function to oven dryness. It is also consistent with the prefractal water retention models proposed by Rieu and Sposito (1991) and Perrier et al. (1996), as will be shown below. Eq. (8) can be rewritten as follows:

$$\theta_{i,j}/\theta_{0,j} = \left[(\Psi/\Psi_0)^{D-3} - (\Psi_{\text{oven}}/\Psi_0)^{D-3}\right]/\left[1 - (\Psi_{\text{oven}}/\Psi_0)^{D-3}\right] \quad (9)$$

Let us denote the experimentally determined volumetric water content at saturation as $\theta_{\text{sat}}$. From Eqs. (3), (6) and (8) we can define $\theta_{\text{sat}}$ as:

$$\theta_{\text{sat}} = 1 - (\Psi_{\text{oven}}/\Psi_0)^{D-3} \quad (10)$$

Substituting Eq. (10) into Eq. (9) and rearranging gives:

$$\theta_{i,j} = A\left[(\Psi/\Psi_0)^{D-3} - 1\right] + \theta_{0,j} \quad (11)$$

where $A = \theta_{0,j}/\theta_{\text{sat}}$ is the ratio of the theoretical water content at saturation to the experimentally determined value. Eq. (11) is similar to the general equation for water retention in prefractal porous media proposed by Perrier et al. (1996). It is to be expected that $A > 1$ when $\Psi_j > \Psi_{\text{oven}}$ since oven drying will underestimate the true saturated water content. For the case where $\Psi_0 < \Psi_j \leq \Psi_{\text{oven}}$, $A = 1$ and Eq. (11) reduces to the earlier Rieu and Sposito (1991) equation.

## 3. Experimental methods

Eqs. (7) and (8) were fitted to water retention curves for six soils from Campbell and Shiozawa (1992). Each curve consisted of between 31 and 39 paired measurements of $S$ and $\Psi$ (expressed as tension), with $\Psi$ ranging from $3.1 \times 10^0$ to $3.3 \times 10^5$ kPa. The reader is referred to the original publication for details on the physical characterization of the soils, and the different experimental methods employed. Eqs. (7) and (8) were also fitted to a truncated subset of these data, in which all values of $\Psi > 1.5 \times 10^3$ kPa were excluded from the fitting. This cutoff was selected because it corresponds to the tension at which most water retention experiments are terminated in soil physics research. The truncated curves consisted of between 15 and 17 paired measurements of $S$ and $\Psi$. The fitting was performed with $\Psi_j$ in Eq. (7) as a free parameter, and $\Psi_{\text{oven}}$ in Eq. (8) as a constant of $10^6$ kPa as suggested by Rossi and Nimmo (1994).

A segmented nonlinear regression procedure (Appendix A) was used for the fitting, and all of the fits converged according to the software default criterion (SAS Institute, 1989). Goodness of fit was assessed using the adjusted coefficient of determination, adj. $R^2$, between observed and predicted values. Parame-

ters from the different fits were compared using linear regression analysis (SAS Institute, 1989).

## 4. Results of nonlinear fits

The results of fitting Eq. (7) as three-parameter model to the complete water retention curves from Campbell and Shiozawa (1992) are summarized in Table 1. The adj. $R^2$ values indicated that Eq. (7) provided an excellent fit to the data regardless of soil type. An example of the relationship between observed and predicted values is presented in Fig. 1.

The estimates of the $\Psi_0$ parameter were all physically reasonable (Table 1). Overall, there was no evidence of any direct textural effect on $\Psi_0$. This is not surprising since the $S(\Psi)$ close to saturation is often more sensitive to soil structure than to soil texture (Campbell and Shiozawa, 1992).

The estimates of $\Psi_j$ for Salkum and Palouse-B (Table 1) were within the theoretical range for oven drying predicted by the ideal gas law (Ross et al., 1991), indicating that $\Psi_j \simeq \Psi_{oven}$ for these soils. The remaining estimates of $\Psi_j$ in Table 1 were much greater than $\Psi_{oven}$, implying the presence of significant quantities of residual water in pores smaller than those that could be emptied by the oven-drying process. Since this trend appeared to be independent of soil type, it may be related to experimental difficulties in accurately determining the $S(\Psi)$ at very high tensions (Campbell and Shiozawa, 1992).

All of the estimates of $D$ in Table 1 were significantly less than three at $P < 0.05$. The fractal dimension was highly sensitive to textural class. The smallest estimates of $D$ were obtained for the coarse-textured soils (L-soil and Royal), with intermediate values for the medium-textured soils (Palouse, Salkum and Walla Walla), and a value approaching three for the finest-textured soil (Palouse-B). These results correspond to varying degrees of curvature in the experimental $S(\Psi)$'s when plotted on a semilog scale: silty clay approximately linear, sand and sandy loam distinctly concave, with the silt loams displaying an

Table 1
Summary of nonlinear fits for Eq. (7) fitted to the complete water retention curves of Campbell and Shiozawa (1992)

| Soil | Texture | $n$ | $\Psi_0$ (kPa) | $\Psi_j$ (kPa) | $D$ | Adj. $R^2$ |
|---|---|---|---|---|---|---|
| L-soil | Sand | 31 | 1.47 | $1.6\times10^{27}$ | 2.65 | 0.96 |
| Royal | Sandy loam | 34 | 5.08 | $4.3\times10^{24}$ | 2.60 | 0.98 |
| Palouse | Silt loam | 39 | 4.20 | $6.2\times10^{12}$ | 2.75 | 0.99 |
| Salkum | Silt loam | 38 | 7.54 | $1.5\times10^{6}$ | 2.79 | 0.99 |
| Walla Walla | Silt loam | 38 | 1.90 | $1.9\times10^{34}$ | 2.72 | 0.99 |
| Palouse-B | Silty clay | 37 | 1.20 | $1.9\times10^{6}$ | 2.90 | 0.98 |

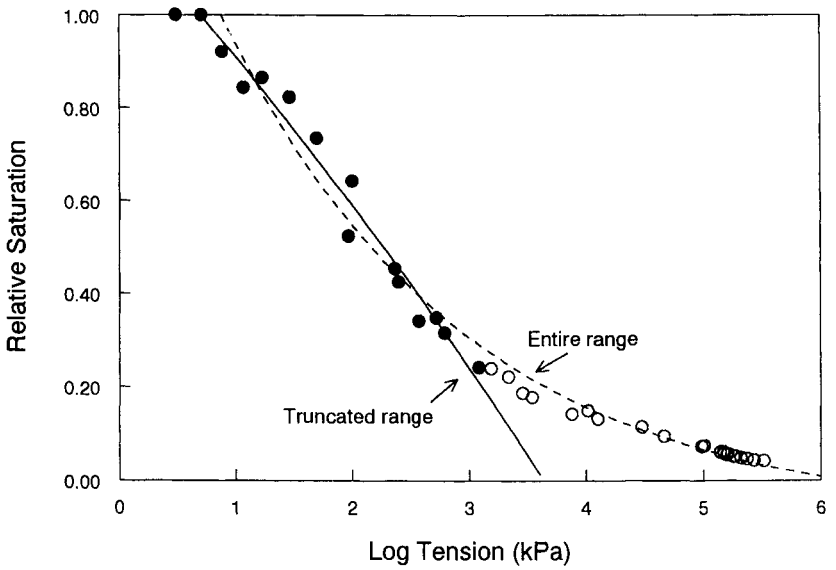


Fig. 1. Semilog plot of experimental water retention data for Salkum silt loam from Campbell and Shiozawa (1992), with Eq. (7) fitted over: (A) the entire range of tensions available (data = open and closed circles, model = dashed line) and (B) the truncated tension range (data = closed circles, model = solid line).

intermediate amount of curvature (Campbell and Shiozawa, 1992). It follows that the void space of sandy soils is dominated by a few relatively large pores (i.e., $D \ll 3$), while clayey soils contain a wide range of pores sizes (i.e., $D \rightarrow 3$). The relationship between mass fractal dimensions and soil texture found in this study is consistent with that reported by other researchers, e.g., Brakensiek and Rawls (1992).

Eq. (7) was also fitted to the truncated water retention curves with $\Psi_j$ as a free parameter (Table 2). The goodness of fit for these nonlinear regressions was only slightly less than that for the complete curves. However, truncating the data

Table 2
Summary of nonlinear fits for Eq. (7) fitted to the truncated water retention curves of Campbell and Shiozawa (1992)

| Soil | Texture | $n$ | $\Psi_0$ (kPa) | $\Psi_j$ (kPa) | $D$ | Adj. $R^2$ |
|---|---|---|---|---|---|---|
| L-soil | Sand | 15 | 1.74 | $2.4\times10^{23}$ | 2.61 | 0.95 |
| Royal | Sandy loam | 16 | 6.07 | $8.6\times10^{20}$ | 2.54 | 0.98 |
| Palouse | Silt loam | 15 | 3.93 | $3.8\times10^{4}$ | 2.82 | 0.99 |
| Salkum | Silt loam | 16 | 4.99 | $4.3\times10^{3}$ | 3.04 | 0.98 |
| Walla Walla | Silt loam | 16 | 4.57 | $7.6\times10^{28}$ | 2.70 | 0.99 |
| Palouse-B | Silty clay | 17 | 0.46 | $1.7\times10^{4}$ | 3.05 | 0.94 |

resulted in significantly different estimates of $\Psi_0$, $\Psi_j$ and $D$. While the estimates of $\Psi_0$ in Table 2 were of the same order of magnitude as those in Table 1, the correlation between the two sets of parameters was only $r = 0.86$. The estimates of $\Psi_j$ for the truncated data were between two and eight orders of magnitude lower than those obtained using the complete curves. This result indicates that $\Psi_j$ is highly sensitive to the range of $\Psi$'s over which Eq. (7) is fitted. The truncated data also resulted in a systematic error in the estimation of $D$ relative to the fits using the complete $S(\Psi)$'s. The magnitude of the difference in $D$ values between the entire and truncated $S(\Psi)$'s was dependent upon soil type. The $D$ was over estimated for the fine-textured soils and under estimated for the coarse-textured soils. As a result the range in $D$ for the truncated curves was much greater (Table 2) than the range in $D$ for the complete curves (Table 1).

Two of the soils (Salkum and Palouse-B) produced estimates of $D > 3$ with the truncated data, while their $D$ values estimated using the entire $S(\Psi)$ were significantly less than three. This switch over from fractal (concave semilog curve) to nonfractal (convex semilog curve) scaling is illustrated in Fig. 1. The use of different methods over different tension ranges, can result in local curvature that does not reflect the shape of the entire curve. As a result, the range of $\Psi$'s included in the fitting can have a profound influence on the estimation of $D$. In order to estimate $D$ accurately, $S(\Psi)$ data covering the entire range from saturation to zero water content are required. It follows that the values of $D > 3$ reported by Perfect et al. (1998) may have been due to the restricted range of tensions over which Eq. (7) was fitted to the experimental data.

Since none of the estimates of $\Psi_j$ in Table 1 were less than $\Psi_{oven}$ predicted from the ideal gas law (Ross et al., 1991), Eq. (8) was fitted to the complete data with $\Psi_{oven}$ set to a constant of $10^6$ kPa, the approximate average tension at oven dryness (Rossi and Nimmo, 1994). The adj. $R^2$ values (not presented) were the same as those for Eq. (7). The results of these fits are summarized in Table 3. The relationships indicate that, for the range of soils considered here, the

Table 3
Relations between parameters estimated using Eq. (7) and those estimated using Eq. (8) with $\Psi_{oven}$ held constant at $10^6$ kPa

| Regression model | Slope | Intercept | $R^2$ |
|---|---|---|---|
| $\Psi_0$ (Eq. (8)) vs. $\Psi_0$ (Eq. (7)) | 1.00(0.07)[a] | −0.14(0.39) | 0.98 |
| $\Psi_0$[b] (Eq. (8)) vs. $\Psi_0$ (Eq. (7)) | 0.98(0.09) | 0.27(0.50) | 0.96 |
| $D$ (Eq. (8)) vs. $D$ (Eq. (7)) | 1.09(0.10) | −0.23(0.02) | 0.97 |
| $D$[b] (Eq. (8)) vs. $D$ (Eq. (7)) | 1.23(0.07) | −0.64(0.01) | 0.99 |

[a]Standard error of estimate in brackets.
[b]From the truncated data.

estimates of $\Psi_0$ and $D$ from Eq. (8) with two fitting parameters were virtually identical to those from Eq. (7) with three.

To further investigate the influence of the range in $\Psi$ on the parameter estimates, Eq. (8) with $\Psi_{oven} = 10^6$ kPa was also fitted to the truncated data. The adj. $R^2$ values ranged from 0.94 to 0.99. The estimates of $\Psi_0$ and $D$ were positively correlated with the corresponding estimates obtained by fitting the complete curves using Eq. (7), and both regression equations were close to a 1:1 relationship (Table 3). While these results are encouraging, the sample size is small and further research is needed to compare estimates of $D$ obtained using limited data and $\Psi_{oven} = 10^6$ kPa, with those obtained using data collected over a much wider range of tensions and $\Psi_j$ as a free parameter.

## 5. Concluding remarks

The water retention properties of natural porous media can be modeled using the capillary equation and a randomized Menger sponge algorithm with upper and lower scaling limits corresponding to the air entry value and the tension at dryness, respectively. Between these two limits the water retention curve is concave when plotted on a semilog scale of $S$ vs. $\log(\Psi)$. The fractal dimension controls the degree of curvature, with decreasing concavity as $D \rightarrow 3$. When fitted to experimental $S(\Psi)$ data for six soils, this model gave fractal dimensions ranging from 2.60 to 2.90; the smallest estimates of $D$ were obtained for coarse-textured soils, and the largest for a fine-textured soil.

Fitting Eq. (7) over a relatively narrow range of $\Psi \leq 1.5 \times 10^3$ kPa can result in physically unreasonable estimates of $D > 3$. To estimate $D$ accurately, water retention data covering the entire range of $S$ from saturation to zero water content are required. In the absence of such data, physically reasonable estimates of $D$ may be obtained by setting $\Psi_{oven} = 10^6$ kPa and fitting Eq. (8) as a two-parameter model. This possibility deserves further investigation since it is difficult and time consuming to determine the complete water retention curve, and most data sets that are currently available terminate at $1.5 \times 10^3$ kPa. Additional research is needed to develop a prefractal water retention model that can accommodate the presence of non-draining water, in disconnected pores and/or in large pores connected to the atmosphere via smaller ones, at any level in the hierarchy.

## Acknowledgements

The water retention data of Campbell and Shiozawa (1992) were kindly provided in worksheet format by J.R. Nimmo.

## Appendix A

SAS program used for the segmented nonlinear regression analyses (SAS Institute, 1989):

proc nlin method = newton;
parms $\Psi_0 = 1$ $\Psi_j = 10^6$ $D = 2.8$;
$x0 = \Psi_0$; $x1 = \Psi_j$;
if $\Psi > x1$ then do;
model $S = 0$;
end;
else
if $\Psi < x0$ then do;
model $S = 1$;
end;
else
model $S = (\Psi^{D-3} - \Psi_j^{D-3})/(\Psi_0^{D-3} - \Psi_j^{D-3})$;
end;
run;

## References


Ahl, C., Niemeyer, J., 1989. The fractal dimension of the pore volume inside soils. Z. Pflanzenernaehr. Bodenkd. 152, 457–458.

Bird, N.R.A., Bartoli, F., Dexter, A.R., 1996. Water retention models for fractal soil structures. Eur. J. Soil Sci. 47, 1–6.

Bird, N.R.A., Dexter, A.R., 1997. Simulation of soil water retention using random fractal networks. Eur. J. Soil Sci. 48, 633–641.

Brakensiek, D.L., Rawls, W.R., 1992. Comment on 'Fractal processes in soil water retention' by Scott W. Tyler and Stephen W. Wheatcraft. Water Resour. Res. 28, 601–602.

Campbell, G.S., 1974. A simple method for determining unsaturated hydraulic conductivity from moisture retention data. Soil Sci. 117, 311–314.

Campbell, G.S., Shiozawa, S., 1992. Prediction of hydraulic properties of soils using particle size distribution and bulk density data. International Workshop on Indirect Methods for Estimating the Hydraulic properties of Unsaturated Soils. University of California Press, Berkeley, CA, pp. 317–328.

Crawford, J.W., Matsui, N., Young, I.M., 1995. The relation between the moisture-release curve and the structure of soil. Eur. J. Soil Sci. 46, 369–375.

Davis, H.T., 1989. On the fractal character of the porosity of natural sandstone. Europhys. Lett. 8, 629–632.

de Gennes, P.G., 1985. Partial filling of a fractal structure by a wetting fluid. In: Adler, D., Fritzsche, H., Ovshinsky, S.R. (Eds.), Physics of Disordered Materials. Plenum, New York, NY, pp. 227–241.

Gardner, W.H., 1986. Water content. In: Klute, A. (Ed.), Methods of Soil Analysis, Part 1, Physical and Mineralogical Methods, 2nd edn. ASA/SSSA Publ., pp. 493–544.

Giménez, D., Perfect, E., Rawls, W.J., Pachepsky, Y.A., 1997. Fractal models for predicting soil hydraulic properties: a review. Eng. Geol. 48, 161–183.

Mandelbrot, B.B., 1982. The Fractal Geometry of Nature. Freeman, San Francisco, CA, 468 pp.
Nimmo, J.R., 1991. Comment on the treatment of residual water content in 'A consistent set of parametric models for the two-phase flow of immiscible fluids in the subsurface' by Luckner et al. Water Resour. Res. 27, 661–662.
Pachepsky, Y.A., Shcherbakov, R.A., Korsunskaya, L.P., 1995. Scaling of soil water retention using a fractal model. Soil Sci. 159, 99–104.
Perfect, E., McLaughlin, N.B., Kay, B.D., Topp, G.C., 1996. An improved fractal equation for the soil water retention curve. Water Resour. Res. 32, 281–287.
Perfect, E., McLaughlin, N.B., Kay, B.D., Topp, G.C., 1998. Reply. Water Resour. Res. 34, 933–935.
Perrier, E., Rieu, M., Sposito, G., de Marsily, G., 1996. Models of the water retention curve for soils with a fractal pore size distribution. Water Resour. Res. 32, 3025–3031.
Pfeifer, P., Orbert, M., 1989. Fractals: basic concepts and terminology. In: Avnir, D. (Ed.), The Fractal Approach to Heterogeneous Chemistry. Wiley, New York, NY, pp. 11–43.
Rieu, M., Sposito, G., 1991. Fractal fragmentation, soil porosity, and soil water properties: I. Theory. Soil Sci. Soc. Am. J. 55, 1231–1238.
Ross, P.J., Williams, J., Bristow, K.L., 1991. Equation for extending water-retention curves to dryness. Soil Sci. Soc. Am. J. 55, 923–927.
Rossi, C., Nimmo, J.R., 1994. Modeling of soil water retention from saturation to oven dryness. Water Resour. Res. 30, 701–708.
SAS Institute, 1989. SAS/STAT User's Guide, Version 6, 4th edn., Vol. 2. SAS Institute, Cary, NC, USA, 846 pp.
Toledo, P.G., Novy, R.A., Davis, H.T., Scriven, L.E., 1990. Hydraulic conductivity of porous media at low water content. Soil Sci. Soc. Am. J. 54, 673–679.
Topp, G.C., Galganov, Y.T., Ball, B.C., Carter, M.R., 1993. Soil water desorption curves. In: Carter, M.R. (Ed.), Soil Sampling and Methods of Analysis. Lewis, Boca Raton, FL, pp. 569–579.
Turcotte, D.L., 1992. Fractals and Chaos in Geology and Geophysics. Cambridge Univ. Press, Cambridge, UK, 221 pp.
Tyler, S.W., Wheatcraft, S.W., 1990. Fractal processes in soil water retention. Water Resour. Res. 26, 1047–1054.

This Page Intentionally Left Blank

*Fractals in Soil Science*
Editors: Ya.A. Pachepsky, J.W. Crawford and W.J. Rawls
© 2000 Elsevier Science B.V. All rights reserved.


# Influence of humic acid on surface fractal dimension of kaolin: analysis of mercury porosimetry and water vapour adsorption data

Z. Sokołowska [a,*], S. Sokołowski [b]

[a] *Institute of Agrophysics, Polish Academy of Science, 20236 Lublin, Poland*
[b] *Department for the Modelling of Physico-Chemical Processes, Maria Curie-Sklodowska University, 20031 Lublin, Poland*

Received 23 September 1997; accepted 28 September 1998

**Abstract**

Samples of kaolin amended with different amounts of humic acid extracted from a Cambic Areosol under forest are investigated. We measure water vapour adsorption isotherms and mercury intrusion pore size distributions. Experimental adsorption isotherms are analyzed by means of Frenkel–Hill–Halsey (FHH) type equation. This analysis leads to the determination of the surface fractal dimension. The fractal dimensions obtained from adsorption isotherms are next compared with those resulting from the analysis of mercury intrusion data. The calculations performed indicate consistently fractally rough surface structure for all the samples. However, the changes of the surface properties of the samples are not proportional to the amount of humic acid added. The fractal dimension is the highest for untreated kaolin, attains a minimum for samples with a small amount of humic acid added and smoothly increases to a constant value, which is significantly lower than that characteristic for pure humic acid. © 1999 Elsevier Science B.V. All rights reserved.

*Keywords:* humic acid; kaolin; fractal dimension; water vapour adsorption; mercury porosimetry

## 1. Introduction

It has been recognized that the geometrical non-uniformity of surfaces of several solids can be characterized by the fractal dimension, $D$ (Avnir, 1989). The values of the fractal dimension belong to the interval [2,3] and indicate the

* Corresponding author. E-mail: sokolows@demeter.ipan.lublin.pl

Reprinted from Geoderma 88 (1999)
© 1999 Elsevier Science B.V. All rights reserved

degree of complexity of the surface and/or porous structure. Several methods have been developed in order to evaluate $D$ from adsorption measurements, mercury porosimetry data, scanning electron microscopy and from X-ray and neutron scattering data (Avnir, 1989; Robbins et al., 1991). The approaches based on adsorption isotherm (Jaroniec and Avnir, 1989; Neimark, 1990a; Yin, 1991; Jaroniec et al., 1997; Jarzebski et al., 1997) and mercury porosimetry (Friesen and Mikula, 1987; Pfeifer, 1987; Spindler and Kraft, 1988; Neimark, 1990b,c; Smith et al., 1990; Bartoli et al., 1991; Neimark, 1992; Bartoli et al., 1993) measurements seem to be ones of the simplest and the most convenient methods, because they require only one complete adsorption isotherm or one mercury intrusion curve to evaluate the value of $D$. Both these methods should be treated as complementary, because the data obtained from analyses of adsorption isotherms and pore size distribution curves can detect irregularities of different parts of the surface.

The content of organic matter in natural soil adsorbents is one of important factors determining their surface properties as, e.g., adhesion, wettability, interparticle attraction, aggregate stability (Theng, 1979; Jouany and Chassin, 1987; Janczuk et al., 1990; Vadarachari et al., 1991; Janczuk et al., 1992; Jozefaciuk et al., 1995). It has been also emphasized that the constant of organic matter can significantly change energetic characteristics (adsorption energy distribution functions) of adsorbents (Sokołowska et al., 1993; Pachepsky et al., 1995a,b; Sokołowska et al., 1997). In some cases, however, the effect of organic matter on some surface properties is not unequivocal. For example, although several published papers report an increase of specific surface area measured by water vapour adsorption together with an increase of organic matter content (Dobrzanski et al., 1972; Curtin and Smillie, 1976; Sequi and Aringhieri, 1977; Pachepsky et al., 1995a,b) inverse effects have been also observed (Sokołowska et al., 1993, 1997) In mineral soils, humic substances are usually bonded by strong forces, so their breaking requires drastic treatments (Theng, 1979; Stepanov and Dokuchayev, 1981; Vadarachari et al., 1991; Murphy et al., 1994). Thus the source of the above mentioned different findings may be due to artefacts produced during organic matter removal procedures, which can cause the formation of highly dispersed mineral phases.

Humic substances comprise a wide class of ubiquitous natural organic materials typically characterized by an extreme physical and chemical heterogeneity and a lack of discrete structure and order in the molecular organization. Consequently, they appear to be highly susceptible of a fractal description (Rice and Lin, 1992; Senesi, 1992; Bartoli et al., 1993; Senesi et al., 1994; Pachepsky et al., 1995a). Obviously, the bonding of humic substances by mineral components of soils can change their organization and the structure. Thus, the objective of this work is to test the fractal nature of clay-humic substance complexes by using data obtained from both: adsorption of water vapour and mercury intrusion measurements. As the model support for humic acid we have

used kaolin. Several samples enriched with known amount of organic material are analyzed by means of mercury porosimetry and water vapour adsorption. The paper is organized as follow. In Section 2, we briefly describe theory used in analysis of the obtained data. Experimental techniques and characteristics of the materials used are given in Section 3, whereas Section 4 contains discussion of the results.

## 2. Theory

### *2.1. Fractal dimension from adsorption isotherm*

The effect of fractal geometry on adsorption isotherms has been intensively researched in recent years (Jaroniec and Avnir, 1989; Yin, 1991; Jaroniec et al., 1997; Jarzebski et al., 1997). A simple method of calculation of the fractal dimension from single isotherm, developed by the above cited authors is based on the following approach. Consider a general form of the adsorption isotherm equation on irregular solid

$$N(\tilde{A}) = \int_{r_{\min}}^{r_{\max}} f(r, \tilde{A})\, J(r)\, \mathrm{d}r, \tag{1}$$

where $r$, $r_{\min}$, and $r_{\max}$ are the pore size, maximum pore size and minimum pore size accessible to adsorption, respectively, $N(\tilde{A})$ is the adsorption quantity, $\tilde{A}$ is the change in the Gibbs free energy of adsorption taken with the minus sign,

$$\tilde{A} = RT \ln p_0/p, \tag{2}$$

$p$ and $p_0$ denote the pressure and the saturated vapour pressure, $R$ is the gas constant, $T$ is the temperature, $f(r, \tilde{A})$ is the function representing the probability of pore filling ('local adsorption isotherm') and $J(r)$ is the pore volume distribution function. If the pore-size distribution is fractal, then

$$J(r) = br^{2-D}, \tag{3}$$

with $b$ being a constant. Except for very small pores (Chmiel et al., 1994) the condensation in the pores with average radius $r_{\mathrm{av}}$ is governed by the Kelvin equation

$$\tilde{A} = \frac{2V_{\mathrm{m}}\gamma \cos\theta}{r_{\mathrm{av}}}, \tag{4}$$

where $V_{\mathrm{m}}$ is the molar volume of adsorbate, $\gamma$ the surface tension and $\theta$ is the contact angle of the adsorbed liquid with the material. Considering next the adsorption process as resulting from the sequential and rapid filling of pores

from small size to larger and that the contact angle is independent of the size of pores, the function $f(r, \tilde{A})$ can be approximated by (Yin, 1991)

$$f(r,\tilde{A}) = \begin{cases} 1 & \text{for } \alpha/\tilde{A} > r \\ 0 & \text{otherwise,} \end{cases} \tag{5}$$

where $\alpha = 2V_m\gamma \cos\theta$. Substituting Eqs. (3) and (5) into Eq. (1) we obtain

$$N(\tilde{A})/N_m = \frac{b\left[\left(c\tilde{A}^{-1}\right)^{3-D} - r_{\min}^{3-D}\right]}{3-D}, \tag{6}$$

with $N_m$ being the maximum of adsorption. The last equation implies that the fractal dimension can be evaluated from

$$\log\left[\frac{\mathrm{d}N(\tilde{A})}{\mathrm{d}A}\right] = \tilde{C} + (D-4)\log A, \tag{7}$$

where $A = \tilde{A}/RT$. Alternatively, if $r_{\min}^{3-D}$ can be neglected, the well-known form of the Frenkel–Halsey–Hill (FHH) isotherm is obtained. Usually, omitting the term corresponding to the smallest pores does not introduce significant errors (Jaroniec et al., 1997) Thus, in the logarithmic coordinates we get

$$\log N(A) = C - \frac{1}{m}\log A, \tag{8}$$

where

$$D = 3 - \frac{1}{m}. \tag{9}$$

In the above $C$ and $\tilde{C}$ are constants.

We stress once more that the derivation of Eq. (6) quoted above is based on the assumption that capillary condensation obeys Kelvin equation. It is thus obvious that this equation is valid at small values of $A$, i.e., within traditional multilayer adsorption regime. At larger values of $A$, i.e., at micropore filling range, the Kelvin equation is not expected to hold for small pore size.

### *2.2. Fractal dimension from mercury porosimetry data*

The basic relationship of the yardstick method used for surface fractal dimension, $D$, calculation has the form (Feder, 1988; Pfeifer and Orbert, 1989):

$$\begin{aligned} N(\epsilon) &\propto \epsilon^{-D}, \\ S(\epsilon) &\propto \epsilon^{2-D}, \end{aligned} \tag{10}$$

where $N(\epsilon)$ is the number of gauges of the size $\epsilon$ which can cover the considered surface and $S(\epsilon)$ is the surface area of the gauges.

In the approach proposed by Neimark (1990b,c, 1992), the role of a gauge is payed by an average radius of curvature of the meniscus at the mercury–sample interface, $r$, when mercury is forced into the sample at the pressure $p$. The average radius of the curvature of the mercury meniscus is related to the pressure by Washburn type relation

$$p = C_1/r, \tag{11}$$

where $C_1$ is a constant. The surface area of the interface can be calculated from the Rootare and Prenzlow (1967) relation

$$S_1 = C_2 \int_0^V p \, dV', \tag{12}$$

where $V$ is the volume of pores of equivalent radius $r$ and $C_2$ is a constant. The area $S_1$ is interpreted as that which would be measured by balls of radius $\epsilon = r$. Assuming thus that $S_1 = S$ and taking into account Eqs. (1) and (3) we get

$$D = 2 + \frac{d \log \int_0^V p \, dV'}{d \log p}, \tag{13}$$

The last equation was proposed by Neimark (1990a,b,c) for calculating the surface fractal dimension from experimental mercury intrusion porosimetry data. It should be stressed, however, that the identification $S_1 = S$ neglects the integration constant in Eq. (4), i.e., the initial surface area, $S_0$. When the identification $S = S_0 + S_1$ is used, Eq. (12) reads

$$D = 2 + \frac{d \log \left[ S_0 + \int_0^V p \, dV' \right]}{d \log p} \tag{14}$$

Obviously, the porosimetric method does not directly measure the initial area $S_0$, this area, however, can be neglected when porosimetric data include information about relatively large pores (Kozak et al., 1995).

## 3. Experimental

We have investigated samples of kaolin Pontedra (Spain) modified by addition of different amounts of humic acid (HA).

The fraction of kaolin with grain size $< 2$ μm used in experiments consisted of 70% kaolinite, 18% mica and 12% quartz. Its CEC at pH = 8.2 was 2.9 cmol $kg^{-1}$ (Wierzchos, 1989).

Humic acid was extracted with water from a sodium homoionic form of an Ah horizon of a Cambic Arenosol under forest (pH = 3.63, clay content less than 1%, 2.45% of organic carbon and 1.42 fulvic to humic acid ratio), taken from the Grunewald experimental plot (Berlin city region). The extract was prepared in the following way. The solution was filtered by G4 glass bed, coagulated with HCl, washed with distilled water by centrifuging and peptized in water. The concentration of the final suspension of HA was $c_0 = 8$ g/dm$^3$. The ash content of the HA was 3.7% (dry mass), its surface area was 345 m$^2$/g and its negative charge at pH = 8.2 was 3.41 mol/kg.

Suspension of the HA was diluted with distilled water to concentrations $1c_0$, $c_0/4$, $c_0/4$, ..., and $c_0/512$ The obtained suspensions were added to kaolin in the ratio 1:1. To get the sample with double amount of HA ($2c_0$), two parts of suspension of concentration $c_0$ were mixed with one part of kaolin. The samples were dried in room temperature and gently ground in a mortar. At the end of drying process the samples were intensively mixed. for convenience, we abbreviate the modified soil samples by using the code: 0 (no HA added), $c_0/512$, $c_0/256, \ldots, 1c_0$ and $2c_0$, respectively.

Additionally, we have also performed experimental determinations by using commercial samples of pure humic acid (Fluka Chemika, Art. No. 53680) and of its sodium salt (C. Roth, Art. No. 7824). We refer to these samples as to CHA and CHA-NA, respectively. Porosimetric measurements have been also carried out for natural HA sample, which has been used as the kaolin modifier.

Water vapour adsorption isotherms were measured by using a vacuum microbalance technique. During measurements the temperature was kept constant at $294 \pm 0.1$ K. The adsorption isotherms were measured within the relative pressure range [0.01,0.9]. The final results were obtained by averaging over three independent measurements; the maximum deviation did not exceed 3%.

The pore size distribution curves were obtained by using Carlo Erba mercury porosimeter series 2000. Before mercury intrusion the samples were dried applying air-drying followed by oven-drying at 105°. Details of the experimental technique have been described by Kozak et al. (1991). The utilization of mercury intrusion porosimetry for the measurements of natural soil pore size distribution may be controversial in some cases. Some possibilities of pore distortion during mercury intrusion, particularly for samples of fine-textured soils were noticed by Sridharan and Venkatappa Rao (1972) and by Murray and Quirk (1981). However, the absence of soil sample damage during mercury intrusion was stated by Lawrence (1978) and Lawrence et al. (1979). In general, the experiments on the influence of clay compaction on the mercury porosimetry results (Volzone and Hipedinger, 1997) indicate that the most probable is a distortion of rather large pores, that are filled at the pressures up to 100 MPa. The question of reliability of mercury intrusion porosimetry results for soils has been discussed in details by Kozak et al. (1991).

## 4. Results and discussion

In Fig. 1 we display some examples of water vapour adsorption isotherms. Part c shows adsorption isotherms evaluated for the samples of pure CHA and for its sodium derivative, CHA-Na; these isotherms have been included for a comparison. The highest values of adsorption are measured on unmodified kaolin sample. The adsorption on the sample $c_0/512$ is only slightly lower, however further increase of the HA content drastically reduces the amount of adsorbed water vapour. The jump in the adsorbed amount is for HA concentration between $c_0/512$ and $c_0/128$. The differences in the adsorption evaluated for the concentration of HA equal to $c_0/128$ or higher are rather small. However, the adsorption isotherms measured on pure CHA and on its sodium

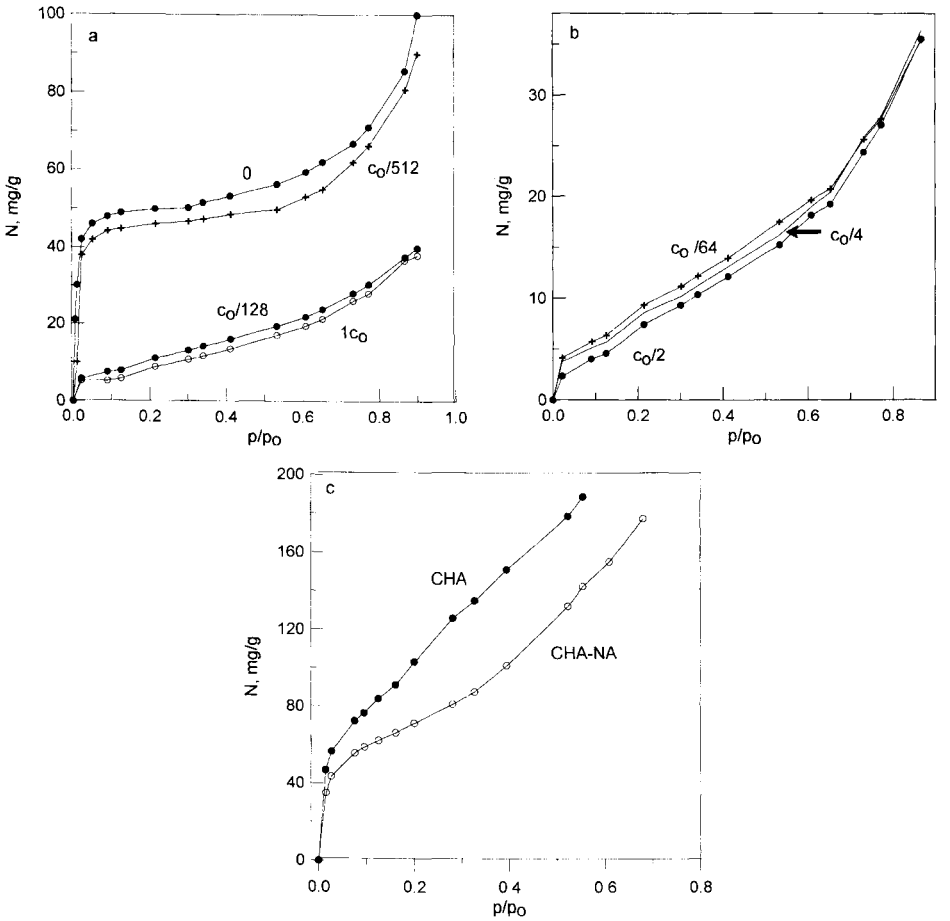


Fig. 1. Examples of the water vapour adsorption isotherms on kaolin modified with different amount of HA, given in the figure. The adsorption is expressed in mg/g of the adsorbent. Part c shows the adsorption isotherms for CHA and for its sodium salt, CHA-NA.

salt, CHA-NA, are several times higher—cf. Fig. 2c. We should stress again that we used different, namely natural HA to modify samples of kaolin.

To obtain estimates of surface area, the adsorption isotherms have been analyzed using the BET equation. Its linearized form can be written as (Oscik, 1982)

$$\frac{1}{N(p_0/p-1)} = \frac{C_{\mathrm{BET}}-1}{C_{\mathrm{BET}}N_{\mathrm{m,BET}}}\frac{p}{p_0} + \frac{1}{C_{\mathrm{BET}}N_{\mathrm{m,BET}}}, \tag{15}$$

where $N_{\mathrm{m,BET}}$ is the BET monolayer capacity and $C_{\mathrm{BET}}$ is a constant. The fit of Eq. (15) to the experimental data provides monolayer capacity and the constant $C_{\mathrm{BET}}$. The BET surface area has been calculated from $N_{\mathrm{m,BET}}$ assuming the area occupied by a single water molecule equal to 10.8 Å.

Fig. 2 illustrates the changes in the BET surface area with the changes of the HA concentration. Initial increase of the HA content leads to rather rapid decrease of the specific surface area of the modified kaolin samples. The minimum values of the surface area are for the samples $c_0/64$, $c_0/32$ and $c_0/16$. Subsequent increase of the HA concentration causes slow rise of the surface area. This rise is not proportional to the amount of HA added. The surface area of pure (natural) HA is equal to 345 $m^2/g$, i.e., it is much higher than the surface area of the sample 2, with the highest HA content.

Determination of the surface area by the BET method is based on the assumptions that: (i) only physical adsorption is involved, (ii) the adsorbent is not changed by the adsorption process, and (iii) no solution is formed by the adsorbate in the adsorbent. In the case of pure HA probably none of the assumptions listed above is fulfilled (cf. Chiou et al., 1990), whereas in the case

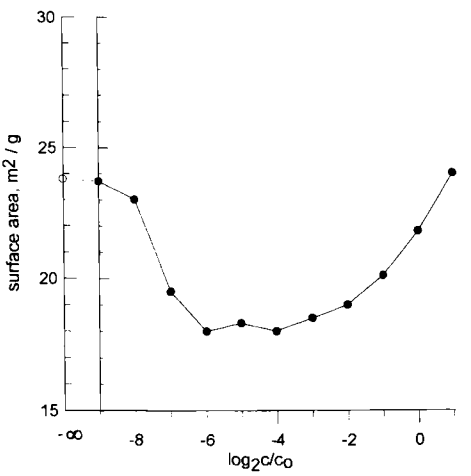


Fig. 2. The dependence of the BET surface area of the modified samples on the concentration of the HA suspension.

of untreated kaolin sample they should be satisfy rather well. Deposition and chemical bonding of a thin-layer of HA with the support delimits possibility of bulk exhaustion (absorption) of water by organic matter.

The percent of the surface of kaolin covered by the HA can be determined from contact angle measurements (Neumann and Good, 1979; Janczuk and Białopiotrowicz, 1989; Jozefaciuk et al., 1995; Hajnos and Matyka-Sarzynska, 1996). By using technique described by Jozefaciuk et al. (1995), the contact angles of glycerol and diiodomethane drops on kaolin modified with HA pellets have been measured. It has been found that remarkable surface coverage of kaolin with HA occurs at very low concentrations. At $c_0/256$ about 14% of the surface of kaolin is covered with HA and at $c_0/128$—about 28%. Further increase of the coverage is slower. At $c_0/32$ the coverage equals to about 30% and at $c_0/2$—to about 40%. At the highest HA concentration, $2c_0$, the coverage of kaolin with HA reaches the level approximately equal to 42%. Thus, with increase of concentration the distribution of organic particles on the kaolin surface changes. At the first stage 'new' parts of kaolin surface are covered, but next the HA builds 'thicker' structure and is deposited on already covered parts of the surface.

Fig. 3 presents examples of the pore size distributions evaluated for samples of kaolin with different amount of HA added by applying mercury intrusion method and cylindrical pore model. Note that only a part of pore size distributions around their maxima displayed in this figure. Beyond of the region shown, the pore size distributions slowly decay to zero. In the case of unmodified kaolin this decay is the slowest and long-range tails occur on both sides of the pore size distribution peak. Within the range of pores shown in Fig. 3 all the curves exhibit similar shape with a single peak, which at its 'top' divides into two maxima, separated by a minimum. The distribution for unmodified kaolin (the curve 1 in Fig. 3a) is broader and possesses lower maxima than all remaining

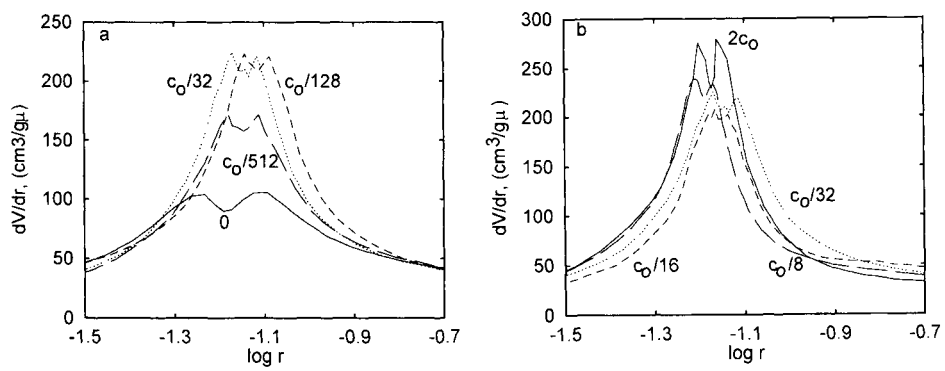


Fig. 3. Examples of the pore size distributions, $dV/dr$, from mercury intrusion measurements. The amount of HA added is marked in the figure. The pore diameter is expressed in microns (μm).

curves. The highest peak exhibits the distribution for the sample richest in HA (the curve 4 in Fig. 2b). However, the average pore radius not much depends on the HA content. The average pore radius equals to 0.074 μm for unmodified sample and 0.0648 μm for the sample $c_0/512$. It attains its minimum equal to 0.0621 μm for the sample $c_0/32$ and reaches plateau equal to 0.0629 μm for concentrations greater than $c_0/8$. Thus, the presence of very small amount ($c_0/512$) of the HA decreases the average pore radius, but subsequent increase of the HA content has only slight effect on the average pore radius. However, the average pore radius of pure CHA is significantly higher and is equal to 2.48 μm, whereas the sodium salt of commercial, CHA-NA, exhibits the average pore radius equal to 1.98 μm.

Our mercury intrusion measurements have indicated that the addition of small amount of HA decreases the total porosity of the samples. Further increase of HA content slightly increases the porosity, however the porosity again decreases for rich in HA samples. For example, untreated kaolin sample rather high total porosity, equal to 64%; the total porosity of the sample $c_0/128$ equals 56%, the sample $c_0/16$–58% and the total porosity of the sample $2c_0$ is 52%. In contrast, the total porosity of pure CHA is rather low and equal to 11%. The total porosity of the sodium salt of the CHA-NA is even much lower and equal to 4.7%. The observed changes in the total porosity of the samples are not proportional to the amount of HA added. Addition of low concentration of HA causes lowering of the total porosity and the pore size distribution becomes narrower, but further changes of porosity with HA are small. At low HA concentration we can expect adsorption of HA on kaolin particles leading to flocculation of this mineral (Jekel, 1986; Wierzchos, 1989; Kretzchmar et al., 1993). With increase of the HA amount formation of steric (e.g., honeycomb), bigger floccules or aggregates and creation of new pores occur. Still further increase of HA content may lead to blocking the pores which have been already formed during flocculation. Thus, the changes in the porosity may be interpreted as the result of an interplay between formation of new pores (flocculation and aggregation) and blocking the pores caused by adsorption. These changes concern wider pores (macro and merozpores); eventual changes in very fine pores are out of mercury intrusion detection range.

Adsorption isotherms and pore mercury intrusion data have been next analyzed using Eqs. (8) and (13), respectively. Let us proceed with the results obtained from experimental adsorption isotherms. In Fig. 4, we have displayed the dependences of the logarithm of the adsorbed amount (expressed in mg/g) vs. log $A$, ($A = \ln p_0/p$). The fitting of these data by linear functions has been done within the multilayer region, log $A \leq 0$. For higher values of log $A$ the deviations from linear behaviour are significant. According to Eq. (8) this analysis gives us the coefficient $1/m$, which is related to $D$ via Eq. (9).

Before discussing the obtained values of the fractal dimension, $D$, let us recall that in the case of non-porous solids the interpretation of the coefficient

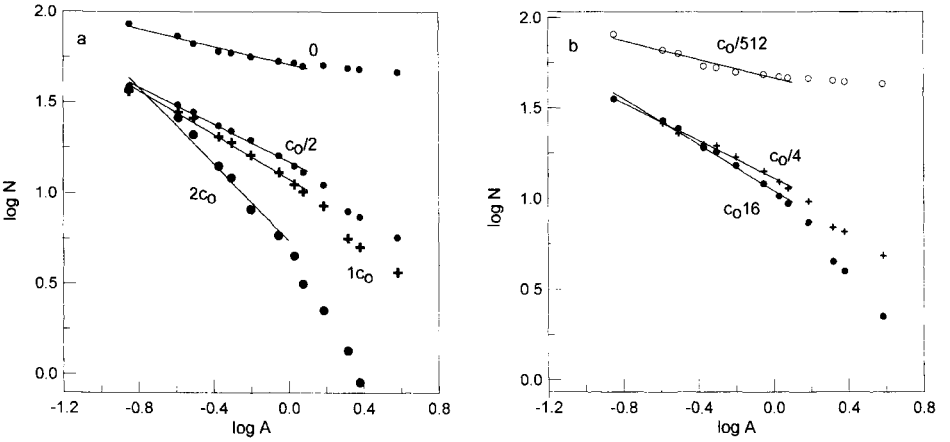


Fig. 4. Adsorption curves in the multilayer region, calculated according to Eq. (8) and presented in the logarithmic coordinates. The amount adsorbed is in mg/g.

$1/m$ entering Eq. (8) as given by Eq. (9) is not unique. Pfeifer et al. (1990) derived an expression similar to Eq. (8), but with different relationship between $1/m$ and $D$, namely (cf. Jarzebski et al., 1997)

$$D = 3(1 - 1/m). \tag{16}$$

The derivation of the last equation is based on the assumption that van der Waals attractive forces govern the formation of the adsorbed film, which is the case for low degrees of the coverage of a surface by the adsorbed film. The applicability of Eq. (16) was questioned, since the same adsorption behaviour can be predicted for simple corrugated surfaces (Robbins et al., 1991). Later, Pfeifer et al. (1991) and Ismail and Pfeifer (1994) extended their model to higher surface coverage for which the adsorption is controlled by the surface tension. In that regime, the resulting definition of $D$ for non-porous solids is *the same* as given by Eq. (9), if applies to *multilayer* adsorption data (Neimark, 1990a; Jaroniec et al., 1997; Jarzebski et al., 1997).

To define linearity ranges we used the technique introduced by Yokoya et al. (1989) (cf. also Pachepsky et al., 1997) According to this approach the linearity measure $L$ is calculated for the set of points in a plane as

$$L = \frac{\sqrt{4\sigma_{xy}^2 + (\sigma_{yy} - \sigma_{xx})^2}}{\sigma_{yy} + \sigma_{xx}}, \tag{17}$$

where $\sigma_{xx}$, $\sigma_{yy}$ and $\sigma_{xy}$ are the variances of $x$-coordinates, the variance of $y$-coordinates and the covariance between $x$ and $y$ coordinate sets, respectively. This measure $L$ falls between 0 and 1, being equal to 1 for points on a straight line and equal to 0 for uncorrelated and random points. To separate linearity intervals on log–log plots, the value of $L$ is computed for the first three points,

then for the first four, five and so on while the value of $L$ increases. The end of the first linearity interval will be in the points after which the value of $L$ begins to decrease. Then the next point is considered to be first points of the next linearity interval, and so on. Note that similar procedure has been also applied in the case of mercury porosimetry data. In the latter case we have started from the point at the highest measured pressure of mercury.

Fig. 4a and b display examples of the log $N$ vs. log $A$ plots for some (untreated and modified) kaolin samples. In Fig. 4c, we show the results for pure CHA and for CHA-NA. In the latter case the coefficient $1/m$ in Eq. (8) is equal 0.54 and 0.71. These values correspond to the fractal dimensions $D = 2.46$ and $D = 2.29$, respectively. The fractal dimension evaluated from Eqs. (8) and (9) for unmodified kaolin (Fig. 4a) is significantly higher and equal to 2.76. Only one linearity interval, corresponding to multilayer adsorption data is displayed in Fig. 4. All remaining data have been not analyzed, as they are for mono- and submonolayer adsorption. One should perhaps mention here that in the case of water vapour adsorption, the coefficient $1/m$ of Eq. (8), from which the fractal dimension in next calculated, contains also some 'hidden' information about specific interaction of water particles with the surfaces. Unfortunately, the adsorption of non-polar substances as nitrogen by humic substances is extremely low. Indeed, the surface area of humic substances measured by nitrogen adsorption is lower than 1 $m^2/g$ (Chiou et al., 1990; Kretzchmar et al., 1993) and thus the accuracy of the adsorption measurements rapidly decreases.

In Fig. 5 we show the dependence of the fractal dimension on the amount of HA used to modify the surface. The error bars have been evaluated assuming 3% uncertainty in the adsorption measurements. The plot of $D$ vs. $\log_2(c/c_0)$

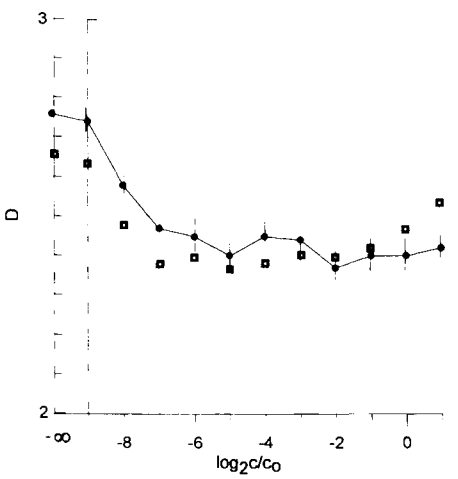


Fig. 5. The dependence of the fractal dimension on the concentration of the HA. Solid circles, connected by solid line denote the results obtained from the analysis of water vapour adsorption data by using Eq. (8). Squares denote the results obtained from the analysis of mercury intrusion data according to Eq. (13)—cf. Fig. 6.

has a similar shape as the plot shown in Fig. 2. The highest fractal dimension exhibits unmodified kaolin surface. The fractal dimension drops rapidly to about 2.4 for $c_0/128$ and remains almost constant up to highest concentrations of the modifier. This constant value is not too much different than that determined for pure CHA.

Fig. 6 shows the log–log plots evaluated according to Eq. (13) from mercury intrusion data. In Fig. 6a–c, we can distinguish two linear parts (the data at low mercury pressures lead to the values of $D$ out of the range [2,3]). The first of them within the range of log $p$ ($p$ is expressed in bars) approximately between 2 and 3, and the second one at highest mercury pressures (corresponding to narrowest pores). Within the second region the values of $D$ evaluated from Eq. (13) are very close to 2. For example, in the case of untreated kaolin we get 2.05, for the sample $1/2$–2.04 and for the sample $1c_0$–2.07. However, the values of $D$ evaluated within the first region of pressures are much higher. These values are shown in Fig. 5 as white squares. In general, except for the samples $1c_0$ and $2c_0$ with the highest HA content, the values of $D$ evaluated from mercury intrusion measurements are lower than those calculated from water vapour adsorption data. However, we can conclude that independently of the source of the data used to fractal dimension calculation, the shape of the curves $D$ vs. $\log_2(c/c_0$ is similar.

The fractal dimension of pure (natural) HA calculated within the same region of pressures as in the case of modified kaolin samples is approximately 2.75, so it is significantly higher than the surface fractal dimension of the sample $2c_0$ (see Fig. 5). Note that the dimension of natural and commercial humic acids are similar. The latter has been found to be 2.71. The value of $D$ for commercial sodium salt, CHA-NA is much lower and equals 2.13. In the case of both

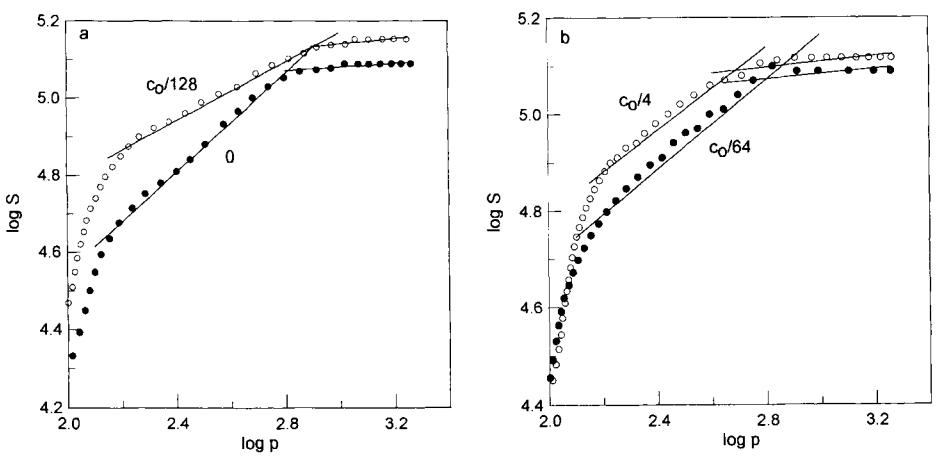


Fig. 6. Analysis of the mercury intrusion data by means of Eq. (13). Amount of the HA added is marked in the figure. Values of the pressure are in bars, values of $S$ are in $mm^2/g$.

commercial HA samples, the region of linearity of log $S$ vs. log $p$ plots (i.e., the fractality range) is wide—see Fig. 6d.

Let us summarize briefly our findings. In the case of water vapour adsorption the fractal dimension of the richest in HA samples is close to the fractal dimension of the HA. The highest fractal dimension exhibits the untreated sample of kaolin. When mercury intrusion data are used, the fractal dimension of the untreated sample is lower than the fractal dimension of HA. In both cases a small amount of HA lowers the fractal dimension of the initial kaolin sample.

Previous investigations (Jozefaciuk et al., 1995) have indicated that wettability (characterized by the contact angle of liquid water) and the average energies of adsorption of water on modified kaolin, as functions of amount of HA added behave similarly to the curves plotted in Figs. 2 and 5. Small amount of HA deposited on kaolin surface blocks the narrowest pores, in which water vapour is strongly adsorbed. These pores cannot be detected by mercury porosimetry measurements. Also, in effect of HA deposition, wider pores, accessible to mercury become narrower. Higher values of $D$, determined from water vapour measurements than the values obtained from mercury intrusion data indicate that finer pores, which can be penetrated by water, are more geometrically heterogeneous than wider pores accessible to mercury. This is not an obvious conclusion, because in the case of some swelling minerals (e.g., montmorillonite) the fractal dimension of external surfaces and wide pores was found to be higher than the fractal dimension of interlamellar space (Sokołowska et al., 1989).

## Acknowledgements

The authors express their appreciation to Dr. Y.A. Pachepsky for helpful discussions and for his suggestions for improvements in the original manuscript. The authors also wish to thank Dr. G. Jozefaciuk and Dr. E. Kozak for stimulating discussions. This work was supported by KBN under the Grant No. 5 P06B 029 14.

## References

Avnir, D., 1989. The Fractal Approach to Heterogeneous Chemistry: Surfaces, Colloids, Polymers. Wiley, Chichester, UK.

Bartoli, F., Philippy, R., Doirisse, M., Niquet, S., Dubuit, M., 1991. Structure and self-similarity in silty and sandy soils: the fractal approach. J. Soil Sci. 42, 167–185.

Bartoli, F., Burtin, G., Philippy, R., Grass, F., 1993. Influence of organic matter on aggregation in Oxisols rich in gibbsite or in goethite: I. Structures: the fractal approach. Geoderma 54, 231–257.

Chiou, C.T., Lee, J.F., Boyd, S.A., 1990. The surface area of soil organic matter. Environ. Sci. Technol. 24, 1164–1166.

Chmiel, G., Karykowski, K., Patrykiejew, A., Rżysko, W., Sokołowski, S., 1994. Adsorption in energetically and geometrically nonuniform pores: a density functional approach. Mol. Phys. 81, 691–705.

Curtin, D., Smillie, G.W., 1976. Estimation of components of soil cation exchange capacity from measurements of specific surface and organic matter. Soil Sci. Soc. Am. J. 40, 461–465.

Dobrzanski, B., Dechnik, J., Stawinski, J., 1972. The organic substance as a factor determining the soil surface area. Pol. J. Soil Sci. IV, 326–331.

Feder, J., 1988. Fractals: Physics of Solids and Liquids. Plenum, New York.

Friesen, W.I., Mikula, R.J., 1987. Fractal dimensions of coal particles. J. Colloid Interface Sci. 120, 263–271.

Hajnos, M., Matyka-Sarzynska, D., 1996. Determination of surface free energy components of kaolin by the thin-layer wicking technique. Pol. J. Soil. Sci. XXIX, 39–45.

Ismail, I.M.K., Pfeifer, P., 1994. Fractal analysis and surface roughness of nonporous carbon fibers and carbon blacks. Langmuir 10, 1532–1538.

Janczuk, B., Białopiotrowicz, T., 1989. Surface free energy components of liquids and low energy solids and contact angles. J. Colloid Interface Sci. 127, 189–203.

Janczuk, B., Hajnos, M., Białopiotrowicz, T., Kliszcz, A., Bilinski, B., 1990. Hydrophobization of the soil by dodecyl ammonium hydroxide and changes of the components of its surface free energy. Soil Sci. 150, 753–762.

Janczuk, B., Białopiotrowicz, T., Zdziennicka, A., Hajnos, M., Jozefaciuk, G., 1992. The influence of soil clay constituents on surface free energy of clay fractions. J. Soil Sci. 43, 27–35.

Jaroniec, M., Avnir, D., 1989. Thermodynamics of gas adsorption on fractal surfaces of heterogeneous microporous solids. Langmuir 5, 1431–1437.

Jaroniec, M., Kruk, M., Olivier, J., 1997. Fractal analysis of composite adsorption isotherms obtained by using density functional theory data for argon in slitlike pores. Langmuir 13, 1031–1035.

Jarzebski, A.B., Lorenc, J., Pajak, L., 1997. Surface fractal characteristics of silica aerogels. Langmuir 13, 1280–1285.

Jekel, M.R., 1986. The stabilization of dispersed mineral particles by adsorption of humic substances. Water Res. 20, 1543–1554.

Jouany, C., Chassin, P., 1987. Determination of the surface energy of clay–organic complexes by contact angle measurements. Colloids and Surfaces 27, 289–303.

Jozefaciuk, G., Hajnos, M., Sokołowska, Z., Renger, M., 1995. Influence of surface coverage by humic acids on surface free energy and wettability of quartz and kaolin. Pol. J. Soil Sci. XXXVII, 29–35.

Kozak, E., Stawinski, J., Wierzchos, J., 1991. Reliability of mercury intrusion porosimetry results for solids. Soil Sci. 152, 1325–1328.

Kozak, E., Sokołowska, Z., Sokołowski, S., Wierzchos, J., 1995. Surface fractal dimension of soil materials from pore size distribution data. A comparison of two methods of determination. Pol. J. Soil Sci. XXVIII, 77–85.

Kretzchmar, R., Robage, W.P., Weed, S.B., 1993. Flocculation of kaolinite solid clays: effect of humic substances and iron oxides. Soil Sci. Soc. Am. J. 57, 1277–1283.

Lawrence, G.P., 1978. Stability of soil pores during mercury intrusion porosimetry. J. Soil Sci. 29, 299–304.

Lawrence, G.P., Payne, D., Greenland, D.J., 1979. Pore size distribution in critical point and freeze dried aggregates from clay subsoils. J. Soil. Sci. 30, 499–516.

Murphy, E.M., Zachar, J.M., Smith, S.C., Philips, J., Wietsma, T.W., 1994. Interaction of hydrophobic organic compounds with mineral-bound humic substances. Environ. Sci. Technol. 28, 1291–1299.

Murray, R.S., Quirk, J.P., 1981. Comments on recent work with critical point dried soils. J. Soil Sci. 32, 161–164.

Neimark, A.V., 1990a. Determination of the surface fractal dimensionality from the results of an adsorption experiment. Russ. J. Phys. Chem. 64, 1397–1403.

Neimark, A.V., 1990b. Thermodynamic method for calculating surface fractal dimension. JETP Lett. 51, 535–538.

Neimark, A.V., 1990c. Calculating surface fractal dimensions of adsorbents. Adsorption Sci. Technol. 7, 210–219.

Neimark, A.V., 1992. A new approach to determination of the surface fractal dimension of porous solids. Physica A 191, 258–262.

Neumann, A.W., Good, R.J., 1979. Techniques of measuring contact angles. In: Good, R.J., Stromberg, R.R. (Eds.), Surface and Colloid Science, 11. Plenum, New York, pp. 31–91.

Oscik, J., 1982. Adsorption. Ellis Horwood, Chichester, pp. 81–87 and 110–117.

Pachepsky, Ya.A., Polubesova, T.A., Hajnos, M., Sokołowska, Z., Jozefaciuk, G., 1995a. Fractal parameters of pore area as influenced by simulated soil degradation. Soil Sci. Soc. Am. J. 59, 68–75.

Pachepsky, Ya.A., Polubesova, T.A., Hajnos, M., Jozefaciuk, G., Sokołowska, Z., 1995b. Parameters of surface heterogeneity from laboratory experiments on soil degradation. Soil Sci. Soc. Am. J. 59, 410–417.

Pachepsky, Y.A., Ritchie, J.C., Gimenez, D., 1997. Fractal modelling of airborne laser altimetry data. Remote Sens. Environ. 61, 150–161.

Pfeifer, P., 1987. Characterization of surface irregularity. In: Laszlo, P. (Ed.), Preparative Chemistry Using Supported Reagents. Academic Press, New York, pp. 13–33.

Pfeifer, P., Orbert, M., 1989. Fractals: basic concepts and terminology. In: Avnir, D. (Ed.), The Fractal Approach to Heterogeneous Chemistry. Wiley, UK, pp. 331–340.

Pfeifer, P., Cole, M.W., Krim, J., 1990. Reply to 'Wetting on fractally rough surfaces' by M. Kardar and J.O. Indekeu. Phys. Rev. Lett. 65, 662–663.

Pfeifer, P., Johnston, G.P., Deshpande, R., Smith, D.M., Hurd, A.J., 1991. Structure-analysis of porous solids from preadsorbed films. Langmuir 7 (11), 2833–2843.

Rice, J.A., Lin, J.S., 1992. Fractal dimension of humic materials. Proc. 6th Int. Meeting IHSS. Elsevier, Amsterdam, p. 44.

Robbins, M.O., Andelman, D., Joanny, J.F., 1991. Thin liquid films on rough or heterogeneous solids. Phys. Rev. A 43, 4344–4354.

Rootare, H.M., Prenzlow, C.F., 1967. Surface areas from mercury porosimeter measurements. J. Phys. Chem. 71, 2733–2736.

Senesi, N., 1992. The fractal approach to the study of humic substances. Proc. 6th Int. Meeting IHSS. Elsevier, Amsterdam, pp. 39, 39a.

Senesi, N., Rizzi, F.R., Dellino, P., Acquafredda, P., Maggipinto, G., Lorusso, G.F., 1994. The fractal morphology of soil humic acids. Transactions of the 15th World Congress of Soil Sci. International Soc. Soil Sci., Acapulco, 3b, pp. 81, 82.

Sequi, P., Aringhieri, R., 1977. Destruction of organic matter by hydrogen peroxide in the presence of pyrophosphate and its effect on the soil specific surface. Soil Sci. Soc. Am. J. 41, 430–432.

Smith, D.M., Johnson, G.P., Hurd, A.J., 1990. Structural studies of vapour-phase aggregates via mercury porosimetry. J. Colloid Interface Sci. 135, 227–237.

Sokołowska, Z., Patrykiejew, A., Sokołowski, S., 1989. A note on fractal analysis of adsorption process by soils and soil minerals. International Agrophysics 5, 3–12.

Sokołowska, Z., Jozefaciuk, G., Sokołowski, S., Ourumova-Pesheva, A., 1993. Adsorption of water vapour by soils. Investigations of the influence of organic matter, iron and aluminum on energetic heterogeneity of soil clays. Clay Miner. 3, 346–352.

Sokołowska, Z., Hajnos, M., Jozefaciuk, G., Hoffmann, C., Renger, J.M., 1997. Influence of humic acid on water adsorption characteristics of kaolin and quartz. Z. Pfl. Bodenk. 160, 327–331.

Spindler, H., Kraft, M., 1988. Fractal analysis of pores. Catalysis Today 3, 395–400.

Sridharan, A., Venkatappa Rao, G., 1972. Pore size distribution of soils from mercury intrusion porosimetric data. Proc. Soil Sci. Soc. Am. 36, 980–981.

Stepanov, I.S., Dokuchayev, V.V., 1981. Physical methods for extracting fractions of organo-mineral substances from solids. Pochvovedeniye 4, 110–121, (in Russian).

Theng, B.K.G., 1979. Formation and Properties of Clay–Polymer Complexes. Elsevier, Amsterdam.

Vadarachari, Ch., Mondal, A.H., Ghosh, K., 1991. Some aspects of clay-humus complexation: effect of exchangeable cations and lattice charge. Soil Sci. 151, 220–227.

Volzone, C., Hipedinger, N., 1997. Mercury porosimetry of compacted clay minerals. Zeitschrift Fur Pflanzenernahrung Und Bodenkunde 160 (No.4), 357–360.

Wierzchos, J., 1989. Analysis of physico-chemical conditions of the formation and stability of soil structure. PhD dissertation, IUNG, Pul/awy, pp. 39–44.

Yin, Y., 1991. Adsorption isotherm on fractally porous materials. Langmuir 7, 216–217.

Yokoya, N., Yamamoto, K., Funakuro, N., 1989. Fractal-based analysis and interpolation of 3D natural surface shapes and their application to terrain modeling. Comput. Vision Graphics Image Process 46, 284–302.

This Page Intentionally Left Blank

*Fractals in Soil Science*
Editors: Ya.A. Pachepsky, J.W. Crawford and W.J. Rawls
© 2000 Elsevier Science B.V. All rights reserved.


# Applications of light and X-ray scattering to characterize the fractal properties of soil organic matter

James A. Rice [a,*], E. Tombácz [b], Kalumbu Malekani [a,1]

[a] *South Dakota State University, Department of Chemistry and Biochemistry, Brookings, SD 57007-0896, USA*
[b] *Attila József University, Department of Colloid Chemistry, Aradi V rtanuk tere 1, Szeged, Hungary*

Received 16 October 1997; accepted 28 September 1998

**Abstract**

Soil organic matter (SOM) is a heterogeneous assemblage of organic molecules that interact in a variety of ways with each other, with soil mineral surfaces, and with soil mineral colloids. Because of SOM's heterogeneity it is very difficult to define its surface, or the surfaces of the composite materials produced by its interaction with soil minerals. Yet it is at these interfaces where chemical reactions that involve SOM take place. Results are presented which describe the fractal characterization of humic materials using static X-ray and light scattering, and dynamic light scattering (DLS) experiments. The applicability of static X-ray scattering to the direct determination of the fractal dimension of humic materials is established using DLS. Over the length scales studied, humic materials are surface fractals in the solid state, and mass fractals in solution. The longer characterization length scales possible in the static light scattering experiments suggest that at longer characterization length scales humic acid is not fractal, at least not under the solution conditions employed in these experiments. Application of fractal analysis to the characterization of the surface morphology of soil and peat humin samples, the calculation of the hydrodynamic radius of humic acid particles, and the study of humic acid aggregation are discussed. © 1999 Elsevier Science B.V. All rights reserved.

*Keywords:* fractal; humic acid; humin; fulvic acid; soil organic matter; dynamic light scattering; static light scattering; small-angle X-ray scattering

* Corresponding author. Tel.: +1-605-688-4252; Fax: +1-605-688-6364; E-mail: ricej@ur.sdstate.edu

[1] Present address: The Connecticut Agricultural Experiment Station, PO Box 1106, New Haven, CT 06504, USA.

Reprinted from Geoderma 88 (1999)
© 1999 Elsevier Science B.V. All rights reserved

## 1. Introduction

Soil organic matter is divided into humic and nonhumic substances (Stevenson, 1982). Nonhumic substances are organic materials that belong to recognizable compound classes such as carbohydrates and other polysaccharides, proteins or peptides, lipids, and lignin. Humic substances are organic materials that are formed by the profound alteration of organic matter in natural environments. They are operationally divided into three fractions based on their solubility as a function of the pH of the aqueous solution used to extract them: humic acid is defined as the fraction soluble at alkaline pH values, fulvic acid is defined as the fraction soluble at all pH values, and humin is defined as the fraction insoluble at any pH value (Hayes et al., 1989). It is possible to fractionate humin into a bound–humic acid fraction, a solvent extractable lipid fraction (bitumen), a bound–lipid fraction, and a mineral component (Rice and MacCarthy, 1990). This paper will focus on the humic materials.

Each humic fraction has been shown to be an extremely complex mixture of organic substances that apparently cannot be described by a single chemical structure (Dubach and Mehta, 1963; Felbeck, 1965; Hurst and Burges, 1967). Essentially all analytical methods that can be used to characterize the structure of a substance, such as NMR or mass spectrometry, operate under the assumption that the material being characterized is a pure substance. But because humic materials are mixtures, the most that can be realistically hoped for from such a chemical characterization is an 'average' or 'bulk' chemical description of the substances that comprise it. While such an approach has some utility describing the chemical and geochemical behavior of humic materials, it provides limited information that can be used to study their structural morphology. Humic materials have proven so intractable to repeated attempts to impose structural order onto them because they may represent the ultimate in molecular disorder (MacCarthy and Rice, 1991). Even lignin, which has been shown to some indication of structure on a long-range scale (Srzic et al., 1995), does not appear to approach the molecular complexity embodied by humic materials. Based on the characteristics that humic materials must possess in order to perform their functions in a natural system, it has been proposed that the fundamental characteristic of humic materials is not a discrete chemical structure (MacCarthy and Rice, 1991). Conversely, it is entirely probable that humic materials are best described by a profound *absence* of discrete structure (MacCarthy and Rice, 1991).

It is only recently that the application of fractal geometry to the study of the nature and chemistry of humic materials in natural systems has been described. In the interval since a fractal nature for humic materials was first reported, there have been few papers to actually exploit the fractal concept to better understand these enigmatic substances. Rice and Lin (1992, 1993, 1994) and Malekani and Rice (1997) have used small-angle X-ray scattering (SAXS) to demonstrate that

all three humic substances are fractal materials in solution or in the solid state. Österberg and Mortensen (1992a,b), Österberg et al. (1994) and Senesi et al. (1994, 1996a,b) using small-angle neutron scattering and turbidimetry, respectively, have also shown that humic materials can be characterized by fractal geometry. These references describe investigations into the effects of concentration, pH, temperature, and ionic strength on the aggregation behavior of humic acids.

The purpose of this paper is to provide an overview of the combination of light and X-ray scattering methods with fractal geometry to probe the chemistry and geochemistry of humic materials.

## 2. Materials and methods

### *2.1. Materials*

A peat and a soil classified as a Cryohemist (Moore, 1986) and a fine-silty, mixed Udic Haploboroll (Malo, 1994), respectively, were the primary source for the humic materials used in this study. Humic acid and fulvic acid were isolated from the peat and the soil using a traditional alkaline extraction procedure. Humin was isolated as the residue remaining after alkaline extraction of the humic and fulvic acids from the soil, and two others as well. Detailed descriptions of these other two soils are given elsewhere (Rice, 1987; Malekani, 1997). Solution samples were prepared by dissolving the humic acid or fulvic acid in 0.1 M NaOH or deionized, distilled water, respectively. When necessary, the pH was adjusted with NaOH or HCl, and the ionic strength was adjusted using NaCl. Prior to scattering measurements, solution samples were filtered through 0.22 μm membrane filters.

The organic components of the humin samples were removed in the following manner. The samples were first extracted with chloroform in a Soxhlet apparatus for 48 h (humin minus lipids), followed by disaggregation of the humin using the MIBK method (Rice and MacCarthy, 1990) and then oxidation of the remaining organic matter with bromine (humin minus organic matter). Malekani and Rice (1997) discuss these procedures in detail.

### *2.2. Scattering methods*

Small-angle X-ray scattering measurements were performed on the 10-m SAXS camera at the Center for Small Angle Scattering at Oak Ridge National Laboratory, Oak Ridge, TN. The instrument has been described by Wignall et al. (1990). A X-ray wavelength of $\lambda = 1.54$ Å was employed for all experiments. Additional methodological details can be found elsewhere (Rice and Lin, 1992, 1993, 1994).

Static light-scattering (SLS) and dynamic light scattering (DLS) measurements were performed on an ALV-5000/E light scattering apparatus fitted with an argon-ion laser operated at $\lambda = 514.5$ nm. Further instrumental details have been described elsewhere (Ren et al., 1996). The correlation functions were evaluated using cumulant and Contin analysis, and the $z$-average particle radius was calculated as described by Martin and Leyvraz (1986) and Martin (1987).

Solid samples were placed into 1 mm thick holders fitted with Kapton windows for SAXS characterization. Solution samples were run in 1 mm flattened Lindeman glass capillaries using the airpath SAXS insert. Quartz cuvettes (8 mm i.d.) were used for SLS characterization of solution samples, DLS measurements were performed in 8 mm (i.d.) glass cuvettes.

### *2.3. Fractal analysis of scattering data*

The scattering vector, $q$, is related to the angle of the scattered radiation, $\theta$, by Eq. (1):

$$q = \frac{4n\pi}{\lambda} \sin\left(\frac{\theta}{2}\right) \tag{1}$$

where $n$ is the refractive index of the scattering medium. The size of the scatterer is described by a characteristic length, $l$ (i.e., the particle diameter), and scattering depends on the product '$ql$'. Most of the information from a scattering measurement can be obtained at scattering angles such that $0.1 \leqslant ql$. The size of the scatterer is inversely related to $q$; larger particles will scatter at smaller angles and smaller values of $q$. Scattering which results from fractal substances conforms to a power law where the intensity of the scattered radiation as a function of $q$ is proportional to $q$ raised to some exponent (i.e., $I(q) \propto q^{-\exp}$) (Schmidt, 1989). The magnitude of this exponent is directly related to the fractal dimension, $D$, of the scatterer. To determine if scattering by humic materials conforms to a power law, log–log plots of $I(q)$ vs. $q$ were constructed. If scattering from a sample obeys a power law, the plot will be a straight line. The slope of this plot is the power law exponent, and can be used to calculate $D$.

Two types of fractals—mass fractals and surface fractals—are relevant to these studies. Mass fractals are objects whose surface and mass distribution are characterized by fractal properties. The power-law behavior of a mass fractal is described by Eq. (2):

$$I(q) \propto q^{-D_m}. \tag{2}$$

For a mass fractal, the power-law exponent is the fractal dimension. A scatterer is a mass fractal when the exponent (and hence the mass fractal dimension, $D_m$) is less than or equal to 3 (Schmidt, 1989). A surface fractal is

one in which only the surface of the scatterer exhibits fractal properties. The power-law scattering behavior of a surface fractal is given by Eq. (3):

$$I(q) = q^{-(6-D_s)}. \tag{3}$$

The power law exponent for a surface fractal falls within the range: $3 < 6 - D_s \leq 4$. Once the exponent is known, the surface fractal dimension, $D_s$, can be readily calculated.

## 3. Results and discussion

### *3.1. Small-angle X-ray scattering*

Figs. 1–3 are log–log plots of the intensity of the scattered X-rays as a function of the scattering vector ($q$) vs. $q$ for the solid- and solution-state peat humic acid and fulvic acid, and the solid-state humin samples used in this study. All plots are straight lines, indicating that SAXS scattering by humic materials

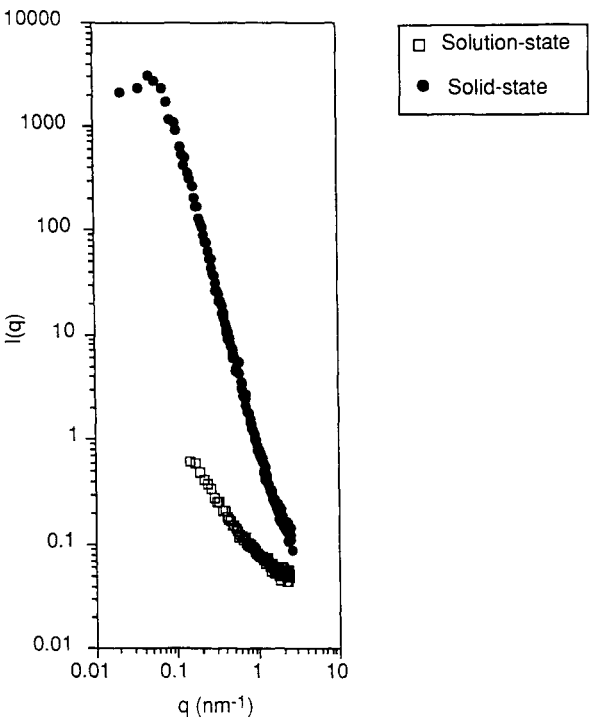


Fig. 1. Log–log plots of $I(q)$ vs. $q$ for the peat humic acid SAXS data. Solution data represent a smaller $q$-range because a shorter sample-to-detector distance was used during data acquisition. The intensity scale [$I(q)$] is in arbitrary units, and each plot has been vertically offset to clarify presentation.

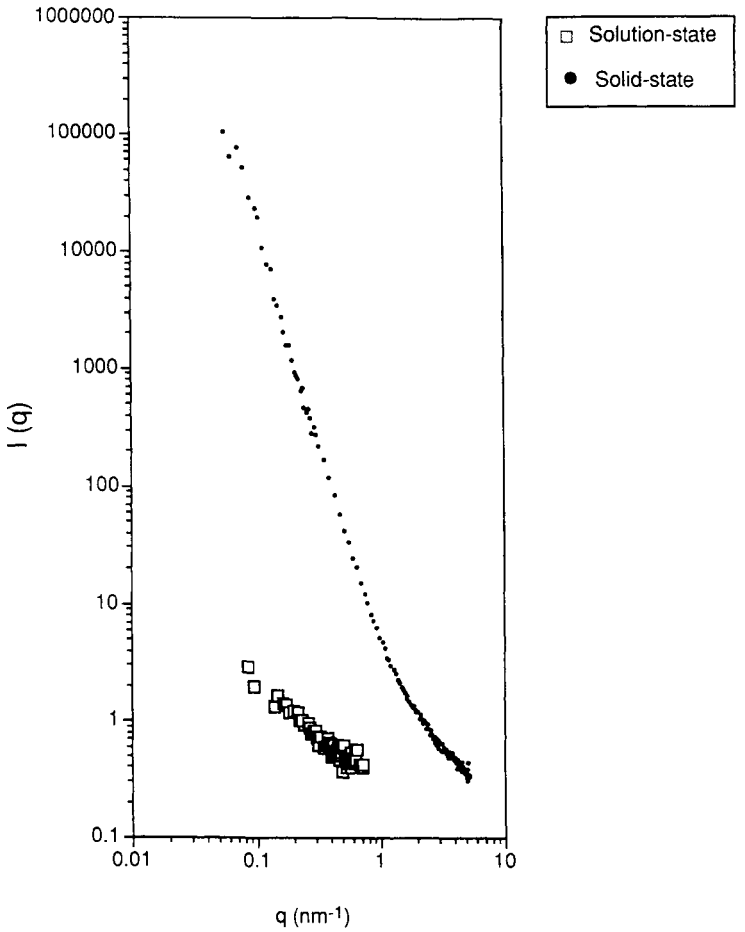


Fig. 2. Log–log plots of $I(q)$ vs. $q$ for the peat fulvic acid SAXS data. Solution data represent a smaller $q$-range because a shorter sample-to-detector distance was used during data acquisition. The intensity scale $[I(q)]$ is in arbitrary units, and each plot has been vertically offset to clarify presentation.

in either form can be described by a power law. The humin scattering curve (Fig. 3) shows a change in slope. This is attributed to the presence of mass and surface fractal scatterers in this sample. This is discussed in more detail in Section 3.3.

Power-law scattering is observed over more than one order of magnitude of $q$. Avnir et al. (1998) have pointed that power-law behavior covering a limited range of characterization lengthscales (in this case, $q$) does not truly conform to Mandelbrot's original definition (Mandelbrot, 1983) of the concept of a fractal. The combination of SAXS and SLS data described in Section 3.2 is a first attempt to try to determine if power-law behavior is actually observed over a wide scaling range. Even if humic materials are not truly fractal, the fractal

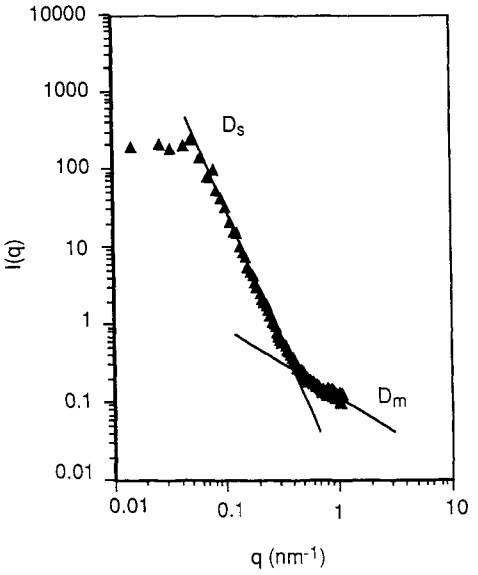


Fig. 3. Log–log plots of $I(q)$ vs. $q$ for the peat humin SAXS data. Because of humin's insolubility, data are for the solid-state.

approach to the analysis of the scattering behavior of humic materials greatly simplifies what is, by almost all accounts, an extraordinarily complex structural geometry and it provides a means to correlate humic material structure to a variety of processes and properties such its aggregation. These are advantages to a fractal approach to data analysis acknowledged by Avnir et al. (1998).

The power-law exponent and the fractal dimension of each humic material are shown in Table 1. In the solid-state, humic materials can be classified as surface fractals. In contrast humic materials in solution are found to be mass fractals. The fractal dimension of each humic material in the solid- and solution-state indicates a convoluted, space-filling morphology for each material. Using dynamic light scattering and dynamic scaling theory, Ren et al. (1996) and Tombácz et al. (1997) have shown that the fractal dimension can, in fact, be calculated directly from the SAXS data without the necessity of correcting for polydispersity, validating these results. For systems with a greater degree of polydispersity, corrections to the measured value of $D$ would have to be made as described by Schmidt (1989) and Martin and Leyvraz (1986). It is apparent from these results that the morphologies of humic materials are amenable to description by fractal geometry.

Scattering by any material can be placed into categories based on the behavior of the scattering intensity as a function of $q$ (Fig. 4). Each of the $q$-regions of a scattering curve provides different types of information about a substance. For example, power-law behavior (and hence, fractal nature) is observed in the Porod region, X-ray diffraction is performed in the Bragg

Table 1
Power-law exponents and fractal dimensions ($D$) for the humic acids, fulvic acids and humins characterized in this study. In the solution-state, humic and fulvic acids are mass fractals, in the solid-state they are surface fractals. Humin is, by definition, insoluble, so there are no solution values. The uncertainty associated with each $D$ value is $\leq 0.1$

| Sample | Power-law exponent | | Fractal dimension | |
|---|---|---|---|---|
| | Solution | Solid | Solution | Solid |
| *Peat* | | | | |
| Fulvic acid | 2.2 | 3.3 | 2.2 | 2.7 |
| Humic acid | 2.5 | 3.8 | 2.5 | 2.2 |
| Humin | – | 3.1 | – | 2.9 |
| *Soil* | | | | |
| Fulvic acid | 2.3 | 3.5 | 2.3 | 2.5 |
| Humic acid | 2.6 | 3.7 | 2.6 | 2.3 |
| Humin | – | 3.5, 3.9[a] | – | 2.5, 2.1[a] |

[a]See Section 3.3.2 for a brief discussion of the two fractal dimensions.

region, and the size of a material can be calculated from data in the Guinier region. In order to extend the $q$-range, and the size of scatterer that can be characterized by fractal geometry, the solution samples were characterized by SLS.

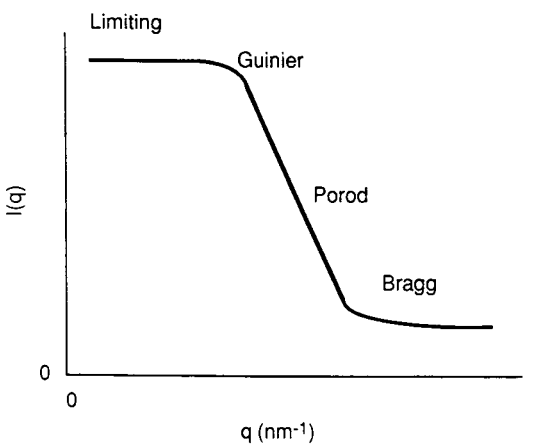


Limiting: uniformity at large length scales

Guinier: information on particle size (correlation length scale)

Porod: scattering by fractal particles

Bragg: atomic level correlations (x-ray diffraction)

Fig. 4. A generalized scattering curve. Modified after Fleischmann (1989).

### 3.2. *Static light scattering*

Fig. 5 shows SLS log–log plot of $I(q)$ vs. $q$ for the peat and soil humic acids. Fulvic acid was found to be too weak a scatterer to characterize at this time. It is evident that the exponent (i.e., the slope) in this $q$-range is very different than that displayed by the same samples in the $q$-range accessible by SAXS (Fig. 1). This indicates that the scattering behavior of humic acid is no longer Porod-type (i.e., fractal) scattering, but has now entered the Guinier or limiting regions of the scattering curve (Fig. 4).

The combination of SAXS and SLS scattering data help to clearly delineate the large-particle limit to the characterization of humic materials in solution by scattering techniques and fractal geometry. Based on these measurements, it appears that humic acid in an alkaline aqueous solution exhibits a fractal nature over a $q$-range of $\sim 0.03$ nm$^{-1}$ to $\sim 3$ nm$^{-1}$. This corresponds to a characterization length-scale of $\sim 3$ Å to $\sim 33$ nm. It is not possible to identify the absolute lower limit of the characterization length scale where humic and fulvic acid are fractal (i.e., the beginning of the Bragg region in Fig. 4). It should be noted that the lower limit in these experiments (3 Å) is approaching molecular

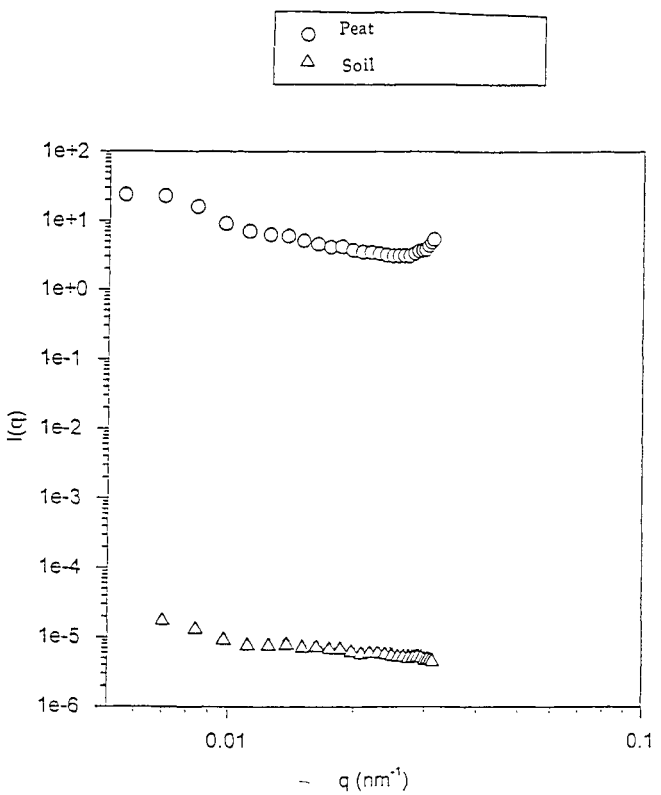


Fig. 5. Log–log plots of $I(q)$ vs. $q$ for the soil and peat humic acid SLS data.

bond lengths, and probably represents a value very near the transition to Bragg scattering.

### *3.3. Applications in studies of soil organic matter*

#### *3.3.1. Particle-size measurement*

An interest in fractal morphology of humic materials leads to an interest in the study of its dynamics in solution. In principle, information on the size of the fractal particle, its growth during aggregation and conformational changes in response to changing solution conditions can be obtained from the autocorrelation function of the temporal variation in light scattered from the particles (Lin et al., 1989). Such determinations are imprecise measurements that depend on many characteristics of the system under investigation, the particle-size distribution. The molecular-weight distribution of humic materials, regardless of the method used for its measurement, typically shows a polydisperse size distribution that displays an asymptotic, high-mass tail (Becket et al., 1989; Hernandez et al., 1989; Novotny et al., 1995). The shape of this distribution suggests power-law polydispersity that is consistent with a fractal nature for humic materials.

Power-law polydispersity makes the interpretation of DLS data on the basis of simple particle dynamics difficult. Martin (1987) has shown that in solutions of power-law polydisperse particles, relaxation rates scale with $q$ in the DLS measurement by noninteger exponents, an observation that is inconsistent with monodisperse or Gaussian-polydisperse particle-size distributions. Martin and Ackerson (1985) and Martin and Leyvraz (1986) have shown that the dynamics of power-law polydisperse fractal aggregates can be scaled with $q$ using a power law whose exponents may have noninteger values that are related to $D$ and the polydispersity of the particle-size distribution. We have recently described the application of this 'dynamic scaling' theory to humic materials (Ren et al., 1996). From the application of this theory to scattering data it is possible to calculate the $z$-averaged particle radius, $R_z$, and in fact the unusual angle dependence often displayed by DLS data from humic acid often make direct calculation of the particle radius essentially impossible without its application (Tombácz et al., 1997).

The $D$ and the polydispersity exponent found by Ren et al. (1996) and Tombácz et al. (1997) are typical of values observed for fractal colloids produced by reaction-limited cluster–cluster aggregation. Reaction-limited cluster–cluster aggregation is a slow process in which clusters must overcome the repulsive forces (in this case, probably the negative charges associated with the humic colloids) before aggregation, and the formation of larger aggregates, can occur. In light of the polyelectrolyte nature demonstrated below, and elsewhere (Swift, 1989; Tombácz and Meleg, 1990), this is an interesting observation on which to base further studies of the aggregation behavior of this environmentally

Table 2
Effect of added electrolyte (NaCl) on the $z$-averaged particle radius ($R_z$) of the peat humic acid

| Electrolyte concentration (mM) | $R_z$ (nm) |
|---|---|
| 5 | 96 |
| 10 | 85 |
| 50 | 66 |
| 100 | 48 |

important colloidal material. Senesi et al. (1996b) also report that a reaction-limited particle–cluster aggregation model can be used to describe the aggregation of fractal humic acid colloids. They also conclude that the applicability of this model may vary as function of pH.

Table 2 shows the effect of increasing added electrolyte concentration on $R_z$. As charge screening effects increase (i.e., the added electrolyte concentration increases), electrostatic repulsion between the individual components of humic acid forming the aggregates decreases. This results in the aggregates shrinking and $R_z$ decreasing which is typical polyelectrolyte behavior.

*3.3.2. Humic organic coatings on mineral surfaces*

The humin samples, and the components of humin, exhibit both mass and surface fractal behavior (Fig. 3 and Table 3). There is precedent for such an observation in mineral-based soils. Avnir et al. (1985) found that fractal dimensions in soils can be different at different observation length scales. In this instance, mass fractal behavior is displayed over a smaller observation range, i.e., 0.4 to $\sim 4$ nm whereas surface fractal behavior is observed over a larger length scale of $\sim 1$ to 10 nm. The two different $D$ values obtained for each of these materials could be attributed to the presence of two different classes of

Table 3
Fractal dimensions of humin, humin after lipid removal (Humin − L), and humin after complete removal of organic matter (Humin − OM, i.e., the mineral surface). Values in brackets represent characterization lengthscale in nanometers. The uncertainty associated with each $D$ value is $\leq 0.1$

| Soil fraction | Fractal dimensions | |
|---|---|---|
| | $D_s$ | $D_m$ |
| Soil Humin | 2.9(1–10) | 2.9(0.4–4) |
| Soil Humin − L | 2.7(1–10) | 2.9(0.4–4) |
| Soil Humin − OM | 2.3(2–8) | 3.0(0.4–3) |
| | 2.9(1–9) | 3.0(0.3–4) |
| Peat Humin | 2.2(2–8) | 2.2(0.5–1) |
| Peat Humin − L | 2.0(2–8) | 2.6(0.4–2) |
| Peat Humin − OM | 2.0(2–8) | 2.6(0.4–1) |

grain size and/or mineral composition (Avnir et al., 1985) in the humin samples characterized here. Further fractionation of these materials into different size/or mineral groups constituting the two fractality regions would be appropriate in attempt to try to resolve these fractal subsets.

The fractal dimensions in Table 3 show that humin and its fractions produced by organic matter removal display surface fractal behavior over length scales ranging from $\sim 1$ to $\sim 10$ Å, with the humin samples having the largest fractal dimension. The removal of organic matter resulted in a decrease in surface fractal dimensions. Malekani et al. (1996) have shown that clay minerals typically have fractal dimensions of $D \sim 2$ which are considerably less than the values for the intact humin samples, indicating that it is the organic matter coatings on mineral surfaces which are responsible for their surface roughness. Thus it seems reasonable to attribute the surface roughness of humin particles to organic matter coatings. Malekani and Rice (1997) have explored the effects of organic matter removal on the surface roughness of soils and humin using surface area measurements and fractal analysis of the soil and humin samples.

## 4. Summary

Humic materials can be characterized by fractal geometry. In addition, fractal geometry has been shown to be applicable to incorporating the polydispersity of humic materials into the characterization of its molecular size in the form of the $z$-averaged particle radius. The information from these experiments has indicated that a reaction-limited aggregation may be appropriate model to study aggregation phenomena that these colloids undergo. Fractal geometry has also been shown to be a valuable tool in elucidating the surface morphology of the organic-coated mineral grains that comprise the humin fraction of soil organic matter, and how the nature of the surface changes as the organic matter is removed.

## Acknowledgements

This work was supported by the National Science Foundation under grants OSR-9452894 and OSR-9108773, and the South Dakota Future Fund.

## References

Avnir, D., Farin, D., Pfeifer, P., 1985. Surface geometric irregularity of particulate materials: the fractal approach. J. Colloid Interface Sci. 103, 113–123.

Avnir, D., Biham, O., Lidar, D., Malcai, O., 1998. Is the geometry of nature fractal?. Nature 279, 39–40.

Becket, R., Jue, T., Giddings, J.C., 1989. Determination of molecular weight distributions of

fulvic and humic acids using flow field–flow fractionation. Environ. Sci. Technol. 21, 289–295.

Dubach, P., Mehta, N.C., 1963. The chemistry of soil humic substances. Soils Fert. 26, 293–300.

Felbeck, G.T. Jr., 1965. Structural chemistry of soil humic substances. Adv. Agron. 17, 327–367.

Fleischmann, M.Y., 1989. Fractals in the natural sciences. In: Fleischmann, M.Y., Tildesley, D.J., Ball, R.C. (Eds.), Fractals in the Natural Sciences. Princeton University Press, Princeton, NJ, USA, 71 pp.

Hayes, M.H.B., MacCarthy, P., Malcolm, R.L., Swift, R.S., 1989. The search for structure: setting the scene. In: Hayes, M.H.B., MacCarthy, P., Malcolm, R.L., Swift, R.S. (Eds.), Humic Substances II: In Search of Structure. Wiley Interscience, Chichester, UK, pp. 3–31.

Hernandez, T., Moreno, J.I., Costa, F., 1989. Molecular size evaluation by gel filtration of humic acids from two sludges and from leonhardite. Geoderma 45, 83–88.

Hurst, H.M., Burges, N.A., 1967. Lignin and humic acids. In: McLaren, A.D., Peterson, G.H. (Eds.), Soil Biochemistry, Marcel Dekker, New York, pp. 261–286.

Lin, M.Y., Lindsay, H.M., Weitz, D.A., Ball, R.C., Klein, R., Meakin, P., 1989. Universality of fractal aggregates as probed by light scattering. In: Fleischmann, M.Y., Tildesley, D.J., Ball, R.C. (Eds.), Fractals in the Natural Sciences. Princeton University Press, Princeton, NJ, USA, pp. 71–87.

MacCarthy, P., Rice, J.A., 1991. An ecological rationale for the heterogeneous nature of humic substances. In: Schneider, S., Boston, P.J. (Eds.), Scientists on Gaia. MIT Press, Cambridge, MA, pp. 339–345.

Malekani, K., 1997. Organic Architecture of Humin. PhD Dissertation, South Dakota State Univ.

Malekani, K., Rice, J.A., Lin, J.S., 1996. Comparison of techniques for determining the fractal dimension of clay mineral surfaces. Clays Clay Miner. 44, 677–685.

Malekani, K., Rice, J.A., 1997. The effect of sequential removal of organic matter on the surface morphology of humin. Soil Sci. 162, 333–342.

Malo, D.D., 1994. South Dakota Soil Classification Key TB-96. Agricultural Experiment Station, Brookings, SD, USA.

Mandelbrot, B.B., 1983. The Fractal Geometry of Nature, revised edition. Freeman, New York.

Martin, J.E., 1987. Slow aggregation of colloidal silica. Phys. Rev. A 36, 3415–3426.

Martin, J.E., Leyvraz, F., 1986. Quasielastic-scattering linewidths and relaxation times for surface and mass fractals. Phys. Rev. A 34, 2346–2350.

Martin, J.E., Ackerson, B.J., 1985. Static and dynamic scattering from fractals. Phys. Rev. A 31, 1180–1182.

Moore, R., 1986. Soil Survey of the Pike and San Isabel National Forest, Northern Part. Soil Survey no. 8657, US Forest Service, GPO, Washington, DC.

Novotny, F.J., Rice, J.A., Weil, D., 1995. Characterization of fulvic acid by laser-desorption FTMS. Environ. Sci. Technol. 29, 2464–2466.

Österberg, R., Mortensen, K., 1992a. Fractal dimension of humic acids. Eur. Biophys. J. 21, 163–167.

Österberg, R., Mortensen, K., 1992b. Fractal geometry of humic substances. Temperature-dependent restructuring studied by small-angle neutron scattering. In: Senesi, N., Miano, T.M. (Eds.), Humic Substances in the Global Environment and Implications on Human Health. Elsevier, Amsterdam, pp. 127–132.

Österberg, R., Szajdak, L., Mortensen, K., 1994. Temperature-dependent restructuring of fractal humic acids: a proton-dependent process. Environ. Int. 20, 77–80.

Ren, S.Z., Tombácz, E., Rice, J.A., 1996. Dynamic light scattering from fractals in solution: application of dynamic scaling theory to humic acid. Phys. Rev. E 53, 2980–2983.

Rice, J.A., 1987. Studies on Humus: I. Statistical Studies on the Elemental Composition of Humus; II. The Humin Fraction, PhD Dissertation T-3204, Colorado School of Mines.

Rice, J.A., MacCarthy, P., 1990. A model of humin. Environ. Sci. Technol. 24, 1875–1877.

Rice, J.A., Lin, J.S., 1992. Fractal nature of humic materials. Prepr. Ext. Abs., Am. Chem. Soc., Environ. Chem. Div., 203rd Natl. Mtg., San Francisco, CA, USA, pp. 11–14.

Rice, J.A., Lin, J.S., 1993. Fractal nature of humic materials. Environ. Sci. Technol. 27, 413–414.

Rice, J.A., Lin, J.S., 1994. Fractal dimensions of humic materials. In: Senesi, N., Miano, T.M. (Eds.), Humic Substances in the Global Environment and Implications on Human Health. Elsevier, Amsterdam, pp. 115–120.

Schmidt, P., 1989. Use of scattering to determine the fractal dimension. In: Avnir, D. (Ed.), The Fractal Approach to Heterogeneous Chemistry. Wiley Interscience, Chichester, UK, pp. 67–79.

Senesi, N., Lorusso, G.F., Miano,T.M., Maggipinto, G., Rizzi, F.R., Capozzi, V., 1994. The fractal dimension of humic substances as a function of pH by turbidity measurements. In: Senesi, N., Miano, T.M. (Eds.), Humic Substances in the Global Environment and Implications on Human Health. Elsevier, Amsterdam, pp. 121–126.

Senesi, N., Rizzi, F.R., Dellino, P., Acquafredda, P., 1996a. Fractal dimension of humic acids in aqueuous suspension as a function of pH and time. Soil Sci. Soc. Am. J. 60, 1773–1780.

Senesi, N., Rizzi, F.R., Dellino, P., Acquafredda, P., 1996b. Fractal humic acids in aqueous suspensions at various concentrations, ionic strengths, and pH values. Colloids Surf. 127, 57–68.

Srzic, D., Martinovic, S., Tolic, L.P., Kezele, N., Shevchenko, S.M., Klasnic, L., 1995. Laser desorption Fourier-transform mass spectrometry of lignins. Rapid. Comm. Mass Spec. 9, 245–249.

Stevenson, F.J., 1982. Humus Chemistry. Wiley, New York.

Swift, R.S., 1989. Molecular weight, shape and size of humic substances by ultracentrifugation. In: Hayes, M.H.B., MacCarthy, P., Malcolm, R.L., Swift, R.S. (Eds.), Humic Substances II: In Search of Structure. Wiley Interscience, Chichester. UK, pp. 449–465.

Tombácz, E., Meleg, E., 1990. A theoretical explanation of the aggregation of humic substances as a function of pH and electrolyte concentration. Org. Geochem. 15, 375–381.

Tombácz, E., Rice, J.A., Ren, S.Z., 1997. Fractal structure of polydisperse humic acid particles in solution studied by scattering methods. ACH Models in Chem. 134, 877–888.

Wignall, G.D., Lin, J.S., Spooner, S., 1990. Reduction of parasitic scattering in small-angle X-ray scattering by a three-pinhole collimating system. J. Appl. Cryst. 23, 241–245.

*Fractals in Soil Science*
Editors: Ya.A. Pachepsky, J.W. Crawford and W.J. Rawls
© 2000 Elsevier Science B.V. All rights reserved.


# Fractal and the statistical analysis of spatial distributions of Fe–Mn concretions in soddy-podsolic soils

Yu.N. Blagoveschensky, V.P. Samsonova *

*Department of Soil Science, Moscow State University, Moscow, 119899, Russian Federation*

Received 17 October 1997; accepted 28 September 1998

**Abstract**

Fe–Mn concretions are stable indicators of water regimes in loamy and clay podsolic and soddy-podsolic soils. Their spatial distribution is, in a large part, an inheritance of several processes in a heterogeneous soil medium. The objective of this study was to examine whether fractal models are appropriate to describe the spatial distributions of concretions. Data were collected at three locations in the Moscow region. At the first location, there were eight plots at depths from 13 to 34 cm and the distributions of concretions larger that 0.5 mm were mapped by staining the individual concretions. At the remaining two locations, soil cores of different sizes were taken from two depths. Concretions were extracted from these cores and sieved to separate them by size. A method of thorough sampling of the area was employed that used estimates of fractal dimension for the every possible position a fixed geometrical form by using the box counting technique. These estimates were studied statistically and by comparison with simulated data. We found concretion distribution on the fixed depth to have at least three components. The first of them represents the background, i.e., it corresponds to the random and independent distributions of concretions. The second component has fractal nature. The third component represents dense nests and it is probably connected with favorable conditions for microorganisms forming concretions. Estimated dimensions greater than 2.5 belong to the nest component and less than 1.6—to the fractal one. The interval (1.6; 2.5) of them can be accounted for only by the random distribution. © 1999 Elsevier Science B.V. All rights reserved.

*Keywords:* Fe–Mn; soddy-podsolic soil; spatial distribution

* Corresponding author. Fax: +7-095-939-0989; E-mail: samson@soil.msu.ru

Reprinted from Geoderma 88 (1999)
© 1999 Elsevier Science B.V. All rights reserved

## 1. Introduction

Hard spherical Fe–Mn concretions are a common component of loamy and clay podsolic and soddy-podsolic soils (Rozanov, 1983). They are located in the upper 50–60 cm soil although mostly confined to the eluvial horizon at depth 10–30 cm. The number, size and chemical composition has been found to be sensitive to soil water regimes. This fact has led to their use as an indicator of hydromorphic processes in the taiga region (Zaidelman, 1974; Zaidelman and Nikiforova, 1997), since even in dry years when others signs of hydromorphism have disappeared from the topsoil horizons, the memory of past events is retained in Fe–Mn concretions.

The coincidence of Fe–Mn concretions with the loamy and clay soils may be considered as evidence that their formation depends on a particular set of circumstances which are favoured in these soils. The process of the segregation of iron and manganese oxides strongly depends on the distribution of water and air in the soil matrix, which in turn depends on the detailed structure of the porous medium. According to Rieu and Sposito (1991), the structure may be modeled as a fractal, and so we might expect that the spatial distribution of Fe–Mn concretions (simply referred to as concretions in the rest of this paper) will have some fractal properties.

In 1985–1989, a study of spatial variability of concretions and their connections with physical and chemical properties of soil mass were carried out on soddy-podsolic soils at the Department of Agriculture of Moscow State University. Although this data was not associated with any analysis of fractal behaviour at the time, we have found that the experimental material is suitable to test the hypothesis that the spatial distribution of concretion content has fractal properties. The basic information provided by the data includes core size, their placement in space, and the number of concretions in each core, and so only fractal properties of the spatial distribution may be considered.

Assuming that on the plot $S$ there is a number, $k$, of thin cores which range in diameter and are placed in a nested arrangement, we can consider the connection between linear sizes of the cores $L = L(A)$ and the number $m(A)$ of concretions in $A \in \{A_1, K, A_k\}$. In this case the embedding dimension is 2, and, if the spatial distribution is fractal, then $m(A)$ can be written as a function of $L(A)$ in the form

$$m(A) = m(L(A)) \cong c_m L(A)^{d_m}, \tag{1}$$

where $c_m$ is a constant and $d_m$ is the fractal dimension of the concretion distribution. If the sampling depth of cores is constant, then the sample is two-dimensional and $d_m \leq 2$. Otherwise it must be the case that $d_m \leq 3$. Estimates for the fractal dimension quoted in the literature often exceed these bounds, and possible reasons stemming from methodology are discussed in

papers of Wu et al. (1993), Perfect et al. (1993), Anderson and McBratney (1995), and Perfect and Kay (1995). Where several local measurements of the fractal dimension, several values can exceed the embedding dimension as a consequence of random noise in the distribution of concretions, and the possibility should be taken into account.

The central element of this paper is the distribution of values for the fractal dimension estimated for a large number of geometrically similar plots covering a thin slab of soil. Statistical distributions of these values and their spatial distribution are related to the area from which the data were collected. An important consideration in this type of analysis is the choice of length scale over which the measurement of the fractal dimension should be made. Since all natural objects may only be approximated by fractals over a finite range in length scale, the choice should be based on some understanding of the factors underlying genesis of the distribution. Our analyses of concretion size and their spatial density shows that a plot measuring 10 cm $\times$ 10 cm is the minimal area for which $d_m$ may be estimated. In addition, many properties of soddy-podsolic soils vary in space with an approximate periodicity of 20–60 cm (Kozlovskii and Sorokina, 1976). Therefore the minimum and maximum length scales between which the distribution of concretions may be approximated using fractals differ by only a factor of 2 to 5. This in turn significantly limits the spatial information in experimental data and the choice of statistical techniques for obtaining reliable estimates of the fractal dimension.

Our approach is therefore of necessity pragmatic. If, in some plot, we find that the fractal dimension significantly exceeds the physical bounds stated above, we can deduce that the distribution cannot be modeled as a fractal. However, if the estimated dimension lies within the physical bounds, then we may say that the distribution is consistent with fractal behaviour, but that our measurements do not constitute proof. Therefore, our approach is to determine the confidence with which the observed distribution is fractal.

## 2. Background

The location and size of the soil samples used in the analysis may influence the estimate of the fractal dimension. This is because the spatial distribution of concretions may be non-stationary, and the scaling properties may be fractal only between upper and lower scale limits which may, or may not, be included in the sampling regime.

To estimate the appropriate size of the soil samples we note the following. Firstly, the concretions vary in size up to, but rarely larger than, 5 mm. This provides an absolute constraint of 0.5 cm for the lower scale limit. Secondly, results of many studies of soil variability show that the spatial correlation of

many soil properties has a sill at 1–3 m, and therefore above that scale the properties are spatially independent. Furthermore, as stated in the introduction, soddy-podsolic soils have an approximate periodicity with period in the range 20–50 cm (Kozlovskii and Sorokina, 1976). From these observations it would seem that appropriate scales to sample would be in the range 10 cm–1 m. Furthermore, it will be necessary to take repeated samples from an area considerably larger than this in order to test for stationary behaviour and to assess the degree of spatial variability of the estimated fractal dimension.

In fact there are two ways to study fractal properties in practice. We can choose several diameters $L_1, L_2, \ldots, L_k$ and for each of them take the same number of cores. Subsequently, we can calculate *mean values* $M_j$ of concretion number for cores with the size $L_j$ and determine the fractal dimension using Eq. (1) for $j = 1, \ldots, k$. But this way does not give us an answer to how fractal dimensions distribute in the soil space. Another way is to calculate fractal dimension from each set of samples, $j = 1.2, \ldots, k$ by the box counting method (Bundle and Havlin, 1994, pp. 17–18). The number of estimates for the dimension is then equal to the number of repeat samples, and each estimate will be associated with a fixed location, in our study plot. Using all samples, it will be possible to determine the spatial structure of the distribution of fractal dimension. For more complete data exploring, we propose to modify the method using the *thorough* sampling of our plot.

To explain the approach we consider a square or rectangular plot divided into the square cells. Let the plot have $n$ cells along each horizontal (row) and $r$ cells along each vertical (column), thus there are $n \times r$ cells in total. A cell will be denoted by $\Delta_{ik}$ where $i$ is the number of its row and $k$ is its column number. Now we define the *form* as the grid of $10 \times 10$ cells together with five nested grids, i.e., the grid $A[10 \times 10]$ itself and the grids $A[7 \times 7]$, $A[5 \times 5]$, $A[3 \times 3]$ and $A[2 \times 2]$ sharing the common cell at the left lower corner of $A[10 \times 10]$ (see Fig. 1). The form can be positioned on the soil plot by the different ways. We will assume that (i) the form lays within our plot and (ii) the position of the form has be determined by that cell $\Delta_{ik}$ which lays in the left lower corner of the form.

Each location of our form results in a data matrix $\mu = \mu(i,k)$. Elements of the $(10 \times 10)$-matrix are total numbers of concretions in the corresponding cells, and the pair $(i,k)$ indexes different matrices. The following data are produced for each matrix $\mu$:

| Cores | $A[2 \times 2]$ | $A[3 \times 3]$ | $A[5 \times 5]$ | $A[7 \times 7]$ | $A[10 \times 10]$ |
|---|---|---|---|---|---|
| Number | $m(A[2 \times 2])$ | $m(A[3 \times 3])$ | $m(A[5 \times 5])$ | $m(A[7 \times 7])$ | $m(A[10 \times 10])$ |
| Size | $s(A[2 \times 2])$ | $s(A[3 \times 3])$ | $s(A[5 \times 5])$ | $s(A[7 \times 7])$ | $s(A[10 \times 10])$ |

where $m(A[B \times B])$ is the number of concretions in a core $A[B \times B]$, i.e., the sum over all cells of the core $A[B \times B]$, and $s(A[B \times B])$ is the area of $A[B \times B]$, where $B = 2$, 3, 5, 7 and 10. Then the fractal dimension $d_m$ can be

| | | | | | | | | | | |
|---|---|---|---|---|---|---|---|---|---|---|
| 10 | 0 | 0 | 1 | 0 | 1 | 2 | 0 | 1 | 1 | 0 |
| 9 | 2 | 0 | 0 | 0 | 0 | 0 | 3 | 0 | 1 | 0 |
| 8 | 0 | 2 | 0 | 0 | 0 | 0 | 2 | 0 | 0 | 0 |
| 7 | 0 | 2 | 0 | 0 | 1 | 1 | 2 | 1 | 1 | 0 |
| 6 | 2 | 0 | 0 | 0 | 2 | 0 | 2 | 1 | 0 | 0 |
| 5 | 0 | 1 | 2 | 0 | 0 | 3 | 1 | 2 | 0 | 1 |
| 4 | 0 | 0 | 0 | 1 | 1 | 1 | 0 | 2 | 1 | 0 |
| 3 | 0 | 2 | 0 | 2 | 2 | 0 | 2 | 0 | 0 | 3 |
| 2 | 0 | 3 | 1 | 1 | 0 | 0 | 0 | 1 | 0 | 2 |
| 1 | 1 | 2 | 0 | 1 | 1 | 0 | 2 | 1 | 0 | 2 |
| | 1 | 2 | 3 | 4 | 5 | 6 | 7 | 8 | 9 | 10 |

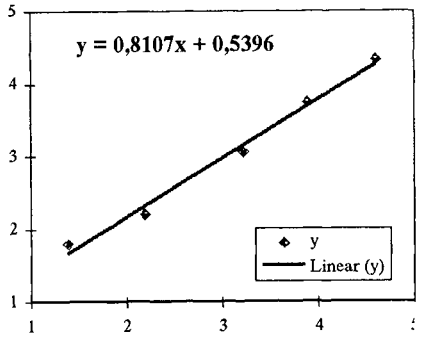


Fig. 1.

estimated from the slope of the assumed linear regression equation which follows from taking the logarithm of Eq. (1),

$$\ln m(A) \equiv \tau(\mu) \ln s(A) + b(\mu), \tag{2}$$

Here $\tau(\mu) = 0.5 d_m$, the equality $L(A) = \sqrt{s(A)}$ has been used, $A$ is any core among $A[B \times B]$, so if $d_m < 2$ then $\tau(\mu) < 1$ and such things (see the example in Fig. 1).

Now suppose that $\min(n,r) > 10$ and there are many possible sites for the form within the plot. We renumber all sites for which conditions (i) and (ii) are satisfied. There will be $N = (n-9) \cdot (r-9)$ proper sites, and we will give them signs $j = 1, 2, \ldots, N$. Further, we calculate the slope $\tau_j$ using Eq. (2) and the data matrix which conforms to the site with the sign $j \in \{1, 2, \ldots, N\}$.

It should be noted that the choice of the form as the grid of $10 \times 10$ cells is somewhat arbitrary. All that is required is that number of cells is large enough to produce a sufficient number of nested grids. If the sampling space is not two-dimensional then we must use a grid volume, or, in the one-dimensional case, a linear grids, in order to determine our form. In general *the thorough sampling* can be characterized by two things. One of them is a form to estimate the local fractal dimension in the plot. The second characteristic is that the form is placed at all possible sites and the corresponding value for the fractal dimension is obtained.

In order to study our new data $\{\tau_1, \tau_2, \ldots, \tau_N\}$ it is necessary to understand the processes that can influence the distribution of the fractal dimension. We propose that the following possibilities exist. First, the spatial distribution can be connected with a soil fractal structure which can impart fractal properties on the concretion distribution. Alternatively, similar properties could be as result of randomness unrelated to the soil matrix. And in addition, we should consider the possibility that tight clusters of concretions will be encountered. If, for example, sizes of these clusters is roughly such as one cell and one cluster falls on 100

cells, then it is quite possible to get $\tau > 1$ (or $d_m > 2$) for several $\tau \in \{\tau_1, \tau_2, \ldots, \tau_N\}$. Although, these possibilities are unlikely to explain the processes underlying the distribution of all concretions, they may represent the main factors explaining the spatial distribution of concretions in soil.

It is proposed that there are three reasons why $d_m \neq d_e$ where $d_e$ is the embedding dimension, and they are associated with the following: (i) *fractal* or properties of the soil matrix, (ii) *random* or uniform spatial distribution unrelated to the soil, and (iii) *nested* or connected with rare clusters near points with soil which are favorable for producing concretions. To differentiate among these possibilities, we complement the experimental data with a simulation of the hypothetical distribution of slopes. In so doing concretions are distributed randomly and uniformly on the same plot with their number equal the experimental value. Comparing the numerical distribution of $\{\tau_1, \tau_2, \ldots, \tau_N\}$ with model data, we can find out that (a) there are $\tau_i \leq \tau_{fr} < 1$ which can not be explained by the random factor, and it is probable that these values relate to a fractal nature of soil matrix, (b) there are $\tau_i \geq \tau_{nest} > 1$ which are too large to be explained by the random placing in space. In the latter case there is the problem in proposing a model explaining these values. Perfect and Kay (1995) give an explanation of similar cases using multifractal model, but we propose a simpler explanation. It seems to us that there is a more natural way to explain it.

As the illustrative example, we consider the new form consisting of two grids. The grid $A[7 \times 7]$ of $7 \times 7$ cells is basic, and the second grid $A[1 \times 1]$ of $1 \times 1$ cells is laid in the centre of the first. In addition we assume the true spatial distribution of concretions is such as it is given in Fig. 2, where we show only a little part of our latticed soil plot. The letter $s$ marks cells with $s$ concretions exactly and the 1 denotes cells containing only one concretion. Although this situation is greatly simplified, however, it allows both exact calculations and

| | | | | | | | | | | |
|---|---|---|---|---|---|---|---|---|---|---|
| 1 | 1 | 1 | 1 | 1 | 1 | 1 | 1 | 1 | 1 | 1 |
| 1 | 1 | 1 | 1 | s | 1 | 1 | 1 | 1 | 1 | s |
| 1 | 1 | 1 | 1 | 1 | 1 | 1 | 1 | 1 | 1 | 1 |
| 1 | 1 | 1 | 1 | 1 | 1 | 1 | 1 | 1 | 1 | 1 |
| 1 | s | 1 | 1 | 1 | 1 | 1 | s | 1 | 1 | 1 |
| 1 | 1 | 1 | 1 | 1 | 1 | 1 | 1 | 1 | 1 | 1 |
| 1 | 1 | 1 | 1 | 1 | 1 | 1 | 1 | 1 | 1 | 1 |
| 1 | 1 | 1 | 1 | s | 1 | 1 | 1 | 1 | 1 | s |
| 1 | 1 | 1 | 1 | 1 | 1 | 1 | 1 | 1 | 1 | 1 |
| 1 | 1 | 1 | 1 | 1 | 1 | 1 | 1 | 1 | 1 | 1 |
| 1 | s | 1 | 1 | 1 | 1 | 1 | s | 1 | 1 | 1 |

Fig. 2.

Table 1
Variants of different samples for the illustrative model

| Numerical characteristics | Different variants of placing of the form | | | |
|---|---|---|---|---|
| | I | II | III | IV |
| $m(A[1\times1])$ | $s$ | 1 | 1 | 1 |
| $m(A[7\times7])$ | $4s+45$ | $4s+45$ | $3s+46$ | $2s+47$ |
| Probability | 1/18 | 1/18 | 4/18 | 12/18 |

examination of the slope distribution obtained by random placing the form within the plot.

In the example each location of the form in the plot gives us two samples. The first sample denoted $m(A[7\times7])$ is the sum of concretions over all cells of the form, and the other, $m(A[1\times1])$, is the number of particles in the centre cell. As the area of sampling is directly proportional to number of cells, we can calculate slopes transforming Eq. (2) to the following relation

$$\tau = \frac{1}{2\ln 7}\left[\ln m(A[7\times7]) - \ln m(A[1\times1])\right]. \tag{3}$$

There are four kind of locations of the form which result in different pairs $m(A[7\times7])$ and $m(A[1\times1])$. All variants and their probabilities are listed in the Table 1. Notice that the probability of the event that the number $s$ is at the centre of the form is 1/18. It follows that probability of relations $m(A[7\times7]) > 2s$ and $m(A[1\times1]) = 1$ is equal $17/18 \approx 0.9444$. And therefore we can show from Eq. (3) that

$$\mathrm{Prob}\left\{\tau > \frac{1}{2\ln 7}\ln 2s\right\} > 0.944. \tag{4}$$

The slopes corresponding to several values of $s$ are given in the Table 2 for four variants and means. The relation (4) and exact mean values from Table 2 yield $\tau > 1$ or $d_m > 2$ for $s \gg 1$. It should be noted that even if $\tau < 1$ all over

Table 2
Slopes as the function of events and $s$

| Values of $s$ | Probability of the event | | | | Values of means |
|---|---|---|---|---|---|
| | 1/18 | 1/18 | 4/18 | 12/18 | |
| 2 | 0.842 | 1.020 | 1.015 | 1.010 | 1.003 |
| 5 | 0.659 | 1.073 | 1.056 | 1.039 | 1.024 |
| 10 | 0.550 | 1.142 | 1.113 | 1.080 | 1.062 |
| 50 | 0.408 | 1.414 | 1.356 | 1.282 | 1.257 |
| 100 | 0.384 | 1.576 | 1.502 | 1.416 | 1.386 |
| 200 | 0.370 | 1.732 | 1.663 | 1.568 | 1.532 |

the entire surface of the plot, we cannot assume that the appropriate model is a fractal model. The same result holds for $\tau > 1$, i.e., both cases can be explained by many ways. So far we considered a strictly simplified illustrative example of nested model. A more general class of nested models can be constructed using Poisson low for the formation of concretion nests. This idea will be exploited to explain our experimental observation.

A value of $\tau > 1$ can also appear if the spatial density of particles is very low. Blagoveschenskiy and Freidlin (1961) proved that there exist random functions which satisfy with probability 1 the following relation

$$|f(z+\Delta) - f(z)| \alpha |\Delta|^H, \quad H > 1, z \text{ and } \Delta \text{ can be vectors,} \tag{5}$$

in contrast with fractal functions for which $H < 1$ in any Euclidian space (Mandelbrot, 1982). This possibility is not investigated in the present paper but we think that this possibility must not be ruled out.

Thus our sampling strategy comprises the following. Firstly, using the method of thorough sampling we obtain the statistical collection $\{\tau_1, \tau_2, \ldots, \tau_N\}$ which gives us the basic information about the spatial distribution of concretions. Secondly, believing that the spatial variability of concretions reflects a complex structure in the properties of soddy-podsolic soil and in the associated physical and chemical processes, we suppose that the concretion distribution is a mixture. Namely, we consider at least three sources and take the distribution unrelated to the soil structure as a base for our statistical analysis of $\{\tau_1, \tau_2, \ldots, \tau_N\}$. Furthermore, we simulate the basic distribution using the experimental number of concretions and experimental scales of our latticed plot. Then we investigate what values out of $\{\tau_1, \tau_2, \ldots, \tau_N\}$ in ranges $\tau < 1$ and $\tau > 1$ can be excluded.

## 3. Methodology

Experimental data were collected at two sites situated 40 km to the north and to the west of Moscow. Both places were under forest comprising the species *Carex pilosa* on soddy-podsolic soil. Two data sets were collected at the first site and one on the second.

In the first experiment the data set (referred to as the pattern data) was obtained from 6 location, 10 m apart, along the transect shown in Fig. 3, and samples were collected from two depths: the middle of $A_2$ horizon (18 cm) and the beginning of the $A_2B$ horizon (28 cm). The thickness of samples was 1 cm. Concretions were extracted by wet sieving using 1 mm sieve. After soil sieving, concretions themselves were sieved to separate by size fraction 1–2 mm, 2–3 mm and $> 3$ mm, and the number in each size fraction was counted.

The second experiment had data set (referred to as the plot data) that concerned the spatial organization of concretions on a meso-level. They was

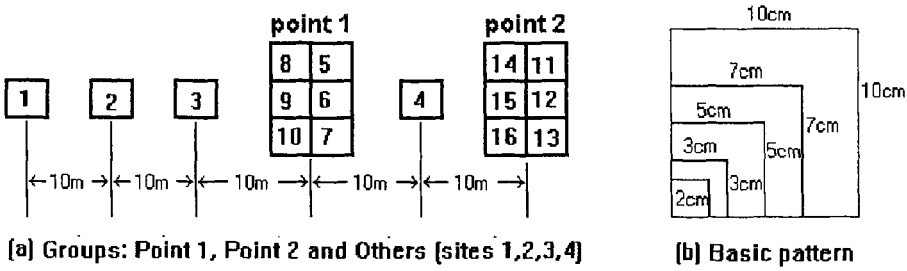


Fig. 3.

collected from consecutive layers (1 m × 0.5 m) 2 cm thick within the soil layer of maximum concretion density as shown in Fig. 4a. The morphology of genetic horizons on the all layers was first drawn to 1:5 scale using Dmitriev's pantograf (Karpachevskiy et al., 1980). The concretions were then stained by applying a 10% solution of potassium iodide and soluble starch. This solution produces dark zones around the concretions arising from the oxidation of $I^{-1}$ by $Fe^{3+}$. Concretions larger than 0.5 mm in diameter and not further than 1 mm from the soil surface could be visualized, and were drawn using the pantograf. After this process was repeated in each layer, the pictures were divided into cells of size 2.5 cm × 2.5 cm and the number of concretions in every cell was counted.

In the third experiment, the spatial variability of concretions along some trench with length 2.5 m was studied. Data (referred to as the box data) was obtained from the analysis of a series of parallel cores of two volumes (10 $cm^3$ and 50 $cm^3$) from two depths 10 and 20 cm in the middle of $A_1A_2$ and $A_2$, respectively, as shown in Fig. 4b. The cores have the same cross section 5 cm × 5 cm and different length (0.4 and 2 cm, respectively). The distance between two series of samples was 0.4 cm. Counting of concretions was as for the pattern data.

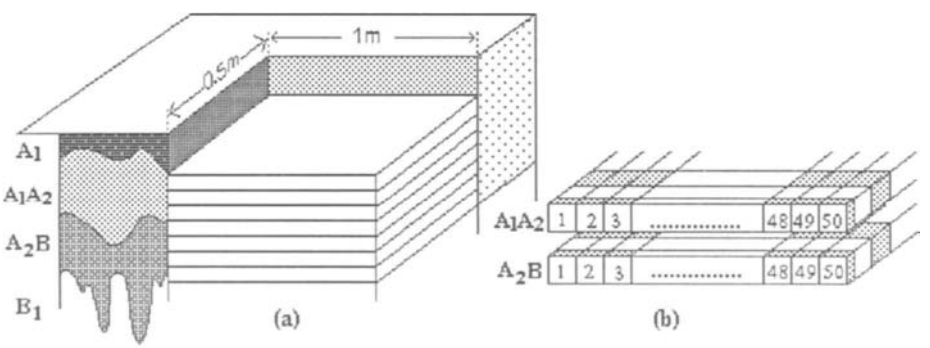


Fig. 4.

## 4. Results

### *4.1. Pattern data*

The method of enclosed samples (cores) for estimating the fractal dimension is well known (Bundle and Havlin, 1994). The pattern data from the first experiment is collected in a manner consistent with the method. In total, there are 16 sites for placing the form, and these sites have been divided into three groups: point 1, point 2 and third group named others (Fig. 3). Each placing of the form had in total six variants of data corresponded to two depths and three sizes of concretions. Some variants were not appropriate for reliable estimation and they were excluded from analysis.

In order to estimate $\tau$ we used a simplified from of Eq. (2). If $y_1$, $y_2$, $y_3$, $y_4$, $y_5$ are ln $m(A[B \times B])$ with $m(A[B \times B]) > 0$ and $B = 2, 3, 5, 7, 10$ accordingly, then we can find $\tau$ as the linear function of them, namely,

$$\tau = -0.2516\,y_1 - 0.1297\,y_2 + 0.0239\,y_3 + 0.1251\,y_4 + 0.2323\,y_5. \qquad (6)$$

Eq. (6) can be easily derived from Eq. (2) since $s(A[B \times B]) = k_a \cdot B^2$ where $k_a$ is the constant of scale. Notice that $\tau$ is independent of $k_a$. Values of $\tau$ for different variants are listed in the Table 3. In addition slopes were calculated for groups and their values are given in the Table 4.

To analyze these data, we used simulated data which was produced in the following way. Firstly we suppose that the simplest spatial distribution of concretions is not related to features of the soil matrix and that number of concretions which are in a random cell in the form can be considered to be a random variable with the probability distribution obtained in experiment. We simulated this simplified situation 500 times and determined the hypothetical

Table 3
Slopes for all different placing of the form

| Number of site | Size and depth | | | | Number of site | Size and depth | | | |
|---|---|---|---|---|---|---|---|---|---|
| | 1–2; 1st | > 2; 1st | > 1; 1st | > 1; 2nd | | 1–2; 1st | > 2; 1st | > 1; 1st | > 1; 2nd |
| 1 | – | – | 1.069 | 1.196 | 9 | 0.970 | – | 0.983 | 1.033 |
| 2 | – | – | *0.773* | 0.974 | 10 | 1.142 | – | 1.142 | 1.016 |
| 3 | – | – | 1.160 | 1.112 | 11 | 0.973 | 1.154 | 0.981 | *1.530* |
| 4 | – | – | 0.994 | *0.701* | 12 | 1.029 | *1.382* | 1.048 | *2.067* |
| 5 | 1.027 | – | 1.020 | 0.959 | 13 | 1.011 | 0.980 | 1.015 | 0.962 |
| 6 | 1.023 | – | 1.001 | 0.855 | 14 | 1.044 | *1.265* | 1.052 | 1.020 |
| 7 | 1.027 | – | 1.012 | *0.786* | 15 | *0.678* | *1.402* | *0.699* | *1.461* |
| 8 | 0.974 | – | 0.979 | 1.156 | 16 | 0.961 | *1.339* | 0.982 | 1.115 |

Table 4
Slopes into groups for the pattern data

| Sizes of fractions | Depth of samples (cm) | Groups of sites for the form | | |
|---|---|---|---|---|
| | | Point 1 | Point 2 | Others |
| > 1 mm | 18–20 | 1.015 (0.028) | 0.961 (0.044) | 1.014 (0.06) |
| > 1 mm | 28–30 | 0.950 (0.06) | 0.1364 (0.11) | 0.998 (010) |
| > 2 mm | 18–20 | 0.938 (0.07) | 1.2520 (0.09) | – |
| 1 mm < ... < 2 mm | 18–20 | 1.021 (0.02) | 0.9531 (0.04) | – |

Values into brackets are standard errors.

distribution of slopes for it. As one would expect from general theoretical considerations, this distribution is well approximated by the Gaussian with mean 1 and standard deviation $\sigma \approx 0.09$ so that

$$\Pr\{|\tau_{\text{hyp}} - 1| > 0.2\} \leq 0.04, \tag{7}$$

and inequalities $\tau_{\text{hyp}} < 0.8$ and $\tau_{\text{hyp}} > 1.2$ have the same probability about 0.02.

If we will look more closely at Table 3 then it can be seen that values $\tau < 0.8$ and $\tau > 1.2$ are more frequent in experimental data than in Gaussian case. More precisely we will find that

| Intervals | $\tau < 0.8$ | $\tau > 1.2$ |
|---|---|---|
| Gaussian frequency | 0.02 | 0.02 |
| Experimental frequency | 0.10 | 0.14 |

These biases are inconsistent with the hypothesis that the concretions are randomly placed. Hence there exist some parts of our soil area which share fractal features with the soil matrix. There are also parts associated with nested sets of concretions, and these are located at point 2 (see Fig. 3) where the values of $\tau$ exceed 1.2.

### *4.2. Plot data*

Data of the second experiment were collected for eight plots which were layered on top of each other (see Fig. 4a). Values of $\tau$ for each plot are estimated according to the regression Eq. (2) using the thorough sampling method described above. Each plot was divided into $20 \times 40$ square cells with the linear size 2.5 cm. Bounding cells were excluded from our consideration, and the form was placed in 261 ($N = (n - 9)(r - 9)$ with $n = 38$ and $r = 18$) positions. This resulted 261 values of $T(p) = \tau_1, \ldots, \tau_{261}$ where $\tau_i$ is the slope calculated for $j$th locating of the form and $p$ is the index of the plot if we numerate them from the top down. Note that these slopes are highly correlated because some forms may overlap by as much as 90%. It is clear that in these circumstances, the usual statistical analysis is not suitable. Therefore we adopt the following methodology.

The actual number of concretions within our plots varies from 459 to 1103 (Table 5) and numbers 500, 750 and 1100 can be adopted as the basis for the models of the distributions. The purpose of the modeling exercise is to understand what part of $T(p)$ can be explained by purely random distribution of concretions. For example, if we randomly distribute 500 concretions in a plot, we can calculate slopes $\tau'_1, \tau'_2, \ldots, \tau'_{261}$. This data can be used to calculate 49 quantiles for $\lambda = 0.02, 0.04, \ldots, 0.96, 0.98$, where $\lambda$-quantile is defined to be that value of $\tau(\lambda)$ for which the inequality $\tau'_k \leq \tau(\lambda)$ is satisfied for a fraction $\lambda$ of the 261 slopes. The means of these quantiles was calculated from 50 model runs. At the end of the procedure we have a good estimation of the model slope distribution and we can compare it with the observed distribution of slopes correlating their $\lambda$-quantiles.

The results of the comparison are shown using the observed and modeled data comprising total numbers of concretions $N = 503$, 736 and 1103 and $N = 500$, 750 and 1100, respectively. The results are displayed in Fig. 5. In the region $x_1 \leq 1$, discrepancies between model and real data are relatively small (right-hand graphs) but the gradients of the curves corresponding to real data are clearly steeper. The three left-hand graphs show that the shape of the curves for the real data are similar in shape. The fact, together with the departure between modeled and observed slope distributions indicates that high values $\tau$ can not be considered to arise as a consequence of randomness or other experimental artifacts. It is more likely to be a consequence of the presence of rare but dense clusters of concretions.

This similar situation frequently arises in studies of spatial distributions of living organisms across some area. The double Poisson distribution was found to be applicable (Vasilevich, 1969) to describe the number of spatial cells containing a given number of single plat species. Using this the double Poisson distribution, we estimated the numbers of cells containing 0, 1, 2, 3 and $> 3$ concretions. Results are shown in Table 6. There is very good agreement between theoretical and observed frequencies for cells containing no concretions. However, predictions for cells with 1 or 2 concretions are generally higher than the observed values, and for cells with $> 2$ concretions, i.e., there are nests, the experimental frequencies are higher than theoretical ones.

Table 5
Statistics for plot data

| General statistics | Plot number | | | | | | | |
|---|---|---|---|---|---|---|---|---|
| | 1 | 2 | 3 | 4 | 5 | 6 | 7 | 8 |
| Number of concretions | 459 | 829 | 1002 | 1103 | 632 | 736 | 1056 | 503 |
| (a) Averages | 0.671 | 1.212 | 1.465 | 1.613 | 0.924 | 1.076 | 1.544 | 0.735 |
| (b) Standard deviation | 0.963 | 1.312 | 1.387 | 1.433 | 1.123 | 1.245 | 1.564 | 1.127 |
| (c) Ratio = (b)/(a) | 1.435 | 1.083 | 0.947 | 0.889 | 1.216 | 1.157 | 1.013 | 1.532 |

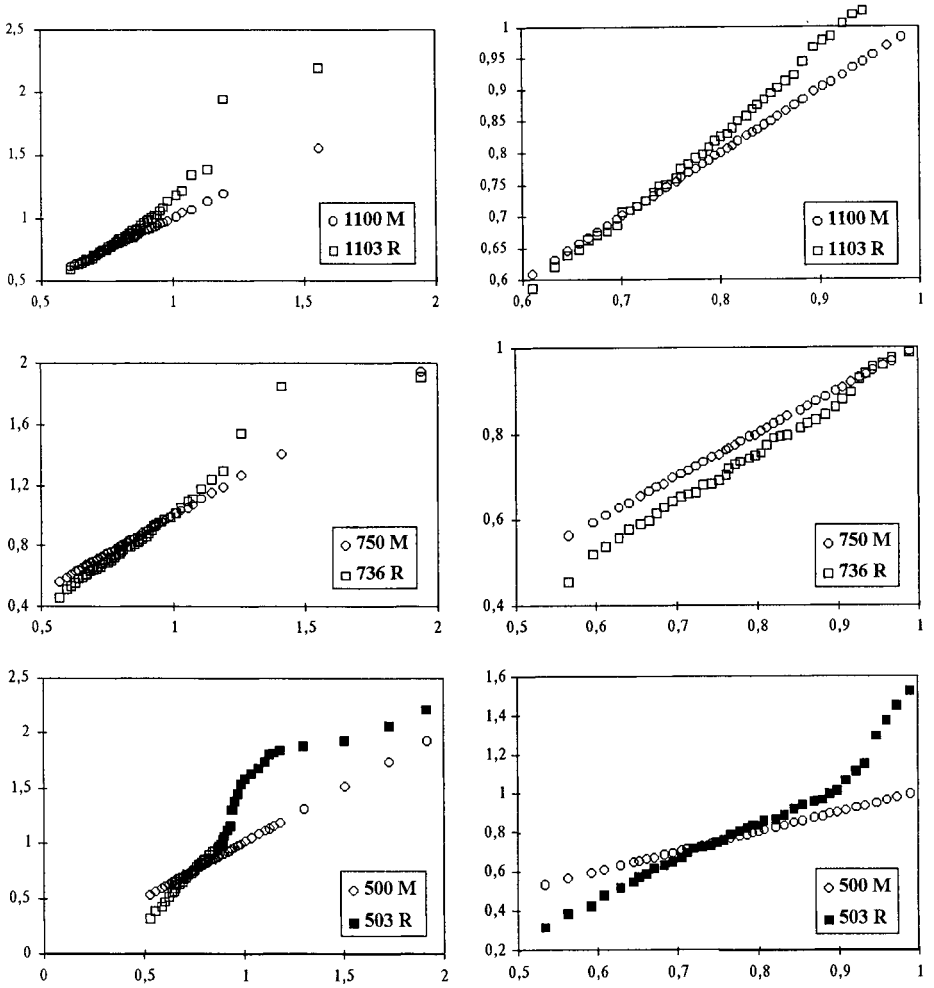


Fig. 5.

### *4.3. Box data*

In contrast with the above, this experiment consists two core sizes which were collected in pairs from each location along two parallel linear transects. Since cores in pairs differ only in length, the embedded dimension is equal to 1. Indeed, the ratio between volumes of cores is the ratio of lengths and we can take volumes in the place of lengths in Eq. (1) to get getting the same estimate of the fractal dimension. Because of that we calculated a separate estimation as slope $\tau$ by the formula

$$\tau = \frac{1}{\ln 5}\left[\ln m(A_2) - \ln m(A_2)\right] \tag{8}$$

Table 6
Distribution of cells with the different content of concretions

| Number of plots | Number of concretions within one cell | | | | | | | | | |
|---|---|---|---|---|---|---|---|---|---|---|
| | 0 | | 1 | | 2 | | 3 | | > 3 | |
| | Model | Real | Model | Real | Model | Real | Model | Real | Model | Real |
| 1 | 396.6 | 401 | 175.9 | 163 | 75.0 | 79 | 26.6 | 29 | 11.9 | 12 |
| 2 | 254.5 | 255 | 201.9 | 192 | 123.0 | 140 | 61.3 | 58 | 43.2 | 39 |
| 3 | 195.7 | 220 | 208.5 | 177 | 143.7 | 120 | 77.7 | 108 | 58.3 | 59 |
| 4 | 166.9 | 185 | 208.5 | 173 | 155.1 | 161 | 87.2 | 104 | 66.3 | 61 |
| 5 | 318.7 | 328 | 200.4 | 182 | 100.8 | 106 | 41.7 | 46 | 22.4 | 22 |
| 6 | 282.1 | 305 | 200.7 | 157 | 113.9 | 123 | 53.1 | 66 | 34.2 | 33 |
| 7 | 212.7 | 226 | 180.4 | 155 | 131.5 | 142 | 79.4 | 76 | 80.0 | 85 |
| 8 | 398.7 | 393 | 152.1 | 159 | 79.1 | 78 | 33.8 | 41 | 24.4 | 13 |

where $m(A_1)$ and $m(A_2)$ are numbers of concretions for lesser and greater cores, respectively. Note that the value of $\tau$ from Eq. (8) is both the slope and the estimate of $d_m$ in contrast with Eq. (6) where $d_m = 2\tau$.

Let $\tau_1, \tau_2, \ldots, \tau_{50}$ be successive values of slopes along the sampling line from one of two depths. They can be considered the trajectory function of $j = 1$,

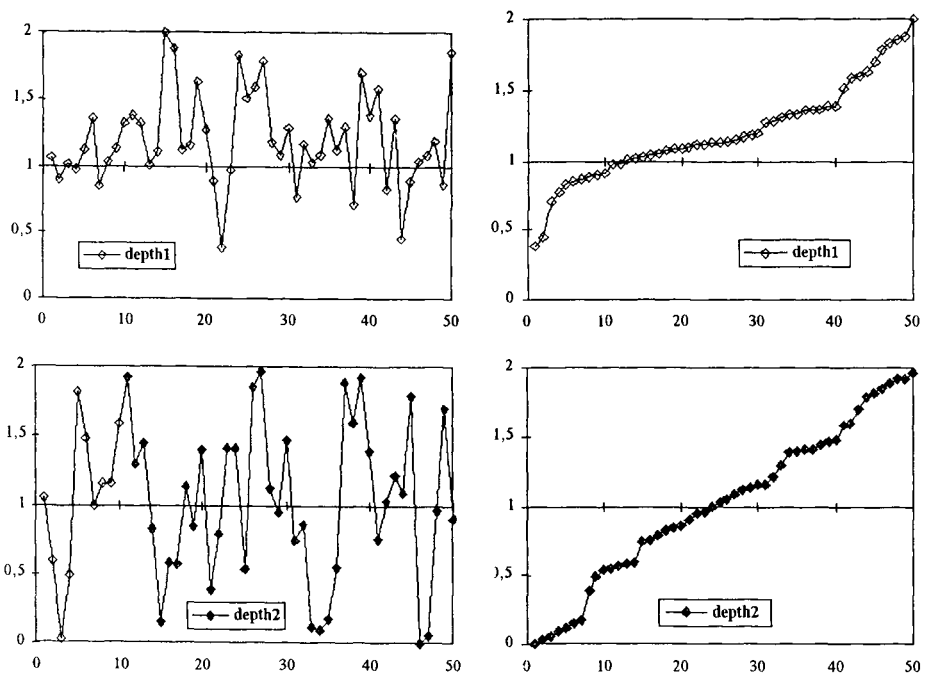


Fig. 6.

2, ..., 50 and as the slope distribution. Both variants are represented by graphs in Fig. 6 for each of two depths. It is easy to see that the mean value of slope at the first depth is significantly greater than 1 while at the second depth it does not markedly deviate from 1.

Since the slopes are measured using only two cores, the results are prone to error. In order to get the more reliable conclusions, we calculated moving averages defined as

$$\tau_i(k) = \frac{1}{2k+1} \sum_{j=i-k}^{i+k} \tau_j, \quad i = k+1, \ldots, 50-k, \tag{9}$$

Trajectory functions $\tau_i(k)$, $i = k+1, \ldots, 50\text{-}k$, for these two values $k$ and for two depths are shown in Fig. 7, on the left hand $k = 3$. The contrast between the different depths is clearly visible. At the first depth almost all values are greater than 1, especially for $k = 7$ whereas at the second depth we quasi-periodic fluctuations are observed, and the distributions of concretions in at least one segment of trench may be considered as having a fractal nature.

Unfortunately, it is not possible to evaluate the reliability of this conclusion using the present data, but in this circumstances computer modeling of the purely random distribution of concretions shows that the hypothesis may be rejected with a probability greater than 0.0995 at both depths.

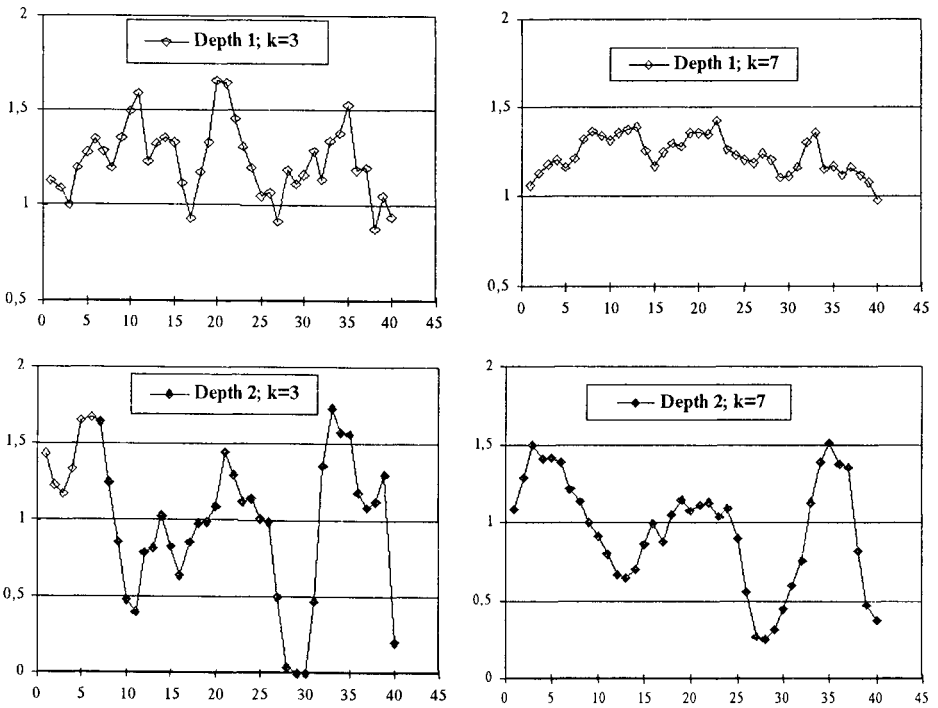


Fig. 7.

## 5. Discussion

Many natural objects may have fractal properties, but are not characterized by any single fractal model. In other words to exploit one or other model we must account for what alternative descriptions there may be.

If the concretion locations can be modeled using fractals rather than some purely random functions, this suggests the existence of a formation mechanism leading to large-scale correlations in their spatial distribution. It is known that the formation of Fe and Mn concretions depends on a combination of factors including a role for microorganism-mediated processes (Aristovskaja, 1965). These factors include (i) the presence of sufficient amount of soluble Fe and Mn compounds, (ii) pore-space restrictions which constrain the solute flow below a critical rate, (iii) alternating redox potential which leads to cycles of dissolution and sedimentation of Fe–Mn oxides, (iv) available organic matter as a substrate for microbial activity. Each of these factors varies from point to point in the soil, and only the locations where they co-exist are suitable for the formation of concretions. In constructing a model for the formation of concretions, we suggest that there are three groups of concretions that spread over the studied area $S$ according to a different mechanism.

The first group represents the background. Every concretion from this group is placed independently and uniformly over area $S$. These background concretions represent the portion of all which may be explained by random coincidence in space of favorable conditions for their formation.

The distribution of the second group can be modeled as a fractal. Let there be $r$ spots $F_1, \ldots, F_r$, with simple boundaries and areas $a(F_1), \ldots, a(F_r)$. Assume that every spot $F_j$, $j = 1, \ldots, r$, contains geometrical fractal $F_j^o$ with the dimension $1 < d_j < 2$. Every concretion from the group of fractals is distributed over set $F^o = U_{j=1}^r F_j^o$ in the following way:

1. first the spot index is chosen with probabilities $p_j = \{[a(F_j)]/[a(F_1) + K + a(F_r)]\}$, $j = 1, \ldots, r$;
2. if $j$th spot is chosen then point $\xi$ is chosen randomly in $F_j$;
3. if $\xi \in F_j^o$ then the concretion is placed in this point;
4. if $\xi \notin F_j^o$ then Brownian particle starts from the point $\xi$ and continues its walk inside $F_j$ until it reaches $F_j^o$ at which point a concretion is placed.

It is likely that fractal concretions have inherited their structure from the fractal geometry of the soil at the locations where this geometry is rather stable.

The third group is nested because its concretions are hierarchically distributed and clustered. According to Poisson law with the parameter $\lambda \geq 5$ we will take a fixed size sample of integers $n_i$, $i = 1, \ldots, k$. Then concretions are distributed among $k$ sites with $n_i$, $i = 1, \ldots, k$, at each site. The points in $S$ are chosen by the following way. For every point $z \in S$, its distance to $F^o$, that is to the set contained all fractals $F_j^o$, may be formally determined. Let the distance be $\delta(z)$ and $\Delta$ be maximum of $\delta(z)$ for all $z \in S$. For every $q \in [0; \Delta]$ we can formally

determine the set $F^q$, of points having distance $q$ from $F^0$. If $i \in \{1, 2, \ldots, k\}$ is given then $q$ is chosen according to the distribution function which is determined phenomenologically as $G(q) = (q/\Delta)^2$ and a point $z_i \in F^q$ is chosen randomly and with equal probability, and $n_i$ concretions are located there. The cluster at each $z_i$ is independent from others. The nests of concretions represent places with favourable and stable conditions for the growth.

## 6. Conclusion

The spatial distribution of Fe–Mn concretions is heterogeneous over distance of 1–3 m and it may be considered as a mixture of at least three components. One of the components is the background and may be described by the model of the random distribution function with exponentially decreasing spatial correlation. Another component is fractal. We can describe it only qualitatively, i.e., there are some locations that are consistent with a fractal hypothesis (spatial correlation decreasing as a power law) associated with a particular fractal dimension. We can estimate the probability of meeting these locations for a concrete scale of sampling. Finally, the third component is nested component. We propose a very simplified model for this component, and use it to provide some support for hypothesis that the origins of some concretions may have a biological nature.

## Acknowledgements

We thank Professors E. Dmitriev and V. Buchshtaber from Moscow State University for the fruitful discussion of this work. We thank Dr. J. Crawford and Dr. D. Gimenez for their comments and suggestions for the improvement of the manuscript. We also are very much obliged to Zheveleva Helen for some part of experimental data.

## References

Anderson, A.N., McBratney, A.B., 1995. Soil aggregates as mass fractals. Aust. J. Soil Res. 35, 757–772.

Aristovskaja, T.V., 1965. Microbiology of Podsolic Soils. Nauka, Moscow (in Russian).

Blagoveschenskiy, Yu.N., Freidlin, M.I., 1961. Some properties of diffusion processes dependent from the parameters. DAN USSR 138, 170–172, (in Russian).

Bundle and Havlin, 1994.

Karpachevskiy, L.O., Voronin, A.D., Dmirtiev, E.A., Stroganova, M.N., Choba, C.A., 1980. Soil and Biogeocenological Experiments in Forest Biogeocenoses. Moscow Univ. Press, Moscow (in Russian).

Kozlovskii, F.I., Sorokina, N.P., 1976. The soil individual and elementary analysis of soil cover pattern. In: Fridland, V.M. (Ed.), Soil Combinations and Their Genesis. Amerind, New Delhi, pp. 55–64.

Mandelbrot, B.B., 1982. The Fractal Geometry of Nature. W.H. Freeman, London.

Perfect, E., Kay, B.D., 1995. Application of fractals in soil and tillage research: a review. Soil and Tillage Research 36, 1–20.

Perfect, E., Kay, B.D., Rasiah, 1993. Multifractal model for soil aggregate fragmentation. Soil Sci. Soc. Am. J. 57, 896–900.

Rieu, M., Sposito, G., 1991. Fractal fragmentation, soil porosity and soil water properties: I. Theory, II. Application. Soil Sci. Soc. Am. J. 55, 1231–1238; 1239–1244.

Rozanov, B.G., 1983. Soil Morphology. Moscow Univ. Press, Moscow (in Russian).

Vasilevich, V.I., 1969. Statistical Methods in Geobotanics. Nauka, Leningrad (in Russian).

Wu, Q., Borkovec, M., Sticher, 1993. On particle-size distribution in soils. Soil Sci. Soc. Am. J. 57, 883–890.

Zaidelman, F.R., 1974. Neubildungen hydrorfer Mineralboden der UdSSR, ihre Klassifcation and diagnostische Bedeutung. Geoderma 12, 121–135.

Zaidelman, F.R., Nikiforova, A.S., 1997. On some general regularities of the formation and changes in properties of Mn–Fe concretions in soils of humid landscapes. Archives of Agronomy and Soil Sci. 41 (5), 367–382.

*Fractals in Soil Science*
Editors: Ya.A. Pachepsky, J.W. Crawford and W.J. Rawls
© 2000 Elsevier Science B.V. All rights reserved.


# Fractal concepts in studies of soil fauna

Christian Kampichler *

*GSF-National Research Centre for Environment and Health, Institute of Soil Ecology, D-85764 Neuherberg, Germany*

Received 4 November 1997; accepted 28 September 1998

**Abstract**

Despite the fact that their objects of study live in a highly complex and irregular environment, soil zoologists have not yet made use of the advantage of fractal geometry in their work. Less than 1% of papers published during the last 3 years that dealt with fractal applications in the field of biological and environmental sciences were directed at studies of soil fauna. This paper tries to initiate a more intensive use of fractals in soil zoology and outlines their potential for different aspects of research. It reviews a fractal approach to describe soil nematode movement patterns in an artificial two-dimensional soil matrix and presents original work on the impact of habitat complexity on the abundance:body size distribution of soil microarthropods and on the potential of detecting scaling regions of microarthropod aggregations by identifying scale-dependent changes of a fractal exponent. © 1999 Elsevier Science B.V. All rights reserved.

*Keywords:* soil fauna; fractals; animal movement; habitat complexity; abundance:body-size distribution; scaling regions

## 1. Introduction

A number of years ago Frontier (1987) and Sugihara and May (1990) outlined the potential of fractal concepts to address some important issues of ecological research. Their list of possible applications included (1) the measurement of available habitat space—e.g., surface availability for invertebrates on plants (Lawton, 1986); (2) the detection of functional hierarchies—e.g., identification of hierarchical size scales by determining different apparent dimensions of forest patches at different scales of observation (Krummel et al., 1987); (3) the analysis of shape and spatial distribution of organisms—e.g., structure of root

* Present address: Institute of Zoology, Free University Berlin, D-12165 Berlin, Germany. Fax: +49-30-8383886; E-mail: kampichl@dezedat.fu-berlin.

Reprinted from Geoderma 88 (1999)
© 1999 Elsevier Science B.V. All rights reserved

systems (Tatsumi et al., 1989) or the structure of plankton swarms (Frontier, 1987); (4) the analysis of animal movement (Dicke and Burrough, 1988); (5) the analysis of time series—e.g., the estimation of the persistence of rare species (Hastings and Sugihara, 1993); and (6) the use of fractals in an abstract representational space—e.g., strange attractors in the dynamics of ecological systems or characterisation of species diversity as a fractal feature of a community (Frontier, 1987).

Frontier (1987) and Sugihara and May (1990) acknowledged fractal geometry as a particularly attractive approach to address problems of scale and hierarchy and expected it to become of fundamental interest for the analysis and modeling of ecosystems. However, their suggestions seem to have had little impact on the study of soil fauna.

A survey of recent literature published between May 1994 and August 1997 reveals a striking dearth of fractal concepts in soil zoological research. Of the 230 articles that include fractal concepts (listed by Current Contents/Agriculture, Biology and Environmental Sciences®) 27.0% (62 articles) explicitly deal with soil research. The majority of these are soil physical papers and describe or model water and solute transport through soil, soil aggregation and related topics. Eleven articles (4.8%) focus on the analysis of root systems and eight articles (3.5%) focus on the analysis of soil microbial growth patterns. Only 0.9% (two articles) refer to soil animals which corresponds to less than 0.5% of all soil zoological papers listed by Current Contents/Agriculture, Biology and Environmental Sciences® in the same time period. These two articles are an analysis of free-living soil nematode movement in an artificial experimental arena (Anderson et al., 1997) and a description of the body-size distribution of microarthropods and its possible relationship to available habitat space in soil (Kampichler, 1995). Also the review by Senesi (1996) on the use of fractals in soil biology and biochemistry reports a rich literature on the fractal nature of humic substances, proteins, enzymes and patterns in microbial morphology but only two articles refer to soil animals (Crawford et al., 1993; Kampichler and Hauser, 1993).

It is unclear whether the lack of fractal applications in studies of soil fauna is caused by ignorance or rejection of the theoretical approach or whether it is a consequence of the methodological difficulties in studying subterranean organisms. Direct observation is generally not possible and destructive sampling is often required (e.g., extraction of soil cores). In this paper I will try to point out that despite these obvious methodological difficulties it actually is possible to apply fractal concepts to various soil zoological questions. I will highlight selected applications: (1) the analysis of animal movement within a pore network referring to the work by Anderson et al. (1997), (2) the analysis of available habitat space for microarthropods of different size following Kampichler and Hauser (1993) and Kampichler (1995) as well as presenting original results, and (3) the identification of ecological hierarchies in aggregations of

Collembola (original data). In each of these sections, I will outline the underlying principle of the application in a short introduction. Finally I will give a few suggestions for further possibilities of fractal applications in studies of soil fauna. All methodological terminology refers to Hastings and Sugihara (1993).

## 2. Analysis of soil animal movement

### *2.1. Outline of principle*

Frontier (1987) and Dicke and Burrough (1988) were the first to suggest the description of animal movement trajectories by means of fractal geometry. Dicke and Burrough (1988) argue that the tortuosity of an animal trail may be characterised by its fractal dimension $D$. The fractal dimension of a trail (or any other curve) usually is determined by the dividers method (cf. Hastings and Sugihara, 1993). This method involves stepping along the trail with a pair of dividers of distance $\delta$ (or with a ruler of length $\delta$). The apparent length $L$ of the trail is the number $N$ of straight-line segments that can be fitted to the trail multiplied by the measurement scale $\delta$ (the length of a single segment). By decreasing $\delta$ the irregularities of the trail can be traced closer and closer, thus the length of the trail will increase with measurement on finer scales. Lenght $L$ depends on measurement scale $\delta$ according to the simple power law

$$L(\delta) \propto \delta^{1-D} \tag{1}$$

$D$ can easily be determined by measuring $L$ at different $\delta$ and calculating a linear regression of log $L(\delta)$ on log $\delta$. $D$ is derived as 1 − slope-value of the regression line. Smooth trails have a $D$ close to 1 with $D = 1$ for a straight line —i.e., the slope-value is 0, apparent lenght is independent of measurement scale —, tortuous trails have larger $D$ with $D$ approaching 2 in the theoretical case of the trail filling the plane completely.

The suggestions of Frontier (1987) and Dicke and Burrough (1988) have been followed by a number of ecologists analysing trajectories of terrestrial arthropods (e.g., Fourcassié et al., 1992; Johnson et al., 1992; Wiens et al., 1995).

A highly magnified portion of a mathematical fractal line—e.g., of the Koch curve (Mandelbrot, 1982)—resembles the line itself, and successive magnifications always show the same structure. This property is called self-similarity (Mandelbrot, 1982). Natural objects, however, usually exhibit self-similarity only within a certain range of scales. For example, a theoretical tree branches ad infinitum, whereas the finest ramifications of a natural tree do not ramify any more, but they bear leaves, and on the other end of the scale, a natural tree does not belong to a larger one, but to a forest (Frontier, 1987). Also animal trails cannot be expected to be self-similar over all spatial scales—i.e., there is no uniform linear relationship between log $L(\delta)$ and log $\delta$ across all values of

δ—and their fractal dimension often may not be constant over some biologically relevant range of spatial scales. Such self-similarity, however, is required if one wants to extrapolate mechanisms from a small to a large spatial scale. This gave rise to criticism on an inappropriate use of the fractal approach: in various articles the fractal dimension of an animal movement trajectory is assumed to be scale-independent without testing this assumption prior to the use of a fractal model (Turchin, 1996). On the other hand, this led to the development of more sophisticated estimators that determine fractal dimension at different spatial scales, give a measure of variance and are able to combine data from separate trail segments measured at various spatial scales (Nams, 1996).

### *2.2. Application: movement of soil nematodes in an artificial heterogeneous environment*

Anderson et al. (1997) were the first to analyse the movement of endogenic animals, namely of free-living soil nematodes, and quantified the interaction between nematode movement along a chemical gradient and a structurally heterogeneous environment. They used 9 cm Petri dishes with a homogeneous layer of nutrient agar as experimental units and applied four different treatments: units with or without a bacterial food-source (*Escherichia coli*, placed left of centre), and units with or without structural heterogeneity established by adding a monolayer of sand grains to the agar surface. Pore space between the grains amounted to approximately 40%. Twenty replicate Petri dishes were used for each treatment. A single specimen of *Caenorhabditis elegans* was placed right of centre of each Petri dish. Their trails were videotaped and the fractal dimension of the movement pathways measured by the dividers method (cf. Hastings and Sugihara, 1993).

The nematode trails from units without structural heterogeneity and without a bacterial food source acting as attractant had the greatest fractal dimension ($D = 1.22 \pm 0.02$ standard error). Movement pathways in these environments were more tortuous, consisting of loops and spirals and were significantly ($p \leq 0.01$) more space filling than the trails in units with bacteria ($D = 1.08 \pm 0.03$ standard error), in units with heterogeneity ($D = 1.08 \pm 0.02$ standard error), and in units with both bacteria and heterogeneity ($D = 1.08 \pm 0.01$ standard error). The presence of a bacterial food source led to a more linear movement, directed towards the bacterial source, most probably due to the influence of a chemical gradient. Also, movement between sand grains led to more linear trajectories even without an attractant being present.

Anderson et al. (1997) also measured the turning-angle distribution of the nematode trails. In the environment without heterogeneity, small changes in direction tended to occur more often than in the environment with heterogeneity. The restrictive pore network minimizes the looping behaviour—pathways with many small changes in angles—and the nematodes follow a trail which is

dictated by the physical structure of the environment. If a blocked pore is encountered, nematodes react with a rapid withdrawal followed by a large change in direction. Anderson et al. (1997) assume that this strategy in a physically structured environment aids the nematodes in escaping structural traps, such as 'dead-end' pores, and then reacting to the attractant gradient again.

As Wiens et al. (1995) point out, different combinations of ecological and behavioural features may produce trails with identical fractal dimensions. Thus, they suggest the use of fractal concepts in concert with other scale-dependent measures. The study of Anderson et al. (1997) reiterates this suggestion; although carried out in only a two-dimensional medium, this experiment illustrates the potential of including fractal concepts in the analysis of faunal interactions with the physical framework of soil.

## 3. Analysis of available habitat space for soil animals

### *3.1. Outline of principle*

Animals live in complexly structured habitats, be it a three-dimensional structure like a tree canopy, a two-dimensional one like a soil surface or a one-dimensional one like a coast-line. Fractal geometry provides a valuable tool for the description of shape and form of natural objects.

The idea of characterising a habitat's complexity by its fractal dimension has mainly been taken up by researchers investigating relationships between plant architecture and its animal community including insects and spiders on vascular plants (Morse et al., 1985; Lawton, 1986; Gunnarsson, 1992), microarthropods on lichens (Shorrocks et al., 1991) and the epifauna on marine macroalgae (Gee and Warwick, 1994a; Davenport et al., 1996). These studies have shown that the greater abundance of small animals can be associated with a greater plant complexity. This is due to the fact that animals of different size perceive their habitat at a different resolution; that is, animals of different size act as 'pair of dividers' or as 'rulers' at different scales $\delta$ (cf. Section 2.1) and according to Eq. (1), habitable space in a fractal habitat is larger for smaller animals than for larger ones. The greater $D$ is, the larger the habitat becomes for a small animal and thus the larger should be density of small animals. Some authors also try to relate species diversity to the fractal geometry of the habitat (e.g., Gee and Warwick, 1994b). The majority of ecologists that apply fractal concepts accept this presumed relationship between the fractal scaling of the habitat and species richness. Fenchel (1993) on the other hand argues that if nature actually shows self-similarity at all scales, the environment should in fact 'appear equally complex to a monkey in a forest, to a tardigrade in a moss cushion or to a protozoan in a bacterial mat, and so there should be equally many habitat niches

available irrespective of body size'. Whether it is habitat space or habitat diversity that most affect species richness at different spatial scales is still under debate. The relationship between the habitat fractal geometry and species number, however, must not be confounded with the much more straight-forward relationship between the habitat fractal geometry and the number of individuals of different size. This section will only deal with the frequency distribution of individuals of different size.

Few attempts have been undertaken to quantify complexity of soil pore surfaces at a scale relevant for soil microarthropods. Since these animals are incapable of digging and thus confined to the surfaces of soil crevices, fractal geometry should permit the measurement of the surface area that is available for them.

### *3.2. Application: habitat space for soil microarthropods in a spruce forest soil*

By applying the area-perimeter exponent—the area and the perimeter of two-dimensional patches are related by $P \propto A^{D/2}$ with $D$ being the fractal dimension of the patch boundary line (cf. Hastings and Sugihara, 1993)—to thin-sections of three different soils, Kampichler and Hauser (1993) estimated the surface dimension $D$ of pores with a sectional area of at least 0.003 mm$^2$ to range between 2.26 and 2.39. Kampichler (1995) found a similar surface dimension with values between 2.33 and 2.38 and the average at 2.36 by measuring outlines of hollow spaces in the humus layer of a spruce forest with the dividers method (cf. Hastings and Sugihara, 1993). Inserting $D = 1.36$—intersections with a plane of dimension $D_{\text{areal}}$ have the dimension $D_{\text{linear}} = D_{\text{areal}} - 1$ (Mandelbrot, 1982)—into Eq. (1) gives

$$L \propto \delta^{1-1.36} \tag{2}$$

For example, halving the scale of linear measurement $\delta$ leads to a $0.5^{-0.36} = 1.28$-fold increase in linear distance. According to Morse et al. (1985), squaring the increase in linear distance gives an estimate for the increase in surface area. Therefore, the respective increase in surface area is $(0.5^{-0.36})^2 = 1.65$. If the way in which soil microarthropods perceive their environment is proportional to their body length we may expect that number of individuals $N$ also scales as

$$N \propto (\delta^{-0.36})^2 \tag{3}$$

Following the reasoning by Morse et al. (1985), let us combine the fractal argument with the assumption that animals with a lower per capita energy demand are able to establish proportionally larger numbers of individuals. This holds independent of habitat complexity. In this case abundance $N$ and biomass $W$ should scale as

$$N \propto W^{-b} \tag{4}$$

where $b$ is the exponent of the allometric relationship $M \propto W^b$ between biomass $W$ and metabolic rate $M$ and equals 0.81 for edaphic arthropods (Ryszkowsky, 1975).

If body mass $W$ and body length $L$ relate as $W \propto L^3$ and $L \propto W^{1/3}$, respectively, Eq. (3) can be written as

$$N \propto \left((W^{1/3})^{-0.36}\right)^2 \tag{5}$$

Consequently the combination of the fractal and the metabolic assumptions leads to $N \propto ((W^{1/3})^{-0.36})^2 \times W^{-0.81}$ and finally

$$N \propto W^{-1.05} \tag{6}$$

Considering that large hollow spaces with large diameter are less abundant than pores with small diameter, large animals have access to fewer crevices than small animals. Thus the expected slope of a plot of log biomass vs. log abundance should be somewhat steeper than $-1.05$. Kampichler (1995) compared this prediction with a sample of soil microarthropods from the same humus layer. He found the slope to equal $-0.80$ which is shallower than the expected slope. His report, however, was based only on a subset of the entire sample (6 out of 17 soil cores). This paper contains a more elaborate analysis of that data-base.

The sample consisted of 17 cylindrical soil cores of 5 cm diameter and 10 cm depth. They were extracted by Berlese–Tullgren-funnels and yielded a total of 5749 mites (predominantly oribatid mites) and collembolans, accounting for 98% of all extracted microarthropods. Therefore, subsequent analysis was restricted to these two taxa. All specimens were measured to the nearest 5 μm using a Wild–Censor binocular microscope and were converted into biomass data using the body length:biomass relationships provided by Edwards (1967), where

$$\mu\text{g biomass}_{\text{Oribatida}} = (4.92 \times \mu\text{m body length})^3 \tag{7}$$

$$\mu\text{g biomass}_{\text{Collembola-Arthropleona}} = (2.64 \times \mu\text{m body length})^3 \tag{8}$$

In a double-logarithmic plot of biomass and abundance, a unimodal curve with the mode in one of the lower size-classes can be expected. Eq. (6) should be valid for the distribution to the right of the mode. Blackburn et al. (1992) showed that the choice of number of size classes can significantly alter the slope of the body-size frequency distribution. They recommend dividing the data to the right of the distribution mode into a number of size classes between 6 and 15 for calculating the slope, since lower numbers produce less acurate and more variable estimates and higher numbers systematically overestimate the slope. Based on their guideline the biomass was divided into octaves (i.e., class limits at $\ldots, 2^{-1}, 2^0, 2^1, \ldots$), and semi-octaves (i.e., class limits at $\ldots, 2^{-1}, 2^{-0.5}, 2^0, 2^{0.5}, 2^1, \ldots$). This yielded 8 and 15 classes—the last semi-octave class was

empty—to the right of the mode. The abundance within each size-class was also $\log_2$-transformed.

The slope of the regression line is $-1.37$ (octaves) (Fig. 1a) and $-1.39$ (semi-octaves) (not shown), respectively. These values fall in line with the prediction of the slope to be somewhat steeper than $-1.05$. They are not statistically different from $-1.05$ ($t = 1.20$ and $t = 0.94$; $p > 0.05$) when tested according to $t = (|b_{obs} - b_{exp}|)/s_b$, where $b_{obs}$ is the observed slope, $b_{exp}$ is the value of a given slope against which $b_{obs}$ is to be compared, and $s_b$ is the standard deviation of $b_{obs}$ (Lozán, 1992).

Obviously, the approximate correspondence between data and prediction does not prove that the fractal nature of soil pore surface adds to an increase of individuals as body size of microarthropods gets smaller. Therefore more studies are needed on the relationship between the shape of the body size distribution

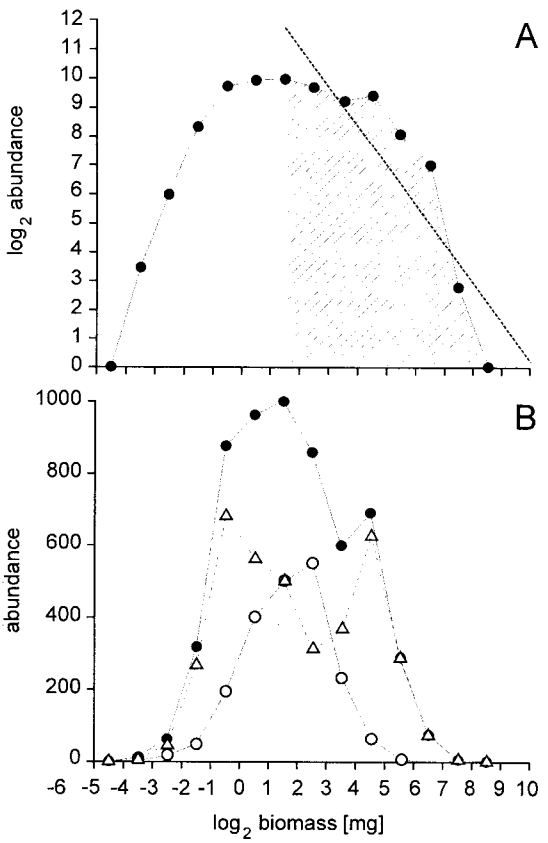


Fig. 1. Body-size distribution of a micoarthropod community (total number of individuals in each size class) in a spruce forest soil (a) in a double-logarithmic plot to show the slope ($b = -1.37$) to the right of the mode (hatched part of the distribution), (b) in a semi-logarithmic plot to show the additive composition of the overall body size distribution (black circles) by the body size distributions of Acarina (white triangles) and Collembola (white circles).

and the fractal geometry of the soil pore surface to find out whether or not different values $D$ actually are reflected in different slopes of a fitted line. Gunnarsson (1992) for example reported that the body size distribution of spiders in tree canopies did not in every case numerically agree with the expected slope for a given $D$ (with $D$ characterising space-filling properties of branches and leaves). A positive relationship between fractal dimension and the slope of the body size distribution, however, was clearly visible. This means, even though the fractal dimension is a weak predictor for a certain value for the slope of the body size distribution, there is obviously a relationship between the fractal dimension and the slope. It must be the aim of future surveys of microarthropod communities to investigate this relationship rather than simply compare prediction and observation in 'one site, one point in time' studies. Patterns of abundance per size-class as well as habitat structure exhibit temporal dynamics: Collembola community patterns for example change distinctively in the course of a year (e.g., Vegter, 1987; Kampichler, 1992), and pore diameter distribution and fractal dimension of pore surface must also be expected to undergo seasonal changes due to biotic (comminution, bioturbation, decomposition, etc.) and abiotic (pressure of a snow cover, etc.) processes.

Despite the appealing simplicity of relating number of individuals in a size-class to the amount of available habitat space, there are some methodological problems in the quantitative analysis of body size:abundance plots (see Loder et al. (1997) for a detailed discussion of these problems in interpreting analogous plots of the body size:species number distribution).

(1) The number of classes into which body size is divided can significantly alter the shape and slope of the body size:abundance distribution. Loder et al. (1997) report on a data-set of North American butterflies, where the fitted slope varies between $-2.05$ (80 size classes) and $-3.36$ (five size classes). In keeping to the recommendations by Blackburn et al. (1992) slopes for the body size distribution of soil microarthropods are obtained that are reasonably similar ($-1.37$ with eight size classes, $-1.39$ with 15 size classes). However, there is no a priori reason to choose any particular number of size classes. Since any slope value reported on in the literature is likely to be largely subjective, the problem arises of how to compare slopes from different distributions. Loder et al. (1997) regard this to be a probably intractable problem.

(2) Body size:abundance distributions will sometimes include empty classes, particularly at the right-hand side of the distribution. Again, there is no a priori reason to include or exclude these size classes containing no individuals from the regression analysis. If their inclusion is desired, the $\log(x + 1)$ transformation to the abundance axis correctly represents empty classes. Loder et al. (1997) regard the potential errors of this procedure to be small. It will, however, depend on how fragmented the distribution is.

(3) In particular when using a high number of size classes, the distribution will sometimes have multiple modes. Again there is no a priori reason to use

either mode. Even when the body size distribution shows a hump rather than an unmistakeable mode (Fig. 1a) the slope value may be affected by the choice of the size classes included in the regression. For example, if the size class left to the mode which contains nearly as many individuals (962) as the modal class (1000) (Fig. 1) is included, the fitted slope changes from $-1.37$ to $-1.15$.

(4) The relationship of body size and abundance to the right of the modal class is often curvilinear rather than linear (e.g., Fig. 1a and figures in the works of Gee and Warwick (1994a) and Gunnarsson (1992)). The fractal/metabolic argument predicts a straight line for the right-hand side of the body size distribution in a double logarithmic plot. It cannot yet be determined whether the bulged curve reflects inefficiencies in the extraction process of smaller animals or whether it is a characteristic feature of the body size distribution of soil microarthropods. However, linear regression may be reasonably well fitted to curvilinear data and may explain much of their variance (e.g., $R^2 = 0.82$ when divided into eight size-classes, $R^2 = 0.81$ when divided into 15 size-classes). Thus the slope value may serve as a heuristic tool for finding out whether or not there actually is a relationship between the fractal geometry of the habitat and the body size distribution. However, more detailed knowledge of the exact shape of the distribution which might be obtained in the future could call for a modification of the initial hypothesis.

These are the methodological problems that may arise in the analysis of soil microarthropod communities. However, at the moment we simply do not know whether empty classes, multiple modes or a curvilinear shape are recurrent patterns in the body size distribution of microarthropods. A few guidelines to be followed in a closer analysis can be given.

(1) The quantitative extraction of small individuals in a soil sample is extremely important, since the number of individuals in the lower size classes may strongly influence the location of the mode. The combination of fractal and metabolic arguments applies only to the right-hand side of the distribution. That fact that small individuals are less abundant than the mode suggests, that there are some other factors than metabolic rate, fractal scaling of the habitat or soil porosity which shape the left-hand part of the body size:abundance relationship. Thus the 'breakpoint' between left-hand and right-hand side of the distribution must by identified as precisely as possible. The location of the median in a middle size-class indicates that smaller individuals have possibly been missed in the extraction process. For future studies it would therefore be advisable to float the soil samples after dynamic extraction in order to minimize such losses, e.g., by using sugar flotation (Snider and Snider, 1997). Loring et al. (1981), for example, report that only 3% of *Tullbergia granulata*, a tiny collembolan species, could be collected by using Tullgren funnels alone.

(2) The analysis must cover the entire microarthropod community. The tradition most zoologists adhere to, namely to deal with single taxonomical groups (cf. Gunnarsson, 1992), would lead to erroneous conclusions. This is

illustrated by the body size distributions of Collembola and oribatid mites which show extremely different shapes (Fig. 1b). While the collembolans have a unimodal distribution with its peak close to the global mode, the oribatids form two distinct modes with a local minimum in the size-class of the collembolan mode. These peaks are due to a set of large species (e.g., *Nothrus silvestris*, *Atropacarus striculus*) and a set of small species (e.g., *Oppiella nova*, *Microppia minus*). Similar bimodal distributions of oribatid mites have recently been observed in a tropical forest in Puerto Rico (L. Heneghan, personal communication). It is yet too early to draw conclusions from a single data-set. The interesting pattern of interwoven peaks, however, suggests that apart from the hypothetical overall effects of habitat fractal geometry and metabolic demands by the individuals within different size-classes, interactions between taxa shape the internal structure of the body size distribution. Whether these interactions act on an ecological—e.g., medium-sized Collembola outcompeting oribatid mites of the same size—or an evolutionary time-scale—different size-specific rates of speciation in Collembola and oribatid mites—must be addressed by future investigations.

## 4. Detecting hierarchical scales

### *4.1. Outline of principle*

Ecosystems can be described as hierarchical systems with processes occurring at various spatial and temporal scales (O'Neill et al., 1986). Sugihara and May (1990) explicitly refer to fractals as a means to address problems like the determination of boundaries between hierarchical levels or the determination of scaling rules within a level. The underlying idea is that changes in dynamics across scales should express themselves in changes of spatial or temporal patterns and thus should be recognisable in the fractal exponents quantifying those patterns. The identification of scaling regions is easy: since fractal scaling rules are expressed by power laws—cf. formulae (1) and (2)—, fractal dimension normally is determined by linear regression on log-transformed data. Therefore one has to find out whether the data are sufficiently well characterised by a global regression or whether they are better fitted using piece-wise linear regression, either by applying a 'rolling regression'—moving a window of a fixed number of points over the entire data-set—or by estimating one or more breakpoints and performing regressions separately for each scaling region (Hastings and Sugihara, 1993). A shift in the slope of the regression line may indicate a shift in the underlying ecological process and may thus help in objectively defining boundaries between different scaling regions. This approach has been mainly undertaken by landscape ecologists (e.g., Krummel et al., 1987; Meltzer and Hastings, 1992).

*4.2. Application: scaling regions in aggregation patterns of Collembola*

In an early work using fractals in ecology, Hastings et al. (1982) applied the determination of the Korcak exponent $B$ to the study of fractal patterns in the distribution of vegetation patches. $B$ was introduced by Korcak (1938) and Mandelbrot (1982) showed it to be a fractal exponent. The Korcak exponent $B$ and fractal dimension $D$ are related by the simple formula $B = D/2$ for fractal islands in the plane and by $B = D/n$ for fractal islands in a $n$-dimensional Euclidean space. The number $N$ of vegetation patches of a size of at least $a$ follows the relationship

$$N(\text{area} > a) \propto a^{-B} \tag{9}$$

Thus, the larger $B$ is, the patchier (= more small patches) is the distribution. Hastings and Sugihara (1993) (pp. 123–124) proved that the Korcak exponent $B$ can also be used in the form

$$N(a \leq \text{area} < ca) \propto a^{-B} \tag{10}$$

where $c$ is a constant. Now let the patches be soil cores and characterise them not by their area but by the numbers of soil animals they contain, thus translating the Korcak exponent $B$ from Euclidean space to an abstract representational space sensu Frontier (1987). Then Eqs. (9) and (10) rewrite to

$$N(\text{number of individuals} > n) \propto n^{-B} \tag{11}$$

and

$$N(n \leq \text{number of individuals} < cn) \propto n^{-B} \tag{12}$$

with larger $B$ denoting larger patchiness. A plot of the number of cores $N$ ($n \leq$ number of individuals $< cn$) as a function of $n$—keeping $c$ constant—will be noisier than the analogous plot of $N$ (number of individuals $> n$), but according to Hastings and Sugihara (1993) it should be easier to recognise break points between scaling regions. Moreover, by applying Eq. (12) rather than Eq. (11) the behaviour at large scales will not interfere with the behaviour at smaller scales (H.M. Hastings, personal communication).

I analysed data on numbers of endogenic and hemiedaphic Collembola in a sample of 400 soil cores from the Scheyern experimental farm of the FAM Munich Research Association for Agricultural Ecosystems (Fromm et al., 1993; Fromm, 1997). The cores (7.8 cm diameter, 5 cm depth) were taken at 400 points distributed over a $50 \times 50$ m$^2$ sampling grid laid over the experimental farm in April 1991. Total numbers of Collembola per core ranged from 0 to 420. I divided that range in semi-octaves ($n = 2^0, 2^{0.5}, 2^1, 2^{1.5}, \ldots$) and chose $c = \sqrt{2}$. Subsequently the number $N$ of soil cores falling in each semi-octave was determined. Fig. 2 shows the graphs for total Collembola and for two

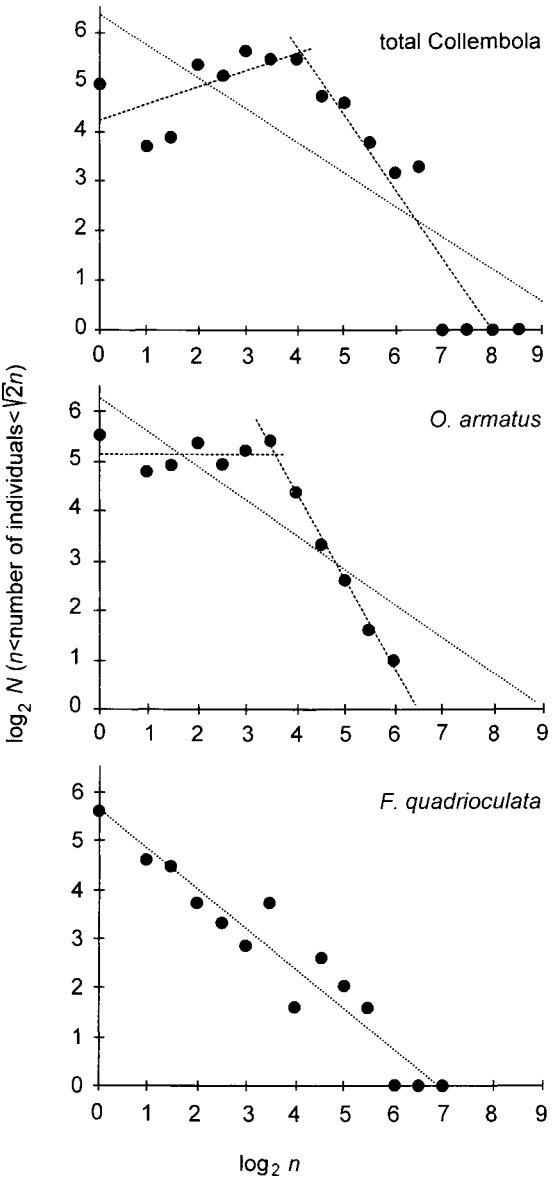


Fig. 2. Relationship between $\log_2 N$ (number of soil cores containing individual numbers $> n$ and $< \sqrt{2}n$) and $\log_2 n$. Hatched lines: regression lines to the left and the right of the breakpoint (breakpoint determined by eye); dotted lines: regression lines of a global regression. See Table 1 for statistics.

dominant species, *Onychiurus armatus* and *Folsomia quadrioculata*. Total Collembola as well as *O. armatus* show distinct breakpoints at an abundance of $2^4 = 16$ and $2^{3.5} \approx 11$ individuals per core, respectively, while the distribution of *F. quadrioculata* is best fit by a global regression (Table 1). Collembola

Table 1
Slope ($-B$) and explained variance ($R^2$) of linear regressions of $\log_2 N$ (number of soil cores containing individual numbers $> n$ and $< \sqrt{2}\,n$ = dependent variable) on $\log_2 n$ (independent variable) (cf. Fig. 2)

| | Range of linear regression | $-B$ | $R^2$ |
|---|---|---|---|
| Total Collembola | left of breakpoint | 0.35 | 0.39 |
| | right of breakpoint | −1.41 | 0.89 |
| | global | −0.64 | 0.60 |
| *O. armatus* | left of breakpoint | 0.00 | 0.00 |
| | right of breakpoint | −1.75 | 1.00 |
| | global | −0.71 | 0.71 |
| *F. quadrioculata* | global | −0.81 | 0.92 |

exhibit vectorial (e.g., aggregations at food sources or microsites with suitable abiotic conditions), social (e.g., aggregations due to pheromone emission) and reproductive (e.g., patches of juveniles slowly dispersing from an egg cluster) clumping patterns (cf. Usher, 1976; Ekschmitt, 1993). It is plausible to assume that the densities above and below the breakpoints are caused by different combinations of these patterns; below-breakpoint densities possibly also show the lack of any aggregation process.

The fractal analysis clearly has an advantage over the widely used approach of fitting the frequency:abundance distribution to a statistical distribution and of taking a distribution parameter as an index of aggregation (e.g., parameter $k$ of the negative binomial distribution; Southwood, 1978). Such a global index cannot distinguish between different scaling regions within the range of observed abundance.

## 5. Further suggestions

These three topics certainly do not exhaust the range of possible applications of fractal concepts in soil zoology. Various bacterial and fungal species have been shown to demonstrate fractal patterns in growth and morphology (cf. Senesi (1996) and Boddy et al. (1999)). Jones et al. (1994) regard fractal dimension as a useful parameter for quantifying the space-filling properties and the degree of self-similarity of fungal mycelia and relate these features to the efficiency of explorative and exploitative growth mechanisms. Several authors successfully quantified the morphological response of fungal growth to nutrient status (Ritz and Crawford, 1991; Crawford et al., 1993) and abiotic conditions like temperature or water potential (Donnelly and Boddy, 1997) by determining the change of the fractal dimension of the hyphal network. Also interactions with fungal grazers cause a significant modification of fungal growth patterns as

shown by Hedlund et al. (1991). However, these modifications have not yet been quantified by means of fractal geometry. The analysis of the response of fungal mycelia to grazing by microarthropods or of bacterial colonies to grazing by protozoans or nematodes could provide valuable insight into the mechanisms of interaction between microbivorous organisms and their prey and its consequences for nutrient cycling and energy flow in soil. If grazing on fungi and bacteria actually modifies their strategies of resource acquisition, e.g., by switching from explorative to exploitative growth patterns, this will have major consequences for defining the role of soil animals in decomposition processes.

Crawford et al. (1993) pointed out that soil structure should have a tremendous impact also on the population dynamics of bacteria due to the fact that the area accessible to bacteria but not accessible to their predators is a function of complexity of soil pore walls. They pointed out that at a fractal dimension of pore surface of $D_s = 2.36$, almost half of the habitable area for bacteria (size $\approx 5$ $\mu$m) is to be regarded as a refuge area where they are safe from protozoan predators (size $\approx 30$ $\mu$m). Although fractal soil features set the limits for predator–prey interactions on the very basis of the bacterial energy channel of below-ground food webs—thus representing an important factor for the dynamics of cycling and transport of nutrients through microbial populations—this concept has not yet been taken up by soil zoologists.

## 6. Summary and conclusions

The examples presented in this paper highlight the diverse range of possibilities for applying fractals to soil zoological problems. These investigations into fractal applications for soil zoologists should be viewed as preliminary, however, as these problems require further research. The measurement of habitat complexity in the pore-space of soils and organic layers needs further development before its impact on the body size distribution of microarthropods can be assessed. Body size most probably is a major factor determining the possible mechanisms of interaction between microarthropods and microflora. Smaller species have access to smaller soil crevices; they should thus be able to exploit additional microbial food resources not available to larger microarthropods and a larger amount of energy should be channelled through populations of smaller species. The slope to the right of the body size distribution mode of $-1.37$ in fact indicates that the amount of energy flowing through a size-class rises approx. 1.5-fold at half the body size ($0.5^{0.81-1.37} = 1.474$). Also, the approach of detecting scaling regions in the aggregation patterns of microarthropods needs careful consideration. The relationships between different types of statistical distributions fitted to frequency:abundance distributions of soil animals (e.g., the negative binomial distribution) and the power law scaling presented above are entirely unknown.

Undoubtedly fractal geometry has the potential to contribute to a number of important questions in studies of soil fauna. Soil zoologists are encouraged to make use of this unique instrument for the analysis of complex patterns.

## Acknowledgements

I am grateful to H.M. Hastings (Hofstra University) for valuable comments on the use of fractal concepts for the detection of scaling regions. I also owe my thanks to L. Miko (Prague) for the identification of oribatid species from spruce forest soil, H. Fromm (Cottbus) for the data-set of Collembola from the Scheyern experimental farm and K. Winter (Neuherberg) and E. Tadsen-Duch (Bonn) for improving the English of the original manuscript. The fractal analysis of the spruce forest humus layer and the analysis of the microarthropod body size distribution was funded by the Austrian Federal Ministry of Science and Research. The analysis of scaling regions in aggregation patterns of Collembola is part of the sub-project I2 'Animal models' of the research network 'Forschungsverbund Agrarökosysteme München' (FAM). The scientific activities of FAM are financially supported by the Federal Ministry of Culture and Science, Research and Technology (BMBF 0339370). Rent and operating expenses are paid by the Bavarian State Ministry for Education and Culture, Science and Art.

## References

Anderson, A.R.A., Young, I.M., Sleeman, B.D., Griffiths, B.S., Robertson, W.M., 1997. Nematode movement along a chemical gradient in a structurally heterogeneous environment: I. Experiment. Fundamentals of Applied Nematology 20, 157–163.

Blackburn, T.M., Lawton, J.H., Perry, J.N., 1992. A method of estimating the slope of upper bounds of plots on body size and abundance in natural animal assemblages. Oikos 65, 107–112.

Boddy, L., Wells, J.M., Culshaw, C., Donelly, D.P., 1999. Fractal analysis in studies of mycelium in soil. Geoderma 88, 301–328, this issue.

Crawford, J.W., Ritz, K., Young, I.M., 1993. Quantification of fungal morphology, gaseous transport and microbial dynamics in soil: an integrated framework utilising fractal geometry. Geoderma 56, 157–172.

Davenport, J., Pugh, P.J.A., McKechnie, J., 1996. Mixed fractals and anisotropy in subantarctic marine macroalgae from South Georgia: implications for epifaunal biomass and abundance. Marine Ecology Progress Series 136, 245–255.

Dicke, M., Burrough, P.A., 1988. Using fractal dimensions for characterizing the tortuosity of animal trails. Physiological Entomology 13, 393–398.

Donnelly, D.P., Boddy, L., 1997. Development of mycelial systems of *Stropharia caerulea* and *Phanerochaeta velutina* on soil: effect of temperature and water potential. Mycological Research 101, 705–713.

Edwards, C.A., 1967. Relationships between weights, volumes and numbers of soil animals. In: Graff, O., Satchell, J.E. (Eds.), Progress in Soil Biology. Vieweg, Braunschweig, pp. 585–594.

Ekschmitt, K., 1993. Über die räumliche Verteilung von Bodentieren. PhD Thesis, University Bremen, Germany.

Fenchel, T., 1993. There are more small than large species? Oikos 68, 375–378.

Fourcassié, V., Coughlin, D., Traniello, J.F.A., 1992. Fractal analysis of search behaviour in ants. Naturwissenschaften 79, 87–89.

Fromm, H., 1997. Räumliche und zeitliche Variabilität der Collembolenfauna und ihre Bedeutung für C- und N-Umsatz in einer Agrarlandschaft. FAM-Bericht 26, Shaker, Aachen.

Fromm, H., Winter, K., Filser, J., Hantschel, R., Beese, F., 1993. The influence of soil type and cultivation system on the spatial distributions of the soil fauna and microorganisms and their interactions. Geoderma 60, 109–118.

Frontier, S., 1987. Applications of fractal theory to ecology. In: Legendre, P., Legendre, L. (Eds.), Developments in Numerical Ecology. NATO ASI Series Vol. G 14. Springer, Berlin, pp. 335–378.

Gee, J.M., Warwick, R.M., 1994a. Body-size distribution in a marine metazoan community and the fractal dimensions of macroalgae. Journal of Experimental Marine Biology and Ecology 178, 247–259.

Gee, J.M., Warwick, R.M., 1994b. Metazoan community structure in relation to the fractal dimensions of marine macroalgae. Marine Ecology Progress Series 103, 141–150.

Gunnarsson, B., 1992. Fractal dimension of plants and body size distribution in spiders. Functional Ecology 6, 636–641.

Hastings, H.M., Sugihara, G., 1993. Fractals—A User's Guide for the Natural Sciences. Oxford University Press, Oxford.

Hastings, H.M., Pekelney, R., Monticciolo, R., vun Kannon, D., del Monte, D., 1982. Time scales, persistence and patchiness. BioSystems 15, 281–289.

Hedlund, K., Boddy, L., Preston, C.M., 1991. Mycelial responses of the soil fungus, *Morteriella isabellina*, to grazing by *Onychiurus armatus* (Collembola). Soil Biology and Biochemistry 23, 361–366.

Johnson, A.R., Milne, B.T., Wiens, J.A., 1992. Diffusion in fractal landscapes: simulations and experimental studies of tenebrionid beetles. Ecology 73, 1968–1983.

Jones, C.L., Lonergan, G.T., Mainwaring, D.E., 1994. A rapid method for the fractal analysis of fungal colony growth using image processing. Binary 5, 171–180.

Kampichler, C., 1992. Community structure and phenology patterns of epedaphic Collembola in a dry-turf grassland. Zoologisches Jahrbuch für Systematik 119, 369–381.

Kampichler, C., 1995. Biomass distribution of a microarthropod community in spruce forest soil. Biology and Fertility of Soils 19, 263–265.

Kampichler, C., Hauser, M., 1993. Roughness of soil pore surface and its effect on available habitat space of microarthropods. Geoderma 56, 223–232.

Korcak, J., 1938. Deux types fondamentaux de distribution statistique. Bulletin de l'Institut International de Statistique 3, 295–299.

Krummel, J.R., Gardner, R.H., Sugihara, G., O'Neill, R.V., Coleman, P.R., 1987. Landscape patterns in a disturbed environment. Oikos 48, 321–324.

Lawton, J.H., 1986. Surface availability and insect community structure: the effects of architecture and fractal dimension of plants. In: Juniper, B.E., Southwood, T.R.E. (Eds.), Insects and the Plant Surface. Edward Arnold, London, pp. 317–331.

Loder, N., Blackburn, T.M., Gaston, K.J., 1997. The slippery slope: towards an understanding of the body size frequency distribution. Oikos 78, 195–201.

Loring, S.J., Snider, R.J., Robertson, L.S., 1981. The effects of three tillage practices on Collembola and Acarina populations. Pedobiologia 22, 172–184.

Lozán, J., 1992. Angewandte Statistik für Naturwissenschaftler. Paul Parey, Berlin.

Mandelbrot, B.B., 1982. The Fractal Geometry of Nature. Freeman, New York.

Meltzer, M.I., Hastings, H.M., 1992. The use of fractals to assess the ecological impacts of increased cattle population: case study from the Runde Communal Land, Zimbabwe. Journal of Applied Ecology 29, 635–646.

Morse, D.R., Lawton, J.H., Dodson, M.M., Williamson, M.H., 1985. Fractal dimension of vegetation and the distribution of arthropod body lengths. Nature 314, 731–733.

Nams, V.O., 1996. The VFractal: a new estimator for fractal dimension of animal movement paths. Landscape Ecology 11, 289–297.

O'Neill, R.V., de Angelis, D.L., Waide, J.B., Allen, T.F.H., 1986. A Hierarchical Concept of Ecosystems. Princeton University Press, Princeton.

Ritz, K., Crawford, J.W., 1991. Quantification of the fractal nature of colonies of *Trichoderma viride*. Mycological Research 94, 1138–1141.

Ryszkowsky, L., 1975. Energy and matter economy of ecosystems. In: van Dobben, W.H., Lowe-McConnel, R.H. (Eds.), Unifying Concepts in Ecology. Junk, The Hague, pp. 109–126.

Senesi, N., 1996. Fractals in general soil science and in soil biology and biochemistry. In: Stotzky, G., Bollag, J.-M. (Eds.), Soil Biochemistry, Vol. 9. Marcel Dekker, New York, pp. 415–472.

Shorrocks, B., Marsters, J., Ward, I., Evennett, P.J., 1991. The fractal dimension of lichens and the distribution of arthropod body lengths. Functional Ecology 5, 457–460.

Snider, R.M., Snider, R.J., 1997. Efficiency of arthropod extraction from soil cores. Entomological News 108, 203–208.

Southwood, T.R.E., 1978. Ecological Methods: With Particular Reference to the Study of Insect Populations, 2nd edn., Chapman and Hall, London.

Sugihara, G., May, R.M., 1990. Applications of fractals in ecology. Trends in Ecology and Evolution 5, 79–86.

Tatsumi, J., Yamauchi, A., Kono, Y., 1989. Fractal analysis of plant root systems. Annals of Botany 64, 499–503.

Turchin, P., 1996. Fractal analyses of animal movement: a critique. Ecology 77, 2086–2090.

Usher, M.B., 1976. Aggregation responses of soil arthropods in relation to the soil environment. In: Anderson, J.M., Macfadyen, A. (Eds.), The Role of Terrestrial and Aquatic Organisms in Decomposition Processes. Blackwell, Oxford, pp. 61–94.

Vegter, J.J., 1987. Phenology and seasonal resource partitioning in forest floor Collembola. Oikos 48, 175–185.

Wiens, J.A., Crist, T.O., With, K.A., Milne, B.T., 1995. Fractal patterns of insect movement in microlandscape mosaics. Ecology 76, 663–666.

*Fractals in Soil Science*
Editors: Ya.A. Pachepsky, J.W. Crawford and W.J. Rawls
© 2000 Elsevier Science B.V. All rights reserved.


# Fractal analysis in studies of mycelium in soil

Lynne Boddy *, John M. Wells, Claire Culshaw, Damian P. Donnelly

*School of Pure and Applied Biology, University of Wales, PO Box 915, Cardiff CF1 3TL, UK*

Received 7 October 1997; accepted 28 September 1998

**Abstract**

Like many naturally irregular structures mycelia are approximately fractal; thus fractal dimension can be used to quantify the extent to which mycelia permeate space in relation to the extent of the system. Since it is important to be able to quantify both space filling at mycelial margins, i.e., 'search fronts', and within systems, both surface/border and mass fractal dimensions are appropriate. The value of employing fractal geometry to describe mycelia is examined by comparison with information from other descriptors, in experiments examining the effects of extracellular concentration of the macronutrients NPK, and endogenous nutrient status of inocula, on development of mycelia of *Hypholoma fasciculare*, *Phanerochaete velutina* and *Phallus impudicus*. Mycelial morphology differed between species and was altered by both soil and inoculum nutrient status. Sensitivity to treatment effects was a major benefit of using fractal dimension (determined by box-counting) as a descriptor. However, complementary descriptors, including mycelial extent and total hyphal cover provided different information and all three should be used in combination. Further, though quantitative measures are attractive because of their objectivity they cannot describe all features of branching pattern, thus visual observation is also essential. © 1999 Elsevier Science B.V. All rights reserved.

*Keywords:* fractal analysis; mycelial morphology; nutrient effects; foraging; basidiomycetes

## 1. Introduction

### *1.1. Mycelia in soil*

Organic resources in soil are discontinuously distributed both spatially and temporally. The fungi which colonize these resources fit into two distinctive

* Corresponding author. Tel.: +44-1222-874000/4776; Fax: +44-1222-874305; E-mail: boddyl@cf.ac.uk

Reprinted from Geoderma 88 (1999)
© 1999 Elsevier Science B.V. All rights reserved

ecological groupings depending on whether or not they are able to grow out of individual resources (Cooke and Rayner, 1985; Rayner and Boddy, 1988). Those which are unable to can be termed 'unit-restricted', and those which can grow out and physically interconnect separate resource units can be termed 'non-unit-restricted'. The operational scales of the latter are variable, but since they are not confined within resources the indeterminate growth form of mycelia means that they are capable of producing among the largest individuals on earth (Smith et al., 1992).

Non-unit-restricted fungi exhibit a spectrum of types with regard to their exploratory mycelium in soil. At one extreme, mycelia are diffuse while at the other mycelia are aggregated to form apically dominant linear organs—rhizomorphs (e.g., *Armillaria* spp. and *Marasmius androsaceus*). In between these, mycelia exhibit various degrees of hyphal aggregation, though all have diffuse growing fronts, and become consolidated into mycelial cords from behind (Thompson, 1984; Rayner et al., 1985; Boddy, 1993).

Those fungi whose mycelia are predominantly diffuse, utilize resources which are relatively common and relatively homogeneously supplied in space. For example, the fairy ring forming fungi of grasslands, e.g., *Marasmius oreades*, and the woodland floor, e.g., members of genera such as *Collybia*, *Clitocybe* and *Mycena* (Rayner and Boddy, 1988; Dowson et al., 1989a). In contrast, those fungi which utilize bulky, relatively uncommon and heterogeneously distributed resources, such as large branches, trunks and tree stumps, predominantly produce extensive and long-lived systems of mycelial linear organs, e.g., *P. velutina* (mycelial cords) and *Armillaria gallica* (rhizomorphs) (e.g., Rayner and Boddy, 1988; Boddy, 1993). Nonetheless, as indeterminate systems, mycelia have the capacity to alter their organizational state according to changing circumstances and functional requirements. Thus at different times, or at the same time in different parts of the system, mycelia may exhibit different branching patterns, degrees of aggregation and hyphal densities (unit length per unit volume).

The extra-resource foraging mycelia of cord-, rhizomorph- and fairy ring-forming fungi mentioned so far all tend to form large systems (easily visible to the naked eye at a macroscopic scale), most commonly at the soil/litter interface. The latter means that they can be considered as approximately 2-D, and that trays containing a thin layer of compact soil provide suitable model systems for studying them. However, this is only an approximation and it may not be entirely appropriate to confine all of these fungi in this way and certainly not those which form small mycelia radiating only a few centimeters into soil from spores or organic resources. Indeed, a reaction–diffusion mathematical model indicates that patterns of mycelial development will differ in 2-D from those in 3-D (Regalado et al., 1996). Nonetheless, in view of ease of observation almost all studies in soil have been performed in 2-D. In the early studies in such model soil systems, apart from recording extension, patterns of mycelial development

could only be described qualitatively (subjectively) (e.g., Dowson et al., 1986, 1988a, 1989b).

### *1.2. Fractal nature of mycelia*

Describing mycelia quantitatively essentially involves estimating their space-filling capacity. Density is inappropriate because the number of units of length, volume or area identified varies with scale of observation. Further by 'averaging' the heterogeneities of mycelial systems, density estimates lose functionally important local details which may be valuable for comparing taxa, genets and organizational states. Like many naturally irregular structures (Richardson, 1961; Morse et al., 1985) mycelia are approximately fractal. Thus fractal dimension can be used to quantify the extent to which mycelia permeate space in relation to extent of the system. Currently this can be achieved most easily using image capture and analysis techniques (e.g., Donnelly et al., 1995; Hitchcock et al., 1996).

It is important to be able to quantify both space filling at mycelial margins, i.e., 'search fronts', and within the system, effectively allowing discrimination between systems which are only fractal at their boundaries (termed surface/border fractal) having entirely plane-filled interiors, and those which are mass fractal where the interior of the system has gaps (Obert et al., 1990). Thus estimates of both mass fractal dimension ($D_{BM}$; which can be considered as a descriptor comparing actual area covered with area enclosed within the minimum perimeter which could contain the whole system) and surface/border fractal dimension ($D_{BS}$; which can be considered as a descriptor comparing the sum of perimeters within the system with its minimum perimeter) are appropriate. The first study of fractal dimensions of mycelia on soil (Bolton and Boddy, 1993), like that of several studies of mycelia on agar (Ritz and Crawford, 1990; Baar et al., 1997) employed the concentric circles method (two point density–density correlation function method) (Witten and Sander, 1981), but this excludes the mycelial growing front from analysis. Subsequently the 'box-counting' method (Obert et al., 1990), which allows estimation of $D_{BM}$ and $D_{BS}$, has been used for mycelia developing on soil (Donnelly et al., 1995; Abdalla and Boddy, 1996; Donnelly and Boddy, 1997a,b; Wells et al., 1997; Donnelly and Boddy, 1998). Likewise, this method has been used on several occasions to quantify fractal dimension of mycelia on agar (Mihail et al., 1994, 1995). Importantly, the box-counting method allows analysis of the whole system, including the growing front. A similar method has been used to examine effects of heterogenous nutrient supply on mycelial growth on cellophane (Crawford et al., 1993).

To date, the fractal nature of mycelia has been studied at two distinct levels. Firstly, several mathematical models have been proposed to explain how the morphogenesis of mycelia (Patankar et al., 1993; Regalado et al., 1996) can be

related to intra- and extracellular substrate concentrations in agar (Jones et al., 1995). Secondly, fractal geometry has been used to quantify interspecific differences in mycelial morphology and relate these to habitat (Donnelly et al., 1995; Mihail et al., 1995), and intraspecific changes induced by introducing new carbon resources or competing fungi to established or establishing mycelial systems (Bolton and Boddy, 1993; Donnelly, 1995; Donnelly and Boddy, 1997b, 1998). Importantly, those concerned with the ecological significance of the fractal nature of mycelia have studied development in non-sterile soils. These studies have revealed clear interspecific differences in morphology (quantified by fractal dimension), especially at initial stages of outgrowth from resources. Some produce surface fractal systems while others produce mass fractal systems, though with time as surface fractal systems cover a large area they become increasingly mass fractal (Donnelly et al., 1995). This may indicate the development of a biomass efficient, persistent mycelial network set up *behind* the foraging margin. Significantly, differences in morphology appear to be associated with differences in extension rate, more aggregated systems (i.e., mass fractal systems) extending faster than surface fractal systems (Donnelly et al., 1995). Morphological and physiological differences have been related to resource specificity, broad-fronted, slowly extending systems utilizing diverse locally abundant resources, while narrow-fronted rapidly extending systems utilize bulky, disparate resources. These contrasting strategies have also been described for clonal plants, the former strategy being termed 'phalangeal' and the latter 'guerrilla' (Schmid and Harper, 1985).

Recently, simulations with a reaction–diffusion model for growth have suggested that the fractal nature of mycelia may be generated in response to the interactions between *intracellular* activators/inhibitors, and *extracellular* substrates (Regalado et al., 1996). The model allows the concentration of the extracellular substrate to be varied and therefore permits predictions of growth form to be made for *heterogeneous* environments. However, the model is based upon growth from a point source, equivalent to a spore or a substrate depleted inoculum. In nature, the situation is often not so simple. Non-unit restricted fungi may be buffered to varying extents from the extremes of a heterogeneous environment by their intracellular nutrient supply, their ability to conserve nutrients within the system, and their ability rapidly to translocate nutrients to different parts of the mycelial system (e.g., Wells et al., 1990, 1995). It is therefore important to consider not only the concentration of substrate within the environment, but also the nutritional history of the resource(s) from which the mycelium is growing and of the mycelium itself.

That extracellular soil nutrient concentration affects fractal morphology has been shown for *Stropharia caerulea*, which is associated with nutrient enriched sites (Donnelly and Boddy, 1998). The extent of the effect depended on the nutrient type and quantity. Importantly, fractal geometry revealed small changes which were undetectable by biomass measurement. Also, it has been shown that

the nutritional quality of the resource from which the mycelium was extending affected both morphology and responsiveness to encounter of new resources (Donnelly and Boddy, 1997b). While these studies focused on the effects of eutrophication, methods have now been developed to examine mycelial growth at naturally occurring and depleted nutrient concentrations in soil (Wells et al., 1997). In this paper we examine further the effect of extracellular concentration of the macronutrients NPK and the endogenous nutrient status of inocula on development of mycelia of *H. fasciculare*, *P. velutina* and *Pha. impudicus*. The value of employing fractal geometry to describe mycelia is examined by comparison with information from other descriptors including mycelial extent, total hyphal cover and visual observation.

## 2. Materials and methods

### *2.1. Fungal isolates*

Fungi, from laboratory stocks, were cultured on 500 $cm^3$ agar in 2-l wide-neck conical flasks, incubated at 20°C. *P. velutina* (DC: Pers.) Parmasto, *H. fasciculare* (Huds.: Fr.) Kummer and *Pha. impudicus* (L.) Pers. were grown on 2% (w/v) malt extract agar (MA: 20 g $l^{-1}$ Munton and Fison spray malt, 15 g $l^{-1}$ Beta Lab agar). Additionally, *P. velutina* was cultured on both noble (NA: 15 g $l^{-1}$ Beta Lab agar) and enriched agar (EA: prepared with 100 mM $NH_4K_2PO_4$).

### *2.2. Preparation of inocula*

Beech (*Fagus sylvatica*) blocks, $1 \times 2 \times 2$ $cm^3$, which had been cut from a freshly felled tree and frozen until required, were soaked overnight in distilled water to defrost, autoclaved at 121°C for 20 min and reautoclaved 24 h later. Approximately 40 blocks were added to 2-week old fungal cultures in flasks, and incubated at 20($\pm$1)°C for 9 (*P. velutina* on MA) or 21 weeks. Blocks were then removed, scraped free of adhering mycelium and agar and weighed prior to use as inocula and placed onto the centre of trays of soil.

### *2.3. Soil preparation*

Soil was collected from a mixed deciduous woodland in the Coed Beddick Inclosure, Tintern, UK (National Grid reference SO 528018). The unsterile loam was air dried in the laboratory and sieved through a 2-mm mesh. 'Dilute' soil was prepared consisting of 1:1 sieved soil:sterile washed sand mixture (by oven dry weight). After thorough mixing, subsamples were removed for water content determinations. The matric potential of the dilute soil was estimated using the

filter paper method of Fawcett and Collis-George (1967), and adjusted to −0.006 MPa by addition of deionised water, compensating for any nutrient solution to be added to the soil before inoculation.

### *2.4. Effects of soil nutrient status on development of mycelial systems of H. fasciculare, Pha. impudicus and P. velutina*

Dilute soil (550 g) was compacted into 24 × 24 $cm^2$ lidded trays. The relative nutrient regimes (RNRs) of the soil trays were either amended, by adding 3.2 $cm^3$ 20 mM (RNR1) or 200 mM (RNR10) $NH_4K_2PO_4$ solutions, or remained 'unamended', receiving 3.2 $cm^3$ deionised water (RNR0.5). The nutrient solution or deionised water was applied evenly to the soil trays by delivery of 0.05 $cm^3$ aliquots via a multi-channel pipette through 64 evenly-spaced holes drilled into a soil tray lid. Applying 3.2 $cm^3$, 20 mM $NH_4K_2PO_4$ raised the available phosphate concentration of the 'dilute' soil approximately to field levels (Wells et al., 1997), and was the datum for defining the RNR of the soils.

Wood block inocula (21-week old) of *H. fasciculare* and *Pha. impudicus* cultured on MA, and inocula of *P. velutina* grown on NA and EA were placed in the centre of the plates, with five to six replicates per treatment. The trays were stacked in polythene bags to minimise moisture loss and incubated at 16(± 1)°C in darkness.

### *2.5. Effect of new wood 'bait' resources on development of mycelial systems of P. velutina*

Dilute soil (700 g) was compacted into 24 × 24 lidded trays. A 9-week old inoculum of *P. velutina* cultured on MA was placed in the centre of the trays and the whole system weighed. Trays were incubated at 16(± 1)°C as described above for 13 days. Systems were then 'baited' by adding either a fresh, unsterile 2 × 2 × 1 $cm^3$ beech wood bait or a control inert Perspex 'bait' of the same contact area (2 × 2 $cm^2$), behind the mycelial growth front, 5 cm from the inoculum. Full details of this experiment are reported by Wells et al. (1997).

### *2.6. Image capture and pre-processing*

The growth and development of the mycelial systems were recorded every 4–21 days, depending on extent of change of systems. Images were captured using a Hitachi KP-MI monochrome CCD video camera with a Canon TV macro-zoom lens, connected to an Optiplex GXMT 5100 computer (Dell Systems, Wicklow, Eire) and stored as digital images in a Synapse frame store (Synoptics, Cambridge, UK). Uniform lighting of the plates was achieved using a circular fluorescent bulb with opalescent diffuser fitted around the camera. All

images were taken with the same illumination from a height of 65 cm. In this paper, images are presented at the same resolution as analysed.

SEMPER 6 (Synoptics, Cambridge, UK) for Windows, was used to pre-process and analyse the images. Each pixel in the $512 \times 512$ array was graded on a scale of 0 (black) to 255 (white) in relation to its shade. Pre-processing reduces this image to a pure 'binary' comprising all black (0) or white (255) pixels as follows (Donnelly et al., 1995).

*2.6.1. High pass filtering*

Any long-range variation in image intensity across the image was reduced by subtracting the mean grey value averaged over the surrounding $120 \times 120$ pixel square, reducing the effect of any soil unevenness on the image.

*2.6.2. Sharpening*

Pixel values were doubled and the local mean grey value (averaged over the surrounding $9 \times 9$ pixel square) subtracted, enhancing the contrast between light and dark areas.

*2.6.3. Histogram equalisation*

After the above adjustments, the pixel values were rescaled over the 0–255 range.

*2.6.4. Windowing*

Inocula, baits and the edge of the plate were removed by manually masking out these regions of the image, using the mouse on a working image screen display. Highlighted soil particles or colonies of other soil fungi could also be removed where necessary.

*2.6.5. Conversion to binary image*

A threshold level for pixel shade values (determined manually by preliminary experimentation and kept constant for all images) was applied to the images; pixel values higher than the threshold were converted to 255 (white, representing mycelium) and lower values to 0 (black, representing soil).

*2.6.6. Particle separation*

Particle separation allows areas of interest to be examined separately from the rest of the mycelium. This is an artificial *visual* separation of distinct regions, which in reality are physiologically interconnected with the whole system. However, in viewing these regions as distinct entities local changes can be detected which may not be discernible when compared on a system wide basis. This feature of SEMPER was used both to separate hyphal 'patches' referred to in the text, and to study mycelial growth in different sectors of the 'baited' *P.*

*velutina* soil trays. In this study, a separating line was drawn through the central inoculum and perpendicular to the alignment of the inoculum and bait. Accordingly, reference in the text is made to 'baited' and 'unbaited' sectors of the mycelial system.

*2.6.7. Particle analysis*

Particles are defined as any region of eight or more connected white pixels surrounded by black pixels. SEMPER assigned a particle identification number for each discrete cluster of pixels within the image. Clusters of less than 20 pixels were automatically removed as these represented reflective soil or sand particles (Wells et al., 1997). Any large reflective particles associated with highlights on the soil surface could also be removed here or the image returned to the windowing phase where they could be masked out. Entire binary images were saved in SEMPER file format at this stage. For baited *P. velutina* systems, 'baited' and unbaited sectors of the image were alternately removed by manually masking out these regions, using the mouse on a working image screen display; the remaining sector could then be saved as a separate binary image for analysis.

*2.7. Image measurements*

The pixel length of a line drawn between the inner edges of a soil tray (length 23.5 cm) within an image was used to calibrate the analysis system. Once calibrated, radial extent (cm) and hyphal cover ($cm^2$, white pixel area) of the image could be determined. Radial extent was determined by drawing 8 lines from the inoculum to the extending mycelial front, aligned on a grid overlaid by SEMPER. Extent was determined until the colony margin reached the edge of the soil trays. Hyphal cover was determined by manual selection of particles. Pixel area, particle type (i.e., 'patch' or 'non-patch') and sector location ('baited' or 'unbaited') were recorded against the identification code for each particle.

*2.8. Estimating fractal dimensions*

The box count method (Obert et al., 1990; Donnelly et al., 1995) was used to determine the fractal dimensions of the mycelial systems. It is an important feature of the method used by Donnelly et al. (1995) that counts of intersected boxes are made by grids of each box size at each possible starting position. For example a grid composed of boxes of 3 pixels side length have nine different starting positions. This greatly increases the confidence in the estimate of $D$ for filamentous colonies (Soddell and Seviour, 1994). Each image was overlaid with grids of square boxes of size 3–61 pixels and the number of boxes intersecting white pixels within the image recorded. For a series of boxes of side length $s$

pixels the number of boxes intersected by the set ($N$) is related to the fractal dimension of the set ($D_B$) by the power law

$$N(s) = cs^{-D_B}$$

Both interior boxes, which are contained wholly within the fractal set (i.e., contain white pixels only), and border boxes, which contain at least one white pixel and which contain or adjoin at least one black pixel, contribute to the total number of boxes ($N$) intersected by the set. Thus,

$$N(s) = N_{\text{border}}(s) + N_{\text{interior}}(s)$$

Practically the image may not be self similar at all length scales, with departure from the power law occurring at very small or very large box sizes (Pfiefer and Obert, 1989; Markx and Davey, 1990; Obert et al., 1990; Donnelly et al., 1995). The fractal range may be determined by the dimensions of the image. The lower limit of resolution is determined by the pixel size of the image, and in mycelial systems this will also be limited to individual hyphae. Box sizes of side length 3 pixels and above were used in the program developed by Donnelly et al. (1995). The upper limit is determined by the largest gap within the image but usually is determined by 25% of the maximum width of the image set (Markx and Davey, 1990; Obert et al., 1990).

An *estimate* of the border fractal dimension is obtained by plotting log $N_{\text{border}}(s)$ against log $s$. Regression analysis of the *linear* portion of this plot yields a gradient of $-D_{BS}$. The mass fractal dimension is similarly estimated by regression analysis on the linear portion of a plot of log $\{N(s) - 1/2N_{\text{border}}(s)\}$ against log $s$, yielding a gradient of $-D_{BM}$. The subtraction term is necessary to avoid an overestimate of the area of the structure at large box sizes since border boxes are not entirely filled by the set (Kaye, 1989).

### *2.9. Statistical analyses*

Treatment means were compared using One-way ANOVA and LSD tests. When data sets had unequal variances, determined by Levene's test, Kruskal–Wallis $H$- and $t$-tests for unequal variances were used (SPSS). Paired $t$-tests were used to compare system characteristics in the 'baited' and unbaited sectors of baited *P. velutina* systems. Unless otherwise indicated, data presented are the means of 3–10 replicates with the standard error of the mean.

## 3. Results

### *3.1. Effect of inoculum and soil nutrient status on development of P. velutina mycelial systems*

On all soils, initial outgrowth from inoculum wood blocks precolonized on NA or EA was as dense, fine white hyphae extending radially with a regular

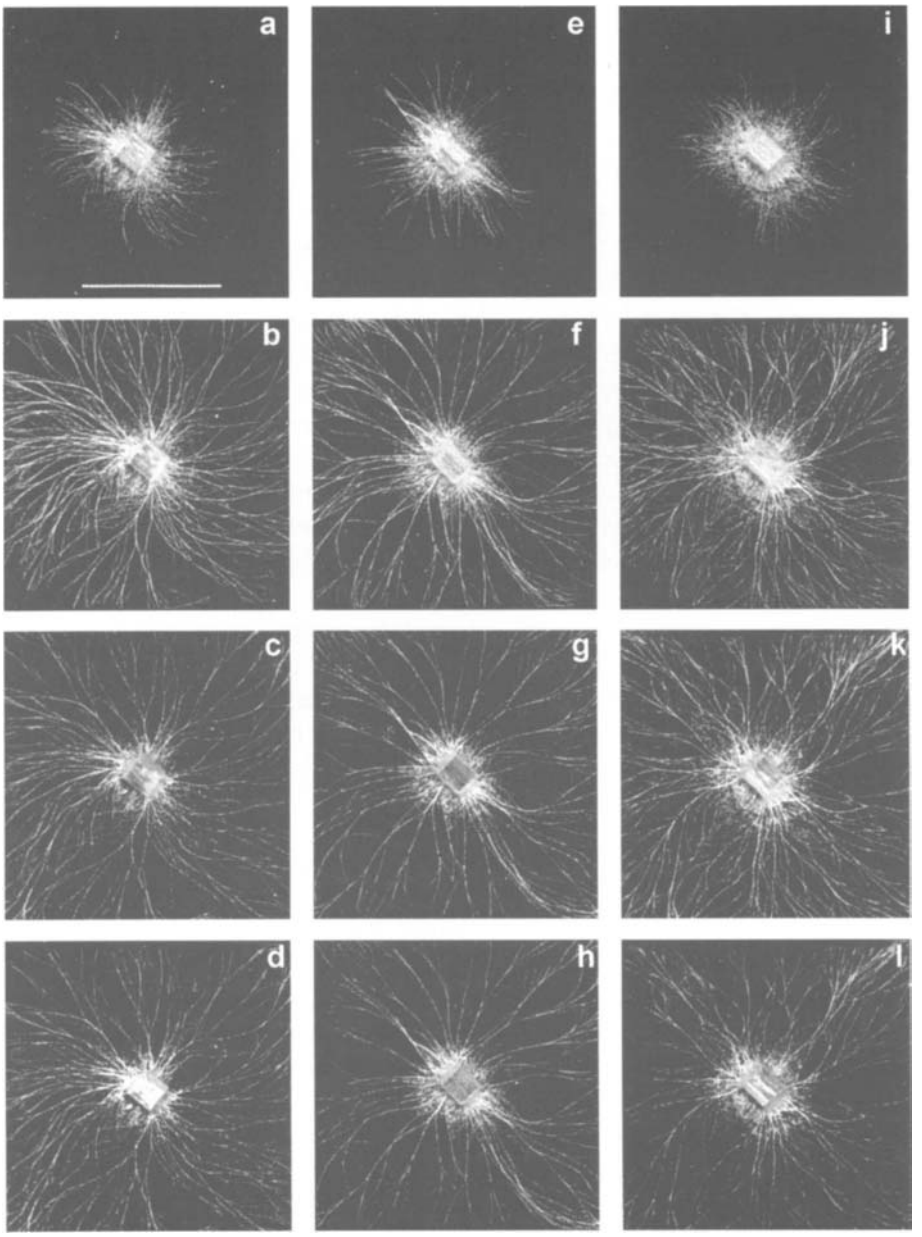


Fig. 1. Digital images of mycelial systems of *P. velutina* grown from noble agar inocula on unsterile 'dilute' soils of different relative nutrient regimes (RNRs) after 11 (a, e, i), 19 (b, f, j), 29 (c, g, k) and 44 days (d, h, l). Soils were either unamended (RNR0.5, a–d), or 'amended' with 20 mM (RNR1, e–h) or 200 mM $NH_4K_2PO_4$ (RNR10, i–l). Scale bar = 10 cm.

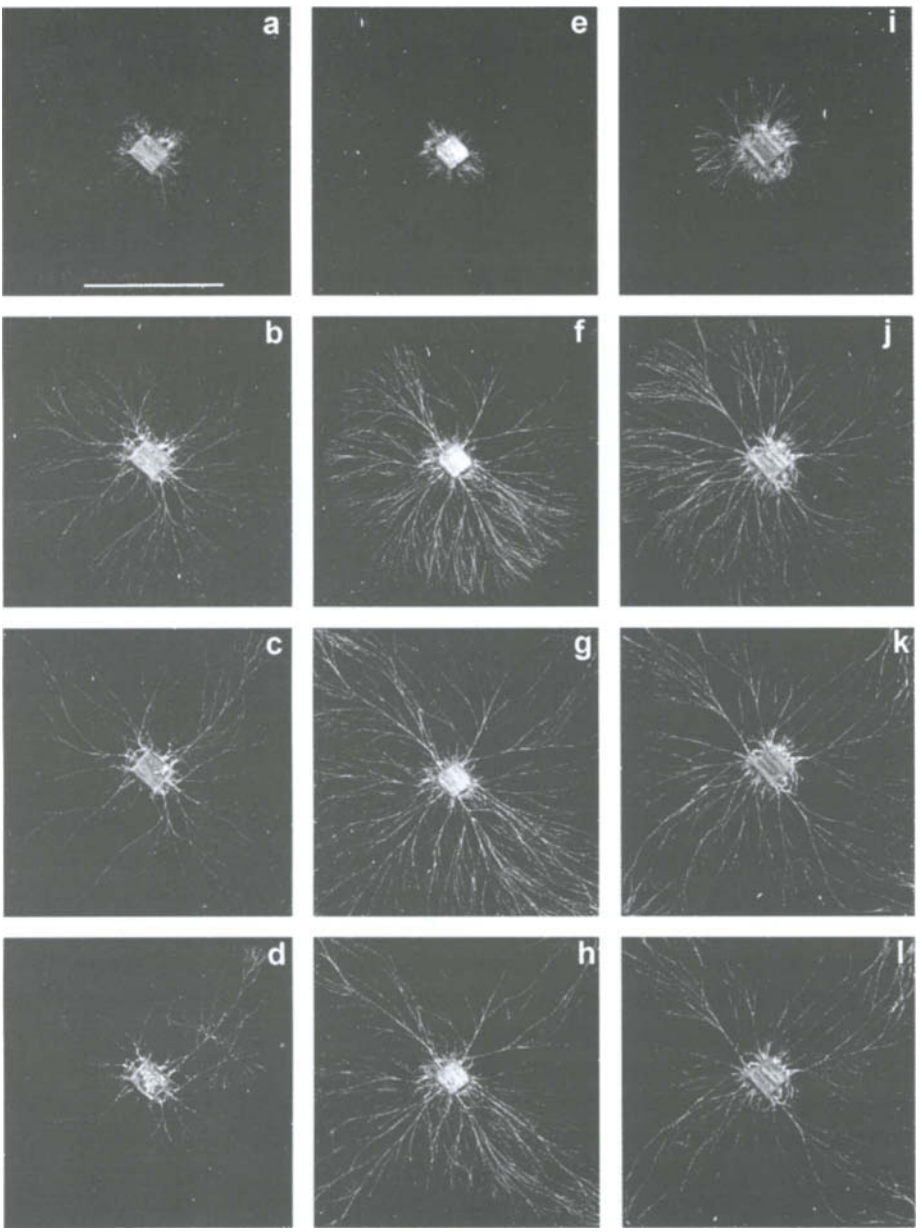


Fig. 2. Digital images of mycelial systems of *P. velutina* grown from enriched agar inocula on unsterile 'dilute' soils of different relative nutrient regimes (RNRs) after 11 (a, e, i), 19 (b, f, j), 29 (c, g, k) and 44 days (d, h, l). Soils were either unamended (RNR0.5, a–d), or 'amended' with 20 mM (RNR1, e–h) or 200 mM $NH_4K_2PO_4$ (RNR10, i–l). Scale bar = 10 cm.

colony margin. Within 11 days development of cords was evident behind the growing front, and the system margins became less regular (Fig. 1a, e, i and Fig. 2a, e, i). The most obvious effects of soil RNR were evident after 11 days at the system margins (Fig. 3). Systems developing from NA inocula had a greater number of discrete hyphae (i.e., greater space filling) at the system margin on RNR0.5 and RNR10 than on RNR1 (Fig. 3a–c). Moreover, with increasing RNR, cords became finer with more compact search fronts (Fig. 3a–c). By contrast, in systems developing from EA inocula both the density of discrete hyphae and discrete cord development increased with increasing RNR (Fig. 3d–f).

From both NA and EA inocula, systems continued to develop as discrete cords, although the latter had fewer fine hyphae close to the inoculum, a trend which continued throughout the experiment (Figs. 1 and 2), even though with time some regression of these fine hyphae occurred. From NA inocula, in most cases, the colony margin reached the edge of the soil trays by 19 days (Fig. 1b, f, j), whereas systems developing from EA inocula extended more slowly (Fig. 2b, f, j). Between 29 and 44 days, there was evidence of a system-wide regression of fine mycelium, leaving a network of discrete mycelial cords on the soil trays (Figs. 1 and 2). While mycelial systems developing from EA inocula

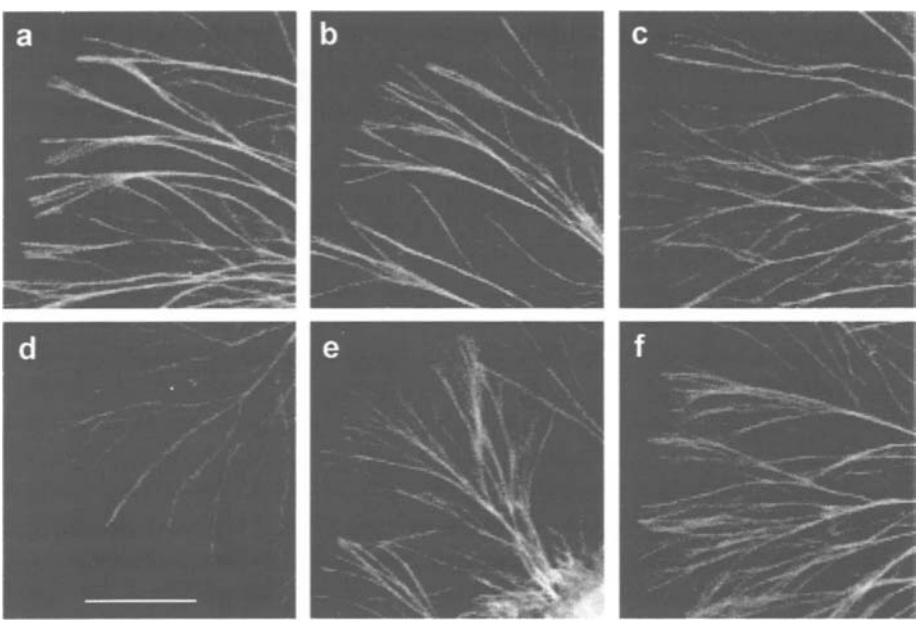


Fig. 3. Digital images showing the foraging fronts of 11-day old mycelial systems of *P. velutina* grown from noble agar (a–c) or enriched agar inocula (d–f) on unsterile 'dilute' soils of different relative nutrient regimes (RNRs). Soils were either unamended (RNR0.5, a, d), or 'amended' with 20 mM (RNR1, b, e) or 200 mM $NH_4K_2PO_4$ (RNR10, c, f). Scale bar = 2 cm.

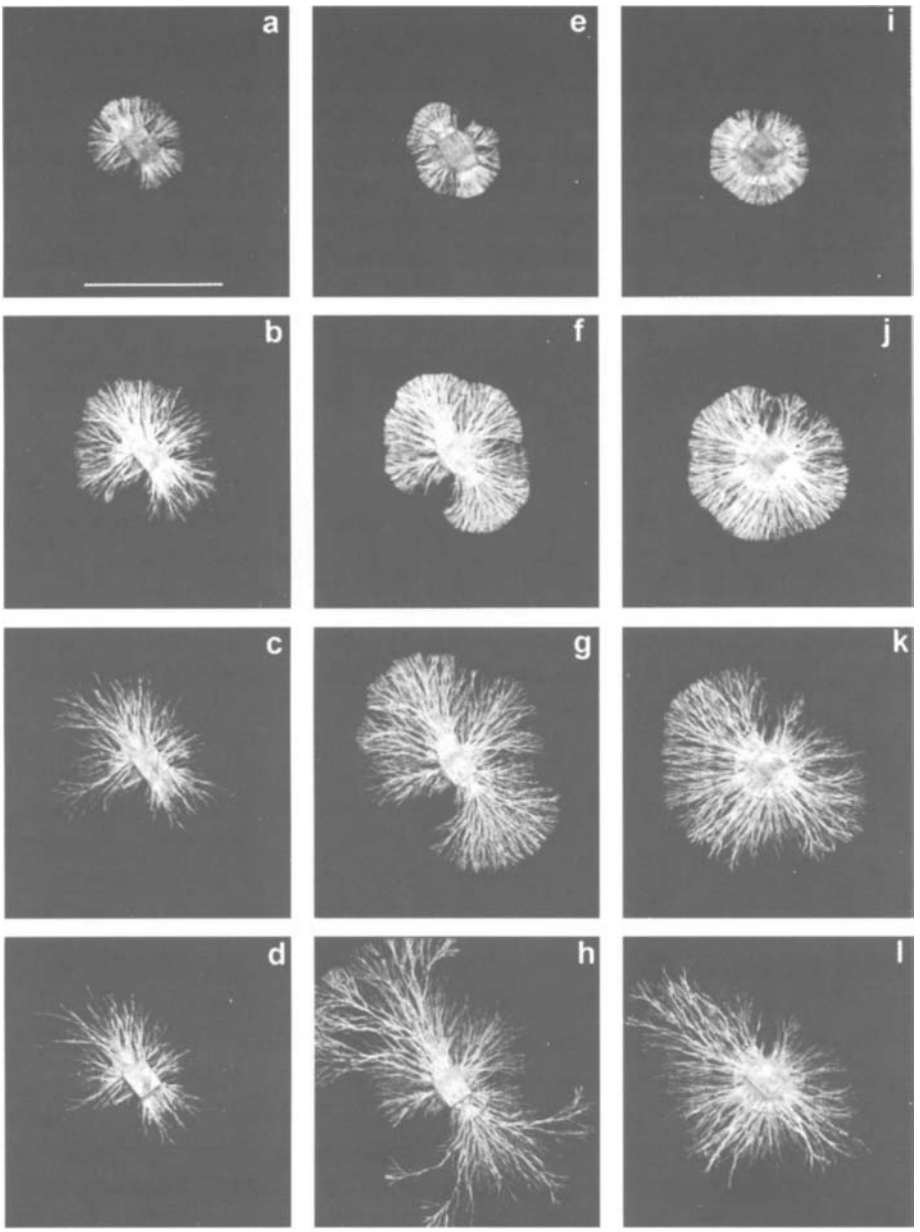


Fig. 4. Digital images of mycelial systems of *H. fasciculare* grown on unsterile 'dilute' soils of different relative nutrient regimes (RNRs) after 11 (a, e, i), 19 (b, f, j), 29 (c, g, k) and 44 days (d, h, l). Soils were either unamended (RNR0.5, a–d), or 'amended' with 20 mM (RNR1, e–h) or 200 mM $NH_4K_2PO_4$ (RNR10, i–l). Scale bar = 10 cm.

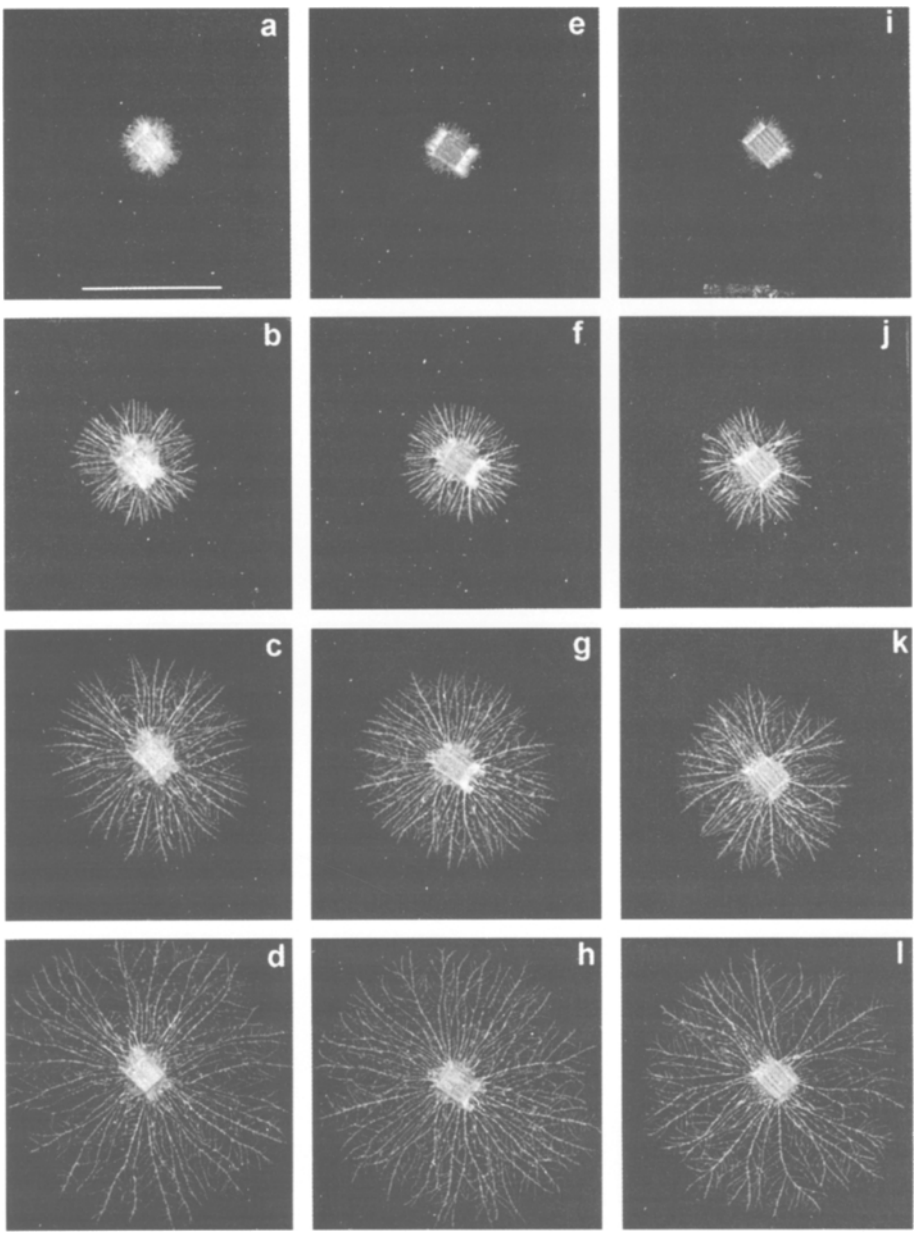


Fig. 5. Digital images of mycelial systems of *Pha. impudicus* grown on unsterile 'dilute' soils of different relative nutrient regimes (RNRs) after 11 (a, e, i), 19 (b, f, j), 29 (c, g, k) and 44 days (d, h, l). Soils were either unamended (RNR0.5, a–d), or 'amended' with 20 mM (RNR1, e–h) or 200 mM $NH_4K_2PO_4$ (RNR10, i–l). Scale bar = 10 cm.

were generally more diffuse with finer cords than those from NA inocula, there was no obvious effect of the soil RNR on overall system form for either NA or EA inocula (Figs. 1 and 2).

### *3.2. Effect of soil nutrient status on development of H. fasciculare and Pha. impudicus mycelial systems*

Like *P. velutina*, on all soils, initial outgrowth of *H. fasciculare* and *Pha. impudicus* was as a dense, fine white mycelium, with cord development evident within 11 days (Figs. 4 and 5). Between 11 and 19 days, *H. fasciculare* on RNR0.5 had a more irregular colony margin with less space filling than on RNR1 and RNR 10, and cords were finer with increasing RNR (Fig. 6). Between 19 and 29 days regression of fine mycelium close to the inoculum occurred in *H. fasciculare* systems (Fig. 4c, g, k). Surface growth of *H. fasciculare* was arrested on the surface of soil RNR0.5 after 29 days (Fig. 4c). This was coincident with hyphae penetrating the soil and continuing to grow at the soil/Perspex interface (*P. velutina* and *Pha. impudicus* grew only on the upper soil surface). On RNR1 and RNR10 *H. fasciculare* continued to grow on the upper surface of the soil for up to 44 days (Fig. 4h, l) although parts of the

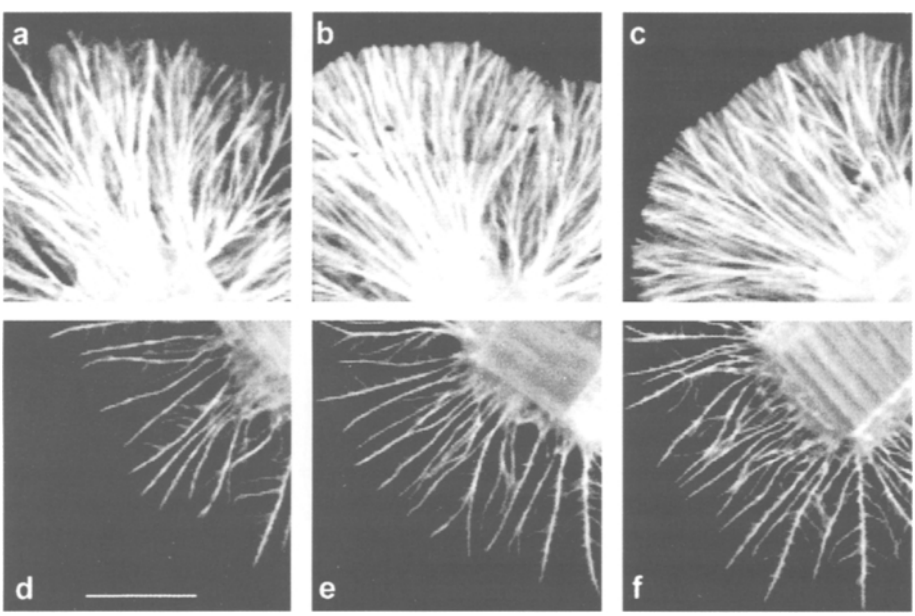


Fig. 6. Digital images showing the foraging fronts of 19-day old mycelial systems of *H. fasciculare* (a–c) and *Pha. impudicus* (d–f) on unsterile 'dilute' soils of different relative nutrient regimes (RNRs). Soils were either unamended (RNR0.5, a, c), or 'amended' with 20 mM (RNR1, b, e) or 200 mM $NH_4K_2PO_4$ (RNR10, c, f). Scale bar = 2 cm.

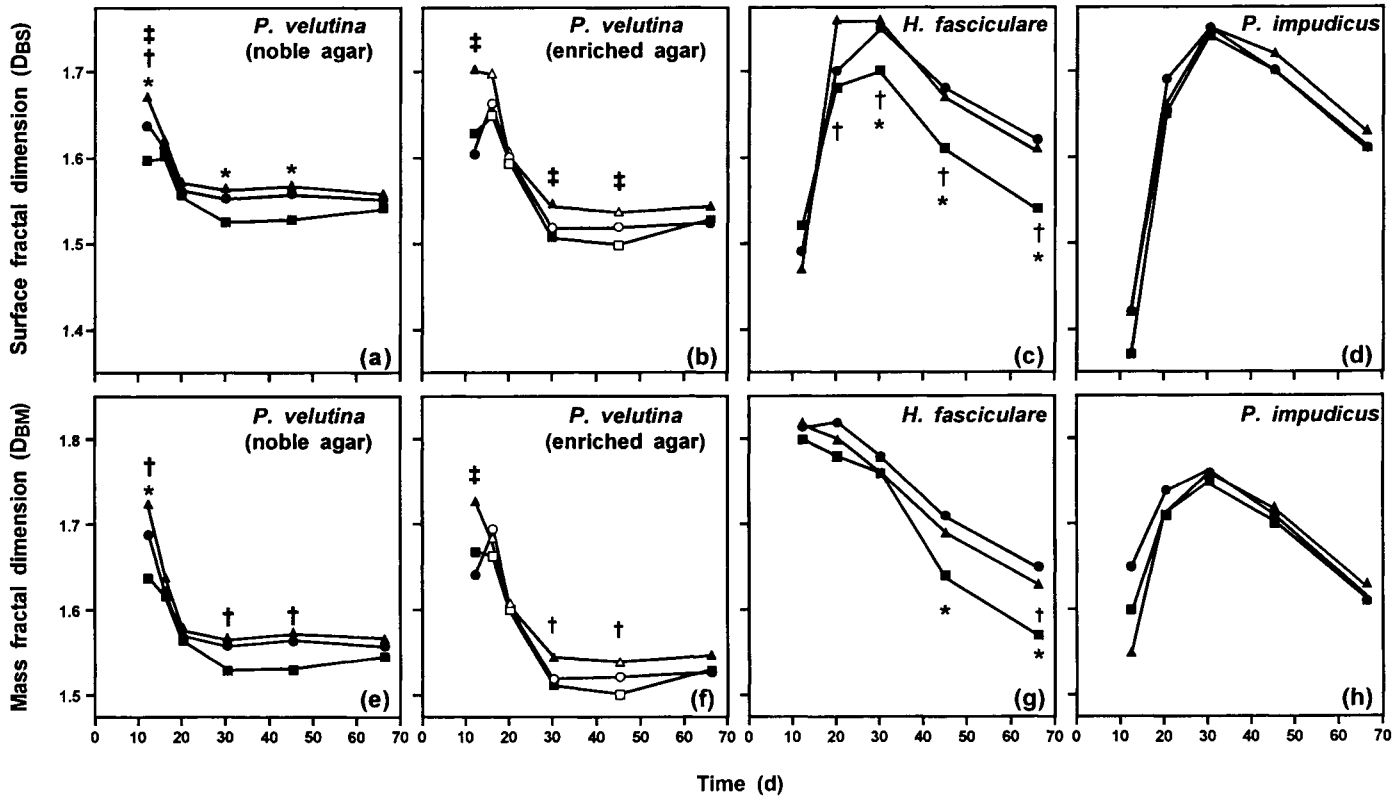


Fig. 7. Surface (a–d) and mass (e–h) fractal dimensions of mycelial systems of *P. velutina* (a, b, e, f), *H. fasciculare* (c, g) and *Pha. impudicus* (d, h) grown on unsterile 'dilute' soils of different relative nutrient regimes (RNRs). Soils were either unamended (RNR0.5, ■), or 'amended' with 20 mM (RNR1, ●) or 200 mM (RNR10, ▲) $NH_4K_2PO_4$. One-way ANOVA and LSD tests indicated significant ($P \leq 0.05$) differences at particular times between means (* RNR0.5 vs. RNR1, † RNR0.5 vs. RNR10, ‡ RNR1 vs. RNR10). Open symbols (b, f) indicate that the fractal dimensions of enriched agar *P. velutina* systems (b, f) differed significantly ($P \leq 0.05$) from noble agar *P. velutina* systems (a, d) of the same RNR at particular times. Error bars omitted for clarity; the standard error ranged from 1 to 7% of the mean of three to six replicates.

system margin did penetrate to the lower soil surface. Unlike *H. fasciculare* or *P. velutina*, systems of *Pha. impudicus* showed no differential response to soil RNR throughout the experiment (Figs. 5 and 6d–f).

### *3.3. Effects of soil and inoculum nutrient status on fractal dimensions*

Fractal dimensions were often greater with greater RNR for *P. velutina* and *H. fasciculare*, although it was not always possible to detect a significant ($P \leq 0.05$) difference between all three soil RNRs (Fig. 7a–c, e–g). There was no significant ($P > 0.05$) effect of soil RNR on fractal dimensions in systems of *Pha. impudicus* (Fig. 7d, h).

Regardless of whether inocula were pre-colonised on NA or EA, surface ($D_{BS}$) and mass ($D_{BM}$) fractal dimensions of *P. velutina* were greatest between 11 and 15 days, declined rapidly between 15 and 29 days, and remained relatively stable thereafter up to 67 days (Fig. 7a, b, e, f). For *H. fasciculare*,

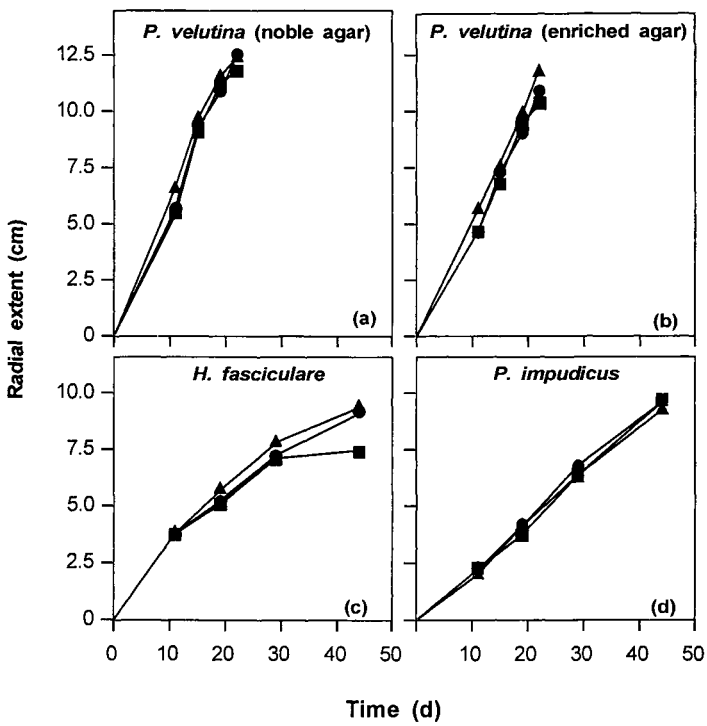


Fig. 8. Change with time in radial extent of mycelial systems of *P. velutina* (a, b), *H. fasciculare* (c) and *Pha. impudicus* (d) grown on unsterile 'dilute' soils of different relative nutrient regimes (RNRs). Soils were either unamended (RNR0.5, ■), or 'amended' with 20 mM (RNR1, ●) or 200 mM (RNR10, ▲) $NH_4K_2PO_4$. One-way ANOVA indicated there were no significant ($P > 0.05$) differences between means at particular times. Error bars omitted for clarity; the standard error ranged from 2 to 29% of the mean of three to six replicates.

$D_{BM}$ was greatest after 11 days (Fig. 7g), while $D_{BS}$ took 18 days longer to reach its greatest value (Fig. 7c). $D_{BS}$ and $D_{BM}$ peaked at 29 days in systems of *Pha. impudicus* (Fig. 7d, h). Unlike *P. velutina,* both $D_{BM}$ and $D_{BS}$ did not stabilise in systems of *H. fasciculare* and *Pha. impudicus* during 67 days (Fig. 7).

For systems of *P. velutina* grown from both NA and EA inocula, there were significant ($P < 0.05$) effects of soil RNR on fractal dimension at some times though not by the end of the experiment (67 days; Fig. 7a, b, e, f). Interestingly, it was not possible to detect significant soil RNR effects ($P > 0.05$) during the steep decline in $D_{BS}$ and $D_{BM}$ between 15 and 29 days (Fig. 7a, b, e, f). This decline appeared to be delayed in systems developed from NA compared to EA inocula, reflected in significantly higher $D_{BS}$ and $D_{BM}$ on day 15 in the latter

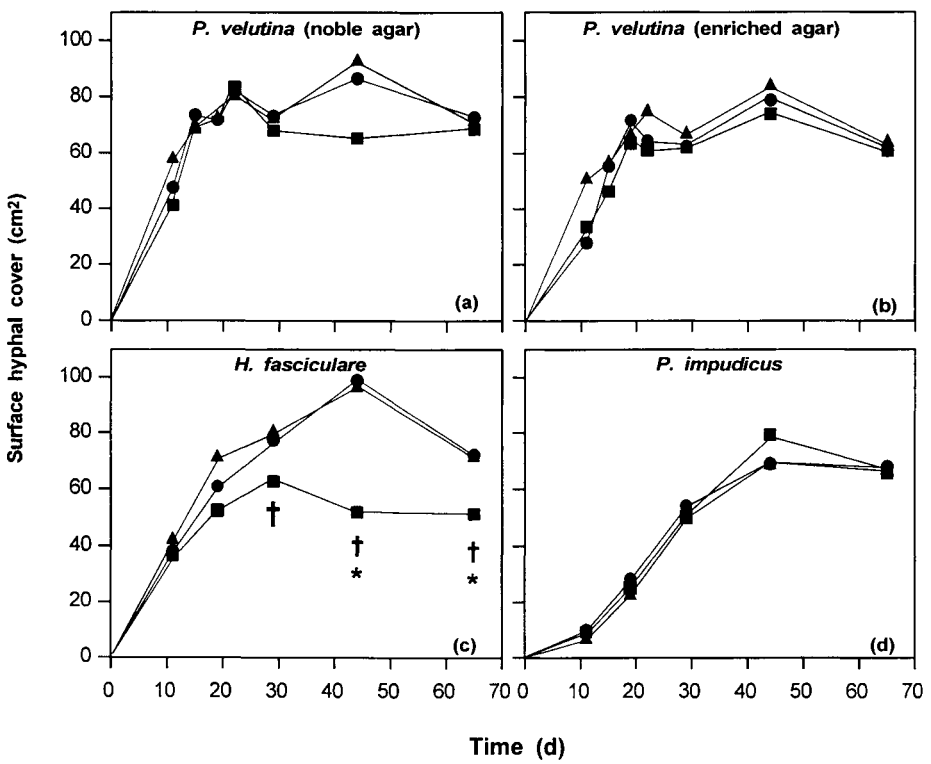


Fig. 9. The change with time of surface hyphal cover of mycelial systems of *P. velutina* (a, b), *H. fasciculare* (c) and *Pha. impudicus* (d) grown on unsterile 'dilute' soils of different relative nutrient regimes (RNRs). Soils were either unamended (RNR0.5, ■), or 'amended' with 20 mM (RNR1, ●) or 200 mM (RNR10, ▲) $NH_4K_2PO_4$. One-way ANOVA and LSD tests indicated significant ($P \leq 0.05$) differences at particular times between means (* RNR0.5 vs. RNR1, † RNR0.5 vs. RNR10). Error bars omitted for clarity; the standard error ranged from 3 to 36% of the mean of three to six replicates.

(cf. Fig. 7a and b, e and f). Thereafter, fractal dimensions tended to be lower in systems developed from EA inocula, although this was not always significant.

### *3.4. Effects of soil and inoculum nutrient status on radial extension and hyphal cover*

In general, initially, both radial extent (Fig. 8) and surface hyphal cover (Fig. 9) increased linearly with time in cord systems of all three fungi, the rate of

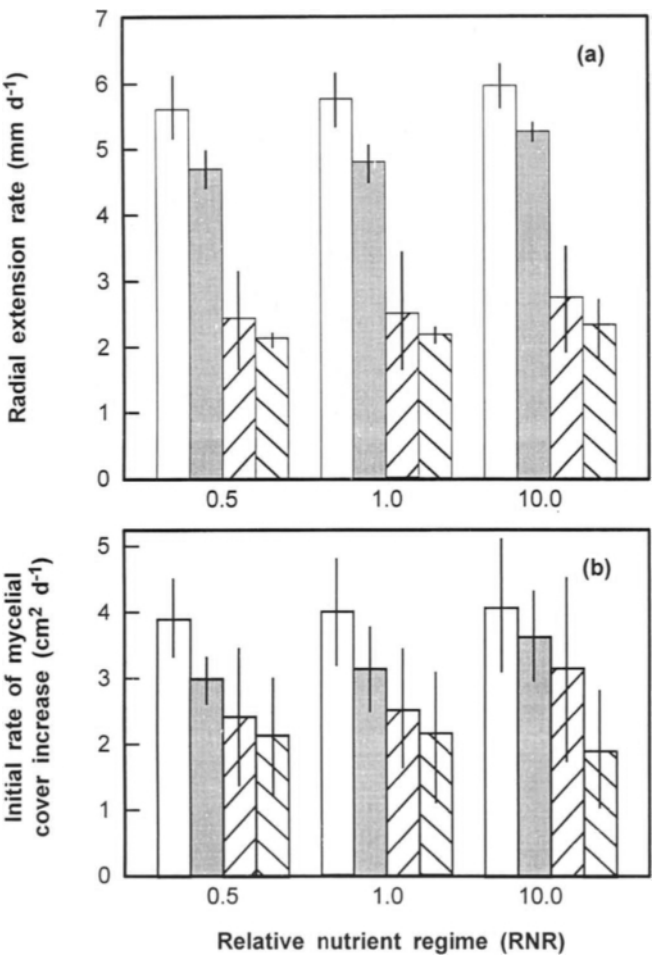


Fig. 10. Initial radial extension (a) and mycelial cover increase (b) rates of mycelial systems of *P. velutina* (0–19 days) developed from noble (□) or enriched (shaded) agar inocula, *H. fasciculare* (0–29 days (diagonal from bottom left to top right)) and *Pha. impudicus* (0–44 days (diagonal from top left to bottom right)). Mycelial systems developed on an unsterile 'dilute' soil which was either unamended (RNR0.5), or 'amended' with 20 mM (RNR1) or 200 mM (RNR10) $NH_4K_2PO_4$. Data presented are regression coefficients determined from results presented in Fig. 8Fig. 9 with 95% confidence intervals.

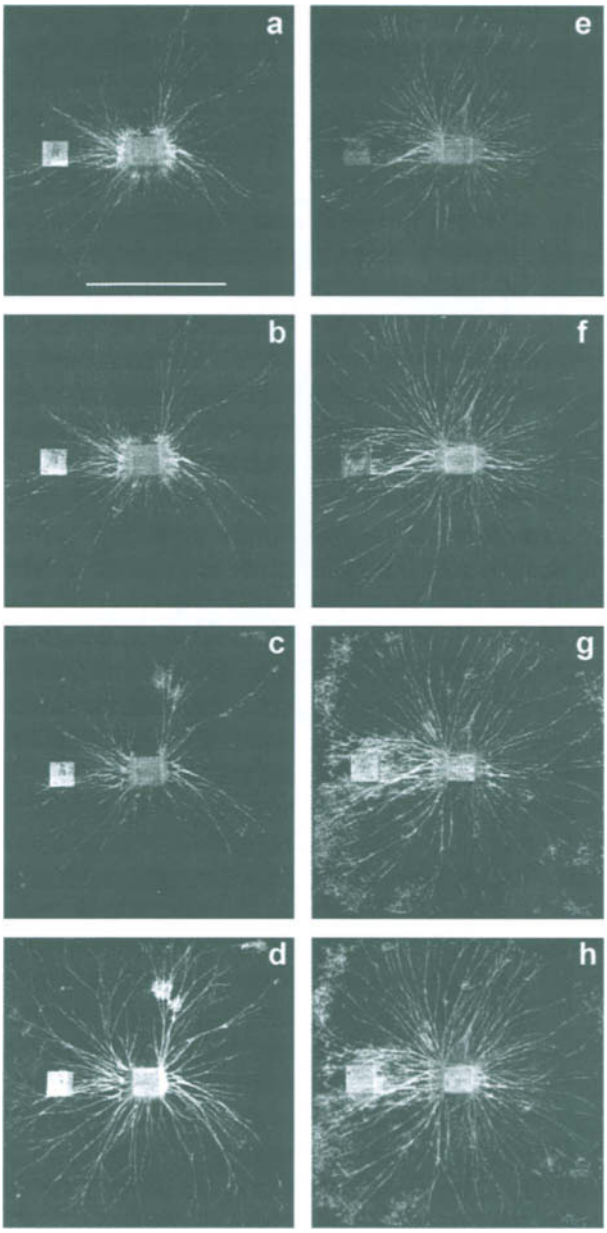


Fig. 11. Digital images of mycelial systems of *P. velutina* grown from 9-week old malt agar inocula on unsterile 'dilute' soil after 18 (a, e), 26 (b, f), 42 (c, g) and 63 days (d, h). Systems were supplied with control Perspex (a–d) or fresh wood baits (e–h) after 8 days. Scale bar = 10 cm.

increase in hyphal cover declining with time (Fig. 9). The only exception was *H. fasciculare* on RNR0.5 which penetrated the soil surface after 19 days (Fig. 8cFig. 9c), resulting in an apparent premature decline in system development. *P. velutina* extended more rapidly than *H. fasciculare* and *Pha. impudicus* (Fig. 8), while the greatest surface hyphal cover was achieved by *H. fasciculare* on RNR10 after 44 days (Fig. 10). For each inoculum type, no significant effect ($P > 0.05$) could be detected between means for radial extent or surface hyphal cover at particular times except for *H. fasciculare* on RNR0.5 (Figs. 8 and 9). However, regression analysis revealed that the initial rates of radial extent for NA *P. velutina* systems were significantly ($P \leq 0.05$) higher than for EA systems on all soil RNRs (Fig. 10a). There were similar, though not significant ($P > 0.05$), differences in surface hyphal cover (Fig. 10b).

### *3.5. Effect of new wood 'bait' resources on development of mycelial systems of P. velutina*

Full details have been published by Wells et al. (1997). Briefly, adding Perspex 'baits' had no discernible effect on development at the border, or within the interior of mycelial systems (Fig. 11a, b). By contrast, within 5 days of adding wood baits the margins of mycelial systems appeared more regular, with more diffuse foraging fronts than in Perspex-baited systems (cf. Fig. 11a and e), due to an increase in density of discrete hyphae at the foraging mycelial front in wood-baited systems (Fig. 12a, b). From 26 to 63 days, mycelial 'patches' comprising discrete, fine, and highly branched hyphae extending radially from their points of origin developed from previously consolidated cords in both Perspex- and wood-baited systems (Fig. 12c), though more frequently (Fig. 11c, d, g, h and Fig. 13) and with greater hyphal area cover in the latter. However, there was no significant effect ($P > 0.05$) on mass ($D_{BM}$) or surface fractal ($D_{BS}$) dimensions or of total hyphal area cover of *entire* systems. Representative patches (e.g., Fig. 12c) in 42-day old wood-baited systems had a $D_{BM}$ of

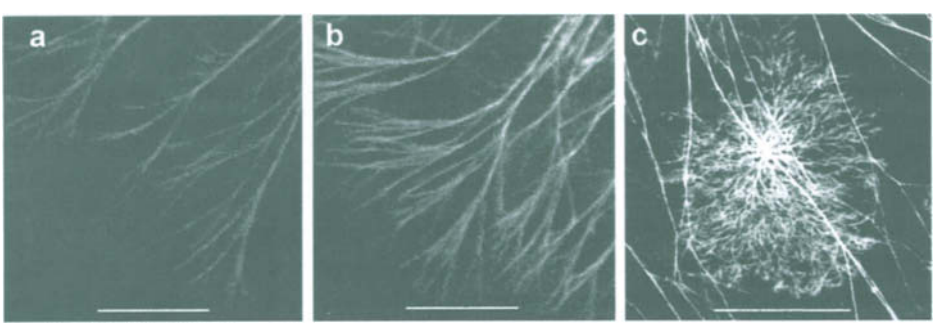


Fig. 12. Digital images showing the foraging fronts of 18-day old Perspex-baited (a) or wood-baited (b) mycelial systems, and a mycelial 'patch' (c) in a 42-day old wood-baited system of *P. velutina* on unsterile 'dilute' soil. Scale bar = 2 cm in (a) and (b) and 1 cm in (c).

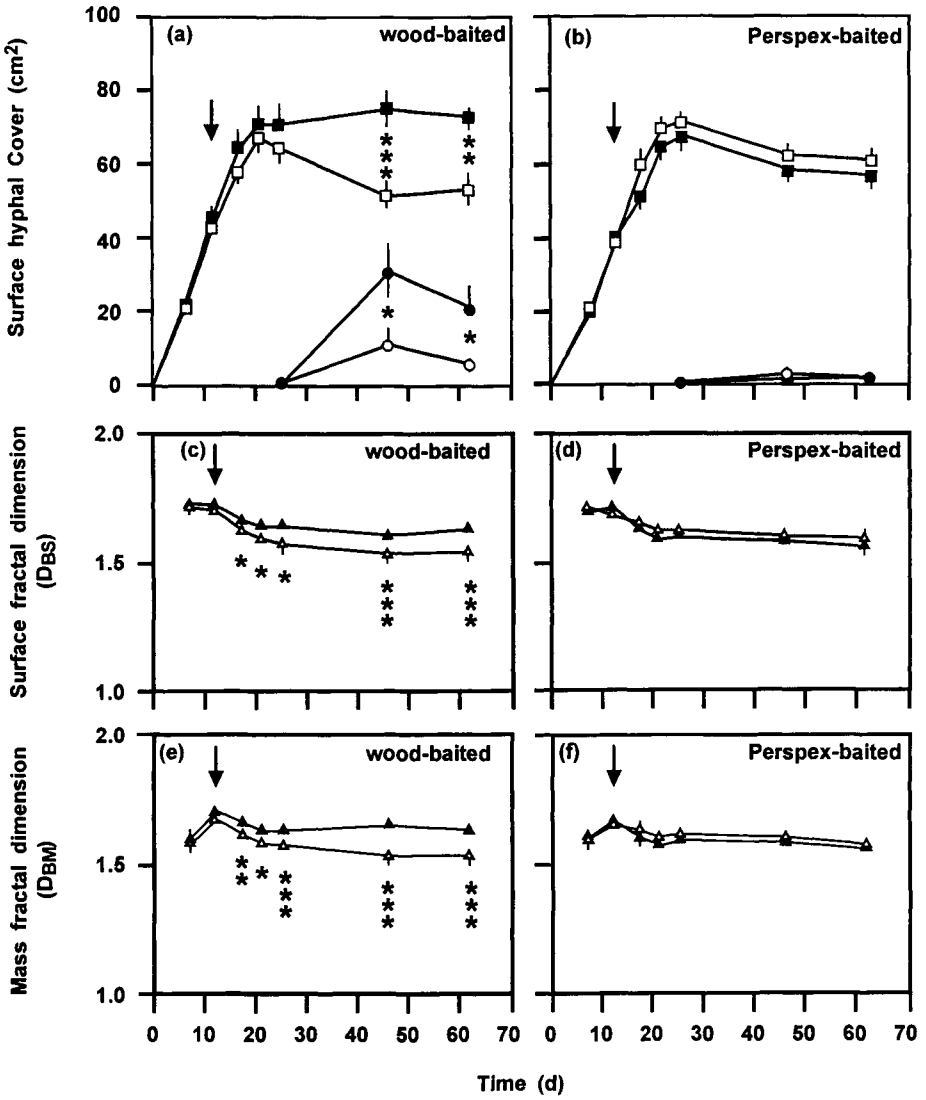


Fig. 13. Changes with time in total hyphal cover (■ □) and 'patch' cover (● ○) in wood-baited (closed symbols) and Perspex-baited systems (open symbols) (a,b); surface (c, d) and mass (e, f) fractal dimensions in 'baited' (▲) and unbaited sectors (△) of wood-baited (c, e) and Perspex-baited (d, f) mycelial systems of *P. velutina* grown on unsterile 'dilute' soil. Bars show the standard error of the mean. Arrow indicates the time of addition of baits. Paired t-tests indicated significant differences ($* P \leq 0.05$, $* * P \leq 0.01$, $* * * P \leq 0.001$) between means at particular times. Modified from Wells et al. (1997).

$1.77 \pm 0.01$ and $D_{BS}$ of $1.80 \pm 0.00$, respectively, 4% and 5% higher than whole system fractal dimensions at this time. Radial extension rates did not differ significantly ($P > 0.05$) between baited and unbaited sectors of wood-baited cord systems.

While *total* hyphal cover declined progressively in both wood- and Perspex-baited systems between 26 and 63 days (data not shown), after 42 days, wood-baited systems maintained hyphal cover in the baited sector of soil trays at the expense of mycelium in the unbaited sector (Fig. 13a). Patch development was also greatest in the baited sector of wood-baited systems, approximately 80% of the difference in total hyphal cover being attributable to patch cover between 42 and 63 days (Fig. 13a). $D_{BM}$ and $D_{BS}$ values were significantly ($P \leq 0.05$) higher in the baited sector of wood-baited cord systems only 5 days after the addition of wood baits (Fig. 13c, e). By contrast, Perspex-baited systems showed no significant ($P > 0.05$) polarity in hyphal/patch cover or fractal dimensions between 'baited' and 'unbaited' sectors throughout the experiment (Fig. 13b, d, f).

## 4. Discussion

Major differences in mycelial morphology were evident between the fungal species examined, and development in general was consistent with previous studies (Donnelly, 1995; Donnelly et al., 1995). Mycelial growth pattern was altered by both soil nutrient concentration and inoculum nutrient status, the extent depending upon treatment combinations and species.

A common feature of mycelial development from colonised wood inocula onto soil for many cord-formers, is the initial emergence of a diffuse mycelium, the foraging front (Donnelly, 1995). This is indicated by high mass fractal values early on in development, demonstrated by *P. velutina* and *H. fasciculare* in this study. Differences in early development are visually apparent but difficult to quantify using traditional geometry, however, comparison of surface and mass fractal values show that *P. velutina* was mass fractal soon after emerging from inocula, whereas *H. fasciculare* was initially border fractal. *H. fasciculare* developed dense mycelial fans with regular margins which coalesced, and *P. velutina* extended as a more open system with regular and aggregated marginal fans.

Species which develop as mass fractal mycelial systems may differ in the pattern formed and patterns may change with time. For example, the low fractal values of *Pha. impudicus* which later increased, compared to the initially high fractal values of *P. velutina* which later declined. This is attributable to *Pha. impudicus* developing as an aggregated system with regular, pinnate branching which with time formed tangential anastomoses behind the foraging front. The effect of this regular network was to substantially increase the mass fractal component of the interior of the system. By contrast, the marginal fans of *P. velutina* were wider with irregularly branched cord aggregations forming much further back from the growing front. Mycelial development in *P. velutina* therefore has a much stronger radial component than *Pha. impudicus*, and the

decline in fractal dimension of *P. velutina* indicated the development of cord aggregates behind the foraging front as the mycelium extended its area of occupation.

Mycelial pattern has also been shown to be related to mycelial extension rate, as explained in the introduction; there often seems to be an inverse relation between fractal dimension and extension rate reflecting contrasting foraging strategies (Donnelly et al., 1995). In this study *P. velutina* extended faster than both *H. fasciculare* and *Pha. impudicus*, which may be attributable to *P. velutina* expending effort to explore areas rapidly rather than either producing a broad margin (*H. fasciculare*) or a highly anastomosed system (*Pha. impudicus*). The establishment of contrasting interspecific mycelial patterns and growth rates has been attributed to differing ecological strategies for the capture of resources which differ in both spatial and temporal distribution (Dowson et al., 1988a, 1989b). The broad marginal foraging front of *H. fasciculare* is an effective strategy for capture of abundant, less dispersed resources; patterns typically exhibited by *P. velutina* are effective for the capture of widely dispersed resources; and the extensive persistent mycelial system of *Pha. impudicus*, with wide diameter cords and large gaps between, effective for capture of temporally dispersed resources. Field observations of both naturally and artificially established cord systems and the nature of resources colonised support these ideas (Thompson and Rayner, 1983; Dowson et al., 1988b).

With increasing soil enrichment, mycelial systems of *H. fasciculare* comprised finer cords and were more regularly margined with greater space-filling (Fig. 6). This has been observed previously with *S. caerulea* where enrichment by N or P generally led to more plane-filled systems compared to controls (Donnelly and Boddy, 1998). It was suggested that this morphological change may represent a switch in primary function from exploration for carbon resources to mineral nutrient uptake. *P. velutina*, though exhibiting attributes of a phalangeal strategy, did increase space-filling with increase in soil nutrient concentration, again presumably a response enabling greater sequestration of soil nutrients. The lack of sensitivity of *Pha. impudicus* to external soil nutrients may in part be due to the thick cords typically produced by this species, which 'insulate' (sensu Rayner, 1991) systems from the environment enabling persistence within a hostile domain. This reduced sensitivity has also been demonstrated during interaction with *S. caerulea*, whereby the fractal dimension of *Pha. impudicus* mycelium growing through mycelial territory of *S. caerulea* was not significantly altered (Donnelly, 1995). Thus a uniform mass fractal mycelium of *Pha. impudicus* is produced despite a range of both abiotic and biotic factors.

That it is not only extra-resource nutrient concentration but also within resource nutrient status that affects foraging is evident from the fact that *P. velutina* exhibited greater space-filling of soil when extending from poorer resources, presumably reflecting the need to obtain additional nutrients from

soil. The production of patches is a more extreme response to demand for nutrients occurring on dilute soil, predominantly when additional carbon resources were available. The striking resemblance of these patches to entire mycelial systems (Fig. 12c) emphasises the self similar nature of mycelial networks. The importance of discrete organic resources to these fungi has been demonstrated previously by the often dramatic changes in allocation of mycelial biomass on encountering new resources (Dowson et al., 1986, 1988a; Wells et al., 1997).

This paper has highlighted the use of fractal analysis in studies of mycelium in soil. A major benefit of employing fractal geometry as a descriptor of mycelial morphology is that its sensitivity to treatments is more easily detected. For example, polarity was detectable far sooner using fractal dimension than hyphal area cover. Effectively, it is a statistical measure which normalises and reduces the variance of data sets. By displaying data quantitatively it emphasises some differences which might not be discernible visually. For example, with *P. velutina* there were initially differences in fractal dimension on soils with different nutrient concentrations, which then became undetectable and later re-emerged. Being able to partition fractal dimension for different parts of systems, whether technically permissible or not, is valuable. Doing this allowed detection of polarising effects of adding wood baits to systems of *P. velutina*, and quantifying foraging behaviour in patches compared with the overall system. Differences in fractal dimension at different places within a colony highlight the danger of trying to obtain a single quantitative descriptor of a system.

However, different descriptors provide complementary information. This is illustrated by comparison of fractal dimension plots (Fig. 7) with those for hyphal area cover (Fig. 9), which reveals no correlation between the two, emphasising that these descriptors are quantifying different aspects of mycelial distribution. Unlike these two measures, which provide information on space filling, radial extension quantifies how quickly a mycelium reaches new areas for exploration. The range of quantitative descriptors should thus be used in conjunction to obtain the whole picture. While quantitative descriptors are attractive because of their objectivity, they cannot completely replace visual observation. This point is borne out here by *Pha. impudicus* and *H. fasciculare* which often have broadly similar values for fractal dimension, surface hyphal cover and extension rate, yet very different branching patterns (cf. Figs. 4 and 5). Further, visual observation is necessary to detect interesting features within systems, such as the patches, that require further analysis.

The use of model soil systems, image processing and various quantitative measures described in this paper have considerably enhanced our understanding of the development of mycelial systems in soil, and will undoubtedly be of immense value in future studies. However, it is important to note that so far only small (0.06 $m^2$) short-lived ( $< 1$ year) systems have been examined which only

represent the beginning of development of a foraging mycelial system compared with naturally established systems (often many $m^2$ and many years old). Further, to facilitate image capture and subsequent analysis, mycelial growth was restricted to the soil surface, allowing a larger component to develop in two dimensions than would usually occur naturally. This may artificially increase the frequency of anastomoses and alter the system's responsiveness to resources. Compressing soil will also alter soil water relations, nutrient movement, etc. Thus, analysis of 3-D soil systems must be a future aim.

## Acknowledgements

This work was partly funded by the Natural Environment Research Council (GR3/10319).

## References

Abdalla, S.H.M., Boddy, L., 1996. Effect of soil and litter type on outgrowth patterns of mycelial systems of *Phanerochaete velutina*. FEMS Microbiol. Ecol. 20, 195–204.

Baar, J., Comini, B., Elferink, M.O., Kuyper, T.W., 1997. Performance of four ectomycorrhizal fungi on organic and inorganic nitrogen sources. Mycol. Res. 101, 523–529.

Boddy, L., 1993. Saprotrophic cord-forming fungi: warfare strategies and other ecological aspects. Mycol. Res. 97, 641–655.

Bolton, R.G., Boddy, L., 1993. Characterisation of the spatial aspects of foraging mycelial cord systems using fractal geometry. Mycol. Res. 97, 762–768.

Cooke, R.C., Rayner, A.D.M., 1985. Ecology of Saprotrophic Fungi. Longman, London.

Crawford, J.W., Ritz, K., Young, I.M., 1993. Quantification of fungal morphology, gaseous transport and microbial dynamics in soil: an integrated framework utilising fractal geometry. Geoderma 56, 157–172.

Donnelly, D.P., 1995. Comparative physiology and ecology of mycelial cord growth of *Stropharia caerulea* and *Phanerochaete velutina*. PhD Thesis, University of Wales, Cardiff.

Donnelly, D.P., Boddy, L., 1997a. Development of mycelial systems of *Stropharia caerulea* and *Phanerochaete velutina* on soil: effect of temperature and water potential. Mycol. Res. 101, 705–713.

Donnelly, D.P., Boddy, L., 1997b. Resource acquisition by the mycelial-cord-former *Stropharia caerulea*: effect of resource quantity and quality. FEMS Microbiol. Ecol. 23, 195–205.

Donnelly, D.P., Boddy, L., 1998. Developmental and morphological responses of mycelial systems of *Stropharia caerulea* and *Phanerochaete velutina* to soil nutrient enrichment. New Phytol., in press.

Donnelly, D.P., Wilkins, M.F., Boddy, L., 1995. An integrated image analysis approach for determining biomass, radial extent and box-count fractal dimension of macroscopic mycelial systems. Binary 7, 19–28.

Dowson, C.G., Rayner, A.D.M., Boddy, L., 1986. Outgrowth patterns of mycelial cord-forming basidiomycetes from and between woody resource units in soil. J. Gen. Microbiol. 132, 203–211.

Dowson, C.G., Rayner, A.D.M., Boddy, L., 1988a. Foraging patterns of *Phallus impudicus*,

*Phanerochaete laevis* and *Steccherinum fimbriatum* between discontinuous resource units in soil. FEMS Microbiol. Ecol. 53, 291–298.

Dowson, C.G., Rayner, A.D.M., Boddy, L., 1988b. Inoculation of mycelial cord-forming basidiomycetes into woodland soil and litter: II. Resource capture and persistence . New Phytol. 109, 343–349.

Dowson, C.G., Rayner, A.D.M., Boddy, L., 1989a. Spatial dynamics and interactions of the woodland fairy ring fungus *Clitocybe nebularis*. New Phytol. 111, 699–705.

Dowson, C.G., Springham, P., Rayner, A.D.M., Boddy, L., 1989b. Resource relationships of foraging mycelial systems of *Phanerochaete velutina* and *Hypholoma fasciculare* in soil. New Phytol. 111, 501–509.

Fawcett, R.G., Collis-George, N., 1967. A filter-paper method for determining the moisture characteristics of soil. Aust. J. Exp. Agric. Anim. Husb. 7, 162–167.

Hitchcock, D., Glasbey, C.A., Ritz, K., 1996. Image-analysis of space-filling by networks—application to a fungal mycelium. Biotechnol. Tech. 10, 205–210.

Jones, C.L., Lonergan, G.T., Mainwaring, D.E., 1995. Acid–phosphatase positional correlations in solid-surface fungal cultivation—a fractal interpretation of biochemical differentiation. Biochem. Biophys. Res. Commun. 208, 1159–1165.

Kaye, B.H., 1989. Image analysis techniques for characterising fractal structure. In: Avnir, D. (Ed.), The Fractal Approach to Heterogenous Chemistry—Surfaces, Colloids, Polymers. Wiley, Chichester, UK, pp. 55–66.

Markx, G.H., Davey, C.L., 1990. Applications of fractal geometry. Binary 2, 169–175.

Mihail, J.D., Obert, M., Taylor, S.J., Bruhn, J.N., 1994. The fractal dimension of young colonies of *Macrophomina phaseolina* produced from microsclerotia. Mycologia 86, 350–356.

Mihail, J.D., Obert, M., Bruhn, J.N., Taylor, S.J., 1995. Fractal geometry of diffuse mycelia and rhizomorphs of *Armillaria* species. Mycol. Res. 99, 81–88.

Morse, D.R., Lawton, J.H., Dodson, M.M., Williamson, M.H., 1985. Fractal dimension of vegetation and the distribution of arthropod body lengths. Nature 314, 731–733.

Obert, M., Pfeifer, P., Sernetz, M., 1990. Microbial growth patterns described by fractal geometry. J. Bacteriol. 172, 1180–1185.

Patankar, D.B., Liu, T.C., Colman, T.A., 1993. Fractal model for the characterization of mycelial morphology. Biotechnol. Bioeng. 42, 571–578.

Pfiefer, P., Obert, M., 1989. Fractal basic concepts and technology. In: Avnir, D. (Ed.), The Fractal Approach to Heterogenous Chemistry—Surfaces, Colloids, Polymers. Wiley, Chichester, UK, pp. 11–43.

Rayner, A.D.M., 1991. The challenge of the individualistic mycelium. Mycologia 83, 48–71.

Rayner, A.D.M., Boddy, L., 1988. Fungal Decomposition of Wood: Its Biology and Ecology. Wiley, Chichester, UK.

Rayner, A.D.M., Powell, K.A., Thompson, W., Jennings, D.H., 1985. Morphogenesis of vegetative organs. In: Moore, D., Casselton, L.A., Wood, D.A., Frankland, J.C. (Eds.), Developmental Biology of Higher Fungi. Cambridge University Press, Cambridge, pp. 249–279.

Regalado, C.M., Crawford, J.W., Ritz, K., Sleeman, B.D., 1996. The origins of spatial heterogeneity in vegetative mycelia: a reaction diffusion model. Mycol. Res. 100, 1473–1480.

Richardson, L.F., 1961. The problem of contiguity: an appendix of statistics of deadly quarrels. Gen. Syst. Yearbook 6, 139–187.

Ritz, K., Crawford, J., 1990. Quantification of the fractal nature of colonies of *Trichoderma viride*. Mycol. Res. 94, 1138–1141.

Schmid, B., Harper, J.L., 1985. Clonal growth in grassland perennials: I. Density and pattern-dependent competition between plants with different growth forms. J. Ecol. 73, 793–808.

Smith, M.L., Bruhn, J.N., Anderson, J.B., 1992. The fungus *Armillaria bulbosa* is among the largest and oldest living organisms. Nature 356, 428–431.

Soddell, J.A., Seviour, R.J., 1994. A comparison of methods for determining the fractal dimension of colonies of filamentous bacteria. Binary 6, 21–31.

Thompson, W., 1984. Distribution, development and functioning of mycelial cord systems of decomposer basidiomycetes of the deciduous woodland floor. In: Jennings, D.H., Rayner, A.D.M. (Eds.), The Ecology and Physiology of the Fungal Mycelium. Cambridge University Press, Cambridge, pp. 185–215.

Thompson, W., Rayner, A.D.M., 1983. Extent, development and function of mycelial cord systems in soil. Trans. Br. Mycol. Soc. 81, 333–345.

Wells, J.M., Hughes, C., Boddy, L., 1990. The fate of soil-derived phosphorus in mycelial cord systems of *Phanerochaete velutina* and *Phallus impudicus*. New Phytol. 114, 595–606.

Wells, J.M., Boddy, L., Evans, R., 1995. Carbon translocation in mycelial cord systems of *Phanerochaete velutina* (DC: Pers.) Parmasto. New Phytol. 129, 467–476.

Wells, J.M., Donnelly, D.P., Boddy, L., 1997. Patch formation and developmental polarity in mycelial cord systems of *Phanerochaete velutina* on a nutrient-depleted soil. New Phytol. 136, 653–665.

Witten, T.A., Sander, L.M., 1981. Diffusion-limited aggregation, a kinetic critical phenomenon. Phys. Rev. Lett. 47, 1400–1403.

*Fractals in Soil Science*
Editors: Ya.A. Pachepsky, J.W. Crawford and W.J. Rawls
© 2000 Elsevier Science B.V. All rights reserved.


# The distribution of anoxic volume in a fractal model of soil

Cornelis Rappoldt [a,*], John W. Crawford [b]

[a] *Research Institute for Agrobiology and Soil Fertility (AB-DLO), PO Box 14, 6700 AA Wageningen, Netherlands*
[b] *Soil – Plant Dynamics Unit, Scottish Crop Research Institute, Invergowrie, Dundee DD2 5DA, UK*

Received 2 December 1997; accepted 28 September 1998

**Abstract**

A simple description of soil respiration is combined with a three-dimensional random fractal lattice as a model of soil structure. The lattice consists of gas-filled pores and soil matrix that is a combination of the solid phase and water. A respiration process is assumed to take place in the soil matrix. Oxygen transport occurs by diffusion in the gas-filled pores and, at a much slower rate, in the soil matrix. The stationary state of this process is characterized by the fraction of the matrix that has zero oxygen concentration, i.e., the anoxic fraction. The anoxic fraction of a three-dimensional lattice appears to be largely determined by the presence and distribution of pores that are not connected to the surface of the lattice. Local gradients in connected gas-filled pores play an insignificant role due to the enormous difference in diffusion coefficient between the gas-filled pores and the saturated soil matrix. Analytical and numerical results for the fractal model are compared with calculations for a dual-porosity model comprising spherical aggregates with a lognormal radius distribution. A one-dimensional fractal lattice and the dual-porosity model yield qualitatively similar predictions, suggesting an anoxic fraction that decreases exponentially with the square root of the local oxygen concentration. However, the anoxic fraction of a three-dimensional fractal lattice decreases much faster than exponentially, implying that large clumps of soil matrix are comparatively rare. We propose that this is due to aggregation of soil particles in more than a single dimension, which has important consequences for anaerobic processes in soil. The fractal model accounts for the geometrical implications of three dimensions. A lognormal radius distribution is essentially a one-dimensional structure model. © 1999 Elsevier Science B.V. All rights reserved.

*Keywords:* soil structure; fractal; diffusion; soil respiration; anoxic fraction; connectivity

* Corresponding author. E-mail: c.rappoldt@ab.dlo.nl

Reprinted from Geoderma 88 (1999)
© 1999 Elsevier Science B.V. All rights reserved

## 1. Introduction

Oxygen transport in soil is implicated in a number of important soil processes. In regions where oxygen is present, mineralization of soil organic matter, oxidation of organic pollutants and nitrification may take place. In regions of low oxygen concentration, a fraction of the microbial community is able to obtain oxygen through the reduction of nitrate that leads to the production of $N_2O$ and $N_2$. These gaseous products represent a loss of nitrogen to the soil–plant system, and the $N_2O$ is an important component of the greenhouse gases implicated in climate change (Houghton et al., 1990). There is considerable ignorance surrounding the spatial partitioning of aerobic and anaerobic processes in soil, and this in turn makes an important contribution to the inability to adequately predict turnover rates for nitrogen and organic matter directly from soil properties. A key role is played by soil structure.

Most models of the oxygen distribution in soil assume greatly simplified models of soil structure. Arah and Vinten (1995) reported huge differences in behavior between two structure models, a random pore model derived from the water retention characteristic, and a dual porosity model comprising discrete soil aggregates. In the latter model, it is assumed that the pore volume is divided between two characteristic scales that define the macropore and micropore space. The micropores are contained within spherical aggregates that are imbedded in a connected macropore matrix, and oxygen availability is assumed to be limited by diffusion into the micropores where it is consumed in microbial respiration. Soil heterogeneity is represented by a distribution function describing the aggregate radius distribution. In this model, anoxic volumes are constrained to lie at the center of the aggregates.

In applying the dual porosity model, the assumption of a spherical aggregate shape is by no means essential (Rappoldt, 1990; Renault and Stengel, 1994). However, it is essential that a distinct class of macropores is present and that the soil between the macropores is homogeneous. For many soils, it is not possible to classify a pore as either a micropore or a macropore. Even if the soil particles form hierarchical clusters, discrete aggregates may only be identifiable upon physical disruption. Such a mechanical definition of aggregates is not operational as a model of soil structure for process-based models.

Most soils have pores distributed across a broad and continuous size range, and their relative configuration determines the distribution of moisture, and water and gas transport. Recently, the structural heterogeneity of soil has been modeled using fractal geometry (e.g., Baveye et al., 1997). These models accommodate the broad range in structural variability observed in soil and the parameters are obtained by direct measurement of the structure rather than by calibration from experiments. Therefore fractal models offer the possibility of elucidating the role of structure in microbial processes.

Table 1
Description of symbols

| Symbol | Description |
|---|---|
| $b$ | the size of a pixel, the smallest cells of the fractal lattice |
| $C$ | boundary concentration in the gaseous phase, with average $\overline{C}$ |
| $c$ | concentration in the gaseous phase |
| $D_m$ | oxygen diffusion coefficient for the soil matrix relative to gaseous gradients |
| $D_p$ | oxygen diffusion coefficient for gas-filled pores |
| $d_m$ | mass fractal dimension |
| $\varepsilon$ | gas-filled porosity |
| $F$ | surface flux |
| $\varphi$ | anoxic fraction |
| $k$ | number of recursion levels |
| $L$ | size of fractal patch |
| $\lambda$ | characteristic length belonging to the diffusion–respiration process |
| $m$ | number of cells at each recursion level |
| $n$ | cluster length in 1D model with average $\bar{n}$ |
| $P(n)$ | probability of finding a cluster of length $n$ |
| $p$ | probability that a cell comprises soil matrix |
| $Q$ | soil respiration constant (amount per unit soil matrix volume per unit time) |
| $\overline{Q}$ | bulk soil respiration (amount per unit soil volume per unit time) |
| $q$ | a function of $p$ and $m$ (Eq. (10)) |
| $R$ | sphere radius |
| $R_g$ | geometrical mean sphere radius |
| $\sigma$ | the standard deviation of the distribution of $\ln(R)$ |
| $V$ | aggregate volume with average value $\overline{V}$ |
| $x$ | penetration depth of oxygen expressed as a number of lattice cells |
| $z$ | distance from the surface |
| $z_0$ | depth of oxic layer for a plane surface |

In this paper, we report on a model for oxygen transport and consumption by microorganisms in soil. The significance of broad range structural heterogeneity is explored by comparing a model of soil structure based on fractal geometry with the dual-porosity model described above. In particular, the dependence of the anoxic fraction on the local oxygen concentration is closely examined. The aspects of structural heterogeneity which are important determinants of the distribution of anoxic volume are determined. Table 1 gives a list of symbols used.

## 2. Description of soil structure and soil respiration

### *2.1. A random fractal lattice*

The structural model is based on a random $n$-dimensional Cantor set (Falconer, 1990). The construction is explained using the two-dimensional case for dia-

grammatic clarity, however, it can easily be extended for the case of one or three dimensions as outlined below. Fig. 1a shows a two-dimensional random lattice build up from primary squares of size $L$. Each primary square is divided into $3 \times 3$ cells ($m = 3$). With probability $p$ a cell comprises soil matrix (black), which is assumed to be a combination of solid particles and water, and therefore with probability $1 - p$, a cell comprises pore space. Hence, on average, each square contains $pm^2$ matrix cells and $(1 - p)m^2$ pores of size $L/m$. Fig. 1b shows the same lattice with the water removed from pores of size $L/m^2$. Thus each matrix cell of Fig. 1a is subdivided into $m \times m$ smaller matrix and pore cells. With the same probability, $p$, these cells comprise solid matrix. Fig. 1c and d show the lattice after three and four levels of recursion, and hence, represent lattices of progressively lower water contents. An obvious effect of decreasing moisture content is an increase in connectivity of the pore space. The

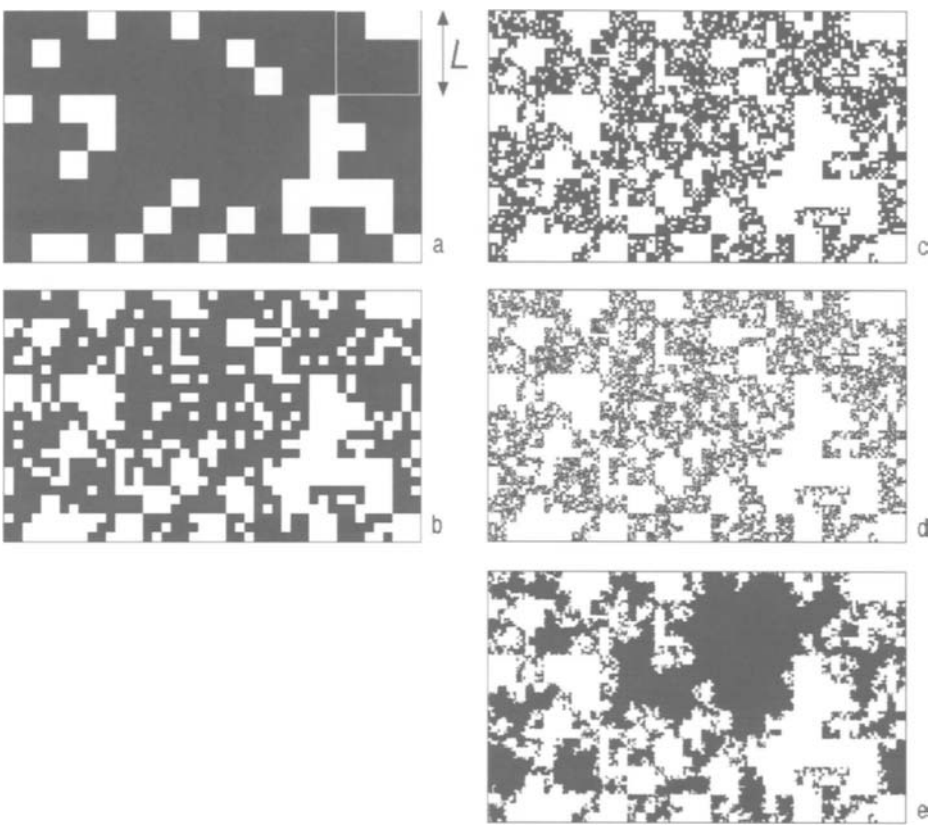


Fig. 1. A random lattice with a fractal patch of size $L$. The soil matrix, which is the combination of the solid phase and water, is black and the pores are white. With decreasing water content, the number of recursion levels increases from 1 in (a) to 4 in (d). In (e) the pores that are not connected to the surface are also black.

mass fractal dimension of the lattice generated in this way is given by (Crawford et al., 1993):

$$d_m = 2 - \frac{\ln(1/p)}{\ln m} \tag{1}$$

Besides the parameters $p$ and $m$, the structure is characterized by the size of the fractal patches, $L$. At scales larger than $L$, the lattice contains random realizations of the same structure. Soil aeration is largely determined by the gas-filled porosity $\varepsilon$, which is given by

$$\varepsilon = 1 - p^k \tag{2}$$

where $k \geq 1$ is the number of levels of recursion in the structure. The smallest fractal scale determines the maximum value of $\varepsilon$. Note that in the absence of knowledge of the structure below the fractal scale, any particular lattice does not have an associated absolute water content. However, the gas-filled porosity, i.e., the amount of water required for saturation, is uniquely determined by the parameters of the lattice.

An important property of a lattice is the continuity of its gas-filled pores. The two-dimensional lattice in Fig. 1d has a porosity of 0.68 and a well-connected gaseous phase in which diffusion may take place. Gas continuity requires a gas-filled porosity of about 0.6 or larger. This implies that either the soil matrix or the gas-filled pore space is discontinuous. This is simply an artifact of working in two dimensions because in three dimensions the threshold value for a continuous phase lies between 0.20 and 0.30. Hence, if the gas-filled porosity exceeds the threshold, both phases are continuous. Even with a porosity well above the threshold, however, there are regions with unconnected pores. Fig. 1e shows in white those pores of Fig. 1d which are connected to either the top or the bottom. The combination of matrix and unconnected pores, shown in black, forms patches which may be much larger than $L$.

### *2.2. The diffusion–respiration process*

Oxygen transport takes place by diffusion in the pore space, and over a much longer timescale, diffusion also takes place in the water component of the soil matrix. Soil respiration is assumed to take place uniformly in the soil matrix. The rate of uptake of oxygen by the microbes, i.e., the respiration rate, is taken to be independent of the oxygen concentration as long as there is any oxygen present. This zero-order respiration model originates from Currie (1961) and Greenwood and Berry (1962). It takes its simplest mathematical form in the case of a plane surface with pore space at a constant concentration $C$ at one side and soil matrix at the other side. If $z$ is the coordinate perpendicular to the surface, the stationary state is described by

$$D_{\mathrm{m}} \frac{d^2 c(z)}{dz^2} = Q, \quad 0 \leq z \leq z_0, \tag{3a}$$

with boundary conditions

$$c(z) = 0, \quad \frac{dc(z)}{dz} = 0 \quad \text{at} \quad z = z_0 \quad \text{and} \quad c(0) = C \tag{3b}$$

in which $z_0$ is the oxygen penetration depth that is determined by the solution of Eqs. (3a) and (3b). The elementary solution is

$$\begin{aligned} c(z) &= C\left(1 - \frac{z}{z_0}\right)^2 = C\left(1 - \frac{z}{\sqrt{2}\,\lambda}\right)^2, \quad 0 \le z \le z_0 \\ c(z) &= 0, \quad z > z_0 \end{aligned} \tag{4}$$

The penetration depth $z_0$ is equal to $\sqrt{2}\lambda$ where $\lambda$ is the characteristic length associated with the diffusion–respiration process in the soil matrix. This length depends on process parameters only and is independent of geometry. It is defined as

$$\lambda = \sqrt{\frac{D_m C}{Q}}\,. \tag{5}$$

The oxygen flux $F$ at the plane surface is equal to the total oxygen use of the aerated layer and is given by

$$F = Q z_0 = \sqrt{2}\sqrt{D_m C Q}\,. \tag{6}$$

The numerical factor $\sqrt{2}$ in the penetration depth depends on the geometry and, for example, is different for spherical or cylindrical geometries. The process length $\lambda$ is a characteristic of all solutions, however.

Eqs. (4)–(6) are based on a constant respiration rate $Q$ as long as there is any oxygen available. For low concentrations this is a simplification. Other models have been proposed (e.g., Greenwood, 1961; Leffelaar, 1986; Arah, 1988; Sierra and Renault, 1996) with first-order behavior at low concentrations or Michaelis–Menten kinetics. Such refinements are important if measured oxygen concentrations inside aggregates are directly compared with model results (Sierra et al., 1995). For exploring the behavior of different soil structure models, however, a constant $Q$ provides a satisfactory description.

The aeration model is based on gaseous concentrations, since gradients in the gaseous concentration are the primary driving force of oxygen transport. For saturated soil matrix the gaseous concentration is the concentration in equilibrium with the liquid phase. The solubility of oxygen in water is a few percent and the diffusion coefficient of oxygen in pure water is about 10,000 times smaller than in air.

At the scale of a soil profile, Eqs. (3a) and (3b) is valid only if the soil is completely oxic. Then the potential oxygen use, $Q$, can be realized everywhere in the soil matrix and the bulk scale oxygen sink $\overline{Q}$ becomes

$$\overline{Q} = (1 - \varepsilon)Q.$$

If it is assumed that a fraction $\varphi(\bar{C})$ of the soil matrix is anoxic, where $\bar{C}$ is the average concentration in the gas-filled pores, then the respiration in the anoxic part is zero and the average oxygen sink becomes

$$\bar{Q}(\bar{C}) = (1-\varepsilon)\big(1-\varphi(\bar{C})\big)Q. \tag{7}$$

This shows that in the presence of local anoxia, the bulk scale oxygen consumption is no longer of order zero.

### *2.3. The anoxic fraction of a 1D lattice*

We apply the diffusion–respiration model described above to a one-dimensional fractal lattice. A one-dimensional lattice is just a single row of cells, constructed using the same rules as used in the lattice construction of Fig. 1. The length $L$ is the length of the fractal structure consisting of $m$ cells, which are either matrix or pore according to the probability, $p$, as before. At the second level of recursion the matrix cells are divided into $m$ smaller ones, etc. The fractal dimension is given by (cf. Eq. (1))

$$d_m = 1 - \frac{\ln(1/p)}{\ln m}. \tag{8}$$

The pore space of a one-dimensional soil clearly cannot be continuous. Therefore, the pores are assumed to be at some fixed concentration $C$. It is assumed that even the smallest gas-filled pores of the lattice contain oxygen. The anoxic fraction of the soil matrix is then determined by the length of the matrix parts at the smallest scale of the structure. At first we derive the statistical distribution of the length of the matrix clusters. Then an expression is derived for the anoxic fraction of the soil matrix as function of process parameters and water content.

We determined the distribution of cluster lengths numerically. For various choices of $m$, the probability $p$, and the number of recursion levels $k$, the probability, $P(n)$, that a cluster consists of $n$ successive matrix cells was determined by analyzing long generated sequences. Fig. 2 shows results based on sequences containing 100,000 clusters. The straight lines are described by

$$P(n) = q^{n-1}(1-q) \tag{9}$$

in which $q$ is related to the group size, $m$, and the probability, $p$, as

$$q = p^{m/(m-1)}. \tag{10}$$

Eq. (9) is not an exact description of $P(n)$. The data points in Fig. 2 show some periodicity with period $m$. This is understandable since if $m = 5$, there is the possibility of five matrix cells in a row, i.e., if all cells of a group of $m$ cells are classified as matrix. A clump of six matrix cells, however, requires two successive matrix groups. This reduces $P(6)$ relative to the average decrease of $P(n)$ with $n$. The numerical results demonstrate, however, that the straight line

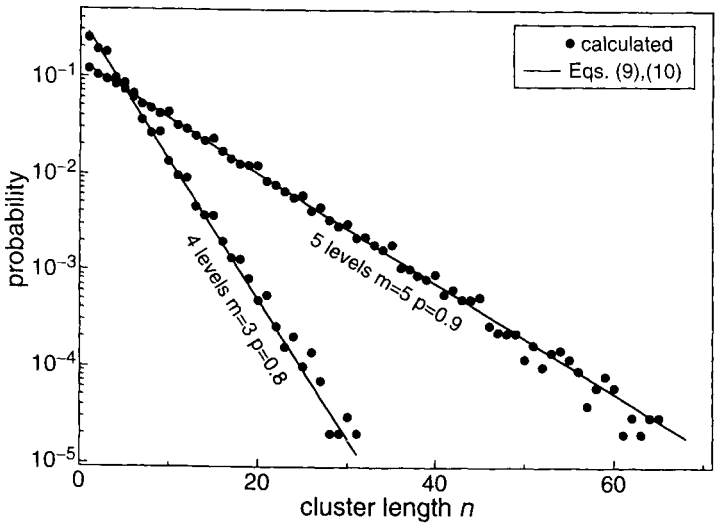


Fig. 2. The probability to find clusters with length $n$ in a 1D random fractal lattice for two choices of the structure parameters. The straight lines are described in Eqs. (9) and (10).

described by Eq. (9) provides a satisfactory description of the cluster size distribution.

The length, $n$, of a piece of soil matrix is equal to the number of cells at the smallest scale of the structure. Therefore, the probability $P(n)$ is largely determined by the structure at the two or three smallest scales. The larger pores are relatively rare, and do not significantly alter the distribution of cluster lengths and because of this, the number of recursion levels $k$ of the fractal structure is not a parameter of Eq. (9).

For large $m$, $P(n)$ approaches $p^{n-1}(1-p)$ which is the probability that a series of matrix cells has length $n$ for an ordinary random sequence of cells with probability $p$ of being matrix. For a given probability, $p$, the clusters in a fractal structure are shorter. The porosity of the random sequence however is $1-p$ and the porosity of the fractal structure is $1-p^k$. Hence, if structures with equal porosity are compared, the fractal structure has longer clusters than an ordinary random sequence.

The overall anoxic fraction of the soil matrix can be calculated by applying the one-dimensional diffusion–respiration model explained above to all matrix clusters. At first, we assume that oxygen penetrates over a distance of $x$ cells in the soil matrix. Later $x$ will be written in terms of the lattice size and the process length, $\lambda$. Clusters which are larger than $2x$ have $n-2x$ anoxic cells in the middle. The overall anoxic fraction becomes

$$\varphi(x) = \frac{1}{\bar{n}} \sum_{n=2x+1}^{\infty} (n-2x)P(n) \tag{11}$$

in which $\bar{n}$ is the average cluster size given by

$$\bar{n} = \sum_{n=1}^{\infty} nP(n) = \sum_{n=1}^{\infty} nq^{n-1}(1-q) = (1-q)\frac{\mathrm{d}}{\mathrm{d}q}\left(\sum_{n=1}^{\infty} q^n\right)$$

$$= (1-q)\frac{\mathrm{d}}{\mathrm{d}q}\left(\frac{q}{1-q}\right) = \frac{1}{1-q}.$$

The anoxic fraction of Eq. (11) becomes

$$\varphi(x) = (1-q)\sum_{n=2x}^{\infty}(n-2x)P(n)$$

$$= \sum_{n=2x}^{\infty} nq^{n-1}(1-q)^2 - 2x\sum_{n=2x}^{\infty} q^{n-1}(1-q)^2$$

$$= (1-q)^2\frac{\mathrm{d}}{\mathrm{d}q}\left(\sum_{n=2x}^{\infty} q^n\right) - 2x(1-q)^2\frac{q^{2x-1}}{1-q} \tag{12}$$

$$= (1-q)^2\frac{\mathrm{d}}{\mathrm{d}q}\left(\frac{q^{2x}}{1-q}\right) - 2x(1-q)q^{2x-1} = q^{2x}$$

In terms of the process length, $\lambda$, and the size of the fractal structure, $L$, $x$ can be written as

$$x = \frac{\sqrt{2}\,\lambda}{Lm^{-k}} = (\sqrt{2}\,\lambda/L)m^k.$$

Substitution in Eq. (12) gives

$$\varphi(\lambda) = \exp\left(-\frac{2\sqrt{2}\,\lambda}{L}m^k \log q^{-1}\right). \tag{13}$$

Finally, with Eqs. (2) and (8), $m^k$ can be written in terms of the fractal dimension and the gas-filled porosity.

$$\varphi(\lambda, \varepsilon) = \exp\left(-\frac{2\sqrt{2}\,\lambda}{L}(1-\varepsilon)^{-1/(1-d_m)} \log q^{-1}\right). \tag{14}$$

Note that $1 - d_m$ corresponds with the Brooks–Corey exponent in the water retention curve of the fractal structure (Crawford et al., 1995). For any particular water content, the anoxic fraction decreases exponentially with the process length, $\lambda$, which in turn is proportional to the square root of the oxygen concentration in the pores (cf. Eq. (5)).

Fig. 3 shows the anoxic fraction as a function of $\varepsilon$, calculated for $\lambda/L = 0.01$ and for several values of $d_m$. The result is weakly dependent on the choice of $m$

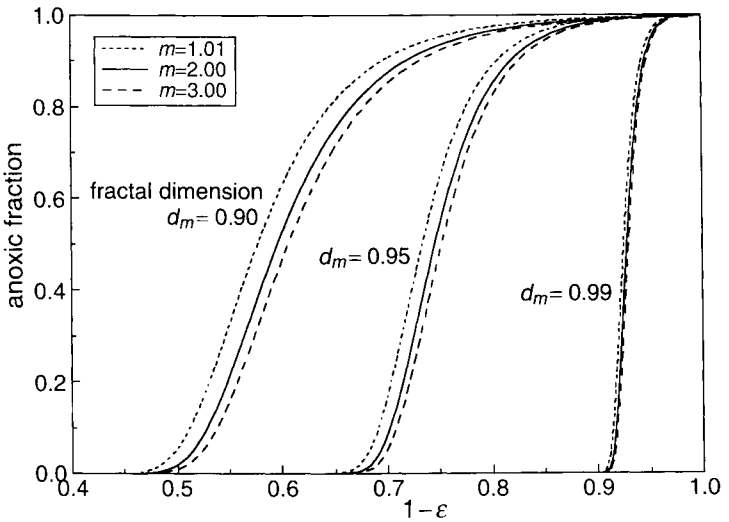


Fig. 3. The anoxic fraction as function of the gas-filled porosity $\varepsilon$ for a 1D random fractal lattice, assuming that there is oxygen in all pores (Eq. (14)).

which determines the value of $q$ through $d_m$ (Eqs. (8) and (10)). The anoxic fraction steeply increases if the size of the saturated clusters is of the order of the oxygen penetration depth.

### *2.4. Numerical calculations for a three-dimensional lattice*

The diffusion–respiration process in a three-dimensional random fractal lattice was determined by numerically solving the diffusion–respiration equation until a stationary state was approached sufficiently closely. A lattice of $81 \times 81 \times 81$ cells was used. The fractal structure inside it was generated using $m = 3$ and three recursion levels, leading to fractal patches of size $27 \times 27 \times 27$ cells, and to 27 different random realizations of the fractal structure within the lattice. The lattice shown in Fig. 5 has been generated using $p = 4/27$. The total gas-filled porosity of the lattice is 0.3997, the surface-connected porosity is 0.3246 and the unconnected porosity 0.0751 The unconnected porosity is of the same order of magnitude as the values measured by Bruckler et al. (1989) (Fig. 11) which varied between 0.00 and about 0.15.

In order to reduce edge effects, the left and right sides of the lattice were treated as if they were connected. This means that the cells of the left most plane have the cells of the right most plane as their immediate neighbors. The same was done for the front and back planes. The oxygen diffusion coefficient for the soil matrix was set 10,000 times smaller than the one for the pore space.

Two types of simulations have been performed. In the first, we assumed a certain fixed concentration in all pores and no oxygen in the matrix. The oxygen

enters the matrix from the pores, and the respiration increases during the simulation. The stationary state is reached when the total respiration is equal to the total inflow. This type of stationary state is the three-dimensional equivalent of the one-dimensional situation analyzed above, where it is also assumed that all pores are at some fixed concentration.

In the second type of simulation, diffusion through the pore space is also taken into account. The source of oxygen is provided by an additional layer of cells at the bottom and at the top of the lattice which is kept at a constant concentration. The oxygen diffuses into the pores and from there into the matrix. This leads to a slowly decreasing flux from the outer layers into the lattice and a slowly increasing oxygen use. If the two are equal to within 2%, it was assumed that the stationary state had been reached.

Diffusion was simulated in an elementary way. Diffusive flows between adjacent cells were calculated explicitly as the product of a concentration difference and the diffusion coefficient. If the cell size is written as $b$, a pore space diffusion coefficient $D_p$ of $0.16b^2$ per time step is sufficient to keep the numerical computations stable. After updating all concentrations, the matrix cells consume oxygen according to the potential respiration rate $Q$ under the restriction that the remaining oxygen concentration cannot become negative.

The computer time is usually determined by the number of time steps required for the approach of stationary concentrations in the pores, and this is of the order of $81^2/D_p = 50{,}000$ steps. If the ratio of outer concentration $C$ and potential respiration rate $Q$ exceeds 50,000 time units, the diffusion respiration process in the matrix becomes the limiting factor. In that situation, it is useful to speed up matrix diffusion by periodically taking a few large time steps without pore diffusion. During these steps the pore concentrations are held constant. Clearly, if no pore space diffusion is simulated, the stationary state can be reached by means of a relatively small number of such large time steps.

If the local pore space concentration is small, the width of the aerated layer of the adjacent soil matrix may become less than one cell. The oxygen use of such a thin aerated layer exceeds the diffusive flow calculated over a full lattice distance. Without a correction this leads to a serious underestimate of the sink strength of pore surfaces at low concentrations. This problem was solved by calculating the flux with Eq. (6) for very low concentrations. Details and test results can be found in Rappoldt and Crawford (1999).

From the stationary states of the oxygen concentration in the lattice, values of the anoxic fraction $\varphi$ as function of the average pore concentration $\overline{C}$ were calculated (cf. Eq. (7)). The averages were calculated by subdividing the 81 rows of the lattice into 9 bands of 9 layers, and averaging the concentration in surface-connected pores over each band. The anoxic fraction of the matrix part was determined by comparing the realized respiration of each band with the potential one. This gives a value of $\varphi(\overline{C})$ for each band. The results for the upper- and lowermost bands were neglected since they contain edge effects.

### 2.5. *Comparison with a model of aggregated soil*

In order to determine the significance of fractal structure we compare the anoxic fraction of a fractal soil with the anoxic fraction of an aggregated soil consisting of homogeneous and spherical soil aggregates. For spherical geometry, there is a diffusion equation similar to Eqs. (3a) and (3b) with an analytical solution given by Smith (1980). The anoxic fraction $\varphi_s(\lambda/R)$ of a sphere depends on the ratio of the process length $\lambda$ (Eq. (5)) and the sphere radius $R$. For $\lambda > R/\sqrt{6}$ there is a stationary anoxic fraction. For a larger process length, the sphere is oxic. Smith (1980) and Arah and Smith (1989) calculated the anoxic fraction of an assembly of spheres with a lognormal radius distribution.

The lognormal distribution is characterized by a geometrical mean aggregate radius $R_g$ and a standard deviation $\sigma$. The assembly anoxic fraction depends on $\lambda/R_g$ and $\sigma$ only, which can be explicitly shown by deriving an expression for $\bar{V}$. This expression is found by noting that the average of $e^y$ for a variable $y$ with normal distribution $n(\mu, \sigma^2)$ is $\exp(\mu + \sigma^2/2)$. This follows by setting $t = 1$ in the moment generating function $E(e^{yt})$ of the normal distribution (e.g., Hogg and Craig, 1978, Section 3.4). Since $\ln(R^3)$ has a normal distribution with mean $\ln(R_g^3)$ and standard deviation $3\sigma$, the average sphere volume is

$$\bar{V} = \tfrac{4}{3}\pi \exp\left(\ln R_g^3 + \frac{1}{2}(3\sigma)^2\right) = \tfrac{4}{3}\pi R_g^3 \exp\left(\frac{9\sigma^2}{2}\right). \tag{15}$$

Using this expression, the integral of the anoxic sphere volume over the sphere size distribution becomes

$$\begin{aligned}\varphi\left(\frac{\lambda}{R_g}, \sigma\right) &= \frac{1}{\bar{V}}\int_0^\infty \varphi_s\left(\frac{\lambda}{R}\right)\tfrac{4}{3}\pi R^3 \frac{1}{\sigma\sqrt{2\pi}} \exp\left\{\frac{(\ln R - \ln R_g)^2}{2\sigma^2}\right\} \mathrm{d}(\ln R) \\ &= \int_0^\infty \varphi_s\left(\frac{\lambda}{R_g}\frac{R_g}{R}\right)\left(\frac{R}{R_g}\right)^3 \frac{1}{\sigma\sqrt{2\pi}} \\ &\quad \times \exp\left\{-\frac{(\ln(R/R_g))^2}{2\sigma^2} - \frac{9\sigma^2}{2}\right\} \mathrm{d}\left(\ln\frac{R}{R_g}\right).\end{aligned} \tag{16}$$

In Eq. (16) the ratio $R/R_g$ is the variable of integration and the result will depend on the remaining variables $\lambda/R_g$ and $\sigma$ only. Fig. 4 gives the anoxic fraction calculated for a standard deviation of ln(2) (which corresponds to the radius interval $[R_g/2, 2R_g]$.

Arah and Smith (1989) and later Arah and Vinten (1995) used a truncated lognormal distribution, probably because the existence of aggregates which are

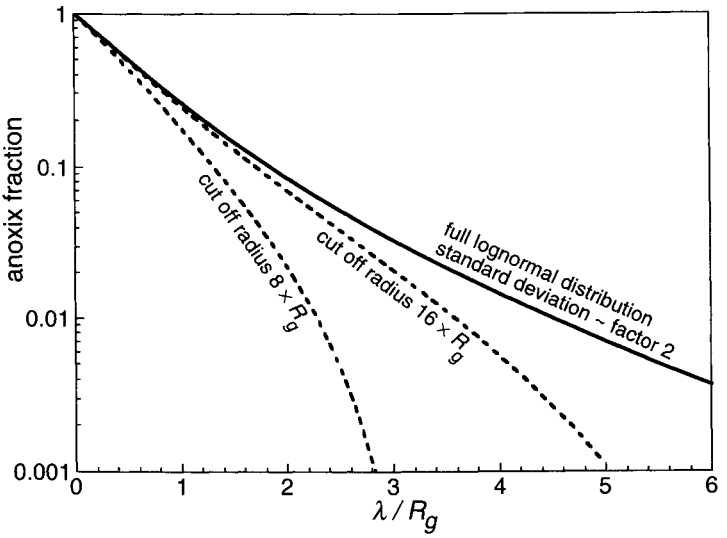


Fig. 4. The anoxic fraction as function of the process length $\lambda$ for a collection of distinct, spherical aggregates with a lognormal radius distribution. The standard deviation corresponds to a factor 2 around the geometrical mean radius $R_g$.

20 or 30 times larger than the geometric mean is highly improbable. Fig. 4 shows that small anoxic fractions are very sensitive to truncation. Clearly, if extremely large aggregates do not exist, the graph of $\ln\varphi$ as function of $\lambda$ must bend downward. The cutoff radius should therefore be considered as a parameter of the aggregate model and not as an insignificant numerical feature.

## 3. Results

Fig. 6 shows cross-sections of stationary states calculated for the diffusion–respiration process in the lattice of Fig. 5. The four stationary states differ only with respect to the outer concentration applied to the top and bottom of the lattice. In Fig. 6a the process length $\lambda$ (Eq. (5)) calculated with the outer concentration is 4.1 times the lattice distance $b$ and there is no anoxic soil. In Fig. 6b ($\lambda = 2.6b$), there are anoxic regions where the respiration rate is zero, but there is still sufficient oxygen available that the pore concentrations in the center of the lattice are similar to the outer concentration at the lattice surface. With decreasing outer concentration in Fig. 6c ($\lambda = 1.8b$) and Fig. 6d ($\lambda = 1.3b$), this situation gradually changes.

The graphs in Fig. 7 show the anoxic fraction as a function of the process length $\sqrt{D_m\overline{C}/Q}$ based on the local average concentration $\overline{C}$ in the surface-connected pores. The lower curve gives the results for a fixed concentration in all pores. The upper curve takes into account diffusion through the pore system and corresponds to stationary states like the ones shown in Fig. 6.

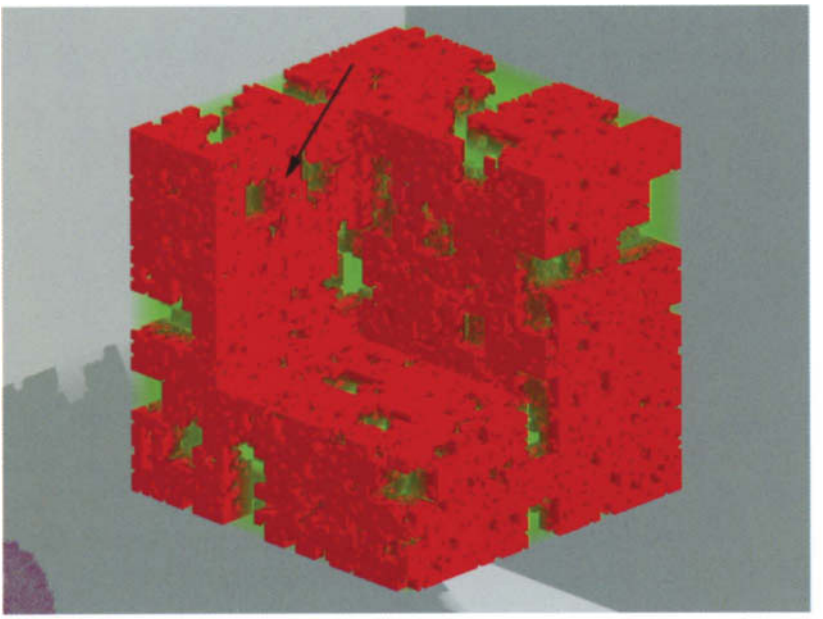

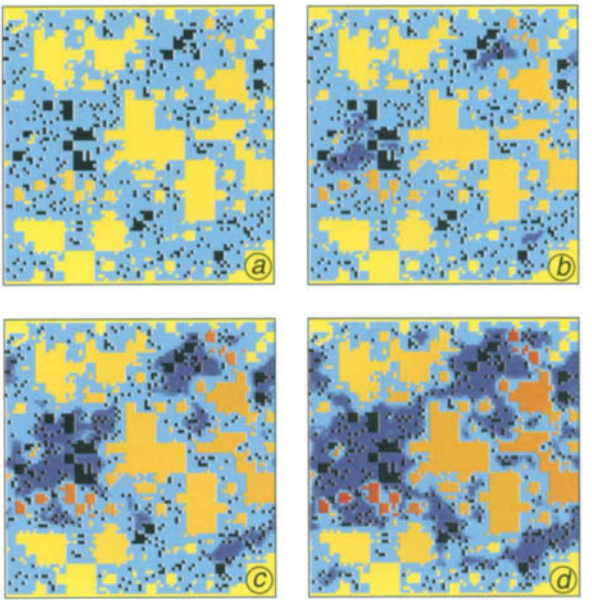
a
b
c
d
oxygen concentration
in connected pores
concentration at
lattice surface
zero
unconnected pores
matrix respiration
potential
anoxic

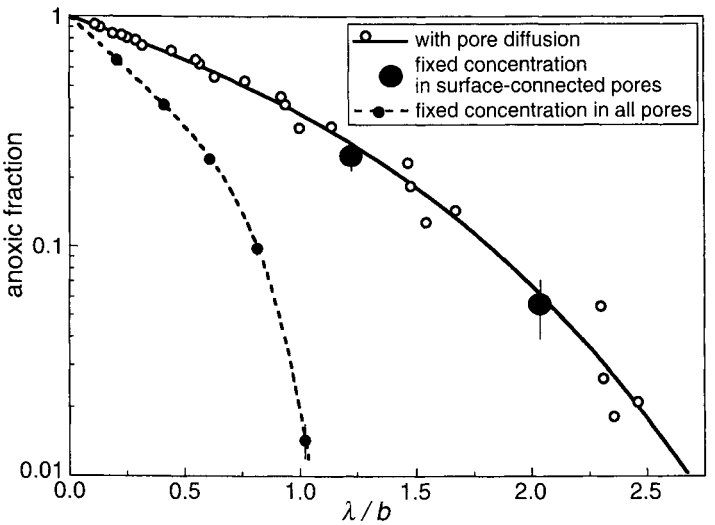


Fig. 7. Simulated anoxic fraction as function of the process length $\lambda$ for a 3D random fractal lattice. The process length is based on the local average concentration in the surface-connected pores. The lower curve has been calculated for a fixed concentration in all pores. The upper curve takes into account pore space diffusion and the presence of unconnected pores.

The lower curve has an estimated initial slope of $-2.11 \pm 0.08$. The slope predicted by Eq. (13) for a one-dimensional lattice is $-2\sqrt{2\log q^{-1}} = 0.680$ (the fractal size, $L$, is equal to $m^k$ lattice distances and the ratio $m^k/L$ cancels). The factor 2 in this equation originates from the number of neighbors that each pixels has in a one-dimensional lattice. In three dimensions, the number of neighbors is three times larger which leads to an estimated value for the three-dimensional case of 2.04, close to the calculated value.

The upper curve includes pore space diffusion and the anoxic fraction is considerably larger. There are potentially two reasons. In the first place, pore space diffusion leads to differences in the local concentration (cf. Fig. 6). At

Fig. 5. Random fractal lattice of $81 \times 81 \times 81$ cells. The porosity is 0.3997 from which 0.0751 is unconnected to the top or bottom surface of the lattice. The size of the fractal patches is $27 \times 27 \times 27$ cells (see Section 2.4 for further details). The arrow points to the plane of the cross-sections below.

Fig. 6. Stationary states for oxygen diffusion and soil respiration in the lattice of Fig. 5. The four cross-sections (a), (b), (c) and (d) correspond to different choices of the surface concentration at top and bottom of the lattice (see text for values). For the surface-connected pores the relative oxygen concentration is given (see color scales). Pores not connected to the surface are black. For the soil matrix the respiration rate is given. The dark blue anoxic zones are characterized by the presence of many disconnected pores.

places which are just oxic such differences may lead to new anoxic spots. Hence, concentration differences tend to increase the anoxic fraction for the same average concentration. Second, the unconnected pores are no longer a source of oxygen. In order to distinguish between these two causes, two runs were made with the same fixed concentration in all surface-connected pores but with diffusion taking place in the unconnected pores. The results are indicated by the large filled circles in Fig. 7 which fall close to the upper curve. This shows that the presence of unconnected pores is a major factor in the relation between the anoxic fraction and the pore space concentration. In our simulations, the local differences in concentration lead to an insignificant increase in the anoxic fraction for a given average concentration.

## 4. Discussion

The bulk scale anoxic fraction has been derived for a one-dimensional lattice in terms of parameters relating both to small-scale processes and the soil structure. The resulting expression describes a simple exponential decrease of the anoxic fraction with the process length $\lambda$. The results for a three-dimensional lattice show that the situation is more complicated.

The first and most important consideration is the dominant role of unconnected pores. Fig. 7 shows that the anoxic fraction can be orders of magnitude larger than the value predicted by assuming that all pores form a source of oxygen. This implies that an anoxic fraction calculated from pore sizes which are derived from the water retention curve may be seriously underestimated. The connectivity of the pore space must be taken into account in any model of soil aeration.

A second consideration is that the curve of the anoxic fraction as a function of the process length bends downward. It is not a simple exponential function. We have also carried out simulations for two-dimensional lattices. Those results confirm the phenomenon. It seems that the anoxic fraction decreases exponentially only for packing in one dimension. This can be understood by realizing that a large clump of matrix should be large in all three dimensions simultaneously. The effective size of a disk shaped region is completely determined by its thickness, for instance. Therefore, the comparative rareness of large clumps of matrix seems to be the consequence of packing in more than one dimension.

We have also shown that for an assembly of aggregates with a lognormal distribution, the anoxic fraction as function of the process length is not a simple exponential relation (Fig. 4). Contrary to the results for the fractal model, the curve for this aggregate model bends upward. Especially for a large standard deviation (a factor of up to 10 around a geometric mean was used by Arah and Smith, 1989), the small anoxic fractions are determined by the rare spheres

having the largest volumes. This may be one of the reasons for truncating the lognormal radius distribution, which obviously eliminates these large volumes. A fractal model achieves the same as the natural consequence of packing.

In principle, downward bending of the curves in Fig. 7 could also be caused by the fact that the lattice size is finite: above some value of $\lambda$ there will be no anoxic soil left. This would imply that the sample size used is too small to simulate an anoxic fraction of a few percent. Inspection of the three-dimensional results, however, shows tens of anoxic spots forming a bulk anoxic fraction of about 2%. Furthermore, if the sample size were too small, it would lead to large differences between different parts of the same lattice. The points and standard deviations in Fig. 7 show that such differences were small compared to the deviation from the initial slope of the curves.

Originally, we expected that the fractal nature of the lattice would lead to important local concentration differences between small and large pores. In that picture the large pores are filled first, if there is little oxygen available. For a larger outer concentration (or smaller demand), the small pores would get filled together with the soil matrix surrounding them. This picture appears to be wrong, at least for the lattices we studied. In three dimensions, the big pores are usually connected by means of small pores. The pores of various sizes are connected on a length scale which is too small for important concentration differences to develop.

The penetration of oxygen into all connected gas-filled pores is due to the factor 10,000 between the diffusion coefficients for air and water. This factor does not yet take into account the low solubility of oxygen in water, just a few percent, and the tortuosity of the water-filled pores inside the matrix. Accounting for these factors as well, oxygen transport in saturated soil is a few hundred thousand times slower than the transport in gas-filled pores (cf. Nye and Tinker, 1977, Eq. 4.20). Therefore, situations in which significant local concentration differences exist will be rare. A truly aggregated (i.e., dual-porosity) soil is an example, however.

Aggregates exist in many soils. Application of the aggregate model, however, requires that the micropores and the soil particles form a homogeneous soil matrix and that the only structure is represented by the macropores. Many soils show an almost continuous range of pore size sizes and there is hierarchy in the structure. In such situations the fractal model is operational and the aggregate model is not.

Tests and practical application of the fractal aeration model require quantitative understanding of its properties. Approximate expressions as function of the structural parameters like the fractal dimension are very desirable. The expression derived in this paper is valid only for small process lengths and large anoxic fractions. A difficulty in all aeration models is that a non-uniform soil activity (e.g., Sierra and Renault, 1996) makes things even more complicated. It is therefore important to describe the essential characteristics of soil structure by

means of just a few parameters. The fractal model, although still difficult to handle, provides such a possibility.

## Acknowledgements

We thank P.A.C. Raats for stimulating discussions and J.R.M. Arah and K.A. Smith for their comments on the manuscript. This work was initiated during a two-month visit of CR in Scotland supported by the OECD. JWC acknowledges the support of the Scottish Office Agriculture, Environment and Fisheries Department.

## References

Arah, J.R.M., 1988. Modelling denitrification in aggregated and structureless soils. In: Jenkinson, D.S., Smith K.A. (Eds.), Nitrogen Efficiency in Agricultural Soils. Elsevier, London, pp. 433–444.

Arah, J.R.M., Smith, K.A., 1989. Steady-state denitrification in aggregated soils: a mathematical model. J. Soil Sci. 40, 139–149.

Arah, J.R.M., Vinten, J.A., 1995. Simplified models of anoxia and denitrification in aggregated and simple-structured soils. Eur. J. Soil Sci. 46, 507–517.

Baveye, P., Parlange, J.Y., Stewart, B.A. (Eds.), 1997. Fractals in Soil Science. Lewis Publishers, Boca Raton, FL.

Bruckler, L., Ball, B.C., Renault, P., 1989. Laboratory estimation of gas diffusion coefficient and effective porosity in soils. Soil Sci. 147, 1–10.

Crawford, J.W., Sleeman, B.D., Young, I.M., 1993. On the relation between number-size distributions and the fractal dimension of aggregates. J. Soil Sci. 44, 555–565.

Crawford, J.W., Matsui, N., Young, I.M., 1995. The relation between the moisture-release curve and the structure of soil. Eur. J. Soil Sci. 46, 369–375.

Currie, J.A., 1961. Gaseous diffusion in aeration of aggregated soils. Soil Science 92, 40–45.

Falconer, K., 1990. Fractal Geometry. Wiley, London.

Greenwood, D.J., 1961. The effect of oxygen concentration on the decomposition of organic materials in soil. Plant Soil 14, 360–376.

Greenwood, D.J., Berry, G., 1962. Aerobic respiration in soil crumbs. Nature 195, 161–163.

Hogg, R.V., Craig, A.T., 1978. Introduction to Mathematical Statistics. Macmillan, New York.

Houghton, J.T., Jenkins, G.J., Ephraums, J.J. (Eds.), 1990. Climate Change. The IPCC scientific assessment. Cambridge Univ. Press, Cambridge.

Leffelaar, P.A., 1986. Dynamics of partial anaerobiosis, denitrification, and water in a soil aggregate: experimental. Soil Sci. 142, 27–41.

Nye, P.H., Tinker, P.B., 1977. Solute Movement in the Soil–Root System. Blackwell, Oxford.

Rappoldt, C., 1990. The application of diffusion models to an aggregated soil. Soil Sci. 150, 645–661.

Rappoldt, C., Crawford, J.W., 1999. Properties of rectangular and hexagonal fractal lattices as a model of soil aeration (in prep).

Renault, P., Stengel, P., 1994. Modeling oxygen diffusion in aggregated soils: I. Anaerobiosis inside the aggregates. Soil Sci. Soc. Am. J. 58, 1017–1023.

Sierra, J., Renault, P., 1996. Respiratory activity and oxygen distribution in natural aggregates in relation to anaerobiosis. Soil Sci. Soc. Am. J. 60, 1428–1438.

Sierra, J., Renault, P., Valles, V., 1995. Anaerobiosis in saturated soil aggregates: modelling and experiment. Eur. J. Soil Sci. 46, 519–531.

Smith, K.A., 1980. A model of the extent of anaerobic zones in aggregated soils, and its potential application to estimates of denitrification. J. Soil Sci. 31, 263–277.

This Page Intentionally Left Blank

*Fractals in Soil Science*
Editors: Ya.A. Pachepsky, J.W. Crawford and W.J. Rawls
© 2000 Elsevier Science B.V. All rights reserved.


# Fractal analysis of spatial and temporal variability [1]

Bahman Eghball [a,*,2], Gary W. Hergert [b], Gary W. Lesoing [c], Richard B. Ferguson [d]

[a] *Department of Agronomy, University of Nebraska, 244 Keim Hall, East Campus, Lincoln, NE 68583, USA*
[b] *West Central Research and Extension Center, North Platte, NE 69101, USA*
[c] *Center for Sustainable Agricultural Systems, University of Nebraska, Lincoln, NE 68583, USA*
[d] *South Central Research and Extension Center, Clay Center, NE 68933, USA*

Received 14 October 1997; accepted 28 September 1998

**Abstract**

Characterizing spatial and temporal variability is important in variable rate (VRAT) or long-term studies. This study was conducted to compare spatial variability of soil nitrate in a VRAT nitrogen (N) application study and temporal variability of soybean (*Glycine max* L.) yield in a long-term organic vs. inorganic study. In the VRAT study, conventional uniform N application was compared with variable rate and variable rate minus 15% N. In the long-term experiment, soybean yields under organic (manure application), fertilizer, and fertilizer plus herbicide systems were studied from 1975 to 1991. Semivariograms were estimated for soil nitrate in the VRAT and for soybean yield in the long-term study. The slope of the regression line of log semivariogram vs. log lag ($h$, distance or year) was used to estimate the fractal dimension ($D$), which is an indication of variability pattern. The intercepts (log $k$) of the log–log lines, which indicate extent of variability, were also compared between treatments. There was no significant effect of the N treatments on the $D$-values in the VRAT study. The extent of spatial variability for residual soil nitrate became significantly less after imposing N application regimes. The variable rate N application had lower log $k$-values than uniform application indicating reduced soil nitrate variability with VRAT N application. In the long-term study, all three management systems had similar $D$ and log $k$-values for soybean yield indicating similar temporal yield variability for the three systems. The three management systems used did not change temporal effects on soybean yield. Rainfall during July and August accounted for 65% of variability in soybean grain yield.

* Corresponding author. E-mail: beghball@unlinfo.unl.edu

[1] Joint contribution of the USDA-ARS and the University of Nebraska Agricultural Research Division, Lincoln, NE as paper no. 12112.

[2] Senior author is with a cooperative agreement between USDA-ARS and University of Nebraska.

Reprinted from Geoderma 88 (1999)
© 1999 Elsevier Science B.V. All rights reserved

Fractal and covariance analyses can be effectively used to compare treatments or management systems for spatial or temporal variability. © 1999 Elsevier Science B.V. All rights reserved.

*Keywords:* manure application; grid sampling; semivariogram; covariance analysis; fractal dimension; variable rate N application; long-term study; site-specific management; precision agriculture

## 1. Introduction

Spatial and temporal variability of soil and plant parameters have been difficult to characterize and quantify. Semivariogram analysis has been used to characterize spatial variability (Clark, 1979; Isaaks and Srivastava, 1989). A semivariogram provides a measure of the degree of spatial or temporal dependence between samples along a line with given direction and can be used to describe spatial and temporal variability. Semivariogram may rise to a constant value (the sill) after a given range, or it may increase continuously without evidence of a definite range and sill (Burrough, 1983).

Fractal analysis has been useful in characterizing plant and soil parameters (Burrough, 1981; Perfect and Kay, 1991; Eghball et al., 1993a). Fractals have also been used in soil and tillage research (Perfect and Kay, 1995). In fractal analysis, the fractal dimension ($D$), which as the name implies can be fractional and is scale independent, is an indicator of the shape (geometry) of the fractal parameter being studied. Fractal dimension is expected to exceed the topological dimension. A continuous series, such as a polynomial, can be split into an infinite number of smooth lines. A non-differentiable continuous series such as a fractal function cannot be split into smooth lines and any attempt to split it up into smaller parts results in the resolution of more structure and roughness (Burrough, 1981).

In spatial and temporal data series, large $D$-values indicate the importance of short-range variation, while small $D$-values reflect the importance of long-range variation (Burrough, 1983). Because of the degree of roughness in spatial and temporal data, it is worth examining the evidence of variation at different scales before attempts are made to interpolate data using least-squares or kriging (Burrough, 1981). For spatial and temporal variability, $D$ can range from 1 (values within spatial and temporal range of analysis fall on a line) to 2 which indicates so much variation that an entire two-dimensional surface is covered by the extent of variation. For surface topography, $D$ can range from 2 which indicates a smooth surface to 3 which indicates a very rough surface.

Fractal analysis can be used to characterize soil spatial variability. Fractal dimensions were calculated for spatial distribution of soil pH, clay content and topographic height (Burrough, 1983), soil nitrate (Eghball et al., 1997), soil strength (Perfect et al., 1990; Folorunso et al., 1994), nutrient content (Burrough, 1981), penetrability (Armstrong, 1986), soil microtopography (Huang and Bradford, 1992), water retention (Pachepsky et al., 1995), and saturated hydraulic

conductivity (Kemblowski and Chang, 1993). Fractal dimension can be used to compare different soil and plant parameters for spatial variability pattern. Eghball et al. (1997) used the fractal dimension to compare treatments that influenced the spatial distribution of soil nitrate and corn grain yield in a site-specific study. Fractal dimension can also be used to compare effects of different management systems on soil properties. Eghball et al. (1993b) and Perfect and Blevins (1997) found that no-till had a smaller fractal dimension of soil fragmentation than other tillage systems indicating a better soil structure for no-till system.

Site-specific application of fertilizer and pesticides is becoming more common because of natural soil variability in any field. Managing variability by variable rate application of fertilizer and pesticide has the potential for increased efficiency, and reduced field variability and environmental impact (Ferguson et al., 1996). By applying inputs where needed instead of to the entire field, a farmer can increase the yield potential of low productivity areas within the field and maintain high productivity in the good areas. Characterizing and comparing spatial variability in these studies is necessary to determine the effectiveness of the treatments used on reducing soil variability.

Temporal variability is an important factor to consider when evaluating the performance of long-term experiments. Fractal analysis has been useful in characterizing temporal variability (Eghball and Power, 1995; Eghball et al., 1995, 1997). Peters (1994) used fractals for analysis of variability of the market. Fractal analysis can be used to distinguish between short-term and long-term variations for parameters collected in time. Eghball and Power (1995) used fractal analysis to characterize temporal variability of average yield of ten crops in the United States with a wide range of yield levels, and found that crops were significantly different in terms of temporal variability. They observed less year-to-year grain yield variability for rice (*Oryza sativa* L.) than other grain crops, which was judged to be due in part to management practices commonly used for this crop. Eghball and Varvel (1997) pointed out that temporal variability may be more dominant than any soil spatial variability that may be present. Year-to-year variation may completely mask the expression of soil spatial variability effects on a crop's performance. Eghball et al. (1995) found that temporal variability of maize grain yield in a long-term manure and fertilizer experiment was due to environmental factors, and management practices did not change this variability.

Characterizing and comparing spatial variability of soil and plant parameters in site-specific application is needed to evaluate the effectiveness of this management system in reducing soil and plant variability. Characterization of temporal variability in long-term studies is also important in order to compare different management systems for sustainability and environmental quality. The objective of this study was to use fractal analysis to characterize and compare spatial and temporal variability of soil and plant parameters in two case studies.

These included a variable rate N application and a long-term organic vs. inorganic study.

## 2. Materials and methods

### *2.1. Case study 1: variable rate nitrogen study*

A variable rate N experiment was initiated in 1993 on a Cozad silt loam (coarse, silty, mixed mesic Fluventic Haplustoll) on a furrow irrigated site in west central Nebraska (Lincoln county). Three N management regimes replicated five times were used: (1) a fixed uniform N rate based on an average expected yield for the field, average soil organic matter content, and the average soil nitrate of the field using the University of Nebraska N recommendations (Hergert et al., 1995); (2) variable rate N based on an average expected goal, varying soil nitrate, and varying soil organic matter determined from grid sampling; and (3) variable rate N calculated as in (2) minus 15% N. Nitrogen treatments were applied in 1994. Uniform N application was made to the entire field in 1993.

Treatment strips were one planter width, 5 m wide for the full field length which was 280 m. A transect of soil samples was taken down the middle of each of the treatment strips using a fixed spacing of 18.3 m on an offset grid. A single 5-cm diameter core was taken at each sampling point to 0.9 m depth for soil nitrate determination.

Fractal analysis was performed on the soil nitrate data to evaluate its pattern and extent of spatial variability based on the method described by Eghball and Power (1995). Briefly, semivariograms were estimated for soil nitrate based on the following equation:

$$\gamma(h) = \Sigma_i^{n-h}(X_i - X_{i+h})^2/2(n-h) \tag{1}$$

where $\gamma(h)$ is the estimated semivariogram, $X_i$ and $X_{i+h}$ are values of a parameter separated by a lag ($h$), and $n$ is the number of points ($n-h$ is the number of intervals or lags). The spatial or temporal structure of a fractal function can be described by the following equation:

$$\gamma(h) \propto kh^H \tag{2}$$

where $\gamma(h)$ is the semivariogram, $h$ is the lag, $H$ is the codimension, and $k$ is a constant related to the extent of variation. Note that $0 < H \leq 2$. Fractal dimension is calculated based on the following relationship:

$$D = d - 1/2H \tag{3}$$

where $d$ is the Euclidean dimension. Thus for a linear transect across a fractal area $D = 2 - 1/2\ H$. Regression of log semivariogram vs. log lag for each

treatment provided an estimation of fractal dimension [$D = 2 - 1/2\ H$] where $H$ is the slope (codimension). Variance of increments of a Weierstrass–Mandelbrot fractal function varies as $h^{4-2D}$ (Berry and Lewis, 1980). In order to compare the intercepts for the extent of short-range spatial variability of soil nitrate, the lag distances were divided by the shortest lag distance (18.3 m) so that the first lag was 1 ($\log 1 = 0$). The intercept of the regression line ($\log k$), which is the log semivariogram at lag equal 1, is an indication of extent of variation and can be compared among treatments. Since the slopes and $D$-values are related by constants, the differences between slopes also reflect differences between $D$-values.

Homogeneity of variability between replications of each treatment was determined using covariance analysis. Since no differences between replications were observed for $D$ for any of the treatments, analysis of covariance was performed on the data to estimate and compare the slopes and log $k$-values among treatments using SAS (SAS, 1985). Semivariograms were estimated using SAS. Seven lags ($h$) out of 15 were used for determination of $D$- and log $k$-values to insure an adequate number of squared differences and use of the linear portion of log semivariogram vs. log $h$. A linear-plateau model was used to determine the linear portion of the log semivariogram vs. log $h$ (Anderson and Nelson, 1975) and seven lags was judged to be an appropriate number to use for all treatments. A probability level $p < 0.10$ was considered significant.

### 2.2. *Case study 2: long-term experiment*

An experiment was initiated in 1975 at the University of Nebraska Agricultural Research and Development Center near Mead, NE. The experiment was conducted on a Sharpsburg silty clay loam (fine, montmorillonitic mesic Typic Argiudoll) under rainfed conditions. The site is gently sloping (0 to 5%), cropped in alfalfa the four years prior to 1975, and receives 680 mm of precipitation per year (16 year average), 65% of which occurs between the months of May and September. Mean annual temperature is 10°C with a mean air temperature between May and September of 21°C.

This experiment was designed to compare chemical-free farming methods that use crop rotation and manure application to crop rotation practices that use agrochemical. Plots (12.2 m × 38.1 m) were arranged in a randomized complete block design, with four replications. A crop rotation of corn (*Zea mays* L.)–soybean–corn–oat (*Avena sativa* L.)/clover [*Avena sativa* (L.), *Melilotus officinalis* (L.) Lam.] was used. Each crop in the rotation sequence was grown every year and received one of three management systems: (1) beef cattle feedlot manure only, designated organic (OR) system; (2) synthetic fertilizer only, designated (FO) system; and (3) synthetic herbicide and fertilizer designated (HF).

In the OR treatment, soybean received manure every other year when manure was applied to corn in rotation with soybean. In the FO treatment, soybean received P fertilizer when soil test indicated low P level. Weed control was achieved by cultivation in the above treatments. In the HF treatment, P fertilizer plus alachlor and metribuzin herbicides were broadcast after planting. A 9.15 m × 38.1 m area within each plot was combined and yield determined. Soybean yields were adjusted for a water content of 130 g $kg^{-1}$. Soybean grain yield from 1976 to 1991 (except 1977) was used for semivariogram and fractal analyses. Fractal dimensions were estimated using semivariograms as described in case study 1. The linear portion of the log semivariogram vs. log lag (year) contained 3 data points based on the linear-plateau model (Anderson and Nelson, 1975). Therefore, these 3 points were used for estimation of the fractal dimensions. Spectral analysis of time series was performed on the soybean yield to determine if periodicity was present in soybean grain yield across 15 years using SAS (SAS, 1984).

## 3. Results and discussion

### *3.1. Variable rate nitrogen study*

The first step in comparing the slopes (or $D$ since slopes and $D$ are related by constants) of log semivariogram vs. log h among treatments is to determine if they are homogeneous across replications of each treatment. Homogeneity tests indicated no significant difference in $D$-values between replications of each treatment as indicated by non-significant log $h$ × replication interactions (Table 1). It seems that nitrate distribution in this field was homogeneous regardless of the location within the field. If the $D$-values were heterogeneous among replications of each treatment, the $D$-value for each replication of a treatment needs to be reported. Semivariograms for the soil nitrate in 1993 and 1994 for the three treatments are given in Fig. 1. Spatial distribution of soil nitrate in 1993 and 1994 are given in Fig. 2.

Table 1
Homogeneity test for the slopes of log semivariogram vs. log $h$ (lag) for the soil nitrate for three N treatments in the variable rate N study

| Variable | *df* | 1993 | | | 1994 | | |
|---|---|---|---|---|---|---|---|
| | | Fixed | Variable | Variable − 15% | Fixed | Variable | Variable − 15% |
| Replication | 4 | 0.01 | 0.01 | 0.01 | 0.10 | 0.01 | 0.01 |
| Log $h$[a] | 1 | 0.01 | 0.05 | 0.01 | 0.03 | 0.01 | 0.01 |
| Log $h$ × replication | 4 | 0.13 | 0.35 | 0.31 | 0.37 | 0.38 | 0.14 |

[a]Seven lags for soil nitrate.

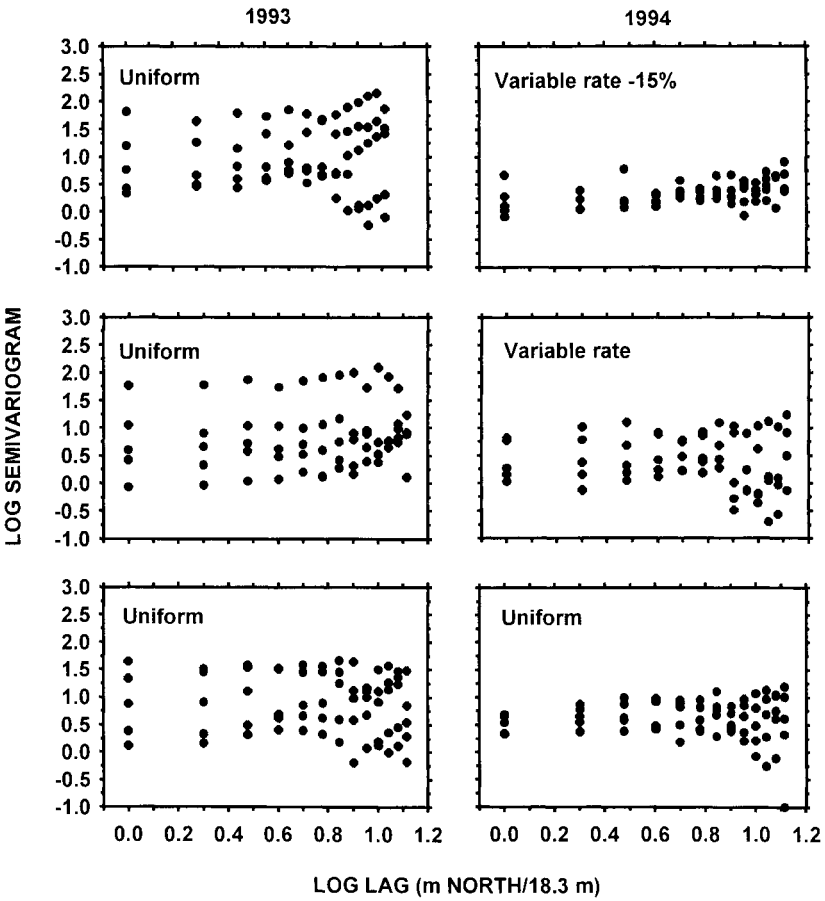


Fig. 1. Log semivariogram of soil nitrate in 1993 and 1994 for three treatments.

Analysis of covariance indicted no significant differences among treatments for the $D$-values of soil nitrate in either year (Table 2). There were significant differences among treatments for the log $k$-values of soil nitrate in 1994 (Table 2). Soil nitrate sampling in 1994 reflected the residual nitrate values after spring application of all three treatments. Variable rate – 15% N application rate had the lowest log $k$-value in 1994 (Fig. 2) indicting lower extent of variation while uniform N application had the highest log $k$-value indicating the greatest extent of variation. In another study with similar N treatments, $D$- and log $k$-values were not different among treatments (Eghball et al., 1997). Nitrate levels in that study were much less than the values reported in this paper. The $D$-values were not significantly different between years for each treatment. The extent of variation decreased from 1993 to 1994 for all treatments as indicated by lower log $k$-values in 1994 compare to 1993. It appears that when N application is made based on soil sampling, spatial soil nitrate variability tends to decrease

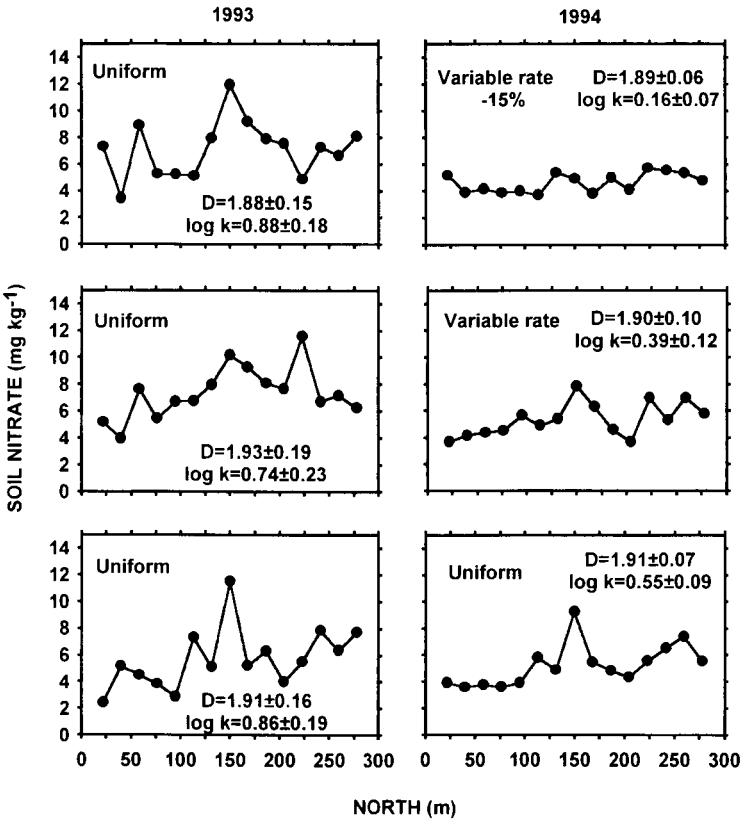


Fig. 2. Soil nitrate concentration to a depth of 0.9 m in 2 years for three treatments. $D$ is fractal dimension and log $k$ is the intercept of log semivariogram vs. log lag ($h$). Fractal dimensions were estimated using seven lags.

Table 2
Analysis of covariance for semivariograms of soil nitrate in the variable rate N study

| Variable | *df* | PR > F | |
|---|---|---|---|
| | | 1993 | 1994 |
| Replication | 4 | 0.01 | 0.01 |
| Treatment[a] | 2 | 0.80 | 0.01 |
| VAR vs. VAR − 15% | 1 | 0.54 | 0.07 |
| FIXED vs. VAR and VAR − 15% | 1 | 0.78 | 0.01 |
| Log $h$[b] | 1 | 0.24 | 0.02 |
| Log $h \times$ treatment[c] | 2 | 0.96 | 0.98 |
| VAR vs. VAR − 15% | 1 | 0.78 | 0.90 |
| FIXED vs. VAR and VAR − 15% | 1 | 0.97 | 0.89 |

[a]The contrasts that follows compare intercepts (log $k$).
[b]Log $h$ is the log of lag (distance).
[c]The contrasts that follows compare slopes (4-2$D$) where $D$ is fractal dimension.

with variable rate N application having the greatest effect. Fractal dimension > 1.8 value for the treatments indicate that nitrate distribution was dominated by short-range spatial variability.

Site-specific management system is supposed to reduce soil and plant variability. The finding in this study that VRAT N application reduced the extent of variation of soil nitrate seems to support this hypothesis. The original soil nitrate level needs to be sufficiently high, as in this study, so that VRAT N application can make a difference in reducing soil nitrate variability.

### *3.2. Long-term study*

Test of homogeneity indicated that the slopes were not significantly different among replications of each treatment as indicated by non-significant log $h \times$ replication interactions in Table 3. A significant log $h \times$ replication interaction indicates that different variability patterns exist among replications. Semivariograms for the three treatments are given in Fig. 3. Soybean grain yields are given in Fig. 4. Average soybean yields across 15 years were 2.29, 2.34, and 2.16 Mg $ha^{-1}$ for FO, HF, and OR, respectively. No significant difference was observed among treatments for grain yield.

Analysis of covariance indicated that no differences existed between *D*- or log *k*-values of the three treatments studied (Table 4). Corn grown organically was reported to have less year-to-year grain yield variation than corn grown with synthetic chemicals (Sahs and Lesoing, 1985). In this study, the variation of the organic system was no different than the systems receiving chemical inputs. The *D*-values were 1.61 for FO, 1.65 for FH and 1.56 for ORG systems indicating that a similar pattern was present in the yield variability of all three systems.

Spectral time series analysis indicated no strong periodicity in the soybean yield across 15 years for any of the treatments. Fractal analysis indicated dominance of short-term (year-to-year) variation in soybean yield for all the three treatments.

Since the treatments did not significantly influence soybean yield temporal variability, effects of other environmental factors on soybean yield were considered by using stepwise regression (SAS, 1985). The factors considered included rainfall from harvest to planting, average low and high temperatures, and rainfall

Table 3
Homogeneity test for the slopes of log semivariogram vs. log *h* (lag, year) for the treatments in the long-term study

| Variable | *df* | Treatment (PR > F) | | |
|---|---|---|---|---|
| | | Fertilizer | Fertilizer + herbicide | Organic |
| Replication | 3 | 0.72 | 0.59 | 0.88 |
| Log *h* | 1 | 0.01 | 0.01 | 0.01 |
| Log $h \times$ replication | 3 | 0.91 | 0.96 | 0.98 |

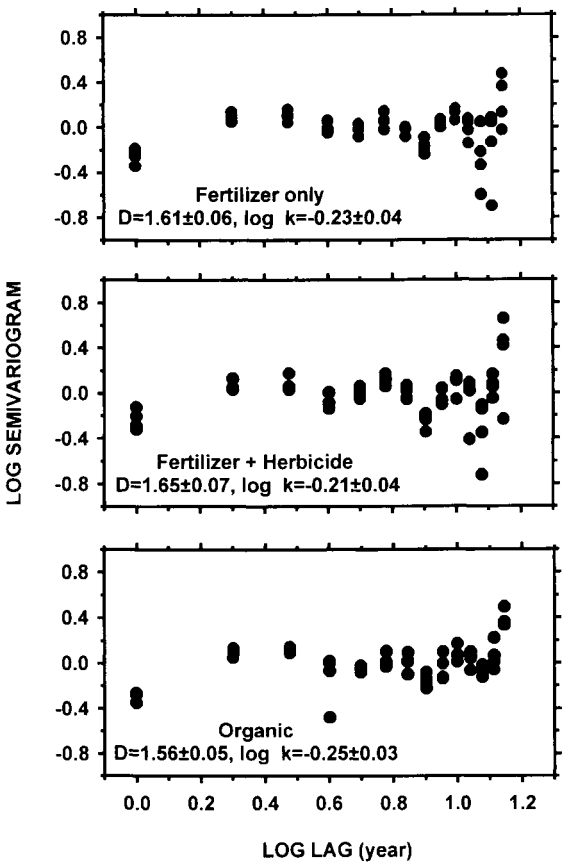


Fig. 3. Log semivariogram of soybean grain yield vs. log lag ($h$, year) for three treatments. $D$ is fractal dimension and log $k$ is the intercept of log semivariogram vs. log lag ($h$, year). Fractal dimensions were estimated using three lags.

during May, June, July, August, and September. August rain accounted for 51% of soybean grain yield variability across 15 years (Table 5). August and July rainfall accounted for 65% of the variability in soybean yield (Table 5). Water availability during July and August seems particularly important for soybean as it goes through flowering and reproductive stages during these months. Other important factors were rainfall during June and September, August average low temperature, and average high temperatures during May and June. For conditions similar to eastern Nebraska, soybean varieties may be chosen that are more drought tolerant. If available, irrigation during August and July would increase soybean grain yield.

### *3.3. Comparison of fractal analysis with other methods*

One of the advantages of using fractal analysis for characterizing and comparing variability of parameters collected in space or time is that fractal

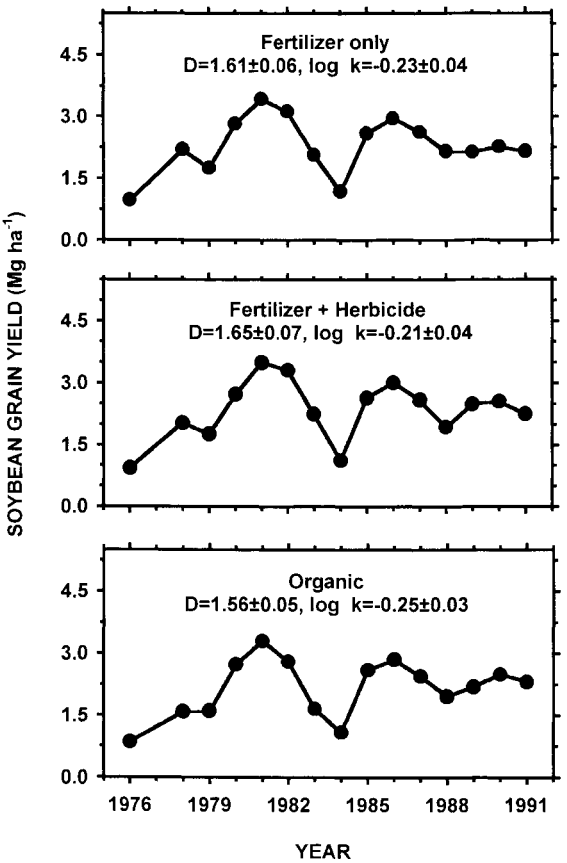


Fig. 4. Soybean grain yield distribution from 1975 to 1991 for three treatments. $D$ is fractal dimension and log $k$ is the intercept of log semivariogram vs. log lag ($h$, year). Fractal dimensions were estimated using three lags.

Table 4
Analysis of covariance for semivariograms of soybean yield from 1976 to 1991 in the long-term study

| Variable | *df* | Probability level |
|---|---|---|
| Replication | 3 | 0.12 |
| Treatment[a] | 2 | 0.66 |
| Organic vs. Fertilizer and Fertilizer + herbicide | 1 | 0.41 |
| Fertilizer vs. Fertilizer and Herbicide | 1 | 0.69 |
| Log $h$[b] | 1 | 0.01 |
| Log $h \times$ treatment[c] | 2 | 0.57 |
| Organic vs. Fertilizer and Fertilizer + herbicide | 1 | 0.36 |
| Fertilizer vs. Fertilizer and Herbicide | 1 | 0.61 |

[a]The contrasts that follows compare intercepts (log $k$).
[b]Log $h$ is the log of lag (year).
[c]The contrasts that follows compare slopes (4-2$D$) where $D$ is fractal dimension.

Table 5
Stepwise regression analysis for the effects of environmental factors on soybean grain yield across three treatments from 1976 to 1991 ($R^2 = 0.831$)

| Variable[a] | Partial $R^2$ | Parameter estimate | Standard error |
|---|---|---|---|
| Intercept | – | −8.2937** | 1.8323 |
| August rain | 0.507 | 0.0731** | 0.0078 |
| July rain | 0.143 | 0.1101** | 0.0154 |
| August average low temperature | 0.049 | 0.2293** | 0.0538 |
| September rain | 0.049 | 0.0420** | 0.0111 |
| May average high temperature | 0.034 | 0.0808* | 0.0367 |
| June average high temperature | 0.027 | 0.0887* | 0.0384 |
| June rain | 0.022 | 0.0336** | 0.0112 |

[a]The analysis included amount of rain from harvest to planting, average low and high temperatures and rainfall during May, June, July, August, and September of each year.
** and * indicate significant at 0.01 and 0.05 probability levels. Other factors did meet the 0.10 probability level.

dimension is scale independent and does not depend on the magnitude of the parameters. In fractal analysis, the pattern of variation of a parameter is characterized not the parameter itself. In standard statistics (CV, SD, etc.), variation of values from the mean is determined while in variogram and fractal analyses, variability along a direction representing space or time is evaluated. Using standard statistics to evaluate temporal or spatial variability may result is misleading conclusion. Eghball and Power (1995) compared average yield of 10 crops for temporal variability across 60 years and found that soybean had the highest $D$-value indicating greatest short-term variation, but CV for soybean was the lowest among the 10 crops.

Domination of short or long-range variation can be determined and compared between treatments or management systems in fractal analysis. This is needed to determine the best management systems to alleviate short or long-range variability. For a discussion of comparing fractal analysis with the stability analysis for characterizing variability see Eghball and Varvel (1997).

Spectral analysis of time series can be used to determine if there is a strong periodicity in data collected in time (Fuller, 1976; Janacek and Swift, 1993). Fractal analysis can be used to characterize variability whether or not there is periodicity in the data.

## 4. Conclusions

Fractal analysis characterized the pattern and extent of spatial and temporal variability in a site-specific and a long-term study. Fractal dimensions and log $k$-values for various parameters were compared among treatments or manage-

ment systems using analysis of covariance. In the VRAT study, the extent of spatial variability for soil nitrate became significantly less after imposing N application regimes, with variable rate − 15% treatment having the lowest and uniform application having the highest log $k$-values. It appears that whenever soil nitrate variability is high and N is applied based on proper soil sampling, residual nitrate distribution in the soil will have less variability. In the long-term study, the organic system had similar temporal soybean yield variability to systems that received chemical inputs. Management system did not change temporal soybean yield variability in this study even though organic systems are claimed to have less year-to-year yield variation than chemical-based systems. Rainfall during August accounted for 51% of the soybean yield variability.

In soil research where spatial or temporal variability is evaluated, semivariogram is usually determined for kriging and mapping. Fractal dimension can also be determine from this semivariogram to evaluate the extent of domination of short and long range-variation. Kriging and mapping may not be useful when there is a strong domination of short-range variation.

The limitation of fractal analysis for temporal variability cases may be the number of observations that is needed for a good approximation of fractal dimension. In agronomic research where observation about crop yield is made once a year, only crop yield data from long-term experiments can be evaluated.

## References


Anderson, R.L., Nelson, L.A., 1975. A family of models involving intersecting straight lines and concomitant experimental designs useful in evaluation response to fertilizer nutrients. Biometrics 31, 303–318.

Armstrong, A.C., 1986. On the fractal dimensions of some transient soil properties. J. Soil Sci. 37, 641–652.

Berry, M.V., Lewis, Z.V., 1980. On the Weierstrass–Mandelbrot fractal function. Proc. R. Soc. London A 370, 459–484.

Burrough, P.A., 1981. Fractal dimensions of landscapes and other environmental data. Nature 294, 240–242.

Burrough, P.A., 1983. Multiscale sources of spatial variation in soil: I. The application of fractal concepts to nested levels of soil variation. J. Soil Sci. 34, 577–597.

Clark, I., 1979. Practical Geostatistics. Applied Science Publishers, London.

Eghball, B., Power, J.F., 1995. Fractal description of temporal yield variability of ten crops in the United States. Agron. J. 87, 152–156.

Eghball, B., Varvel, G.E., 1997. Fractal analysis of temporal yield variability of crop sequences: implications for site-specific management. Agron. J. 89, 851–855.

Eghball, B., Settimi, J.A., Maranville, J.W., Parkhurst, A.N., 1993a. Fractal analysis for morphological description of corn roots under nitrogen stress. Agron. J. 85, 287–289.

Eghball, B., Mielke, L.N., Calvo, G.A., Wilhelm, W.W., 1993b. Fractal description of soil fragmentation for various tillage methods and crop sequences. Soil Sci. Soc. Am. J. 57, 1337–1341.

Eghball, B., Binford, G.D., Power, J.F., Baltensperger, D.D., Anderson, F.N., 1995. Maize temporal yield variability under long-term manure and fertilizer application: fractal analysis. Soil Sci. Soc. Am. J. 59, 1360–1364.

Eghball, B., Ferguson, R.B., Varvel, G.E., Hergert, G.W., Gotway, C.A., 1997. Fractal characterization of spatial and temporal variability in site-specific and long-term studies. In: Novak, M.M., Dewey, T.G. (Eds.), Fractal Frontiers. World Scientific, Singapore, pp. 339–348.

Ferguson, R.B., Gotway, C.A., Hergert, G.W., Peterson, T.A., 1996. Soil sampling for site-specific management. In: Roberts, P.C., Rust, R.H., Larson, W.E. (Eds.), Precision Agriculture. Proceedings of the 3rd International Conference. American Society of Agronomy, Madison, WI, pp. 13–22.

Folorunso, O.A., Puente, C.E., Rolston, D.E., Pinzon, J.E., 1994. Statistical and fractal evaluation of the spatial characteristics of soil surface strength. Soil Sci. Soc. Am. J. 58, 284–294.

Fuller, W.A., 1976. Introduction to Statistical Time Series. Wiley, New York.

Hergert, G.W., Ferguson, R.B., Shapiro, C.A., 1995. Fertilizer suggestions for corn. NebGuide G74–174 (revised). Univ. of Nebraska Cooperative Extension Service.

Huang, C., Bradford, J.M., 1992. Application of a laser scanner to qualify soil microtopography. Soil Sci. Soc. Am. J. 56, 14–21.

Isaaks, E.H., Srivastava, R.M., 1989. An Introduction to Applied Geostatistics. Oxford Univ. Press, New York.

Janacek, G., Swift, L., 1993. Time Series: Forecasting, Simulation, Application. Ellis Horwood, New York.

Kemblowski, M.W., Chang, C.M., 1993. Infiltration in soils with fractal permeability distribution. Groundwater 31, 187–192.

Pachepsky, Y.A., Shcherbakov, R.A., Korsunskaya, L.P., 1995. Scaling of soil water retention using a fractal model. Soil Sci. 159, 99–104.

Perfect, E., Kay, B.D., 1991. Fractal theory applied to soil aggregation. Soil Sci. Soc. Am. J. 55, 1552–1558.

Perfect, E., Kay, B.D., 1995. Applications of fractals in soil and tillage research: a review. Soil and Tillage Research 36, 1–20.

Perfect, E., Blevins, R.L., 1997. Fractal characterization of soil aggregation and fragmentation as influenced by tillage treatments. Soil Sci. Soc. Am. J. 61, 896–900.

Perfect, E., Groenevelt, B.D., Kay, B.D., Grant, C.D., 1990. Spatial variability of soil peneterometer measurements at the mesoscopic scale. Soil and Tillage Research 16, 257–271.

Peters, E.E., 1994. Fractal Market Analysis: Applying Chaos Theory to Investment and Economics. Wiley, New York.

Sahs, W.W., Lesoing, G.W., 1985. Crop rotations and manure versus agricultural chemicals in dryland grain production. J. Soil and Water Conserv. 40, 511–516.

SAS, 1984. SAS/ETS User's Guide. SAS Institute, Cary, NC.

SAS, 1985. SAS User's Guide. SAS Institute, Cary, NC.

*Fractals in Soil Science*
Editors: Ya.A. Pachepsky, J.W. Crawford and W.J. Rawls
© 2000 Elsevier Science B.V. All rights reserved.


# Bibliography on applications of fractals in soil science

Yakov A. Pachepsky [1], Daniel Giménez [2], Walter J. Rawls [1]

[1] *USDA-ARS, Hydrology Laboratory, Beltsville, MD 20705, USA*
[2] *Department of Environmental Sciences, Rutgers, The State University of New Jersey, New Brunswick, NJ 08901, USA*

Abdalla, S.H.M., Boddy, L., 1996. Effect of soil and litter type on outgrowth patterns of mycelial systems of Phanerochaete velutina. FEMS microbiology ecology 20, 195–204.

Agnese, C., Crescimanno, G., Lovino, M., 1994. On the possibility of predicting the hydrological characteristics of soil from the fractal structure of porous media. Annals of Geophysics 12, suppl. II, 482–494.

Ahl, C., Niemeyer, J., 1989. The fractal dimension of the pore-volume inside soils. Zeitschrift Pflanzenernährung und Bodenkunde 152, 457–458.

Ahl, C., Niemeyer, J., 1989. Fractal geometric objects in the soil. Mitt. Deutsch. Bodenk. Gesellschaft 59, 93–98.

Amin, M.H.G., Richards, K.S., Chorley, R.J., Gibbs, S.J., Carpenter, T.A., Hall, L.D., 1995. Studies of soil water transport by MRI. Magnetic Resonance Imaging 14, 879–882.

Anderson, A.N., McBratney, A.B., 1995. Soil aggregates as mass fractals. Australian Journal of Soil Research 33, 757–772.

Anderson, A.N., McBratney, A.B., Fitzpatrick, E.A., 1996. Soil mass, surface, and spectral fractal dimensions estimated from thin section photographs. Soil Science Society of America Journal 60, 962–969.

Anderson, A.N., McBratney, A.B., Crawford, J.W., 1998. Applications of fractals to soil studies. Advances in Agronomy 63, 1–76.

Anderson, A.R.A., Young, I.M., Sleeman, B.D., Griffiths, B.S., Robertson, W.M., 1997. Nematode movement along a chemical gradient in a structurally heterogeneous environment. I. Experiment. Fundamental and Applied Nematology 20, 157–163.

Anderson, S.H., Liu, X., Peyton, R.L., Gantzer, C.J., 1998. Fractal analysis of CT-measured solute transport parameters. In: Proceedings of the World Congress of Soil Science, 20–26 August 1998, Montpellier, France. CD-ROM.

Arias, M., Lopez, E., Barral, T., 1997. Comparison of functions for evaluationg the effect of Fe and Al oxides on the particle size distribution of kaolin and quartz. Clay minerals 32, 3–11.

Armstrong, A.C., 1986. On the fractal dimensions of some transient soil properties. Journal of Soil Science 37, 641–652.

Arnold, R.W., 1990. Fractal dimensions of soil map units. In Transactions of 14th International Congress of Soil Science, Japan, Vol. V, pp. 92–97.

Aubertot, J.N., Durr, C., Kieu, K., Richard, G., 1999. Charcaterization of sugarbeet seedbed structure. Soil Science Society of America Journal 63, 1377–1384.

Avnir, D., Farin, D., Pfeifer, P., 1985. Surface geometric irregularity of particulate materials: The fractal approach. Journal of Colloid and Interface Science 103, 112–123.

Bacchi, O.O.S., Reichardt, K., Villa Nova, N.A., 1998. Fractal, particle size distribution, pore size distribution, soil water retention, soil hydraulic conductivity. In: Proceedings of the World Congress of Soil Science, 20–26 August 1998, Montpellier, France. CD-ROM.

Barak, P., Seybold, C.A., McSweeney, K., 1996. Self-similitude and fractal dimension of sand grains. Soil Science Society of America Journal 60, 72–76.

Bartoli, F., Philippy, R., Doirisse, M., Niquet, S., Dubuit, M., 1991. Structure and self-similarity in silty and sandy soil: the fractal approach. Journal of Soil Science 42, 167–185.

Bartoli, F., Philippy, R., Burtin, G., 1992. Influence of organic matter on aggregation in Oxisols rich in gibbsite or in goethite. I. Structures: the fractal approach. Geoderma 54, 231–257.

Bartoli, F., Philippy, R., Burtin, G., 1992. Influence of organic matter on aggregation in Oxisols rich gibbsite or in goethite. II. Clay dispersion, aggregate strength and water-stability. Geoderma 54, 257–274.

Bartoli, F., Philippy, R., Burtin, G., 1992. Poorly-ordered hydrous Fe oxides, colloidal dispersion and soil aggregation. II. Modification of silty soil aggregation by addition of Fe(III) polycations and model humic macromolecule models. Journal of Soil Science 43, 59–75.

Bartoli, F., Burtin, G., Philippy, R., Gras, F., 1993. Influence of fir root zone on soil structure in a 23 m forest transect: The fractal approach. Geoderma 56, 67–85.

Bartoli, F., Burtin, G., Royer, J.J., Gury, M., Gomendy, V., Phillppy, R., Leviandier, T., Gafrej, R., 1995. Spatial variability of topsoil characteristics within one silty soil type. Effect on clay migration. Geoderma 68, 279–300.

Bartoli, F., Dutartre, P., Gomendy, V., Niquet, S., Dubuit, M., Vivier, H., 1997. Fractals and soil structure. In: Baveye, P., Parlange, J.-Y., Stewart, B.A. (Eds.), Fractals in Soil Science, CRC Press, Boca Raton, FL, pp. 203–232.

Bartoli, F., Bird, N., Gomendy, V., Vivier, H., 1999. The relationship between silty soil structures and their mercury porosimetry curve counterparts: fractals and percolation. European Journal of Soil Science 50, 9–22.

Baveye, P., Boast, C.W., 1997. Fractal geometry, fragmentation processes and the physics of scale-invariance: an introduction. In: Baveye, P., Parlange, J.-Y., Stewart, B.A. (Eds.), Fractals in Soil Science. Lewis Publishers, Boca Raton, FL, pp. 1–54.

Baveye, P., Boast, C.W., 1998. Concepts of "fractals" in soil science: demixing apples and oranges. Soil Science Society of America Journal 62, 1469.

Baveye, P., Boast, C.W., Ogawa, S., Parlange, J.Y., Steenhuis, T., 1998. Influence of image resolution and thresholding on the apparent mass fractal characteristics of preferential flow patterns in field soils. Water Resource Research 34, 2783–2796.

Beauvais, A., Dubois, J., Badri, A., 1994. Application d'une analyse fractale a l'etude morphometrique du trace des cours d'eau methode de Richardson. Academie des Sciences 318, Serie II, 219–225.

Berntson, G.M., 1994. Root systems and fractals: How reliable are calculations of fractal dimensions? Annals of Botany 73, 281–284.

Berntson, G.M., 1997. Topological scaling and plant root system architecture: Developmental and functional hierarchies. New Phytologist 135, 621–634.

Berntson, G.M., Lynch, J., Snapp, S., 1997. Fractal geometry and the description of plant root systems: Current perspectives and future applications. In: Baveye, P., Parlange, J.-Y., Stewart, B.A. (Eds.), Fractals in Soil Science, CRC Press, Boca Raton, FL, pp. 113–152.

Bertuzzi, P., Rauws, G., Courault, D., 1990. Testing roughness indices to estimate soil surface roughness changes due to simulated rainfall. Soil and Tillage Research 17, 87–99.

Biondini, M.E., Crygiel, C.E., 1994. Landscape distribution of organisms and the scaling of soil resources. American Naturalist 143, 1026–1059.

Bird, N.R.A., 1997. Comments on 'The relation between the moisture-release curve and the structure of soil' by J.W. Crawford, N. Matsui, and I.M. Young. European Journal of Soil Science 46, 188–189.

Bird, N.R.A., 1998. Comment on 'An improved fractal equation for the soil water retention curve' by E. Perfect et al. Water Resources Research 34, 929–930.

Bird, N.R.A., Bartoli, F., Dexter, A.R., 1996. Water retention models for fractal soil structures. European Journal of Soil Science 47, 1–6.

Bird, N.R.A., Dexter, A.R., 1997. Simulation of soil water retention using random fractal networks. European Journal of Soil Science 48, 633–641.

Bird, N.R.A., Perrier, E., Rieu, M., 2000. The water retention function for a model of soil structure with pore and solid fractal distributions. European Journal of Soil Science 51, 55–63.

Bitelli, M., Campbell, G.S., Flury, M., 1999. Characterization of particle size distribution in soil with a fragmentation model. Soil Science Society of America Journal 63, 782–788.

Blagoveschensky, Y.N., Samsonova, V.P., 1999. Fractal and the statistical analysis of spatial distributions of Fe-Mn concretions in soddy-podsolic soils. Geoderma 88, 265–282.

Boddy, L., 1999. Saprotrophic cord-forming fungi: meeting the challenge of heterogeneous environment. Mycologia 91, 13–32.

Boddy, L., Wells, J.M., Culshaw, C., Donelly, D.P., 1999. Fractal analysis in studies of mycelium in soil. Geoderma 88, 301–328.

Bolton, R.G., Boddy, L., 1993. Characterization of the spatial aspects of foraging mycelial cord systems using fractal geometry. Mycological Research 97, 762–768.

Bonala, M.V.S., Reddi, L.N., 1999. Fractal representation of soil cohesion. Journal of Geotechnical and Geoenvironmental Engineering 125, 901–904.

Booltink, H.W.G., Hatano, R., Bouma, J., 1993. Measurement and simulation of bypass flow in a structured clay soil: A physico-morphological approach. Journal of Hydrology 148, 149–168.

Borkovec, M., Wu, Q., Dedovics, G., Laggner, P., Sticher, H., 1993. Surface area and size distributions of soil particles. Colloids Surf. A 73, 65–76.

Brakensiek, D.L., Rawls, W.J., Logsdon, S.D., Edwards, W.M., 1992. Fractal description of macroporosity. Soil Science Society of America Journal 56, 1721–1723.

Brakensiek, D.L., Rawls, W.J., 1992. Comment on 'Fractal processes in soil water retention' by S.W. Tyler and S.W. Wheatcraft. Water Resources Research 28, 601–602.

Burrough, P.A., 1981. Fractal dimensions of landscapes and other environmental data. Nature 294, 240–242.

Burrough, P.A., 1983. Multiscale sources of spatial variation in soil. I. The application of fractal concepts to nested levels of soil variation. Journal of Soil Science 34, 577–597.

Burrough, P.A., 1983. Multiscale sources of spatial variation in soil. II. A non-Brownian fractal model and its application in soil survey. Journal of Soil Science 34, 599–620.

Burrough, P.A., 1983. Problems of superimposed effects in the statistical study of the spatial variation of soil. Agricultural Water Management 6, 123–144.

Castrignanò, A., Stelluti, M., 1997. Appliazione dello "Scaling" frattale alla suddivisione a secco degli aggregati: Analisi e Limitazioni. Rivista di Agronomia 3, 832–839 (In Ital.).

Castrignanò, A., Stelluti, M., 1999. Fractal geometry and geostatistics for describing the field variability of soil aggregation. Journal of Agricultural Engineering Research 73, 13–18.

Chang, C.-M., Kemblowski, M.W., 1995. Stochastic analysis of unsaturated transport in soils with fractal log-conductivity distribution. Stochastic Hydrology and Hydraulics 9, 297–304.

Chang, W.-L., Biggar, J.W., Nielsen, D.R., 1994. Fractal description of wetting front instability in layered soils. Water Resources Research 30, 125–132.

Chen, S.C., 1998. Estimating the hydraulic conductivity and diffusivity in unsaturated porous media by fractal capillary model. Journal of the Chinese Institute of Engineering 21, 449–458.

Chicushi, J., Hirota, O., 1998. Simulation of root development based on the dielectric breakdown model. Hydrological Sciences Journal 43, 549–560.

Classen, J.J., Liu, W., Kenerleg, C.M., Whitakker, A.D., 1996. Fractal analysis of subsurface growth of a genetically modified strain of Gliocladium virens and its parental strain. Transactions of the ASAE 39, p. 2271–2276.

Comegna, V., Damiani, P., Sommella, A., 1998. Use of a fractal model for determining soil water retention curves. Geoderma 85, 307–323.

Cosh, M.H., Brutsaerts, W., 1999. Aspects of soil moisture variability in the Washita 92 study region. Journal of Geophysical Research 104, 19751–19757.

Coulombe, C.E., Wilding, L.P., Dixon, J.B., 1995. Overview of vertisols: Characteristics and impacts on society. Advances in Agronomy 57, 289–375.

Crawford, J.W., 1994. The relationship between structure and the hydraulic conductivity of soil. European Journal of Soil Science 45, 493–502.

Crawford, J.W., Ritz, K., Young, I.M., 1993. Quantification of fungal morphology, gaseous transport and microbial dynamics in soil: an integrated framework utilizing fractal geometry. Geoderma 56, 157–172.

Crawford, J.W., Sleeman, B.D., Young, I.M., 1993. On the relation between number-size distribution and the fractal dimension of aggregates. Journal of Soil Science 44, 555–565.

Crawford, J.W., Matsui, N., Young, I.M., 1995. The relation between the moisture release curve and the structure of soil. Eur. J. Soil. Sci. 46, 369–375.

Crawford, J.W., Matsui, N., 1996. Heterogeneity of the pore and solid volume of soil: distinguishing a fractal space from its non-fractal complement. Geoderma 73, 183–195.

Crawford, J.W., Verrall, S., Young, I.M., 1997. The origin and loss of fractal scaling in simulated soil aggregates. European Journal of Soil Science 48, 643–650.

Crawford, J.W., Young, I.M., 1997. The interactions between soil structure and microbial dynamics. In: Baveye, P., Parlange, J.-Y., Stewart, B.A. (Eds.), Fractals in Soil Science, CRC Press, Boca Raton, FL. pp. 233–260.

Crawford, J.W., Matsui, N., Young, I.M., 1997. Reply to "Comments on 'The relation between the moisture-release curve and the structure of soil' by N.R.A. Bird". European Journal of Soil Science 46, 189–191.

Crawford, J.W., Pachepsky, Ya.A., Rawls, W.J., 1999. Integrating processes in soils using fractal models. Geoderma 88, 103–107.

Crawford, J.W., Baveye, P., Grindrod, P., Rappoldt, C., 1999. Application of fractals to soil properties, landscape patterns and solute transport in porous media. In: Corwin, D.L., Loague, K., Ellsworth, T.W. (Eds.), Advanced Information Technologies for Assessing Non-point Source Pollutants in the Vandose Zone. American Geophysical Union, Washington, DC.

Crestana, S., Posadas, A.N.D., 1997. 2-D and 3-D fingering in unsaturated soils investigated by fractal analysis, invasion percolation modeling and non-destructive image processing In: Baveye, P., Parlange, J.-Y., Stewart, B.A. (Eds.), Fractals in Soil Science, CRC Press, Boca Raton, FL. pp. 293–332.

Crestana, S., Vaz, C.M.P., 1998. Non-invasive instrumentation opportunities for characterizing soil porous media. Soil and Tillage Research 47, 61–66.

Culling, W.E.H., 1986. Highly erratic spatial variability of soil-pH on Iping Common, West Sussex, Catena 13, 81–98.

Culling, W.E.H., 1988. Dimension and entropy in the soil-covered landscape. Earth Surface Processes and Landforms 13, 619–648.

Culling, W.E.H., 1989. The characterization of regular/irregular surfaces in the soil-covered landscape by Gaussian random fields. Computers and Geosciences 15, 219–226.

Culling, W.E.H., Datko, M., 1987. The fractal geometry of the soil-covered landscape. Earth Surface Processes and Landforms 12, 369–385.

Czirok, A., Somfai, E., Vicsek, T., 1997. Fractal scaling and power law landslide distribution in a micromodel of geomorphic evolution. Geologische Rundschau 86, 525–530.

Daccord, G., Touboul, E., Lenormand, R., 1989. Chemical dissolution of a porous medium: Limits of the fractal behaviour. Geoderma 44, 159–165.

Dachs, J., Bayona, J.M., 1997. Langmuir-derived model for diffusion- and reaction-limited adsorption of organic compounds on fractal aggregates. Environmental Science and Technology 31, 2754–2760.

Dachs, J., Bayona, J.M., 1998. On the occurrence of microscale chemical patches in fractal aggregates. Ecological Modelling 107, 87–92.

Davies, S., Hall, P., 1999. Fractal analysis of surface roughness by using spatial data. Jornal of Royal Statistical Society, Ser. B – Statistical methodology 61, 3–29.

Degovics, G., Laggner, P., Borkovec, M., 1993. Fractal structures of soil particles as revealed by small-angle X-ray scattering studies. Progress in Colloid and Polymer Science 93, 209–218.

Donnelly, D.P., Wilkins, M.F., Boddy, L., 1995. An integrated image analysis approach for determining biomass, radial extent and box-count fractal dimension of macroscopic mycelial systems. Binary 7, 19–28.

Donnelly, D.P., Boddy, L., 1997. Resource acquisition by the mycelial-cord-former Stropharia caerulea: effect of resource quantity and quality. FEMS Microbiology Ecology 23, 195–205.

Donnelly, D.P., Boddy, L., 1997. Development of mycelial systems of Stropharia caerulea and Phanerochaete velutina on soil: effect of temperature and water potential. Mycological Research 101, 705–713.

Donnelly, D.P., Boddy, L., 1998. Developmental and morphological responses of mycelial systems of Stropharia caerulea and Phanerochaete velutina to soil nutrient enrichment. New Phytologist 138, 519–531.

Donnelly, D.P., Boddy, L., 1998. Repeated damage results in polarised development of foraging mycelial systems of Phanerochaete velutina. FEMS Microbiology and Ecology 26, 101–108.

Droogers, P., Stein, A., Bouma, J., Boer, G.D., 1998. Parameters for describing soil macroporosity derived from staining patterns. Geoderma 83, 293–308.

Eghball, B., Mielke, L.N., Calvo, G., Wilhelm, W., 1993. Fractal description of soil fragmentation for various tillage methods and crop sequences. Soil Science Society of America Journal 57, 1337–1341.

Eghball, B., Settimi, J.R., Maranville, J.W., Parkhurst, A.M., 1993. Fractal analysis for morphological description of corn roots under nitrogen stress. Agronomy Journal 85, 287–289.

Eghball, B., Binford, G.D., Power, J.F., Baltensperger, D.D., Anderson, F.N., 1995. Maize temporal yield variability under long-term manure and fertilizer application: Fractal analysis. Soil Science Society of America Journal 59, 1360–1364.

Eghball, B., Power, J.F., 1995. Fractal description of temporal yield variability of 10 crops in the United States. Agronomy Journal 87, 152–156.

Eghball, B., Ferguson, R.B., Varvel, G.E., Hergert, G.W., Gotway, C.A., 1997. Fractal characterization of spatial and temporal variability in site-specific and long-term studies. In Novak, M.M., Dewey, T.G. (Eds.), Fractal Frontiers, World Scientific, Singapore, pp. 339–347.

Eghball, B., Varvel, G.E., 1997. Fractal analysis of temporal yield variability of crop sequences: Implications for site-specific management. Agronomy Journal 89, 851–855.

Eghball, B., Hergert, G.W., Lesoing, G.W., Ferguson, R.B., 1999. Fractal analysis of spatial and temporal variability. Geoderma 88, 349–362.

Eltz, F.L.F., 1997. Surface roughness changes as affected by rainfall erosivity, tillage, and canopy cover. Soil Science Society of America Journal. Soil Science 61, 1746–1755.

Emerman, S.H., 1995. The tipping bucket equation as a model for macropore flow. Journal of Hydrology 171, 23–47.

Ewing, R.P., Jaynes, D.D., 1995. Issues in single fracture transport modeling – scales, algorithms, and grid types. Water Resource Research 31, 303–312.

Fenton, G.A., 1999. Estimation for stochastic soil models. Journal of Geotechnical and Geoenvironmental Engineering 125, 470–485.

Fenton, G.A., 1999. Random field modeling of CPT data. Journal of Geotechnical and Geoenvironmental Engineering 125, 486–498.

Filgueira, R.R., Sarli, G.O., Piro, A.I., Fournier, L.L., 1997. Determination of the specific surface of soils with nitrogen. The fractal dimension and some experimental difficulties. In: Novak, M.M., Dewey, T.G. (Eds.), Fractal Frontiers. World Scientific, Singapore, p. 477.

Filgueira, R.R., Fournier, L.L., Piro, A., Sarli, G.O., Aragón A., 1997. Aplicación de la matemática fractal a la fragmentación de un suelo. Ciencia del Suelo 15, 33–36 (In Span.).

Filgueira, R.R., Sarli, G.O., Piro, A.I., Fournier, L.L., 1998. Surface-fractal dimension of soil aggregates and rock particles. In: M.M., Novak (Ed.), Fractals and Beyond: Complexities in the Science. World Scientific Publishing, Singapore, pp. 223–229.

Filgueira, R.R., Sarli, G.O., Fournier, L.L., Garcia, M.I., Aragón, A., 1998. El proceso de fragmentación del suelo: Un ehfoque fractal. In: Balbuena, R.H., Benez, S.H., Jorajuría, D. (Eds.), Avances en el Manejo del Suelo y Agua en la Ingeniería Rural Latinoamericana. Editorial de la UNLP (Universidad Nacional de La Plata), La Plata, Argentina, pp. 82–87. (In Span.).

Filgueira, R.R., Pachepsky, Ya.A., Fournier, L.L., Sarli, G.O., Aragón, A., 1999. Comparison of fractal dimensions estimated from aggregate mass-size distribution and water retention scaling. Soil Science 164, 217–223.

Filgueira, R.R., Fournier, L.L., Sarli, G.O., Aragón, A., Rawls, W.J., 1999. Sensitivity of fractal parameters of soil aggregates to differences in managements practices. Soil and Tillage Research 52, 217–222.

Fitter, A.H., Stickland, T.R., 1992. Fractal characterization of root system architecture. Functional Ecology 6, 632–635.

Flury, M., Flühler, H., 1995. Modeling solute leaching in soils by diffusion-limited aggregation: Basic concepts and application to conservative solutes. Water Resources Research 31, 2443–2452.

Folorunso, O.A., Puente, C.E., Rolston, D.E., Pinzon, J.E., 1994. Statistical and fractal evaluation of the spatial characteristics of soil surface strength. Soil Science Society of America Journal 58, 284–294.

Fuentes, C., 1992. Approache fractale des transferts hydriques deans les sols nonsaturés. Ph.D. thesis. University of Grenoble, France.

Fuentes, C., Vauclin, M., Parlange, J.-Y., Haverkamp, R., 1996. A note on the soil-water conductivity of a fractal soil. Transport in Porous Media 23, 31–36.

Fuentes, C., Vauclin, M., Parlange, J.-Y., Haverkamp, R., 1997. Soil-water conductivity of a fractal soil. In: Baveye, P., Parlange, J.-Y., Stewart, B.A. (Eds.), Fractals in Soil Science, CRC Press, Boca Raton, FL, pp. 333–340.

Gallart, F., Padini, G., 1996. Perfilru un programa para el analysis de perfiles microtopograficos mediante el estudio de la geometria fractal. Gadernos Xeoloxico de Laxe 21, 163–176.

Gantzer, C., Zeng, Y., Anderson, S., Peyton, L., 1998. Fractal dimension and lacunarity of a claypan soil as affected by drying. In: Proceedings of the

World Congress of Soil Science, 20–26 August 1998, Montpellier, France. CD-ROM.

Ghilardi, P., Kai, A.K., Menduni, G., 1993. Self-similar heterogeneity in granular porous media at the representative elementary volume scale. Water Resources Research 29, 1205–1214.

Ghilardi, P., Menduni, G., 1996. Scaling properties of porous media with power law particle size distributions. Journal of Hydrology 187, 223–230.

Giménez, D., 1995. Functional Characterization of Soil Structure: The Fractal Approach. Ph.D. dissertation, University of Minnesota, St. Paul.

Giménez, D., Allmaras, R.R., Nater, E.A., Huggins, D.R., 1997. Fractal dimensions for volume and surface of interaggregate pores: scale effects. Geoderma 77, 19–38.

Giménez, D., Perfect, E., Rawls, W.J., Pachepsky Ya., 1997. Fractal models for predicting soil hydraulic properties: a review. Engineering Geology 48, 161–183.

Giménez, D., Allmaras, R.R., Huggins, D.R., Nater, E.A., 1997. Prediction of the saturated hydraulic conductivity-porosity dependence using fractals. Soil Science Society of America Journal 61, 1285–1292.

Giménez, D., Allmaras, R.R., Nater, E.A., Huggins, D.R., 1997. Fractal dimensions for volume and surface of interaggregate pores – scale effects. Geoderma 77, 19–38.

Giménez, D., Allmaras, R.R., Huggins, D.R., Nater, E.A., 1998. Mass, surface, and fragmentation fractal dimensions of soil fragments produced by tillage. Geoderma 86, 261–278.

Giménez, D., Rawls, W.J., Lauren, J.G., 1999. Scaling properties of saturated hydraulic conductivity in soil. Geoderma 88, 205–220.

Gomendy, V., Bartoli, F., Burtin, G., Doirisse, M., Rhilippy, R., Niquet, S., Vivier, H., 1999. Silty topsoil structure and its dynamics: the fractal approach. Geoderma 88, 165–189.

Grant, C.D., Dexter, A.R., Huang, C., 1990. Roughness of soil fracture surfaces as a measure of soil microstructure. Journal of Soil Science 41, 95–110.

Grant, C.D., Watts, C.W., Dexter, A.R., Frahn, B.S., 1995. An analysis of the fragmentation of remolded soils with regard to self-mulching behavior. Australian Journal of Soil Science 33, 569–583.

Grout, H., Tarquis, A.M., Wiesner, M.R., 1998. Multifractal Analysis of Particle Size Distributions in Soil. Environmental Science and Technology 32, 1176–1182.

Guerrini, I.A., Swartzendruber, D., 1994. Fractal characteristics of the horizontal movement of water in soils. Fractals 2, 465–468.

Guerrini, I.A., Swartzendruber, D., 1997. Fractal concepts in relation to soil water diffusivity. Soil Science 162, 778–784.

Hadas, A., 1997. Soil tilth – the desired soil structural state obtained through proper soil fragmentation and reorientation processes. Soil and Tillage Research 43, 7–40.

Hajnos, M., Sokołowska, Z., Jozefaciuk, G., Hoffmann, Ch., Renger, M., 1999. Effect of leaching of DOC on pore characteristic of a sandy soil. Journal of Plant Nutrition and Soil Science 162, 19–25.

Hallet, P.D., Bird, N.R.A., Dexter, A.R., Seville, J.P.K., 1998. Investigation into the fractal scaling of the structure and strength of soil aggregates. European Journal of Soil Science 49, 203–211.

Hansen, J.P., Muller, J., 1992. Mean field calculation of effective permeability based on fractal pore soil. Transport in Porous Media 8, 93–97.

Hatano, R., 1998. Regression model to predict travel time for chloride leaching through pedons using soil morphological characteristics. Nutrient Cycling in Agroecosystems 50, 267–269.

Hatano, R., Kawamura, N., Ikeda, J., Sakuma, T., 1992. Evaluation of the effect of morphological features of flow paths on solute transport by using fractal dimensions of methylene blue staining pattern. Geoderma 53, 31–44.

Hatano, R., Boolink, H.W.G., 1992. Using fractal dimensions of stained flow patterns in a clay soil to predict bypass flow. Journal of Hydrology 135, 121–131.

Hatano, R., Booltink, H.W.G., 1994. A morphological approach to describe solute movement influenced by bypass flow in a structured clay soil. Soil Science and Plant Nutrition 40, 573–580.

Hatano, R., Boolink, H.W.G., 1997. Using fractal dimensions of stained flow patterns in clay soils to predict bypass flow. In: P. Baveye, Parlange, J.-Y., Stewart, B.A. (Eds.), Fractals in Soil Science. CRC, Boca Raton, FL, pp. 261–291.

Helfenstern, P., Shepard, M.K., 1999. Submillimeter-scale topography of the lunar regolith. ICARUS 141, 107–131.

Herrmann, H.J., Sahimi, M., Tzchichholz, F., 1993. Examples of fractals in soil mechanics. Fractals 1, 795–805.

Holden, N.M., 1993. A 2-dimensional quantification of soil ped shape. Journal of Soil Science 44, 209–219.

Homer, V.J., 1997. Fractal probes of humic aggregation: Scattering techniques for fractal dimension determinations In: Baveye, P., Parlange, J.-Y., Stewart, B.A. (Eds.), Fractals in Soil Science, CRC Press, Boca Raton, FL, pp. 75–112.

Huang, C.-H., 1997. Quantification of soil microtopography and surface roughness. In: Baveye, P., Parlange, J.-Y., Stewart, B.A. (Eds.), Fractals in Soil Science. CRC Press, Boca Raton, FL, pp. 153–168.

Huang, C., Bradford, J.M., 1992. Applications of a laser scanner to quantify soil microtopography. Soil Science Society of America Journal 56, 14–21.

Hyslup, J.P., Vallejo, L.E., 1997. Fractal analysis of the roughness and size distribution of granular materials. Engineering Geology 48, 231–244.

Izumi, Y., Kono, Y., Yamauchi, A., Iijima, M., 1997. Quantitative analysis of the architecture of seminal root system of rice (Oryza sativa L.) grown under

different soil moisture conditions. Japanese Journal of Crop Science 66, 418–426.

Jong, S.M.D., Burrough, P.A., 1995. A Fractal Approach to the Classification of Mediterranean Vegetation Types in Remotely Sensed Images. Photogrammetric Engineering & Remote Sensing 61, 1041–1053.

Jun-Zheng, P., Zhi-Xiong, L., 1994. Fractal dimensions of soil strengths for paddy fields in China. Journal of Terramechanics 31, 1–9.

Kampichler, C., 1995. Biomass distribution of a microarthropod community in spruce forest soil. Biology and fertility of soils 19, 263–265.

Kampichler, C., 1999. Fractal concepts in studies of soil fauna. Geoderma 88, 283–300.

Kampichler, C., Hauser, M., 1993. Roughness of soil pore surface and its effect on available habitat space of microarthropods. Geoderma 56, 223–232.

Kemblowski, M.W., Chang, C.-M., 1993. Infiltration in soils with fractal permeability distribution. Ground Water 31, 187–192.

Kemblowski, M.W., Wen, J.-C., 1993. Contaminant spreading in stratified soils with fractal permeability distribution. Water Resources Research 29, 419–425.

Korvin, G., 1992. Fractal Models in the Earth Sciences. Elsevier, Amsterdam.

Kozak, E., Sokołowska, Z., Sokołowski, S., Wierzchos, J., 1995. Surface fractal dimension of soil materials from pore size distribution data. I. A comparison of two methods of determination. Polish Journal of Soil Science XXXVIII, 76–85.

Kozak, E., Pachepsky, Ya.A., Sokołowski, S., Sokołowska, Z., Stępniewski, W., 1996. A modified number-based method for estimating fragmentation fractal dimensions of soils. Soil Science Society of America Journal 60, 1291–1297.

Koutika, L.S., Bartoli, F., Andreux, F., Cerri, C.C., Burtin, G., Chone, T., Philippy, R., 1997. Organic matter dynamics and aggregation in soils under rain forest and pastures of increasing age in the Eastern Amazon Basin. Geoderma 76, 87–112.

Kravchenko, A.N., Zhang, R.D., 1997. Estimation of soil water retention function from texture and structure data: fractal approach. In: Novak, M.M., Dewey, T.G. (Eds.), Fractal Frontiers. World Scientific, Singapore, pp. 329–338.

Kravchenko, A.N., Zhang, R.D., 1998. Estimating the soil water retention from particle-size distributions: a fractal approach. Soil Science 163, 171–179.

Li, B.-L., Loehle, C., Malon, D., 1994. Microbial transport through heterogeneous porous media: random walk, fractal, and percolation approaches. Ecological Modeling 85, 285–302.

Li, R., Takayasu, H., Inaoka, H., 1996. Water erosion on fractal surface. Fractals 4, 385–392.

Liddell, C.M., Mansen, D., 1993. Visualizing complex biological interactions in the soil ecosystem. Journal of Visualization and Computer Animation 4, 3–12.

Ling, F., Wu, Z.-W., Zhu, Y.-L., 1999. Fractal approximation of the stress-strain curve of frozen soil. Science in China, Series D, Earth Sciences 42 (supplementum), 17–26.

Lipiec, J., Hatano, R., Slowinska-Juriewicz, A., 1998. The fractal dimension of pore distribution patterns in variously compacted soil. Soil and Tillage Research 47, 61–66.

Lui, C., Huang, P.M., 1999. Atomic force microscopy and surface characteristics of iron oxides formed in citrate conditions. Soil Science Society of America Journal 63, 65–72.

Loehle, C., Li, B.-L., 1994. Statistical properties of ecological and geologic fractals. Ecological Modelling 85, 271–284.

Logsdon, S.D., 1995. Analysis of aggregate fractal dimensions and aggregate densities back-calculated from hydraulic conductivity. Soil Science Society of America Journal 59, 1216–1221.

Logsdon, S.D., Giménez, D., Allmaras, R.R., 1996. Fractal characterization of aggregate-size distribution: The question of scale invariance. Soil Science Society of America Journal 60, 1327–1330.

Lynch, J., 1993. Growth and architecture of seedling roots of common bean genotypes. Crop science 33, p. 1253–1257.

Lynch, J.P., Nielsen, K.L., Davis, R.D., Jablokow, A.G., 1997. SimRoot: Modeling and visualization of root systems. Plant and Soil 188, 139–151.

Malekani, K., Rice, J.A., Lin, J.S., 1996. Comparison of techniques for determining the fractal dimension of clay mineral surfaces. Clays and Clay Minerals 44, 677–685.

Malekani, K., Lin, J.S., Rice, J.A., 1997. Fractal characterization of the surface of the humin fraction of soil organic matter. In: Novak, M.M., Dewey, T.G. (Eds.), Fractal frontiers. World Scientific, Singapore, pp. 367–381.

Malekani, K., Rice, J.A., Lin, J.-S., 1997. The effect of sequential removal of organic matter on the surface morphology of humin. Soil Science 162, 333–342.

Malekani, K., Rice, J.A., Lin, J.-S., 1997. Fractal character of humin and its components. Fractals 5, 83–100.

Martín, M.A., Taguas, F.J., 1998. Fractal modelling, characterization and simulation of particle-size distributions in soil. Proceedings of the Royal Society of London, A 454, 1457–1468.

Martinez-Mena, M., Deeks, L.K., Williams, A.G., 1999. An evaluation of a fragmentation fractal dimension technique to determine soil erodibility. Geoderma 90, 87–95.

Masi, C.E.A., Maranville, J.W., 1998. Evaluation of sorghum root branching using fractals. The Journal of Agricultural Science 131, 259–265.

McBratney, A.B., 1993. Comments on 'Fractal Dimensions of Soil Aggregate-Size Distributions Calculated by Number and Mass' by E. Perfect, V. Rasiah, B.D. Kay. Soil Science Society of America Journal 57, 1393–1395.

McBratney, A.B., 1998. Some considerations on methods for spatially aggregating and disaggregating soil information. Nutrient Cycling in Agroecosystems 50, 51–62.

McBratney, A.B., Moran, C.J., 1992. Soil pore structure modeling using fuzzy pseudofractal sets. In: Ringrose-Voase, A.J., Humphreys, G.S. (Eds.), Soil Micromorphology, Vol. 22, Elsevier, Amsterdam; New York. pp. 495–507.

McDowell, G.R., Bolton, M.D., Robertson, D., 1996. Fractal crushing of granular materials. Journal of mechanics and physics of solids 44, 2079–290.

Mikhail, J.D., Obert, M., Bruhn, J.M., Taylor, S.J., 1995. Fractal geometry of diffuse mycelia and rhizomorphs of Armillaria species. Mycological Research 99, 81–88.

Molz, F.J., Boman, G.K., 1993. A fractal-based stochastic interpolation scheme in subsurface hydrology. Water Resources Research 29, 3769–3774.

Molz, F.J., Boman, G.K., 1995. Further evidence of fractal structure in hydraulic conductivity distributions. Geophysical Research Lettters 22, 2545–2548.

Molz, F.J., Liu, H.H., 1997. Fractional Brownian motion and fractional Gaussian noise in subsurface hydrology: A review, presentation of fundamental properties, and extensions. Water Resources Research 33, 2273–2286.

Molz, F.J., Hewett, T.A., Boman, G.K., 1997. A pseudo-fractal model for hydraulic property distributions in porous media. In: Baveye, P., Parlange, J.-Y., Stewart, B.A. (Eds.), Fractals in Soil Science. CRC Press, Boca Raton, FL, pp. 341–372.

Moore, C.A., and Donaldson, C.F., 1995. Quantifying soil microstructure using fractals. Géotechnique, London 45, 105–116.

Moreau, E., Velde, B., Terribile, E., 1999. Comparison of 2D and 3D images of fractures in Vertisol. Geoderma 92, 55–72.

Morse, D.R., Lawton, J.H., Dodson, M.M., Williamson, M.H., 1985. Fractal dimension of vegetation and the distribution of arthropod body lengths. Nature 314, 731–733.

Mukhopadhyay, S., Cushman, J.H., 1998. Diffusive transport of volatile pollutants in nonaqueous-phase liquid contaminated soil: a fractal model. Transport in porous media 30, 125–134.

Nielsen, K.L., Lynch, J.P., Weiss, H.N., 1997. Fractal geometry of bean root systems: correlations between spatial and fractal dimension. American Journal of Botany 84, 26–33.

Nielsen, K.L., Miller, C.R., Beck, D., Lynch, J.P., 1998/99. Fractal geometry of root systems: Field observations of contrasting genotypes of common bean (*Phaseolus vulgaris* L.) grown under different phosphorus regimes. Plant and Soil 206, 181–190.

Niemeyer, J., Ahl, C., 1991. Die Fractale Verteilung der Minerale und deren Bedeutung fur die Sorption. Mitt. Dtsch. Bodenk. Ges. 66, 217–274.

Niemeyer, J., Machulla, G., 1999. Description of soil pore systems accessible for water by fractal dimensions. Physica A 266, 203–208.

Nizovtsev, V.V., Panchenko, O.V., Garigullin, R.G., 1998. Investigation into the instability of water front under satiation of a modeled ground. Eurasian Soil Science 31, 649–652.

Ogawa, S., Baveye, P., Boast, C., Parlange, J.-Y., Steenhuis, T., 1999. Surface fractal characteristics of preferential flow patterns in field soils: evaluation and effect of image processing. Geoderma 88, 109–136.

Okuda, I., 1993. Sorption and transport in heterogeneous porous media: Applications of fractal and stochastic approaches. Ph.D. Thesis. University of Florida, Gainesville, FL, 227 pp.

Oleschko, K., 1998. Delesse principle and statistical fractal sets: 1. Dimensional equivalents. Soil and Tillage Research 49, 255–266.

Oleschko, K., 1998. Delesse principle and statistical fractal sets: 2. Unified fractal model for soil porosity. Soil and Tillage Research 52, 247–257.

Oleschko, K., Fuentes, C., Brambila, F., Alvarez, R., 1997. Linear fractal analysis of three Mexican soils in different management systems. Soil Technology 10, 207–223.

Oleschko, K., Brambila, F., Acess, F., Mora, L.P., 1998. From fractal analysis along a line to fractals on the plane. Soil and Tillage Research 45, 389–406.

Ong, C.K., Deans, J.D., Wilson, J., Mutua, J., Khan, A.A.H., Lingren, E.M., 1998. Exploring below ground complementarity in agroforestry using sap flow and root fractal techniques. Agroforesry systems 44, 87–103.

Onody, R.N., Posadas, A.N.D., Crestana, S., 1995. Experimental studies of the fingering phenomena in two dimensions and simulation using a modified invasion percolation model. Journal of Applied Physics 78, 2970–2976.

Österberg, R., Mortensen, K., Ikai, A., 1995. Direct observation of humic acid clusters, a nonequilibrium system with a fractal structure. Naturwissenschaften 82, 137–139.

Österberg, R., Mortensen, K., 1994. Fractal geometry of humic substances. Temperature-dependent restructuring studied by small-angle neutron scattering. In: Senesi, N., Miano, T.M. (Eds.), Humic Substances in the Global Environment and Implications on Human Health. Elsevier Science, pp. 127–132.

Österberg, R., Mortensen, K., 1992. Fractal Dimension of Humic Acids. European Biophysical Journal 21, 163–167.

Österberg, R., Mortensen, K., 1994. The growth of fractal humic acids: cluster correlation and gel formation. Radiation and Environmental Biophysics 33, 269–276.

Österberg, R., Szajdak, L., Mortensen, K., 1994. Temperature-dependent restructuring of fractal humic acids: A proton-dependent process. Environ. International 20, 77–80.

Ouchi, S., Matsushita, M., 1992. Measurement of self-affinity on surfaces as a trial application of fractal geometry to landform analysis. Geomorphology 5, 115–130.

Outcalt, S.I., Hinkel, K.M., Nelson, F.E., 1992. Spectral signature of coupled flow in the refreezing active layer, Northern Alaska. Physical geography 93, 273–284.

Ozhovan, M.I., Dmitriev, I.E., Batyukhnova, O.G., 1993. Fractal structure of pores in clay soil. Atomic Energy. Translated from Atomnaya Energiya 74, 241–243.

Ozier-Lafontaine, H., Lecompte, F., Sillon, J.F., 1999. Fractal analysis of the root architecture of *Gliricidia sepium* for the spatial prediction of root branching, size and mass model development and evaluation of agroforestry. Plant and Soil 209, 167–180.

Pachepsky, Ya.A., Shcherbakov, R.A., Korsunskaya, L.P., 1995. Scaling of soil water retention using a fractal model. Soil Science 159, 99–104.

Pachepsky, Ya.A., Polubesova, T.A., Hajnos, M., Sokołowska, Z., Jozefaciuk, G., 1995. Fractal parameters of pore surface area as influenced by simulated soil degradation. Soil Science Society of America Journal 59, 68–75.

Pachepsky, Ya., Yakovchenko, V., Rabenhorst, M.C., Pooley, C., Sikora, L., 1996. Fractal parameters of pore surface as derived from micromorphological data: effect of long-term management practices. Geoderma 74, 305–320.

Pachepsky, Ya.A., Korsunskaia, L.P., Hajnos, M., 1996. Fractal parameters of soil pore surface area under a developing crop. Fractals 4, 97–104.

Pachepsky, Ya.A., Ritchie, J.C., Gimenez, D., 1997. Fractal modeling of airborne laser altimetry data. Remote Sensing and Environment 61, 150–161.

Pachepsky, Ya.A., Giménez, D., Logsdon, S., Allmaras, R., Kozak, E., 1997. On interpretation and misinterpretation of fractal models: a reply to "Comment on number-size distributions, soil structure, and fractals". Soil Science Society of America Journal 61, 1800–1801.

Pachepsky, Ya.A., Ritchie, J.C., 1998. Seasonal changes in fractal landscape surface roughness estimated from airborne laser altimetry data. International Journal of Remote Sensing 19, 2509–2516.

Pachepsky, Ya., Rawls, W.J., Giménez, D., Watt, J.P.C., 1998. Data Mining to Develop Pedotransfer Functions. In: Proceedings of the World Congress of Soil Science, 20–26 August 1998, Montpellier, France. CD-ROM.

Pachepsky, Ya.A., Rawls, W., Giménez, D., Watt, J.P.C., 1998. Use of soil penetration resistance and group method of data handling to improve soil water retention estimates. Soil and Tillage Research 49, 117–128.

Pachepsky, Ya., Timlin, D., 1998. Water transport in soils as in fractal media. Journal of Hydrology 204, 98–107.

Pan, J.-Z., Lu, Z.-X., 1994. Fractal dimensions of soil strengths for paddy fields in China. Journal of Terramechanics 31, 1–9.

Pardini, G., Gallart, F., 1989. A combination of laser technology and fractals to analyze soil surface roughness. European Journal of Soil Science 49, 197–202.

Pastor-Satorras, R., Rothman, D.H., 1998. Scaling of a slope, the erosion of tilted landscapes. Journal of Statistical Physics 43, 477–500.

Pelletier, J.D., Malamud, B.D., Blodgett, T., Turcotte, D.L., 1997. Scale invariance of soil moisture variability and its implications for the frequency-size distribution of landslides. Engineering Geology 48, 255–268.

Perfect, E., 1996. Soil management effects on planting and emergence of no-till corn. Transactions of the ASAE 39, 1611–1615.

Perfect, E., 1997. Fractal models for the fragmentation of rocks and soils: a review. Engineering Geology 48, 185–207.

Perfect, E., 1997. On the relationship between mass and fragmentation fractal dimensions. In: Novak, M.M., Dewey, T.G. (Eds.), Fractal Frontiers. World Scientific, Singapore, pp. 349–358.

Perfect, E., 1997. Fractal characterization of soil aggregation and fragmentation as influenced by tillage treatment. Soil Science Society of America Journal 61, 896–900.

Perfect, E., 1999. Estimating soil mass fractal dimensions from water retention curves. Geoderma 88, 221–231.

Perfect, E., Groenevelt, P.H., Kay, B.D., Grant, C.D., 1990. Spatial variability of soil penetrometer measurements at the mesoscopic scale. Soil and Tillage Research 16, 257–271.

Perfect, E., Kay, B.D., 1991. Fractal theory applied to soil aggregation. Soil Science Society of America Journal 55, 1552–1558.

Perfect, E., Rasiah, V., Kay, B.D., 1992. Fractal dimensions of soil aggregate-size distributions calculated by number and mass. Soil Science Society of America Journal 56, 1407–1409.

Perfect, E., Kay, B.D., Rasiah, V., 1993. Reply to "Comments on 'fractal dimensions of soil aggregate-size distributions calculated by number and mass'". Soil Science Society of America Journal 57, 1394–1395.

Perfect, E., Kay, B.D., Rasiah, V., 1993. Multifractal model for soil aggregate fragmentation. Soil Science Society of America Journal 57, 896–900.

Perfect, E., Kay, B.D., Rasiah, V., 1994. Unbiased estimation of the fractal dimension of soil aggregate size distributions. Soil and Tillage Research 31, 187–198.

Perfect, E., Kay, B.D., 1995. Applications of fractals in soil and tillage research: a review. Soil and Tillage Research 36, 1–20.

Perfect, E., Kay, B.D., 1995. Brittle fracture of fractal cubic aggregates. Soil Science Society of America Journal 59, 969–974.

Perfect, E., McLaughlin, N.B., Kay, B.D., Topp, G.C., 1996. An improved fractal equation for the soil water retention curve. Water Resources Research 32, 281–287.

Perfect, E., Blevins, R.L., 1997. Fractal characterization of soil aggregation and fragmentation as influenced by tillage treatment. Soil Science Society of America Journal 61, 896–900.

Perfect, E., McLaughlin, N.B., Kay, B.D., 1997. Energy requirements for conventional tillage following different crop rotations. Transactions of the ASAE 40, 45–49.

Perfect, E., McLaughlin, N.B., Kay, B.D., Topp, G.C., 1998. Comment on 'An improved fractal equation for the soil water retention curve' by E. Perfect et al. – Reply. Water Resources Research 34, 933–935.

Perfect, E., Zhai, Q., Blevins, R.V., 1998. Estimation of Weibull brittle fracture parameters for heterogeneous materials. Soil Science Society of America Journal 62, 1212–1219.

Perrier, E., Mullon, C., Rieu, M., de Marsily, G., 1995. Computer construction of fractal soil structures: Simulation of their hydraulic and shrinkage properties. Water Resources Research 31, 2927–2943.

Perrier, E., Rieu, M., Sposito, G., Marsily, G.D., 1996. A computer model of the water retention curve for soils with a fractal pore size distribution. Water Resources Research 32, 3025–3031.

Perrier, E., Rieu, M., Sposito, G., de Marsily, G., 1996. Models of the water retention curve for soils with fractal pore-size distributions. Water Resources Research 32, 3025–3031.

Perrier, E., Rieu, M., Sposito, G., de Marsily, G., 1998. Comment on 'An improved fractal equation for the soil water retention curve' by E. Perfect et al. Water Resources Research 34, 931–932.

Perrier, E., Bird, N.R.A., Rieu, M., 1999. Generalizing the fractal model of soil structure: the pore-solid fractal approach. Geoderma 88, 137–164.

Peyton, R.L., Gantzer, C.J., Anderson, S.H., Haeffner, B.A., Pfeifer, P., 1994. Fractal dimension to describe soil macropore structure using X ray computed tomography. Water Resources Research 30, 691–700.

Posadas, D., Crestana, S., 1993. Application of fractal theory for characterizing fingering phenomenon in unsaturated soils. Revista brasileira de ciencia do solo 17, 1–25 (in Port.).

Posadas, D.A.N., Tannus, A., Panepucci, H., Creastana, S., 1996. Magnetic resonance imaging as a new non-invasive techniques for investigating 3-D preferential flow occurring within stratified soil samples. Computers and electronics in agriculture 14, 255–267.

Preston, S., Griffiths, B.S., Young, I.M., 1997. An investigation into sources of soil crack heterogeneity using fractal geometry. European Journal of Soil Science 48, 31–37.

Qian, Z.W., 1995. Fractal dimensions of sediments in nature. Physical Review E 53, 2304–2306.

Raes, F., De Cort, M., 1991. Multi-fractal nature of radioactivity deposition on soil after the Chernobyl accident. Health physics 61, 271.

Rappoldt, C., Crawford, J.W., 1999. The distribution of anoxic volume in a fractal model of soil. Geoderma 88, 329–347.

Rasiah, V., 1995. Fractal dimension of surface-connected macropore count-size distribution. Soil Science 159, 105–108.
Rasiah, V., 1996. Comments on 'Fractal dimension of surface connected macropore count–size distribution' by V. Rasiah. Soil Science 161, 543–544.
Rasiah, V., 1997. Parameterizing temporal changes in aggregation in sludge amended soil. Soil Science Society of America Journal 61, 579–585.
Rasiah, V., 1998. Assessing tillage- and cropping-induced changes in relative conductivity. Australian Journal of Soil Research 36, 799–807.
Rasiah, V., Kay, B.D., Perfect, E., 1992. Evaluation of selected factors influencing aggregate fragmentation using fractal theory. Canadian Journal of Soil Science 72, 97–106.
Rasiah, V., Kay, B.D., Perfect, E., 1993. New mass-based model for estimating fractal dimensions of soil aggregates. Soil Science Society of America Journal 57, 891–895.
Rasiah, V., Biederbeck, V.O., 1995. Fractal dimension of soil aggregates: influence of bulk density, fitting procedure, and oily waste sludge incorporation. Soil Science160, 250–255.
Rasiah, V., Perfect, E., Kay, B.D., 1995. Linear and nonlinear estimates of fractal dimension for soil aggregate fragmentation. Soil Science Society of America Journal 59, 83–87.
Rasiah, V., Aylmore, L.A.G., 1998. Characterizing the changes in soil porosity by computer tomography and fractal dimension. Soil Science 163, 203–211.
Rasiah, V., Aylmore, L.A.G., 1998. Estimating microscale spatial distribution of conductivity and pore continuity using computed tomography. Soil Science Society of America Journal 62, 1197–1202.
Rawls, W.J., 1996. Estimation of macropore properties for no-till soils. Transactions of the ASAE, 91–95.
Rawls, W.J., Brakensiek, D.L., Logsdon, S.D., 1993. Predicting saturated hydraulic conductivity utilizing fractal principles. Soil Science Society of America Journal 57, 1193–1197.
Rawls, W.J., Brakensiek, D.L., 1995. Utilizing fractal principles for predicting soil hydraulic properties. Journal of Soil and Water Conservation 50, 463–465.
Regalado, C.M., Crawford, J.W., Ritz, K., Sleeman, B.D., 1996. The origins of spatial heterogeneity in vegetative mycelia: A reaction-diffusion model. Mycological Research 100, 1473–1480.
Rice, J.A., Lin, J.-S., 1993. Fractal nature of humic materials. Environmental Science and Technology 27, 413–414.
Rice, J.A., Lin, J.-S., 1994. Fractal dimensions of humic materials. In: Senesi, N., Miano, T.M. (Eds.), Humic Substances in the Global Environment and Implications on Human Health. Elsevier, Amsterdam, pp. 115–120.
Rice, J.A., Tombácz, E., Malekani, K., 1999. Applications of light and X-ray scattering to characterize the fractal properties of soil organic matter. Geoderma 88, 251–264.

Rieu, M., Sposito, G., 1991. Relation pression capillaire–teneur en eau dans les milieux poreux fragmentes et identification du caractere fractal de la structure des sols. Comptes Rendus de l'Acadèmie des Sciences de Paris 312 Serie II, 1483–1489.

Rieu, M., Sposito, G., 1991. The water characteristic curve of fragmented porous media and the fractal nature of soil structure. C.R. Acad. Sci. Paris 312 Serie II, 1483–1489.

Rieu, M., Sposito, G., 1991. Fractal fragmentation, soil porosity, and soil water properties: I. Theory. Soil Science Society of America Journal 55, 1231–1238.

Rieu, M., Sposito, G., 1991. Fractal fragmentation, soil porosity, and soil water properties: II. Applications. Soil Science Society of America Journal 55, 1239–1248.

Rieu, M., Perrier, E., 1994. Modélisation fractale de la structure des sols. Comptes Rendus Académie Agriculture 80, 21–39.

Rieu, M., Perrier, E., 1997. Fractal models of fragmented and aggregated soils. In: Baveye, P., Parlange, J.-Y., Stewart, B.A. (Eds.), Fractals in Soil Science. CRC Press, Boca Raton, FL, 169–202.

Ritz, K., Crawford, J.W., 1990. Quantification of the fractal nature of colonies of Trichoderma viride. Mycological research 94, 1138–1141.

Sakamoto, Y., 1994. Fractal dimension of water path through unsaturated media and its simulation using water path invasion model. Journal of Hydroscience and Hydraulic Engineering 11, 19–30.

Salabo, F.K., Babalola, O., Houser, S., Kang, B.T., 1999. Soil macroaggregate stability under different management systems and cropping intensities in South Western Nigeria. Geoderma 91, 103–123.

Semkov, T.M., 1997. Neighborhood volume for bounded locally self-similar fractals. Fractals 5, 23–33.

Senesi, N., 1994. The fractal approach to the study of humic substances. In: Senesi, N., Miano, T.M. (Eds.), Humic Substances in the Global Environment and Implications on Human Health. Elsevier Science, pp. 3–41.

Senesi, N., 1996. Fractals in general soil science and in soil biology and biochemistry. In: Stotzky, G., Bollag, J.-M. (Eds.), Soil Biochemistry Vol. 9, Marcel Dekker, New York. pp 415–472.

Senesi, N., 1999. Aggregation patterns and macromolecular morphology of humic substances: A fractal approach. Soil Science 164, 841–856.

Senesi, N., Rizzi, F.R., Dellino, P., Acquafredda, P., Maggipinto, G., Lorusso, G.F., 1994. The fractal morphology of soil humic acids. Trans. 15th World Congr. Soil Sci. 3b, 81–82.

Senesi, N., Rizzi, F.R., Acquafredda, P., 1996. Fractal dimension of humic acids in aqueous suspensions as a function of pH and time. Soil Science Society of America Journal 60, 1773–1780.

Senesi, N., Rizzi, F.R., Dellino, P., Acquafredda, P., 1997. Fractal humic acids in aqueous suspensions at various concentrations, ionic strengths, and pH values. Colloids and Surfaces 127, 57–68.

Senesi, N., Bourrie, G., 1998. Heterogeneity of Physico-Chemical Processes in Soils. In: Proceedings of the World Congress of Soil Science, 20–26 August 1998, Montpellier, France. CD-ROM.

Shcherbakov, R.A., Korsunskaia, L.P., Pachepskiy, Y.A., 1995. A stochastic model of the soil pore space. Eurasian Soil Science 27, 93–100.

Shepard, S.J., 1993. Using a fractal model to compute the hydraulic conductivity function. Soil Science Society of America Journal 57, 300–306.

Shibusawa, S., 1992. Fractals in clods formed with rotary tillage. Journal of Terramechanics 29, 107–115.

Shibusawa, S., 1994. Modelling the branching growth fractal pattern of the maize root system. Plant and soil 165, 339.

Soddell, J.A., Seviour, R.J., 1994. A comparison of methods for determining the fractal dimensions of colonies of filamentous bacteria. Binary 6, 21–31.

Sokołowska, Z., 1989. On the role of energetic and geometric heterogeneity in sorption of water vapour by soils: Application of a fractal approach. Geoderma 45, 251–265.

Sokolowska, Z., Hajnos, M., Borowko, M., Sokolowski, S., 1999. Adsorption of nitrogen on thermally treated peat soils: the role of energetic and geometric heterogeneity. Journal of Colloid and Interface Science 219, 1–10.

Sokołowska, Z., Patrikiejew, A., Sokołowski, S., 1989. A note on fractal analysis of adsorption process by soils and soil minerals. International Agrophysics 5, 3–12.

Sokołowska, Z., Sokołowski, S., 1989. Water sorption by soil: The role of energetic and geometric heterogeneity. International Agrophysics 5, 247–259.

Sokołowska, Z., Sokołowski, S., 1999. Influence of humic acid in surface fractal dimension of kaolin: analysis of mercury porosimetry and water vapor adsorption data. Geoderma 88, 233–245.

Spadotto, A.J., 1998. Processamento e estabilidade de rações através da dimensão fractal. Botucatu, 1998. 122p. Doutorado – Faculdade de Ciências Agronômicas, UNESP – Botucatu (in Port.).

Spadotto, A.J., and Seraphim, O.J., 1998. Determinação da dimensão fractal pela fórmula Spadotto e pelo MC-D. Energia na Agricultura 12, 24–31 (In Port.).

Spek, L.Y., van Noordwijk, M., 1994. Proximal root diameter as predictor of total root size for fractal branching models. II. Numerical model. Plant and soil 164, 119–127.

Spek, L.Y., 1997. Generation and visualization of root-like structures in a three-dimensional space. Plant and Soil 197, 9–18.

Sposito, G., 1995. Recent advances associated with soil water in unsaturated zone. Reviews in Geophysics 33, 1059–1065.

Stork, N.E., Blackburn, T.M., 1993. Abundance, body-size, and biomass of arthropods in tropical forest. OIKOS 67, 483–489.

Swift, R.S., 1989. Molecular weight, size, shape, and charge characteristics of humic substances: Some basic considerations. In: Hayes, M.H.B. et al. (Eds.), Humic substances II: In search of structure. John Wiley & Sons, New York, pp. 449–465.

Taguas, F.J., Martín, M.A., Perfect, E., 1999. Simulation and testing of self-similar structures for soil particle-size distributions using iterated function systems. Geoderma 88, 191–203.

Tatsumi, J., 1996. Fractal analysis of root distribution. In Ito, O., et al. (Eds.), Dynamics of Roots and Nitrogen in Cropping Systems of the Semi-arid tropics. Japan International Research Center for Agricultural Sciences, pp. 547–557.

Tatsumi, J., and Takagai, K., 1997. Fractal characterization of root system architecture in legume seedlings. In: Novak, M.M., Dewey, T.G. (Eds.), Fractal Frontiers. World Scientific, Singapore, pp. 359–368.

Tatsumi, J., Yamauchi, A., Kono, Y., 1989. Fractal analysis of plant-root systems. Annals of Botany 64, 499–503.

Taylor, C.C., Burrough, P.A., 1986. Multiscale sources of variation in soil: III. Improved methods for fitting the nested model to one-dimensional semivariograms. Mathematical Geology 18, 811–821.

Thevanayagam, S., Nasarajah, S., 1998. Fractal model for flow through saturated soils. Journal of Geotechnical and Geoenvironmental Engineering 124, 53–66.

Thimm, H.F., Poon, D.C., McCormack, N., 1997. Some applications of fractal mathematics in evaluation of the environmental problems. Journal of Canadian Petroleum Technology 36, 31–35.

Tombácz, E., Rice, J.A., Ren, S.Z., 1997. Fractal structure of polydisperse humic acid particles in solution studied by scattering methods. ACH Models in Chemistry 134, 877–888.

Toledo, P.G., Novy, R.A., Davis, H.T., Scriven, L.E., 1990. Hydraulic conductivity of porous media at low water content. Soil Science Society of America Journal 54, 673–679.

Tyler, S.W., 1990. The consequences of fractal scaling in heterogeneous soils and porous media. In: Scaling in Soil Physics: Principles and Applications. SSSA special publication series 25, 109–122.

Tyler, S.W., Wheatcraft, W., 1989. Application of fractal mathematics to soil water retention estimation. Soil Science Society of America Journal 53, 987–996.

Tyler, S.W., Wheatcraft, S.W., 1990. Fractal processes in soil water retention. Water Resources Research 26, 1047–1054.

Tyler, S.W., Wheatcraft, S.W., 1990. The consequences of fractal scaling in heterogeneous soils and porous media. In: Hillel, D., Elrick, D. (Eds.), Scaling in soil physics: principles and applications. Proceedings of a symposium, 1989, October 18, Las Vegas, Special Publication 25, Madison, WI, SSSA, pp. 109–122.

Tyler, S.W., Wheatcraft, S.W., 1992. Fractal scaling of soil particle-size distributions: Analysis and limitations. Soil Science Society of America Journal 56, 362–369.

Valdez-Cepeda, R.D., Olivares-Saenz, E., 1998. Fractal analysis of Mexico's annual mean yields of maize, bean, wheat and rice. Field Crops Research 59, 53–63.

Vallejo, L.E., 1995. Fractal analysis of granular materials. Géotechnique 45, 159–163.

Vallejo, L.E., Zhou, Y., 1995. The Relationship between the Fractal Dimension and Krumbein's Roundness Number. Soils and foundations 35, 163–168.

Van Damme, H., 1995. Scale invariance and hydric behaviour of soils and clays. Comptes Rendus à l'Academie des Sciences 320, Series I, 665–681.

Van Damme, H., 1998. Structural hierarchy and molecular accessibility in clayey aggregates. In: Baveye, P., Parlange, J.-Y., Stewart, B.A. (Eds.), Fractals in Soil Science, CRC Press, Boca Raton, FL, pp. 55–74.

Van Noordwijk, M., Spek, L.Y., de Willigen, P., 1994. Proximal root diameter as predictor of total root size for fractal branching models. I. Theory. Plant and Soil 164, 107–117.

Van Noordwijk, M., Purnomosidhi, P., 1995. Root architecture in relation to tree–soil–crop interactions and shoot pruning in agroforestry. Agroforestry Systems 30, 161–173.

Van Noordwijk, M., van de Geijn, S.C., 1996. Root, shoot and soil parameters required for process-oriented models of crop growth limited by water or nutrients. Plant and Soil 183, 1–25.

Van Noordwijk, M., Cerri, C., Woomer, P.L., Nughoro, K., Bernaux, M., 1997. Soil carbon dynamics in the humid tropical forest zone. Geoderma 79, 187–225.

Velde, B., 1999. Structure of surface cracks in soil and muds. Geoderma 93, 101–124.

Vieux, B., Farajalla, N., 1994. Capturing the essential spatial variability in distributed hydrological modelling: Hydraulic roughness. Hydrological Processes 8, 221–236.

Wang, Y.Q., Zhang, H.J., Yang, D., Bai, K.Z., Kuang, T.Y., 1998. Fractal analysis for root growth of plant seedlings under doubled CO2 concentration. Chinese Science Bulletin 43, 1891–1893.

Wells, J.M., Harris, M.J., Boddy, L., 1999. Dynamics of mycelial growth and phosphorus partitioning in developing mycelial cord systems of Phanerochaete velutina: dependence on carbon availability. New Phytologist 142, 325–332.

Wheatcraft, S.W., Tyler, S.W., 1988. An explanation of scale-dependent dispersivity in heterogeneous aquifers using concepts of fractal geometry. Water Resources Research 24, 566–578.

Wu, Q., Borkovec, M., Sticher, H., 1993. On particle-size distribution in soils. Soil Science Society of America Journal 57, 883–890.

Yordanov, O I., Guissard, A., 1997. Approximate self-affine model for cultivated soil roughness. Physica A 238, 49–65.

Young, I.M., Crawford, J.W., 1991. The fractal structure of soil aggregates: its measurement and interpretation. Journal of Soil Science 42, 187–192.

Young, I.M., Crawford, J.W., 1992. The analysis of fracture profiles of soil using fractal geometry. Australian Journal of Soil Research 30, 291–295.

Young, I.M., Crawford, J.W., Anderson, A., McBratney, A., 1997. Comment on number–size distributions, soil structure, and fractals. Soil Science Society of America Journal 60, 1799–1800.

Zeng, Y., Gantzer, C.J., Payton, R.L., Anderson, S.H., 1996. Fractal dimension and lacunarity of bulk density determined with X-ray computer tomography. Soil Science Society of America Journal 60, 1718–1724.

Zhang, R., 1997. Scale-dependent soil hydraulic conductivity. In: Novak, M.M., Dewey, T.J (Eds.). Fractal Frontiers. World Scientific, pp. 383–392.

Zhou, B.I., 1996. Some progress in the biomimetic study of composite materials. Materials chemistry and physics 45, 114–199.

This Page Intentionally Left Blank